

VOLUME 77

JULY 19, 1973

NUMBER 15

JPCA x

T H E J O U R N A L O F

PHYSICAL
CHEMISTRY

ห้องสมุด กรมวิทยาศาสตร์

PUBLISHED BIWEEKLY BY THE AMERICAN CHEMICAL SOCIETY

THE JOURNAL OF PHYSICAL CHEMISTRY

BRYCE CRAWFORD, Jr., *Editor*

STEPHEN PRAGER, *Associate Editor*

ROBERT W. CARR, Jr., FREDERIC A. VAN-CATLEDGE, *Assistant Editors*

EDITORIAL BOARD: A. O. ALLEN (1970-1974), C. A. ANGELL (1973-1977),
J. R. BOLTON (1971-1975), F. S. DAINTON (1972-1976), M. FIXMAN (1970-1974),
H. S. FRANK (1970-1974), R. R. HENTZ (1972-1976), J. R. HUIZENGA (1969-1973),
W. J. KAUZMANN (1969-1973), R. L. KAY (1972-1976), W. R. KRIGBAUM (1969-1973),
W. J. MOORE (1969-1973), R. M. NOYES (1973-1977), J. A. POPLE (1971-1975),
B. S. RABINOVITCH (1971-1975), H. REISS (1970-1974), S. A. RICE (1969-1975),
F. S. ROWLAND (1973-1977), R. L. SCOTT (1973-1977), W. A. ZISMAN (1972-1976)

AMERICAN CHEMICAL SOCIETY, 1155 Sixteenth St., N.W., Washington, D. C. 20036

Books and Journals Division

JOHN K. CRUM, *Director*

RUTH REYNARD, *Assistant to the Director*

CHARLES R. BERTSCH, *Head, Editorial Processing Department*

D. H. MICHAEL BOWEN, *Head, Journals Department*

BACIL GUILLEY, *Head, Graphics and Production Department*

SELDON W. TERRANT, *Head, Research and Development Department*

©Copyright, 1973, by the American Chemical Society. Published biweekly by the American Chemical Society at 20th and Northampton Sts., Easton, Pa. 18042. Second-class postage paid at Washington, D. C., and at additional mailing offices.

All manuscripts should be sent to *The Journal of Physical Chemistry*, Department of Chemistry, University of Minnesota, Minneapolis, Minn. 55455.

Additions and Corrections are published once yearly in the final issue. See Volume 76, Number 26 for the proper form.

Extensive or unusual alterations in an article after it has been set in type are made at the author's expense and it is understood that by requesting such alterations the author agrees to defray the cost thereof.

The American Chemical Society and the Editor of *The Journal of Physical Chemistry* assume no responsibility for the statements and opinions advanced by contributors.

Correspondence regarding accepted copy, proofs, and reprints should be directed to Editorial Processing Department, American Chemical Society, 20th and Northampton Sts., Easton, Pa. 18042. Head: CHARLES R. BERTSCH, Assistant Editor: EDWARD A. BORGER, Editorial Assistant: JOSEPH E. YURVATI.

Advertising Office: Centcom, Ltd., 142 East Avenue, Norwalk, Conn. 06851.

Business and Subscription Information

Send all new and renewal subscriptions *with payment* to: Office of the Controller, 1155 16th Street, N.W., Washington, D. C. 20036. Subscriptions should be renewed promptly to avoid a break in your series. All correspondence and telephone calls regarding changes of

address, claims for missing issues, subscription service, the status of records, and accounts should be directed to Manager, Membership and Subscription Services, American Chemical Society, P. O. Box 3337, Columbus, Ohio 43210. Telephone (614) 421-7230.

On changes of address, include both old and new addresses with ZIP code numbers, accompanied by mailing label from a recent issue. Allow four weeks for change to become effective.

Claims for missing numbers will not be allowed (1) if loss was due to failure of notice of change in address to be received before the date specified, (2) if received more than sixty days from date of issue plus time normally required for postal delivery of journal and claim, or (3) if the reason for the claim is "issue missing from files."

Subscription rates (1973): members of the American Chemical Society, \$20.00 for 1 year; to nonmembers, \$60.00 for 1 year. Those interested in becoming members should write to the Admissions Department, American Chemical Society, 1155 Sixteenth St., N.W., Washington, D. C. 20036. Postage to Canada and countries in the Pan-American Union, \$5.00; all other countries, \$6.00. Single copies for current year: \$3.00. Rates for back issues from Volume 56 to date are available from the Special Issues Sales Department, 1155 Sixteenth St., N.W., Washington, D. C. 20036.

Subscriptions to this and the other ACS periodical publications are available on microfilm. Supplementary material not printed in this journal is now available in microfiche form on a current subscription basis. For information on microfilm or microfiche subscriptions, write Special Issues Sales Department at the address above.

THE JOURNAL OF
PHYSICAL CHEMISTRY

Volume 77, Number 15 July 19, 1973

JPCHAx 77(15) 1819-1928 (1973)

Photochemical Formation of Free Radicals from Chloroolefins as Studied by Electron Spin Resonance	T. Richerzhagen, P. Svejda, and D. H. Volman*	1819
An Investigation of the Mechanism of the Trisbipyridylruthenium(II) Photosensitized Redox Decomposition of Cobalt(III) Complexes and the Reactivity Patterns of Some Primary Radicals	P. Natarajan and John F. Endicott*	1823
Fluorescence of Cycloalkanones	M. O'Sullivan and A. C. Testa*	1830
Pulse Radiolysis Studies of Nitrofurans. Radiation Chemistry of Nifuroxime	C. L. Greenstock* and I. Dunlop	1834
Yields and Decay of the Hydrated Electron at Times Greater than 200 Picoseconds	C. D. Jonah,* E. J. Hart, and M. S. Matheson	1838
Hydrogen Isotope Effects in the Reaction of Water Vapor with Alkali Metal Mirrors	R. O. Bremner and D. H. Volman*	1844
Adsorption of Gases on Gold Films	J. M. Saleh	1849
Temperature-Dependent Splitting Constants in the Electron Spin Resonance Spectra of Cation Radicals. IV. The Ethoxy Group	Paul D. Sullivan	1853
Raman Spectra of Sulfur Dissolved in Primary Amines	Francis P. Daly and Chris W. Brown*	1859
The Tetrathiotetracene Cation Radical	William E. Geiger, Jr.	1862
Carbon-13 Chemical Shifts of Benzocycloalkenes	Edwin L. Motell, Dieter Lauer, and Gary E. Maciel*	1865
Proton Magnetic Resonance Chemical Shifts and the Hydrogen Bond in Concentrated Aqueous Electrolyte Solutions	E. J. Sare, C. T. Moynihan, and C. A. Angell*	1869
Proton Magnetic Resonance Investigations of Alkylammonium Carboxylate Micelles in Nonaqueous Solvents. III. Effects of Solvents	O. A. El Seoud, E. J. Fendler, J. H. Fendler,* and R. T. Medary	1876
Spectroscopic Studies of Solvation in Sulfolane	T. L. Buxton and J. A. Caruso*	1882
Transport Property Investigation of Ammonium and Tetraalkylammonium Salts in 1,1,3,3-Tetramethylurea	Barbara J. Barker and Joseph A. Caruso*	1884 ■
Uracyl Radical Production in the Radiolysis of Aqueous Solutions of the 5-Halouracils	Kishan Bhatia and Robert H. Schuler*	1888
σ - π Polarization Parameters for Oxygen-17 in Organic and Inorganic π Radicals	E. Melamud and Brian L. Silver*	1896
Secondary and Solvent Deuterium Isotope Effects on Electronic Absorption Spectra of Anilines	J. L. Jensen* and M. P. Gardner	1900
Isotopic Exchange Reactions between Thallium(III) in Complex Compounds and ²⁰⁴ Thallium(I)	Al. Cecal* and I. A. Schneider	1904
Hydration and Association Equilibria in Molten Salts Containing Water. III. The Association of Cadmium Ion with Bromide in the Solvent Calcium Nitrate—Water	H. Braunstein, J. Braunstein,* and P. T. Hardesty	1907 ■

ต้องสมมติ กรมวิทยาศาสตร์
- X 10.8. 7516

Infrared Study of the Interaction between Anhydrous Perchloric Acid and Acetonitrile Masanori Kinugasa,* Kosaku Kishi, and Shigero Ikeda	1914
The Effect of Pressure on the Dimerization of Carboxylic Acids in Aqueous Solution Keizo Suzuki,* Yoshihiro Taniguchi, and Takashi Watanabe	1918

COMMUNICATIONS TO THE EDITOR

Temperature-Jump Experiments on the System Acridine Orange-Poly(styrenesulfonic acid) Vincenzo Vitagliano	1922
An Electron Spectroscopy for Chemical Analysis Study of Lead Adsorbed on Montmorillonite Mary Ellen Counts, James S. C. Jen, and James P. Wightman*	1924
On the Decay of Hydrated Electrons in Radiolytic Spurs at Picosecond Times Stefan J. Rzed and Robert H. Schuler*	1926

■ Supplementary material for this paper is available separately, in photocopy or microfiche form. Ordering information is given in the paper.

* In papers with more than one author, the asterisk indicates the name of the author to whom inquiries about the paper should be addressed.

AUTHOR INDEX

Angell, C. A., 1869	El Seoud, O. A., 1876	Kinugasa, M., 1914	Saleh, J. M., 1849
	Endicott, J. F., 1823	Kishi, K., 1914	Sare, E. J., 1869
Barker, B. J., 1884	Fendler, E. J., 1876	Lauer, D., 1865	Schneider, I. A., 1904
Bhatia, K., 1888	Fendler, J. H., 1876		Schuler, R. H., 1888, 1926
Braunstein, H., 1907		Maciel, G. E., 1865	Silver, B. L., 1896
Braunstein, J., 1907	Gardner, M. P., 1900	Matheson, M. S., 1838	Sullivan, P. D., 1853
Bremner, R. O., 1844	Geiger, W. E., Jr., 1862	Medary, R. T., 1876	Suzuki, K., 1918
Brown, C. W., 1859	Greenstock, C. L., 1834	Melamud, E., 1896	Svejda, P., 1819
Buxton, T. L., 1882		Motell, E. L., 1865	
	Hardesty, P. T., 1907	Moynihan, C. T., 1869	Taniguchi, Y., 1918
Caruso, J. A., 1882, 1884	Hart, E. J., 1838		Testa, A. C., 1830
Cecal, A., 1904		Natarajan, P., 1823	Vitagliano, V., 1922
Counts, M. E., 1924	Ikeda, S., 1914	O'Sullivan, M., 1830	Volman, D. H., 1819, 1844
	Jen, J. S. C., 1924		
Daly, F. P., 1859	Jensen, J. L., 1900	Richerzhagen, T., 1819	Watanabe, T., 1918
Dunlop, I., 1834	Jonah, C. D., 1838	Rzed, S. J., 1926	Wightman, J. P., 1924

THE JOURNAL OF PHYSICAL CHEMISTRY

Registered in U. S. Patent Office © Copyright, 1973, by the American Chemical Society

VOLUME 77, NUMBER 15 JULY 19, 1973

Photochemical Formation of Free Radicals from Chloroolefins as Studied by Electron Spin Resonance

T. Richerzhagen, P. Svejda, and D. H. Volman*

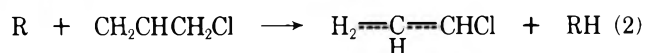
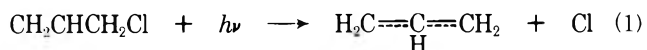
The Department of Chemistry, University of California, Davis, California 95616 (Received February 9, 1973)

Publication costs assisted by the University of California

The esr spectra of uv-irradiated allyl chloride frozen neat or together with methanol, of 2,3-dichloro-1-propene frozen neat, and of allyl chloride, 1-chloro-1-propene, 1,1-dichloro-1-propene, 1,3-dichloro-1-propene, 3-chloro-2-methyl-1-propene, and 1-chloro-2-butene irradiated as inclusion compounds in adamantane matrices showed that the primary process is cleavage of the allylic bond, C-Cl if Cl is in an allylic position or C-H if Cl is absent. The esr spectra of uv-irradiated liquid solutions of di-*tert*-butyl peroxide in allyl chloride, 1,3-dichloro-1-propene, 2,3-dichloro-1-propene, and 1,2,3-trichloro-1-propene showed that the secondary process following formation of the *tert*-butoxy radical was abstraction of an allylic H atom. The hydrocarbon radicals identified were allyl, 2-methylallyl, and *cis*-1-methylallyl. The Cl-containing radicals identified were 1-chloroallyl, 2-chloroallyl, 1,2-dichloroallyl, 1,3-dichloroallyl, 1,1-dichloroallyl, and 1,2,3-trichloroallyl. The esr spectra of the hydrocarbon radicals formed in this work have been observed previously but the esr spectra of the Cl-containing radicals have not heretofore been observed.

Introduction

In previous work from this laboratory¹ we have reported results of esr studies of some uv-irradiated chloropropenes and chlorobutenes: allyl chloride; 1,3-dichloro-1-propene; 2,3-dichloro-1-propene; 2-chloro-2-butene; and 1-chloro-1-butene. After irradiation in the frozen state at 77 K, the chloropropenes gave spectra which we attributed to allenyl free radical, and the chlorobutenes gave spectra which we attributed to methylallenyl free radical. The same result with allyl chloride has since been obtained by Grotorex and Kemp² who attempted to produce a solid-state esr spectrum of allyl radical by uv irradiation in the frozen state. These results were surprising because, by analogy to our earlier results with hydroxypropenes and hydroxybutenes,³ the expected major free-radical-producing processes, taking allyl chloride as an example, would be



Thus the expected radicals would be allyl and/or chloroallyl. We suggested that the precursor of the allenyl radicals were allenylic or propargylic compounds formed by molec-

ular elimination in the primary process. Subsequently, we found that uv irradiation of allyl chloride produced both allene and methylacetylene from the solid state and allene from the liquid state.⁴ However, the primary process indicated was fission of the carbon-chlorine bond.

Although our identification of allenyl radicals seemed reasonable, it was not completely unambiguous. In glassy systems at low temperatures, resolution is relatively poor, and the hydroxyallyl radical³ yields an equally spaced four-line esr spectrum with an average peak separation of 15 G while allenyl radical yields a four-line spectrum with peak-to-peak separations of 18, 14, and 18 G. Thus for hydroxyallyl, coupling with the central proton, some 4 G, is not resolved; for allenyl, $\text{HC}=\overset{\text{H}}{\text{C}}=\text{CH}_2$, although the CH_2 and CH protons under high resolution have coupling constants of 18.9 and 12.6 G, respectively,^{5,6} which yield a six-line spectrum, in the glassy state only four lines are evident.^{1,2,7} For chloroallyl in the glassy state four lines would be expected because the small splittings due to the central proton and the Cl atom would not be resolved. It is possible that the effect of Cl on the spectrum would be different from that of OH and therefore that the coupling constants for CH_2 and CHCl protons in allyl chloride would yield the nonequally spaced spectrum which was

found. Therefore it seemed possible, albeit improbable, that the radical from allyl chloride which we have identified as allenyl was really chloroallyl. Similar arguments apply to the other chloroolefins studied.

In consequence of the above, we have carried out further studies directed at clarification of both the photochemistry and esr spectroscopy of uv-irradiated chloroolefins. Additional compounds have been investigated and the esr studies have been carried out not only in frozen solid systems but also in adamantane matrices and in liquid solutions containing di-*tert*-butyl peroxide yielding *tert*-butoxy as the primary radical.

Experimental Section

3-Chloro-1-propene, allyl chloride (MCB White Label), and 2,3-dichloro-1-propene (Columbia Organic Chemicals) were purified by vpc as previously described.⁴ All the other chloroolefins were used as received: 1-chloro-1-propene (K & K Laboratories); 1,1-dichloro-1-propene (Columbia Organic Chemicals); 1,3-dichloro-1-propene (Columbia Organic Chemicals low boiling isomer); 1,2,3-trichloropropene (K & K Laboratories); 3-chloro-2-methyl-1-propene (Eastman Organic Chemicals); and 1-chloro-2-butene (K & K Laboratories). Di-*tert*-butyl peroxide, DTBP (K & K Laboratories), was also used as received.

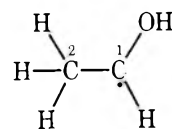
The usefulness of adamantane as a free-radical matrix was discovered by Wood and Lloyd⁸ who obtained radical species from aliphatic amine inclusions by exposure to X-rays. Radical species were also obtained by dual irradiation, exposure to X-rays followed by exposure to uv, but attempts to obtain spectra by exposure to uv only were unsuccessful.⁹ We, however, were able to obtain free-radical species by uv irradiation using a modified technique:¹⁰ the small crystals of adamantane containing guest molecules were subject to high pressure which yielded a translucent pellet, suitable for uv studies.

In the present work adamantane (Aldrich Puriss) was dissolved in warm spectrograde *n*-hexane, treated with activated carbon, and collected by filtration and evaporation of the solvent. Prepared in this fashion, adamantane produced virtually no background esr signal on irradiation at 254 or 185 nm. Inclusions were prepared by cooling a solution of adamantane in the compound of interest to give rapid crystallization. The resulting small white crystals were subjected to a pressure of 1.0×10^9 Nm⁻² whereupon milky translucent pellets, 1.1 cm in diameter, were produced. Samples were irradiated at 254 nm using a low-pressure mercury resonance arc housed in Vycor and ambient temperature unless otherwise noted. To eliminate spectra originating from quartz, the sample was transferred to an unexposed quartz tube following irradiation.

The DTBP esr method, wherein liquid solutions containing DTBP are irradiated to yield the *tert*-butoxy radical which subsequently abstracts an hydrogen atom from the solvent, was independently discovered by Adams¹¹ and by Krusic and Kochi.⁶ In the work reported herein, 1 part of DTBP and 2 parts of the chloroolefin were placed in a quartz tube, degassed by several freeze-pump-thaw cycles, and sealed off under vacuum. Samples were irradiated in the esr cavity using a 2-kVA high-pressure mercury capillary arc housed in quartz and focused on the cavity. Best results were obtained using temperatures slightly above the solidification temperature of the solution.

As will be shown below, the DTBP method gave generally low-intensity broad-line spectra. However, we were able to convince ourselves that this was not due to poor

experimental technique by carrying out the method with ethanol as solvent. A well-resolved spectrum was obtained at 168 K. The coupling constants for the radical



are $a_{2H} = 22.0 \pm 0.1$, $a_{1H} = 15.1 \pm 0.1$ and $a_{OH^H} = 1.50 \pm 0.03$ G. These results are in good agreement with results reported in flow systems by Adams¹¹ using the DTBP method, except that he did not resolve the OH proton coupling, and with results reported in flow systems by Livingston and Zeldes¹² on irradiating solutions of hydrogen peroxide in ethanol; in particular, our value of 1.50 G for the OH proton coupling at 168 K compares with 1.13 G at 206 K and 0.98 at 240 K found by Livingston and Zeldes, showing a further increase in coupling constant with decreasing temperature.

Results and Interpretation

Irradiated in adamantane the compounds gave the spectra shown in Figure 1. Not shown are spectra from 2,3-dichloro-1-propene, which gave only a very broad single line, from 1,2,3-trichloro-1-propene, in which adamantane is only slightly soluble and which yielded only a background of irradiated adamantane, and from 1,3-dichloro-1-propene, which was identical with that obtained from 1-chloro-1-propene. Irradiation of some of the compounds according to the DTBP method yielded the spectra shown in Figure 2.

The coupling constants obtained for the radicals identified from the figures are given in Table I. Coupling constants for the 2-chloroallyl radical obtained as discussed below are also given. The spectra of the radicals identified in Figure 1 were computer simulated using Gaussian-line shape, line widths of 2.1 G, and, for the hydrocarbon radicals, the values reported by Kochi and Krusic.¹³ The coupling constants given are those used for the simulations and are not to be construed as representing the accuracy of the experimental results because variations of some ± 0.3 G in the constants chosen for the simulations would not seriously affect comparisons with the experimental spectra. For the spectra in Figure 2, the coupling constants are the average peak-to-peak separations attributed to protons attached to the 1 and 3 carbon positions.

The 1-chloroallyl radical spectra obtained from irradiation in adamantane, Figure 1B, and by the DTBP method, Figure 2A, are clearly not the same as the four-line spectrum previously observed on irradiation of frozen allyl chloride.¹ Since neither of these experiments produced evidence for the formation of allenyl radical, additional studies of the frozen system were made. It was found that short irradiation, less than 3 min with low-intensity 254-nm light at 77 K, gave the spectrum of allyl radical as usually observed in frozen media, five lines with an equal separation of 15 G, by ourselves and others.³ More prolonged irradiation, up to 15 min, yielded a mixture of two spectra and finally on further irradiation a single spectrum which was identical with that previously assigned to allenyl.¹ At times when the allyl spectrum was observed, irradiation was accompanied by a greenish emission centered at 525 nm; the emission did not accompany the formation of allenyl radical. Upon warming samples irradiated at 77 K, which exhibited both radical spectra, the allenyl spectrum diminished much more rapidly than the

TABLE I: Radicals and Coupling Constants

Figure	Radical	Compound and method	Coupling constants, ^c G
1A	CH ₂ CHCH ₂	CH ₂ CHCH ₂ Cl, A, ^a 176 K	1,3 α H, 14.8; 1,3 β H, 13.9; 2H, 4.1
None		Neat, 77 K	1,1,3,3H = 15.0 \pm 0.5
1D	CH ₂ C(CH ₃)CH ₂	CH ₂ C(CH ₃)CH ₂ Cl, A, 298 K	1,3 α H, 14.7; 1,3 β H, 13.8; H _{CH₃} , 3.2
1E	CH(CH ₃)CHCH ₂	CH(CH ₃)CHCH ₂ Cl, A, 298 K	3 α H, 14.9; 1H, 14.2; H _{CH₃} , 14.0; 3 β H, 13.5; 2H, 3.8
1B	CHCICHCH ₂	CHCICHCH ₃ , A, 298 K	{3 α H, 14.8; 1,3 β H, 13.9
None		CHCICHCH ₂ Cl, A, 298 K	{2H, 4.1; Cl, 1.2
2A		CH ₂ CHCH ₂ Cl, D, ^b 133 K	1,3,3H = 14.0 \pm 0.5
None	CH ₂ CClCH ₂	CH ₂ CClCH ₂ Cl, neat, 123 K	1,1,3,3H = 15.0 \pm 0.5
1C	CCl ₂ CHCH ₂	CCl ₂ CHCH ₃ , A, 298 K	3 α H, 14.8; 3 β H, 13.9; 2H, 4.1; Cl, 1.2
2B	CHCICHCHCl	CHCICHCH ₂ Cl, D, 173 K	1,3H = 13.2 \pm 0.5
2C	CH ₂ CClCHCl	CH ₂ CClCH ₂ Cl, D, 198 K	1,1,3H = 13.5 \pm 0.5
2D	CHCICClCHC	CHCICClCH ₂ Cl, D, 198 K	1,3H = 13.5 \pm 0.5

^a Adamantane. ^b DTBP. ^c Position of the coupling nucleus given by number of the carbon of the allylic system from left to right in the radical formula. α and β distinguish two protons on the same carbon with different coupling constants.

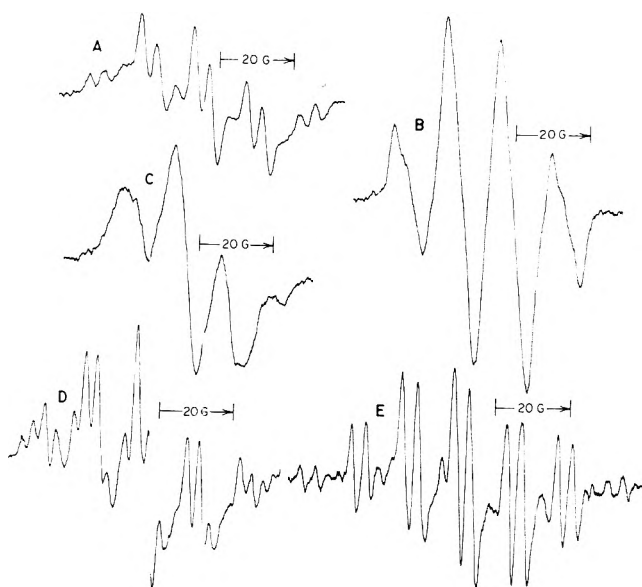


Figure 1. ESR spectra from irradiation in adamantane: (A) CH₂CHCH₂Cl, 176 K; (B) CHCICHCH₃, 298 K (also from CHCICHCH₂Cl); CCl₂CHCH₃, 298 K; (D) CH₂C(CH₃)CH₂Cl, 298 K; (E) CH(CH₃)CHCH₂Cl, 298 K.

allyl until at 110 K it was not observable while the allyl spectrum persisted to 135 K. Irradiation in the cavity at 100 K yielded only an allyl radical spectrum which grew in intensity to a level which remained constant under prolonged irradiation, 3 hr. Mixtures of methanol and allyl chloride were also irradiated at 77 K. With 2 parts methanol to 1 part allyl chloride, the spectrum was predominantly allyl radical but with an admixture of allenyl on prolonged irradiation. With 3 or 4 parts methanol to 1 part of allyl chloride, only the allyl spectrum was observed.

Additional studies of the 2,3-dichloro-1-propene frozen system were also made and yielded results similar to those observed for allyl chloride. Irradiation at 123 K gave an equally spaced five-line spectrum identified as 2-chloroallyl radical.

Discussion

Spectra. The spectra of the hydrocarbon radicals found in this study, allyl, 2-methylallyl, and *cis*-1-methylallyl, have been observed in other studies and are well charac-

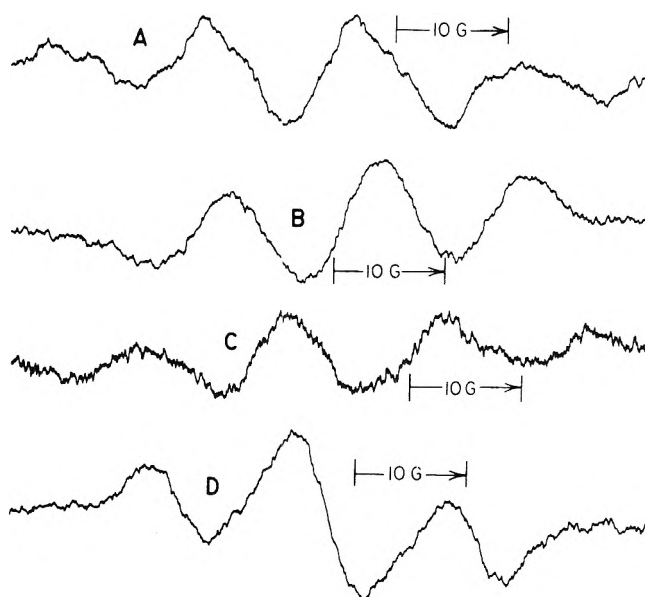


Figure 2. ESR spectra from DTBP method: (A) CH₂CHCH₂Cl, 133 K; (B) CHCICHCH₂Cl, 173 K; (C) CH₂CClCH₂Cl, 198 K; (D) CHCICClCH₂Cl, 198 K.

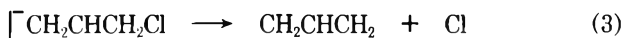
terized by Kochi and Krusic.¹³ We are, however, unaware of any ESR spectral data on the chlorine-substituted radicals found in this study: 1-chloroallyl; 2-chloroallyl; 1,1-dichloroallyl; 1,3-dichloroallyl; 1,2-dichloroallyl; and 1,2,3-trichloroallyl. Few studies of chlorine couplings in aliphatic radicals have been reported. Substitution of a chlorine atom for an hydrogen atom in methyl yields $a_{Cl} = 2.8$ and $a_H = 22$ G.¹⁴ Thus the chlorine coupling is some 12% of the proton coupling in methyl radical and the substitution only slightly reduces the proton coupling. The strong electric quadrupole moment of chlorine allows a breakdown of the Δm_1 selection rule, and hence there are spectral lines from $\Delta m_1 = 0, 1, 2$ transitions. Further, ³⁵Cl and ³⁷Cl, both having nuclear spins of 3/2, are appreciably present in normal chlorine. Because the nuclear magnetic moment ratio $\mu(^{35}\text{Cl})/\mu(^{37}\text{Cl}) = 1.2$, the small difference in coupling constants will merely give additional line width. These multiple effects would result in spectra in which the principal proton couplings appear broadened. Indeed this broadening, as our spectra and simulations show, is sufficient to obviate resolution of the 4.1-G proton coupling of the central proton.

Although the identification of the radical species leaves little ambiguity, extraneous spectral lines are apparent where resolution is greatest, the hydrocarbon radicals in adamantane. Four sources seem possible: secondary radical reactions; impurities; alternate primary processes; uv absorption by the initial radical. These background spectra are not serious enough to negate the principal conclusions.

Mechanism. The spectra obtained show clearly that a photochemical primary process is cleavage of the allylic bond (Scheme I). The spectra of the allylic radicals in-

Scheme I

$h\nu(254\text{ nm}) +$



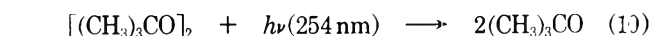
dicated in eq 3, Figure 1A, 4, Figure 1B, 5, Figure 1C, 6, Figure 1B, 8, Figure 1D, and 9, Figure 1E, were obtained in adamantane matrices. The spectrum of the allyl radical, eq 3, was also obtained from irradiation of frozen neat allyl chloride and from irradiation of a frozen mixture of allyl chloride and methanol. The spectrum of the 2-chloroallyl radical was obtained from irradiation of frozen neat 2,3-dichloro-1-propene. If a chlorine atom is in the allylic position, the C-Cl bond is broken; otherwise a C-H allylic bond is broken.

Although in this work we have obtained evidence for the formation of allyl radical by irradiation of frozen neat allyl chloride and 2-chloroallyl radical by irradiation of frozen neat 2,3-dichloro-1-propene, we still cannot explain the formation of allenyl radicals observed in earlier experiments. However, the observation that irradiation of frozen allyl chloride to yield allyl radical was accompanied by emission at 525 nm, which was not observed when allenyl radical was formed, suggests that perhaps an excited state of allyl is involved. Primary process 1 is about 217 kJ exothermic if a value of 250 kJ is used for the carbon-chlorine bond dissociation energy in allyl chloride,¹⁵ very close to 227 kJ, the energy at 525 nm. It is possible to

write a number of concerted mechanisms between an energy-rich allyl radical and allyl chloride which could yield allenyl radical but these would be highly speculative at this time. However, mechanisms of this type are alternatives to our earlier proposal¹ that allenyl radicals were formed by H-atom elimination from allenic compounds formed by irradiation.

The spectra obtained according to the DTBP method demonstrate the sequences shown in Scheme II. In each

Scheme II



$(\text{CH}_3)_3\text{CO} +$



case, the spectrum of an allylic radical corresponding to the abstraction of an allylic hydrogen atom by *tert*-butoxy radical was formed.

Acknowledgment. We are grateful to the National Science Foundation for financial support of this research.

References and Notes

- (1) D. H. Volman, K. A. Maas, and J. Wolstenholme, *J. Amer. Chem. Soc.*, **87**, 3041 (1965).
- (2) D. Greatorex and T. J. Kemp, *Trans. Faraday Soc.*, **67**, 1576 (1971).
- (3) K. A. Maas and D. H. Volman, *Trans. Faraday Soc.*, **60**, 1202 (1964).
- (4) R. W. Phillips and D. H. Volman, *J. Amer. Chem. Soc.*, **91**, 3418 (1969).
- (5) R. W. Fessenden and R. H. Schuler, *J. Chem. Phys.*, **39**, 2147 (1963).
- (6) P. J. Krusic and J. K. Kochi, *J. Amer. Chem. Soc.*, **90**, 7155 (1968).
- (7) C. U. Morgan and K. J. White, *J. Amer. Chem. Soc.*, **92**, 3309 (1970).
- (8) D. E. Wood and R. V. Lloyd, *J. Chem. Phys.*, **52**, 3840 (1970), *et seq.*
- (9) D. E. Wood, R. V. Lloyd, and D. W. Pratt, *J. Amer. Chem. Soc.*, **92**, 4115 (1970).
- (10) T. Richerzhagen and D. H. Volman, *J. Amer. Chem. Soc.*, **93**, 2062 (1971).
- (11) J. O. Adams, *J. Amer. Chem. Soc.*, **90**, 5363 (1968).
- (12) R. Livingston and H. Zeldes, *J. Chem. Phys.*, **44**, 1245 (1966).
- (13) J. K. Kochi and P. J. Krusic, *J. Amer. Chem. Soc.*, **90**, 757 (1968).
- (14) J. P. Michaut and J. Roncin, *Chem. Phys. Lett.*, **12**, 95 (1971).
- (15) T. L. Cottrell, "The Strengths of Chemical Bonds," 2nd ed, Butterworths, London, 1958, p 276.

An Investigation of the Mechanism of the Trisbipyridylruthenium(II) Photosensitized Redox Decomposition of Cobalt(III) Complexes and the Reactivity Patterns of Some Primary Radicals¹

P. Natarajan and John F. Endicott*

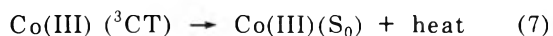
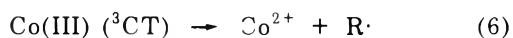
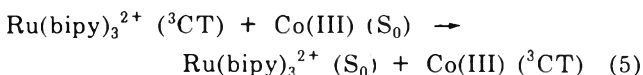
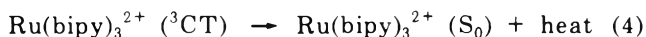
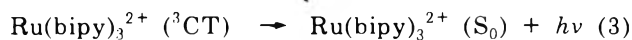
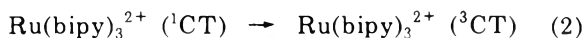
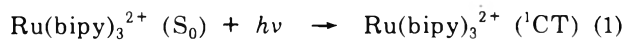
The Department of Chemistry, Wayne State University, Detroit, Michigan 48202 (Received December 15, 1972)

Publication costs assisted by the National Science Foundation

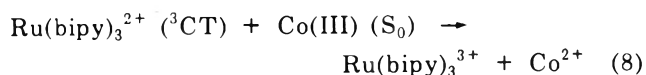
Investigations have been made of the identities and the stoichiometries of products formed in the Ru(bipy)₃²⁺ sensitized redox decompositions of Co(NH₃)₅Br²⁺, Co(EDTA)⁻, and Co(HEDTA)X⁻ (X = Cl, Br, NO₂) substrates. When reactions were carried out in strongly acidic aqueous solution with purified materials, and when proper account was made for dark reactions, the redox products were found to be Co²⁺, Ru(bipy)₃³⁺, and CO₂ with yields in a 1:1:1 ratio. In the presence of 50% 2-propanol the Ru(bipy)₃³⁺ yield was greatly diminished while the Co²⁺ yield was markedly increased. This indicates that a primary radical is formed and reacts competitively with 2-propanol and Ru(bipy)₃²⁺ with the resulting 2-hydroxy-2-propyl radical reducing the cobalt(III) substrate. The nearly diffusion-controlled oxidation of Ru(bipy)₃²⁺ by primary radicals has been confirmed in flash photolysis studies. It is concluded that the dominant mode of Ru(bipy)₃²⁺ sensitized redox decomposition of these cobalt(III) substrates is triplet-to-triplet energy transfer and that there is no evidence for electron transfer from the triplet excited states of the sensitizer. Aspects of the very complex primary and secondary radical reactions have been investigated and are described in detail.

Introduction

A recent communication from this laboratory² reported on the photosensitized redox decomposition of ethylenediaminetetraacetate (EDTA) complexes of cobalt(III) using Ru(bipy)₃²⁺ as a triplet sensitizer.³⁻⁵ It has been suggested^{2,3} that the sensitized reaction proceeded by means of triplet-to-triplet energy transfer, a reaction scheme represented in eq 1-7, and where R· is a primary radical ob-



tained from the 1 equiv oxidation of one of the ligands of the cobalt(III) substrate. The mechanistic significance of (5) has recently been challenged by Adamson and coworkers^{6,7} who have proposed that the critical mechanistic step is electron transfer from the charge transfer triplet state of Ru(bipy)₃²⁺ to the cobalt(III) substrate, (8), and that no radical species are produced in the primary step. Both mechanistic suggestions have attracted considerable interest and establishing the nature of the key mechanistic step, *i.e.*, whether it is (6) or (8), is of fundamental



significance in understanding the photochemical behavior

of cobalt(III) complexes; therefore we have undertaken a critical investigation of this question. This report of our studies has been separated from the reports of our investigations of the photochemical behavior of transition metal-EDTA complexes⁸ in order that the experimental evidence and the contrasting mechanistic arguments may be presented in detail.

Experimental Section

Most of the chemical⁸ and photochemical^{8,9} techniques, preparation, characterization, and analysis of complexes,⁸ and the analytical techniques^{8,9} are described in detail elsewhere.

In the flash photolysis studies reported here we used an unfiltered 250-J flash and monitored changes in absorbance at 480 nm (20-cm optical path length).

Continuous irradiations were performed in the focal plane of the irradiator grating at 450 ± 30 nm. Samples were irradiated in 1-cm quartz cells, following 20-30 min deaeration (with Cr²⁺ scrubbed N₂) at 4 ± 1°. Exposure time was limited to less than or equal to 2 min. The photolyte solutions were diluted twofold with 1 M H₂SO₄ (at 4°) immediately after irradiation and absorbance changes at 480 nm were determined in the Cary 14 with cell compartment maintained at 4 ± 2°. All operations from the commencement of irradiation were timed with a stopwatch. In general the absorbance at 480 nm was found to have decreased during irradiation in 1 M H₂SO₄, due to formation of Ru(bipy)₃³⁺, and for all such solutions the initial absorbance intensity of the Ru(bipy)₃²⁺ was eventually recovered (to within 5% of the initial value). The rate of recovery was timed, the pseudo-first-order recovery rate was extrapolated back to the termination of irradiation, and an initial yield of Ru(bipy)₃³⁺ was estimated. The amount of Ru(bipy)₃³⁺ estimated to have decom-

posed during the irradiation period was negligible in continuous photolysis experiments.

Pseudo-first-order rate constants for the reaction of 2-propanol and $\text{Ru}(\text{bipy})_3^{3+}$ were determined by following the increase in absorbance at 480 nm. Rate constants were obtained from a plot of $\log(A - A_t)$ vs. time. In some cases deviations from pseudo-first-order behavior were observed after three reaction half-lives.

The 2-propanol used was generally Merck Spectral Quality. For some experiments we used redistilled analytical reagent grade 2-propanol.

The solutions of $\text{Ru}(\text{bipy})_3^{3+}$ in 1 M H_2SO_4 were prepared by means of the PbO_2 oxidation of $\text{Ru}(\text{bipy})_3^{2+}$, using the minimum necessary amount of PbO_2 .

For the radiolysis studies a U. S. Nuclear GR-9 ^{60}Co γ -irradiator¹⁰ was used. The nominal dose rate was 6.3 Mrads hr^{-1} . Six samples of each solution were irradiated simultaneously to average out differences in flux.

Results

The 450-nm light stimulated phosphorescent emission of $\text{Ru}(\text{bipy})_3^{2+}$ has been found to be efficiently quenched by $\text{Co}(\text{NH}_3)_5\text{Br}^{2+}$,⁶ by $\text{Co}(\text{EDTA})^-$,⁸ and by all the acid EDTA complexes of cobalt(III).⁸ The efficient production of cobalt(III) has been found to occur concomitantly with the quenching of charge transfer triplet state of ruthenium(II).^{6,8} Our studies of the intermediates produced in these reactions are described below.

A. $\text{Ru}(\text{bipy})_3^{2+}$ Sensitized Photolysis. Our studies of the production and stability of $\text{Ru}(\text{bipy})_3^{3+}$ under various conditions are summarized in Table I. Although $\text{Ru}(\text{bipy})_3^{3+}$ is reasonably stable in 1 M H_2SO_4 ($t_{1/2} \sim 30$ min), it does react with EDTA in this medium to give numerous gaseous products (CO_2 and nitrogen oxides detected gas chromatographically). In view of this we have observed the pseudo-first-order rates of decomposition of $\text{Ru}(\text{bipy})_3^{3+}$ under a variety of relevant solvent conditions. Of particular interest was the stability of $\text{Ru}(\text{bipy})_3^{3+}$ in 50% 2-propanol, since the flash photolysis studies described below indicated very efficient scavenging of the primary radicals in this medium. We have found the pseudo-first-order rate of decay of $\text{Ru}(\text{bipy})_3^{3+}$ in 2-propanol to vary a great deal; however, reasonably reproducible pseudo-first-order rate constants could be obtained with the highly purified reagent. Such impurities as copper and acetone shortened the lifetime of $\text{Ru}(\text{bipy})_3^{3+}$ in 2-propanol.

We obtained evidence for some formation of $\text{Ru}(\text{bipy})_3^{3+}$ in all the sensitized redox decompositions of cobalt(III) substrates, even when these were run in 50% 2-propanol. However, the initial yield of $\text{Ru}(\text{bipy})_3^{3+}$ was in each case greatly diminished in 50% 2-propanol.

B. Flash Photolysis Studies of Radical Oxidations of $\text{Ru}(\text{bipy})_3^{2+}$. We have flash photolyzed solutions containing $\text{Ru}(\text{bipy})_3^{2+}$ and various cobalt(III) substrates in 1 M H_2SO_4 , using an unfiltered flash, in order to examine directly the chemical reactions between $\text{Ru}(\text{bipy})_3^{2+}$ and the radicals produced in the photoredox decomposition of various cobalt(III) substrates. In each case there is a very limited range of cobalt(III) and $\text{Ru}(\text{bipy})_3^{2+}$ concentrations over which such reactions may actually be observed. The important considerations in this regard are the following: (1) that radiation from the photolysis flash penetrate significantly throughout the sample cell (i.e., sample solutions must be optically dilute, absorption $< \sim 0.5$, in some spectral region where the cobalt(III) complex has a

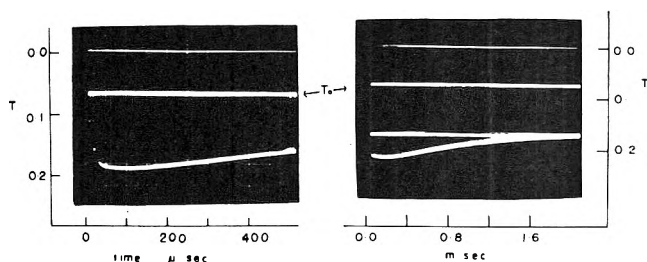


Figure 1. Flash photolysis of $\text{Co}(\text{HEDTA})\text{Cl}^-$ and $\text{Ru}(\text{bipy})_3^{2+}$ in 1 M H_2SO_4 . Transmittance monitored at 480 nm; $[\text{Co}(\text{HEDTA})\text{Cl}^-] = 2.3 \times 10^{-4}$ M, $[\text{Ru}(\text{bipy})_3^{2+}] = 8.2 \times 10^{-6}$ M. Note difference in times scales; trace on right shows all of reaction II and transmittance at "infinite" time. Initial transmittance indicated by T_0 .

charge transfer to metal absorption); (2) $\text{Ru}(\text{bipy})_3^{2+}$ absorbs strongly in the near ($\lambda_{\text{max}} 450$ nm; $\epsilon_{\text{max}} 1.4 \times 10^4$ $\text{M}^{-1} \text{cm}^{-1}$) and deep ultraviolet with a "window" centered around 350 nm through which CTTM bands of cobalt(III) complexes may be irradiated; and (3) the $[\text{Ru}(\text{bipy})_3^{2+}]$ must be large enough that the ruthenium complex can effectively compete with the natural decay modes of the radicals produced. Fortunately the rate constants for radical oxidations of $\text{Ru}(\text{bipy})_3^{2+}$ are large enough (nearly diffusion controlled) that very dilute solutions can be used. In practice most of the solutions flash photolyzed were dilute enough that little photochemistry could have been produced by energy (or electron) transfer as the lifetime of the charge transfer triplet state of $\text{Ru}(\text{bipy})_3^{2+}$ is only about 0.6×10^{-6} sec,^{4,5} and quenching rate constants (inferred from Stern-Volmer plots) vary from 3×10^8 to 4×10^9 $\text{M}^{-1} \text{sec}^{-1}$ for the several substrates included in this report.^{6c,8a} Also note that $[\text{Ru}(\text{bipy})_3^{3+}]_{t=0}$ did not vary significantly for a twofold reduction in $[\text{Co}(\text{HEDTA})\text{Cl}^-]$ (Table II).

An example of our observations, the flash photolysis of $\text{Co}(\text{HEDTA})\text{Cl}^-$ and $\text{Ru}(\text{bipy})_3^{2+}$ in 1 M H_2SO_4 , is shown in Figure 1. For most of our studies with the cobalt(III)-EDTA complexes we observed two distinct reactions following flash irradiation: (1) the very rapid decrease in absorptivity at 450 nm due to formation of $\text{Ru}(\text{bipy})_3^{3+}$ and (2) a much slower partial recovery of the $\text{Ru}(\text{bipy})_3^{2+}$ absorbance. These reactions are conveniently designated I and II, the associated rate constants k_I and k_{II} , respectively. The rate for reaction I increased with $[\text{Ru}(\text{bipy})_3^{2+}]$, but was nearly independent of $[\text{Co}(\text{III})]$. The extent to which II occurred decreased with decreases in $[\text{Ru}(\text{bipy})_3^{2+}]$ or with increases in $[\text{Co}(\text{III})]$. Over the very limited range of $[\text{Ru}(\text{bipy})_3^{2+}]$ where I was observable (note that the flash duration was about 40 μsec in our system), and with a correction for the pseudo-first-order back reaction II, the initial decrease in absorbance of the $\text{Ru}(\text{bipy})_3^{2+}$ following the flash could be accounted for by the extrapolated change in $[\text{Ru}(\text{bipy})_3^{2+}]$ (using a plot of $[\text{Ru}(\text{II})]^{-1}$ vs. t^{-1} to determine $[\text{Ru}(\text{bipy})_3^{2+}]$ at "infinite time" for I) during I (see Table II). In the case of $\text{Co}(\text{HEDTA})\text{Cl}^-$ we have been able to observe part of the initial disappearance of $\text{Ru}(\text{bipy})_3^{2+}$ absorbance, over a narrow range of $[\text{Ru}(\text{bipy})_3^{2+}]$, and find that this process appears to be pseudo first order in $[\text{Ru}(\text{bipy})_3^{2+}]$; our observations lead to an apparent second-order rate constant, $k_I = (6 \pm 1) \times 10^8$ $\text{M}^{-1} \text{sec}^{-1}$. The variations in $[\text{Ru}(\text{bipy})_3^{3+}]$ at $t = 0$ and $[\text{Ru}(\text{bipy})_3^{3+}]_f$ for the case of $\text{Co}(\text{HEDTA})\text{Cl}^-$ in Table II reflect the several competitive reactions in this system and the delicate balance of conditions necessary for detection of reactions I and II.

TABLE I: Products from the Ru(bipy)₃²⁺ Sensitized Redox Decompositions of Various Cobalt(III) Complexes and Kinetics of the Ru(bipy)₃³⁺-2-propanol Reaction^a

Cobalt(III) substrate	[Co(III)] × 10 ³ , M	[Ru(bipy) ₃ ²⁺] × 10 ⁴ , M	Exposure time, min	[2-propanol], % v/v	[Co(II)] ^c × 10 ⁴ , M	[Ru(bipy) ₃ ³⁺] _{t=0} ^c × 10 ⁴ , M	k ^b × 10 ³ , sec ⁻¹
Co(NH ₃) ₅ Br ²⁺	1.0	2.5	2.0	0	2.0 ± 0.3	1.9 ± 0.3	0.4 ± 0.1
	1.0	2.5	2.0	50	3.7 ± 0.3	0.8 ± 0.2	3.0 ± 0.3
Co(EDTA) ⁻	1.0	2.0	2.0	0	1.4 ± 0.1	1.2 ± 0.2	3.4 ± 0.3
	1.0	2.0	2.0	50	2.0 ± 0.2	0.25 ± 0.05	2.5 ± 0.3
Co(HEDTA)Cl ⁻	1.0	2.0	2.0	0	1.8 ± 0.2	1.7 ± 0.2	2.4 ± 0.2
	1.0	2.0	2.0	50	2.7 ± 0.2	0.41 ± 0.06	8 ± 1
Co(HEDTA)Br ⁻	1.0	2.0	1.0	0	1.6 ± 0.2	1.9 ± 0.3	1.0 ± 0.1
	1.0	2.0	1.0	50	2.0 ± 0.2	<0.2	~2
Co(EDTA) ⁻	2.0		0	50		2 ^d	3.2 ± 0.3
Co(HEDTA)Cl ⁻	0.5 ^e		0	50	5 ± 1 ^e	2 ^d	3.6 ± 0.4
None	0		0	50	0	2 ^d	6 ^f
	0		0	50	0	2 ^d	3.5 ± 0.4
	0		0	40	0	2 ^d	3.0
[Cu(II)] ^g	0		0	50	0	2 ^d	6 ^g
[(CH ₃) ₂ CO] ^h	0		0	50	0	2 ^d	13 ^h

^a All reactions in 1 M H₂SO₄; [Ru(bipy)₃³⁺] determined from absorptivity of solutions at 480 nm and total [Ru(bipy)₃ⁿ⁺]. T = 4 ± 2°, except as indicated, for both the irradiation and the determination of absorbance change. Irradiations performed at 45°C. ^b Pseudo-first-order recovery of [Ru(bipy)₃²⁺] absorbance at 480 nm. Mean and mean deviations. ^c Concentrations estimated at the termination of irradiation. ^d Thermally prepared Ru(bipy)₃³⁺. ^e Reactant solution prepared using a solution containing 50% photolyzed Co(HEDTA)Cl⁻. T = 25°. ^f Reactant solution contained 10⁻⁶ M Cu(ClO₄)₂. ^g Reactant solution contained 1% acetone.

TABLE II: Reactions of Trisbipyridylruthenium Complexes with Radicals Produced in the Photoredox Decomposition of Cobalt(III) Substrates^a

Cobalt complex	[Co(III)] × 10 ⁴ , M	[Ru(bipy) ₃ ²⁺] × 10 ⁵ , M	[2-propanol], % v/v	k ₁₁ × 10 ³ , sec ⁻¹	[Ru(bipy) ₃ ³⁺] _{t=0} ^b × 10 ⁶ , M	[Ru(bipy) ₃ ³⁺] _t ^c × 10 ⁶ , M
Co(NH ₃) ₅ Br ²⁺	6.0	0.8	0	d		5.6 ± 0.5
	6.0	0.8	50	d		<0.2
Co(EDTA) ⁻	2.0	1.0	0	2.0 ± 0.3	12 ± 2	2.8 ± 0.3
	2.0	1.0	50	d		<0.2
Co(HEDTA)Cl ⁻	2.3	0.8	0	1.6 ± 0.2	6.0 ± 1 ^e	2.9 ± 0.3
	2.3	1.2	0	f	3.9 ± 0.5	2.1 ± 0.3
	1.25	0.89	0	1.3	6.4 ± 1	1.3 ± 0.2
	2.3	1.2	50	d		~0.2
Co(HEDTA)Br ⁻	1.0	1.4	0	1.0 ± 0.2	7 ± 1	3.9 ± 0.4
	1.0	1.0	50	d		<0.2
Co(HEDTA)NO ₂ ⁻	2.0	0.9	0	3.7 ± 0.5	9 ± 2	6 ± 1 ^g
	2.0	0.9	50	d		<0.3

^a All solutions 1 M in H₂SO₄; unfiltered 250-J flash; 25°. Absorbance changes monitored at 480 nm. ^b Determined from extrapolation of reaction II to t = 0. ^c Determined from "final" solution absorbance at 480 nm a few minutes after the flash. ^d No back reaction observed. ^e In this and similar experiments experiment observation of reaction I allowed us to estimate that (5 ± 1) × 10⁶ M Ru(bipy)₃³⁺ was formed in reaction I. ^f Not determined. ^g In the case of the nitro complex a slower reaction (lifetime of the order of seconds) eventually consumed all the Ru(bipy)₃³⁺.

For the case of Co(NH₃)₅Br²⁺ we have described the Br₂⁻ oxidation of Ru(bipy)₃²⁺ in detail elsewhere¹¹ and no back reaction was observed on the flash photolysis time scale. In the case of Co(HEDTA)NO₂⁻ two back reactions were observed to regenerate the Ru(bipy)₃²⁺ absorptivity at 480 nm; the first was relatively rapid and we have associated it with II, the second was much slower and eventually resulted in complete recovery of the ruthenium(II) absorbance. This second reaction probably accounts for the failure to observe the formation of Ru(bipy)₃³⁺ in the sensitized photolysis of Co(HEDTA)NO₂⁻ and is most likely due to the NO₂⁻ reduction of Ru(bipy)₃³⁺.

Finally, we have found that in flash photolysis of solutions containing cobalt(III) complexes and Ru(bipy)₃²⁺ in 1 M H₂SO₄ and 50% 2-propanol, the radical oxidations of Ru(bipy)₃²⁺ are suppressed in each case (Figure 2, Table II).

It is to be noted that the changes in Ru(bipy)₃²⁺ absorptivity described in this report are from 10–100 times as great as the "transient bleaching" effects we noted previously¹² for this substrate in the absence of cobalt(III) complexes.

C. *Some Observations on the Reactions of Primary Radicals from the Photoredox Decomposition of Cobalt(III) Substrates.* We have used 2-propanol and bromide as scavengers for the radicals produced from the photoredox decomposition of several cobalt(III) substrates. We have found that 50% 2-propanol does not compete effectively with 10⁻² M Br⁻ for the Br⁻ radical, whereas the radicals produced in the photoredox decomposition of all the EDTA complexes are scavenged more efficiently by 50% 2-propanol than by 10⁻² M Br⁻ (Table III). The product yields (i.e., φ(Co²⁺)) are not very sensitive to the [2-propanol] for the EDTA complexes, but φ(Co²⁺) ap-

TABLE III: Products of Primary Radical Reactions with Bromide and with 2-Propanol^a

Complex irradiated	[2-propanol], % v/v	$\phi(\text{Co}^{2+})^b$	$\phi(\text{CO}_2)^c / \phi(\text{Co}^{2+})$	Br_2^- ^d absorbance at $t = 0$	
$\text{Co}(\text{NH}_3)_5\text{Br}^{2+}$	0	0.30 ± 0.03		0.40 ± 0.06	
	25			0.40 ± 0.06	
	50			0.38 ± 0.06	
$\text{Co}(\text{EDTA})^-$	0	0.05 ± 0.01		0.25 ± 0.02	
	6			0.14 ± 0.02	
	10			0.12 ± 0.01	
	50			0.00	
$\text{Co}(\text{HEDTA})\text{Cl}^-$	0	0.18 ± 0.02	1.0 ± 0.1 0.71 ± 0.03^e	0.21 ± 0.02	
	0			0.15 ± 0.02	
	10		0.12 ± 0.01		
	20		0.12 ± 0.01		
	50		0.19 ± 0.02	0.55 ± 0.06	0.00
	50		0.19 ± 0.02	0.33 ± 0.06^e	
$\text{Co}(\text{HEDTA})\text{Br}^-$	0	0.14 ± 0.02	0.72 ± 0.06 1.0 ± 0.2^e	0.41 ± 0.06	
	0			0.30 ± 0.04	
	10			0.27 ± 0.04	
	20			0.27 ± 0.04	
	50			0.00	

^a All solutions at 25°. 0.1 M HClO_4 , (and no Br^-) except as indicated. ^b For irradiation at 254 nm. ^c Gas analyses discussed in detail in ref 8. ^d Br_2^- transient monitored at 360 nm. All solutions for flash photolysis were 0.01 M in Br^- . Unfiltered 250-J flash of 20- μsec lifetime. ^e For $\text{Ru}(\text{bipy})_3^{2+}$ sensitization; $\text{Ru}(\text{bipy})_3^{2+}$ irradiated at 450 nm ($I_a = 1.4 \times 10^{-4}$ einstein $\text{l}^{-1} \text{min}^{-1}$); 0.1 M H_2SO_4 .

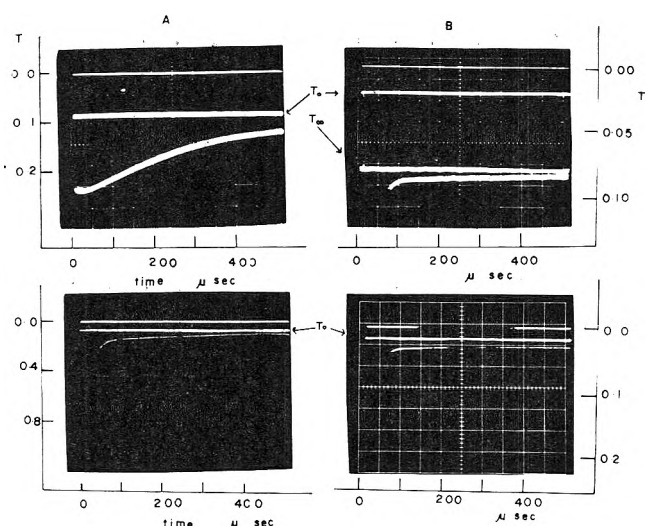
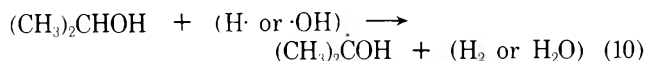
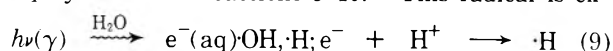


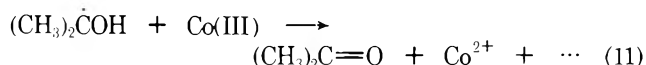
Figure 2. Flash photolysis of solutions of cobalt(III) complexes, $\text{Ru}(\text{bipy})_3^{2+}$, and 1 M H_2SO_4 without 2-propanol (top) and with 50% 2-propanol (bottom). For series A, $[\text{Co}(\text{HEDTA})\text{Cl}^-] = 1.2 \times 10^{-4}$ M and $[\text{Ru}(\text{bipy})_3^{2+}] = 8.9 \times 10^{-5}$ M; for series B, $[\text{Co}(\text{NH}_3)_5\text{Br}^{2+}] = 6 \times 10^{-4}$ M and $[\text{Ru}(\text{bipy})_3^{2+}] = 1.8 \times 10^{-5}$ M. Transmittance monitored at 480 nm; T_0 = transmittance before flash; T = transmittance several minutes after flash.

proximately doubles in 50% 2-propanol in the case of $\text{Co}(\text{NH}_3)_5\text{Br}^{2+}$. A few CO_2 yields are noted in Table III; most of our studies of the CO_2 yields are being presented elsewhere.⁸ It should be observed that for all the cobalt(III)-EDTA complexes photoredox decomposition leads to nearly equal yields of Co^{2+} and CO_2 regardless of whether the excitation is by direct absorption of radiation or by $\text{Ru}(\text{bipy})_3^{2+}$ sensitization.⁸

D. Reactions of $(\text{CH}_3)_2\dot{\text{C}}\text{OH}$ with $\text{Co}(\text{NH}_3)_5\text{Br}^{2+}$ and $\text{Co}(\text{EDTA})^-$. The 2-hydroxy-2-propyl radical was generated in the γ -radiolysis of 50% 2-propanol solutions 0.1 M in HClO_4 by means of reactions 9-10.¹³ This radical is ex-



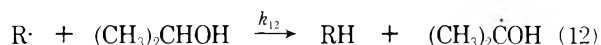
pected to react efficiently with most cobalt(III) substrates (11).^{14,15} Since $\phi(\text{Co}^{2+})$ proved to be nearly independent



of [2-propanol] for the EDTA complexes, it was necessary to demonstrate that reactions of the type of (11) do indeed occur for these complexes. To this end we have irradiated 10^{-3} M solutions of $\text{Co}(\text{NH}_3)_5\text{Br}^{2+}$ or $\text{Co}(\text{EDTA})^-$. After 40-min irradiation we found these solutions to be $(1.3 \pm 0.1) \times 10^{-4}$ and $(0.95 \pm 0.1) \times 10^{-4}$ M, respectively, in Co^{2+} , demonstrating the similar stoichiometric efficiency of (11) for both substrates.

Discussion

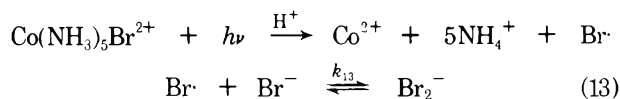
The observation that the cobalt(II) yield in the $\text{Ru}(\text{bipy})_3^{2+}$ sensitized redox decompositions of cobalt(III) complexes is always higher in 50% 2-propanol (1 M H_2SO_4) than in the absence of 2-propanol (Table I) is compelling evidence that radicals are produced in these reactions. Thus we would propose that reactions 1-6 are followed by (12), then (11) as has been observed in a number of other



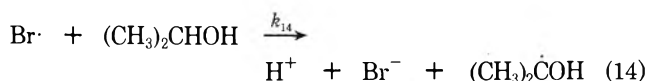
systems.^{9,14,15} It will be seen below that this proposed mechanism for the sensitized reaction is strongly supported by our observations; however, the complexity and intricacy of the various radical reactions in these systems require a very careful and detailed discussion.

A. The Nature and Reactivity of the Primary Radicals from Photoredox Reactions. The photoredox reactions which are stimulated by direct excitation of charge transfer to metal transitions in cobalt(III) complexes produce cobalt(II) and some radical derived from oxidation of a ligand of the substrate.¹⁶ The formation of $\text{Br}\cdot$ from the photoreduction of $\text{Co}(\text{NH}_3)_5\text{Br}^{2+}$ is readily inferred from

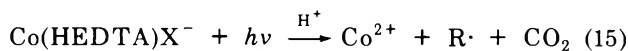
the observation of Br_2^- in dilute bromide solutions^{17,18}



In the present study we have demonstrated that although the $\text{Br}\cdot$ radical reacts with 2-propanol (Figure 2) the Br_2^- radical does not (Table III), and that $k_{13} \geq 10^3 k_{12}$ (note that $k_{13} \sim 10^{10} \text{ M}^{-1} \text{ sec}^{-1}$).¹⁷ It is also evident (from Figure 2 and ref 11) that both $\text{Br}\cdot$ and Br_2^- oxidize $\text{Ru}(\text{bipy})_3^{2+}$ very rapidly, the latter reaction has been shown to have a specific rate constant of $3 \times 10^9 \text{ M}^{-1} \text{ sec}^{-1}$ in 1 *M* H_2SO_4 .¹¹ The flash photolysis studies show that the $\text{Br}\cdot$ oxidation of $\text{Ru}(\text{bipy})_3^{2+}$ is repressed in 2-propanol.



The situation with regard to the EDTA complexes is not so straightforward. By analogy with the case of $\text{Co}(\text{NH}_3)_5\text{O}_2\text{CCH}_3^{2+}$,^{9b} and from points developed below we may write the primary photochemical reaction as in (15)¹⁹



where $\text{R}\cdot$ may be thought of as the *N*-methyleneethylenediaminetriacetate radical (or a protonated form of that radical). Since $\text{R}\cdot$ oxidizes Br^- (Table III) to $\text{Br}\cdot$ (detected as Br_2^-), and since the standard reduction potential of the $\text{Br}\cdot|\text{Br}^-$ couple is about 1.9 V,^{18,20} the radical $\text{R}\cdot$ is a very powerful oxidant; for comparison note that the potential of the $\text{Ru}(\text{bipy})_3^{3+}|\text{Ru}(\text{bipy})_3^{2+}$ couple is only 1.26 V.²¹ In view of the energetics of the reaction, and in comparison to the rate of the Br_2^- oxidation of $\text{Ru}(\text{bipy})_3^{2+}$,¹¹ the $\text{R}\cdot$ oxidation of $\text{Ru}(\text{bipy})_3^{2+}$ seems a bit slow (we estimate $k_{16} = k_1 \approx 6 \times 10^8 \text{ M}^{-1} \text{ sec}^{-1}$). By using the facile oxidation of $\text{Ru}(\text{bipy})_3^{2+}$ (16) as a means of detecting $\text{R}\cdot$, we have demonstrated that this radical is efficiently scavenged by 2-propanol; on the basis of ruthenium(III) yields with and without 2-propanol, we would estimate $10^6 k_{12} \geq k_{16}$. In connection with the 2-propanol scavenging of $\text{R}\cdot$,

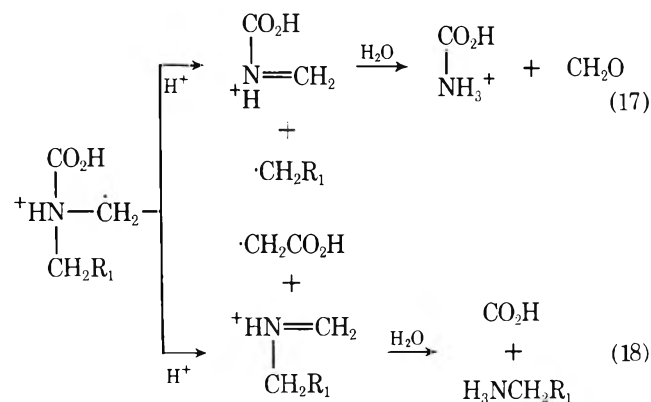


it is important to observe that the ratio of $\phi(\text{CO}_2)/\phi(\text{Co}^{2+})$ is reduced approximately twofold in 50% 2-propanol. Since the $(\text{CH}_3)_2\dot{\text{C}}\text{OH}$ radical efficiently reduces cobalt(III) substrates^{14,15} (see also Results section D above and the discussion below) this argues that decarboxylation has occurred by the time the photoredox fragments achieve independent solvent environments (certainly in a very, very short time after the primary step since the carboxylate radical is not scavenged and reactions of $\text{R}\cdot$ are observed after $\sim 40 \mu\text{sec}$) as indicated in (15). The contrasting insensitivity of $\phi(\text{Co}^{2+})$ to [2-propanol] suggests that $\text{R}\cdot$ (or some species derived from $\text{R}\cdot$) reacts with the $\text{Co}(\text{HEDTA})\text{X}^-$ substrate to produce Co^{2+} so that (12) may be equivalent to changing one reducing radical for another.

B. Possible Secondary Radicals and Radical Reduction of Substrates for Species Obtained from Photooxidation of EDTA. Our principal concern in this report has been to establish the nature of the primary photochemical process. The generation of similar radicals in the $\text{Ru}(\text{bipy})_3^{2+}$ sensitized decomposition of $\text{Co}(\text{NH}_3)_5\text{Br}^{2+}$, $\text{Co}(\text{EDTA})^-$,

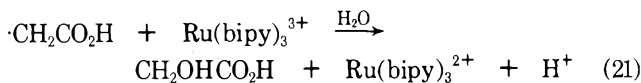
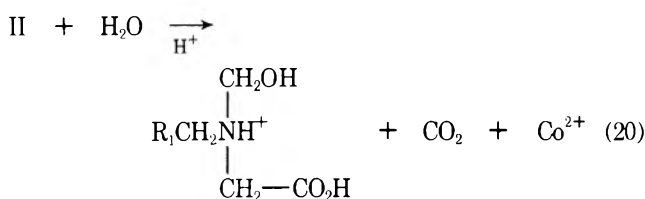
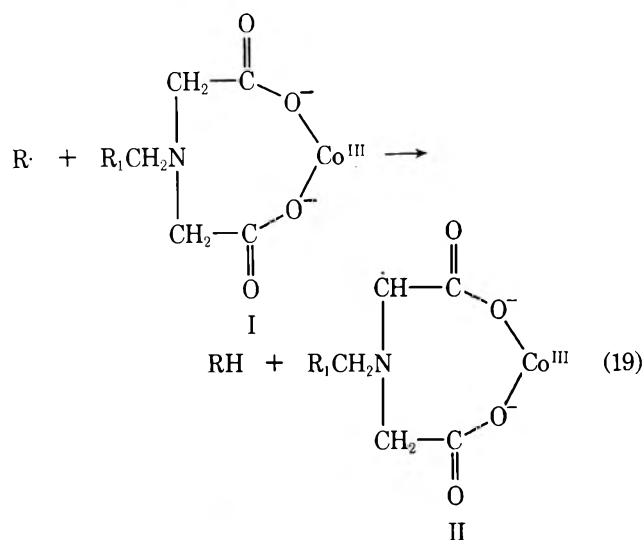
and $\text{Co}(\text{HEDTA})\text{X}^-$ ($\text{X} = \text{Cl}, \text{Br}, \text{NO}_2$) and the directly stimulated photoredox decompositions of these complexes serves to distinguish the two proposed mechanisms. The EDTA systems are complicated by the instability of the primary radical, apparently *N*-methyleneethylenediaminetriacetate, and the different reactivities of the species resulting from the decomposition of this radical. In the present section we wish to point out how some of the likely successors to this primary radical may ultimately affect product yields.

In our flash photolysis studies of the EDTA complexes, we have observed, I, a strongly oxidizing species (denoted as $\text{R}\cdot$ above), which oxidizes $\text{Ru}(\text{bipy})_3^{2+}$ in competition with a reaction (or reactions) generating a species which, in stage II, reduces $\text{Ru}(\text{bipy})_3^{3+}$ + 22,23 (Figures 1 and 2, Table II). If left to its own devices, one would expect the *N*-methyleneethylenediaminetriacetate radical, $\text{R}_1\text{CH}_2\text{-N}(\text{CH}_2)\text{CH}_2\text{CO}_2\text{H}$, to fragment²⁴ as in (17) or (18).²⁵ We have little basis for the choice between these paths.²⁶ Each of the radicals $\text{R}_1\text{CH}_2\text{N}(\text{CH}_2)\text{CO}_2\text{H}$, $\cdot\text{CH}_2\text{R}_1$, and



$\cdot\text{CH}_2\text{CO}_2\text{H}$ should be reasonably oxidizing²⁶ and could in principle be identified with $\text{R}\cdot$, above; on the other hand, oxidation of each of these radicals would result in an alcohol, so each could also in principle act as a reductant.²⁶ Owing the apparent relative "stability" of $\cdot\text{CH}_2\text{CO}_2\text{H}$,²⁶ (18) seems the most likely fragmentation mode. In principle a fragmentation sequence such as (18) could transform an "oxidizing" radical, $\text{R}_1\text{CH}_2\text{N}(\text{CH}_2)\text{CO}_2\text{H}$, into a relatively good "reducing" radical, $\cdot\text{CH}_2\text{CO}_2\text{H}$.²⁶

Although we were not able to vary concentrations over as great a range as we had hoped, we did observe that a twofold decrease in $[\text{Co}(\text{HEDTA})\text{Cl}^-]$, with $[\text{Ru}(\text{bipy})_3^{2+}]$ nearly constant, did result in about a twofold decrease in the extent of II (Table II). This and the inference (from data in Tables I and III) that radical reattack on the cobalt(III)-EDTA substrate produces approximately stoichiometric amounts of Co^{2+} and CO_2 is consistent with the reaction sequence 16, 18, and 19-21, for $\text{R}\cdot = \text{R}_1\text{CH}_2\text{N}(\text{CH}_2)\text{CH}_2\text{CO}_2\text{H}$ and where I is an EDTA complex of cobalt(III). In experiments in which $[\text{Co}(\text{HEDTA})\text{Cl}^-]$ was varied twofold (Table III) the yield of $\text{R}\cdot$ may be presumed to have been varied by twofold (the 1-cm absorbance due to cobalt(III) in the 350-nm "window" of $\text{Ru}(\text{bipy})_3^{2+}$ was < 0.5), and the approximate constancy of the yield of $\text{Ru}(\text{bipy})_3^{3+}$ may be attributed to the change in competition between (16) and (19); the smaller observed extent of stage II at the lower $[\text{Co}(\text{HEDTA})\text{Cl}^-]$ may be presumed to arise from the lower initial $[\text{R}\cdot]$ and the competition between (18) and (16) and (19).



For the more concentrated solutions used in the sensitization studies, (16) and (19) are expected to predominate over (18).

The above scheme provides a plausible and self-consistent account of the observed secondary radical reactions. These secondary reactions are not a primary concern of this report, and the assessment of merits of the scheme proposed here over any plausible alternatives must await additional information.

In discussing the possible secondary reaction scheme we have postulated that CO_2 is evolved in reaction 20. The evolution of CO_2 in some secondary radical reaction with the cobalt substrate is required by a careful consideration of data in Table I. As noted in section C below these data argue for the production of radicals and the mechanisms outlined in (1)–(6) for the $\text{Ru}(\text{bipy})_3^{2+}$ sensitized redox decomposition of these cobalt(III) substrates. Furthermore, the radicals, $\text{R}\cdot$, produced under these conditions from the EDTA complexes may be identified with the radicals which result from direct irradiation of these cobalt substrates. An appreciable percentage of these radicals have been shown in our flash photolysis studies to be scavenged efficiently by $[\text{Ru}(\text{bipy})_3^{2+}] \approx 10^{-5} \text{ M}$ (Table II), so all the radicals $\text{R}\cdot$ should be scavenged by $\text{Ru}(\text{bipy})_3^{2+}$ under the sensitization conditions; this is confirmed by the equality²⁷ of $[\text{Co}(\text{II})]$ and $[\text{Ru}(\text{bipy})_3^{3+}]_{t=0}$ in Table I, in the absence of 2-propanol. Thus under these conditions, with (18) and/or (20) suppressed (the ratio of [ruthenium(II)] to [cobalt(III)] is in every case greater for the sensitization than for the flash photolysis reactions), the yields of Co^{2+} and CO_2 stand in about a 1:1 ratio, as previously proposed for the primary photochemical step in (15). Furthermore, in 50% 2-propanol, where reactions 12 and 11 should dominate, the yields of Co^{2+} and CO_2

stand in approximately a 2:1 ratio, consistent with (11), (12), and (15). Similarly, for direct excitation of $\text{Co}(\text{HEDTA})\text{Cl}^-$ in 50% 2-propanol the Co^{2+} and CO_2 yields were found to stand approximately in a 2:1 ratio, contrasting to a 1:1 ratio in the absence of 2-propanol; however, $\phi(\text{Co}^{2+})$ was found to be insensitive to [2-propanol]. These observations are readily reconciled with (15) as the primary photochemical step in each case followed by (12) and (11) in 2-propanol, by (16) when $\text{Ru}(\text{bipy})_3^{2+}$ is present, or by (18) and (19) when efficient radical scavengers are absent.

It should be observed that all continuous photolyses were performed to limited extents of reaction to minimize contributions from reactions such as (22). When $[\text{Ru}(\text{bipy})_3^{2+}] \geq [\text{Ru}(\text{bipy})_3^{3+}]$ this reaction could become important since $K_{22} \sim 7 \times 10^{12}$.^{18,20,21}

C. Mechanism of the $\text{Ru}(\text{bipy})_3^{2+}$ Sensitized Redox Reactions. We have demonstrated the following points in the present study.

(1) The radicals produced by photoreduction of $\text{Co}(\text{NH}_3)_5\text{Br}^{2+}$, $\text{Co}(\text{EDTA})^-$, and $\text{Co}(\text{HEDTA})\text{X}^-$ oxidize $\text{Ru}(\text{bipy})_3^{2+}$ at nearly diffusion-controlled rates.

(2) The $\text{Ru}(\text{bipy})_3^{2+}$ sensitized redox decomposition of the EDTA complexes in 1 M H_2SO_4 produces Co^{2+} , $\text{Ru}(\text{bipy})_3^{3+}$, and CO_2 in nearly stoichiometric amounts; for the $\text{Co}(\text{NH}_3)_5\text{Er}^{2+}$ substrate, Co^{2+} and $\text{Ru}(\text{bipy})_3^{3+}$ are produced in stoichiometric amounts.

(3) The $\text{Ru}(\text{bipy})_3^{2+}$ sensitized redox decompositions of each of these cobalt(III) substrates in 50% 2-propanol results in an increase (approaching twofold in $[\text{Co}^{2+}]$) and a large decrease in $[\text{Ru}(\text{bipy})_3^{3+}]$ compared to reactions described in 2 above.

The postulated excited state electron transfer mechanism⁶ (8) cannot account for either 2 or 3. On the other hand, we infer that in each case the sensitized reaction generates the same primary radical species found to result from the redox decompositions stimulated by direct absorption of radiation. Reactions 1–7 are consistent with all the points raised above.

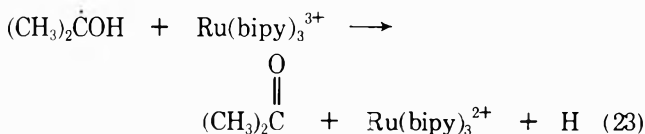
The complexity of the EDTA systems prevents us from altogether ruling out some contribution from an excited state electron transfer reaction. However, careful consideration of the data in Table I indicates that the triplet-to-triplet energy transfer mechanism 1–7 could in principle account for all the observed sensitization reactions as is indicated by the following considerations.

(1) $[\text{Ru}(\text{bipy})_3^{2+}]$ was at least 20 times greater in the sensitization studies than in the flash photolysis studies; thus the competition between (12) and (16) is expected to be an order of magnitude less favorable in the former case; *i.e.*, all the $\text{Ru}(\text{bipy})_3^{3+}$ we have observed could come from (16) if $10^6 k_{12} \geq k_{16} \geq 5 \times 10^4 k_{12}$.

(2) If in the case of $\text{Co}(\text{NH}_3)_5\text{Br}^{2+}$ we take 2.0×10^{-4} as the primary yield of Co^{2+} under the photolysis conditions given in Table I, then the yields of primary radicals in our analysis should be equal to the increase in the Co^{2+} yields in 2-propanol plus the yield of $\text{Ru}(\text{bipy})_3^{3+}$ at $t = 0$, also in 2-propanol; the latter sum is $2.5 \times 10^{-4} \text{ M}$ of radicals, certainly not different from $2.0 \times 10^{-4} \text{ M}$ within the error limits of these determinations.

(3) An analysis, similar to that in 2 above, for the EDTA complexes shows a defect in apparent radical concentration of about $6 \times 10^{-5} \text{ M}$. This is outside our esti-

mated error limits, but could be easily accounted for by an effective competition of $\text{Ru}(\text{bipy})_3^{2+}$ with 2-propanol for $R\cdot$, (12) vs. (16), under sensitization conditions and an effective competition between (23) and (11); this requires $k_{23} > k_{11}$.

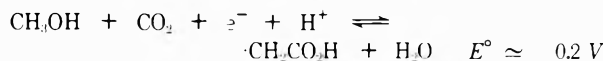
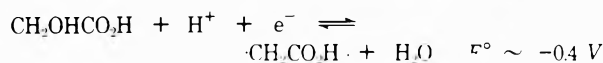
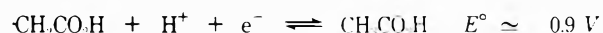
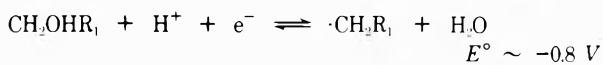
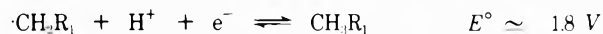
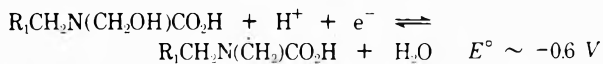
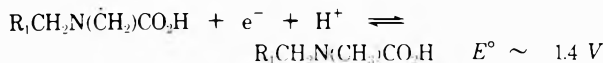


For the $\text{Ru}(\text{bipy})_2^{2+}$ sensitized redox decompositions of $\text{Co}(\text{NH}_3)_5\text{Br}^{2+}$, $\text{Co}(\text{EDTA})^-$, and $\text{Co}(\text{HEDTA})\text{X}^-$ ($\text{X} = \text{Cl}, \text{Br}, \text{NO}_2$) we conclude that there is definitive evidence that radicals are formed in the primary step and therefore that the reaction proceeds in these systems predominately by means of the triplet-to-triplet energy transfer mechanism 1-7 as originally proposed.^{2,3} Furthermore there is no experimental evidence demonstrating any contribution from an electron transfer mechanism, such as (8) in these systems. On the other hand, we see no reason why the demonstration of this reaction mode should not eventually be possible for some systems.

Finally we should like to note that there has been some discussion of the minimum sensitizer energy required to stimulate redox decomposition of cobalt(III)^{6,8,16,28,29} substrates. A more careful discussion of this question will be presented elsewhere,³⁰ but for the present we would like to note that the minimum free energy required, that for redox dissociation of the ground state, is readily calculated from standard reduction potentials of the cobalt(III)|cobalt(II) and the appropriate radical couples.^{18,20,23} Enthalpy changes are expected to dominate^{20,23,31} both couples, so these free energy changes can be taken as a crude first approximation to the required minimum excitation energy. For example, we would estimate this minimum sensitizer energy as about $21 \times 10^4 \text{ cm}^{-1}$ for $\text{Co}(\text{NH}_3)_6^{3+}$ and about $12 \times 10^4 \text{ cm}^{-1}$ for $\text{Co}(\text{NH}_3)_5\text{Br}^{2+}$;^{32,33} thus it is not surprising that $\text{Ru}(\text{bipy})_3^{2+}$ ($17.3 \times 10^4 \text{ cm}^{-1}$ emission) is an effective triplet sensitizer for $\text{Co}(\text{NH}_3)_5\text{Br}^{2+}$ but not for $\text{Co}(\text{NH}_3)_6^{3+}$.

References and Notes

- (1) Partial support of this research by the National Science Foundation (Grant No. GP 15070) is gratefully acknowledged.
- (2) P. Natarajan and J. F. Endicott, *J. Amer. Chem. Soc.*, **94**, 3635 (1972).
- (3) J. N. Demas and A. W. Adamson, *J. Amer. Chem. Soc.*, **93**, 1800 (1971).
- (4) J. N. Demas and G. A. Crosby, *J. Mol. Spectrosc.*, **26**, 72 (1968).
- (5) F. E. Lytle and D. M. Hercules, *J. Amer. Chem. Soc.*, **91**, 253 (1969).
- (6) (a) A. W. Adamson, "Proceedings XIV International Conference on Coordination Chemistry," Toronto, June, 1972, p 240; (b) Abstracts of the 164th National Meeting of the American Chemical Society, New York, N. Y., Aug 1972, INORG 2; (c) H. D. Gafney and A. W. Adamson, *J. Amer. Chem. Soc.*, **94**, 8238 (1972).
- (7) Although Gafney and Adamson stated in ref 6c that they could not rule out the possibility of radical oxidation of $\text{Ru}(\text{bipy})_3^{2+}$, the prevailing attitude in that report does not seem to reflect this reservation.
- (8) (a) P. Natarajan and J. F. Endicott, *J. Amer. Chem. Soc.*, **95**, 2470 (1973); (b) *J. Phys. Chem.*, submitted for publication.
- (9) (a) G. Caspari, R. G. Hughes, J. F. Endicott, and M. Z. Hoffman, *J. Amer. Chem. Soc.*, **92**, 6801 (1970); (b) E. R. Kantrowitz, J. F. Endicott, and M. Z. Hoffman, *J. Phys. Chem.*, **75**, 1914 (1971); (c) T. L. Kelly and J. F. Endicott, *J. Amer. Chem. Soc.*, **94**, 1797 (1972).
- (10) We wish to thank Professor L. Kevan for the use of this facility.
- (11) P. Natarajan and J. F. Endicott, *J. Phys. Chem.*, **77**, 971 (1973).
- (12) P. Natarajan and J. F. Endicott, *J. Amer. Chem. Soc.*, **94**, 5909 (1972).
- (13) J. K. Thomas, *Advan. Radiat. Chem.*, **1**, 103 (1969).
- (14) (a) E. R. Kantrowitz, M. Z. Hoffman, and K. M. Schilling, *J. Phys. Chem.*, **76**, 2492 (1972); (b) A. F. Jaudo, E. R. Kantrowitz, M. Z. Hoffman, E. Papacoustantinou, and J. F. Endicott, *J. Amer. Chem. Soc.*, **94**, 6655 (1972).
- (15) (a) H. Cohen and D. Meyerstein, *J. Amer. Chem. Soc.*, **94**, 6944 (1972); (b) M. Z. Hoffman and M. Simic, *ibid.*, **94**, 1757 (1972).
- (16) For example, see V. Balzani and V. Carassiti, "Photochemistry of Coordination Compounds," Academic Press, New York, N. Y., 1970, Chapter 11.
- (17) L. I. Grossweiner and M. Matheson, *J. Phys. Chem.*, **61**, 1089 (1957).
- (18) S. D. Malone and J. F. Endicott, *J. Phys. Chem.*, **76**, 2223 (1972).
- (19) Evidence is analyzed in detail elsewhere^{8a} that the radicals produced in these systems do not derive from oxidation of the ligands X^- .
- (20) W. H. Woodruff and D. W. Margerum, *Inorg. Chem.*, **12**, 962 (1973).
- (21) D. B. Buckingham and A. M. Sargeson, "Chelating Agents and Metal Chelates," F. P. Dwyer and D. P. Mellor, Ed., Academic Press, New York, N. Y., 1964, Chapter 6.
- (22) It is to be observed that radicals which undergo spontaneous redox disproportionations can function as either an oxidant or reductant. This behavior, for example, is characteristic of $\text{Br}_2^{18,20}$ and $(\text{CH}_3)_2\dot{\text{C}}\text{OH}$ as well as such better known species as H_2O_2 .²³ The reaction which predominates for such species depends on energetic and kinetic considerations and on substrate concentrations. In our flash photolysis studies $[\text{Ru}(\text{bipy})_3^{2+}]_{t=0} \gg [\text{Ru}(\text{bipy})_3^{3+}]_{t=0}$.
- (23) W. Latimer, "Oxidation Potentials," Prentice Hall, Englewood Cliffs, N. J., 1952.
- (24) For example, compare the behavior proposed for $(\text{H}_2\text{NCH}_2\text{CH}_2\text{NH}_2)^+$ by D. Klein and C. W. Moeller, *Inorg. Chem.*, **4**, 394 (1965).
- (25) Langford and coworkers have claimed that CH_2O is obtained from photoredox decomposition of $\text{Co}(\text{EDTA})^-$ with $\phi(\text{CH}_2\text{O}) \approx 0.5\phi(\text{Co}^{2+})$. (C. H. Langford, private communication to J. F. Endicott.)
- (26) We can, however, make crude estimates of standard reduction potentials for the radical couples from tabulated bond energies and other thermodynamic quantities.²²



On the basis of these estimates (18) is far the most likely fragmentation mode and $\text{R}_1\text{CH}_2\text{N}(\text{CH}_2)\text{CO}_2\text{H}$ and $\text{CCH}_2\text{CO}_2\text{H}$ have properties consistent with those of $R\cdot$ and its "reducing" successor. Although values of potentials as estimated here are no more reliable than $\pm 0.2 \text{ V}$, they do help focus our discussion and draw attention to the fact that radicals which disproportionate are not properly characterized as "oxidizing" or "reducing." Note that our observation that $R\cdot$ oxidizes Br^- suggests that $\text{R}\cdot\text{CH}_2\text{N}(\text{H})(\text{CH}_2)\text{CO}_2\text{H}$, or a coordinated analog, is about 0.6 V better oxidant than the unprotonated species discussed above.

- (27) Gafney and Adamson^{6c} recently reported a 40% excess of Co^{2+} over $\text{Ru}(\text{bipy})_3^{3+}$ in the $\text{Ru}(\text{bipy})_3^{2+}$ sensitized redox decomposition of $\text{Co}(\text{NH}_3)_5\text{Br}^{2+}$. Although we have no way of accounting for this stoichiometric defect, since experimental details were not reported, it is not unusual to find such defects in the stoichiometry of radical reactions run under conditions of very high local concentrations of radicals or when scavenging impurities are present. For example, we have observed similar stoichiometric defects in the $\text{Ru}(\text{bipy})_3^{2+}$ sensitized decomposition of $\text{Co}(\text{HEDTA})\text{Cl}$ at very high concentrations of sensitizer. When proper care is taken to exclude stray radical scavengers and when proper account is taken of dark reactions which result in reduction of $\text{Ru}(\text{bipy})_3^{3+}$, good stoichiometric ratios can be obtained as in Table I.

(28) M. A. Scandola and F. Scandola, *J. Amer. Chem. Soc.*, **92**, 5943 (1970).

(29) H. D. Gafney and A. W. Adamson, *J. Phys. Chem.*, **76**, 1105 (1972).

(30) J. F. Endicott, manuscript in preparation.

- (31) J. J. Christensen and R. M. Izatt, "Handbook of Metal Ligand Heats," Marcel Dekker, New York, N. Y., 1970.
- (32) In these estimates we have assumed $\cdot\text{NH}_2$ to be about as good an oxidant as $\text{Cl}^{\cdot 9a}$ and that the potentials of cobalt(III)|cobalt(II)

- couples change about as observed previously³³ when coordinated NH_3 is replaced by Br^- .
- (33) D. P. Rillema, J. E. Endicott, and E. Papaconstantinou, *Inorg. Chem.*, **10**, 1739 (1971).

Fluorescence of Cycloalkanones

M. O'Sullivan and A. C. Testa*

The Department of Chemistry, St. John's University, Jamaica, New York 11439 (Received February 26, 1973)

The fluorescence of a series of cycloalkanones has been studied at room temperature. Results indicate that the contour of the emission spectrum remains the same and exhibits a wavelength maximum at ~ 405 nm, and that the α -CH stretching mode appears to be a factor in radiationless deactivation from the excited singlet state. The fluorescence yield of cyclopentanone and cyclohexanone is an order of magnitude greater than the value for cyclobutanone, increases with α substitution, and is not affected by β substitution. The fluorescence yield of cyclopentanone, 2-methylcyclopentanone, 2,5-dimethylcyclopentanone, and 2,2,4,4-tetramethylcyclopentanone increase in the ratio 1.0:1.6:3.4:3.6. Polar and hydrogen bonding solvents as well as methyl substitution affect the vibration structure in the ${}^1n,\pi^*$ absorption band of cyclopentanone, which is probably due to reduced interaction between the carbonyl group and the α -CH₂ group.

Introduction

Although the photochemistry of cycloalkanones has been widely studied,^{1,2} relatively little information is available regarding the fluorescence of these molecules. La Paglia and Roquette³ reported that the fluorescence of cyclopentanone is unstructured with a peak at ~ 405 nm; however, there has been no attempt to correlate the fluorescence yield of these molecules with ring size and substitution. Recently, Closs and Doubleday⁴ concluded that the type I cleavage in cycloalkanones becomes less pronounced with increasing ring size of the ketone. Lee, *et al.*,^{5,6} have reported that the fluorescence yield for cyclobutanone, CB, cyclopentanone, CP, and cyclohexanone, CH, is approximately 0.002 in the gas phase, while in cyclohexane the fluorescence yield, using 313-nm excitation, for CP ($6 \pm 2 \times 10^{-4}$) and CH ($9 \pm 2 \times 10^{-4}$) is significantly larger than for CB ($1.0 \pm 0.3 \times 10^{-4}$). The lifetime of the lowest excited singlet state in CB was estimated to be $\sim 10^{-10}$ sec. It has been observed that the unimolecular photodecomposition of cyclobutanone is not quenched by high concentrations of 1,3-pentadiene.² Lee and Metcalfe⁷ have shown that in *n*-propylcyclobutanone the internal conversion, $S_1 \rightsquigarrow S_0$, involves biradical intermediates as the main path of deactivation and that the triplet yield is < 0.05 . Chandler and Goodman⁸ have investigated the ${}^1n,\pi^*$ absorption spectra of cycloalkanones and concluded that this transition has increasing allowed character with increasing deviation from C_{2v} symmetry, *i.e.*, cyclopentanone $>$ cycloheptanone $>$ cyclohexanone. In cyclobutanone it was suggested that an a_2 vibration was the dominant intensification path.

In a previous report from this laboratory we studied the fluorescence of a series of alkyl ketones and presented evidence that the α -CH stretching mode is a factor in radiationless deactivation from the lowest excited singlet state.⁹ The fluorescence wavelength maximum remained constant at 405 ± 3 nm and the fluorescence yield of di-*tert*-butyl ketone in τ -hexane was determined to be larger than the value for acetone by a factor of 4.4. In the present investigation we have measured the fluorescence yield of 17 cycloalkanones with the aim of demonstrating the effect of ring size and substitution on the fluorescence process and also to see if our earlier conclusions regarding alkyl ketones also apply to cycloalkanones.

Experimental Section

Materials. The ketones used in this study were vacuum distilled prior to use and their purity checked with a 6 ft, 0.25-in. o.d., Carbowax 20 M column with a Perkin-Elmer Model 145B gas chromatograph. Spectrograde solvents were used as received since they exhibited no interfering spectral properties.

Apparatus and Procedures. Fluorescence measurements were made with equipment described previously.⁹ All ketones were excited with 285-nm light, which was isolated with an interference filter from an Osram HBO 100W/2 high-pressure mercury lamp. The fluorescence quantum yield was measured relative to $\phi_F = 0.09$ for tryptophan.¹⁰ Absorption spectra were obtained with either a Bausch and Lomb Model 5C5 or a Beckman Model DU spectrophotometer. The natural radiative singlet lifetime, τ_F^0 ,

was estimated from the integrated absorption of the lowest transition of the ketone.

Results

The fluorescence spectrum of each of the compounds studied is unstructured with a wavelength maximum at ~ 405 nm, similar to that observed for alkyl ketones. Of the five unsubstituted cycloalkanones investigated, cyclobutanone, which possesses the most ring strain, has a much lower fluorescence yield than the C_5 - C_8 ring ketones. In Table I are summarized the extinction coefficients, the absorption wavelength maxima, the natural singlet radiative lifetimes, and the fluorescence quantum yields for various cycloalkanones, measured in *n*-hexane. The results of Lee, *et al.*,⁶ for CB, CP, and CH in cyclohexane are also included in Table I for comparison. The singlet radiative lifetime is approximately constant for all the ketones and is, within experimental uncertainty, equal to the value previously determined for alkyl ketones.⁹ The cyclopentanones have the highest absorption wavelength maxima (300 nm in *n*-hexane), while cyclobutanone exhibits the lowest wavelength maximum (281 nm in *n*-hexane). Measurements were also performed in acetonitrile and methanol and the results are, in general, the same as in *n*-hexane. There is no significant solvent effect on the fluorescence yield, although the ϵ_{\max} were $\sim 30\%$ larger in acetonitrile and methanol, which resulted in approximately 30% decrease in τ_F^0 .

In contrast to the unstructured ${}^1n,\pi^*$ absorption band of alkyl ketones, there is a distinct vibrational structure in the spectra of CB and CP. That these vibrational bands are solvent dependent is seen in Figures 1 and 2, where the vibronic bands appearing in *n*-hexane disappear when changing to acetonitrile and methanol. In the latter solvent there is complete loss of the structure. In the case of cyclopentanone the first four bands appear at 34,480, 33,330, 32,150, and 30,950 cm^{-1} , which corresponds to a vibrational band ranging from 1150-1200 cm^{-1} . This band is most likely the intense skeletal mode appearing at 1160 cm^{-1} in the ir spectrum of cyclopentanone.¹¹ Goodman and Chandler⁸ have also observed the same progression. The loss of vibrational structure is also apparent as the ring size increases. In Figure 3 the absorption spectra of the ketones cyclobutanone to cyclooctanone clearly show this effect. Substitution at the position α to the carbonyl group in cyclopentanone causes a similar change in the spectrum. No shift of the absorption maximum occurs upon methyl substitution. It is seen that 2,2,4,4-tetramethylcyclopentanone, which has one methylene group replaced, has lost most of its vibrational structure.

The fluorescence yields of all the ketones studied (with the exception of CB) are small ($\sim 10^{-3}$); however, there is a measurable variation of the fluorescence yield with methyl substitution at the α position of the cyclic ketones. Substitution at the β position, however, has no effect on the fluorescence yield of the molecule. The most significant variation in the fluorescence yield is seen in the sequence CP, 2-methylcyclopentanone, 2,5-dimethylcyclopentanone, and 2,2,4,4-tetramethylcyclopentanone, which increases in the ratio 1.6:2.6:5.4:5.8. These results parallel the trend observed with aliphatic ketones.⁹ The fluorescence lifetime also increases with α substitution: 1.9 nsec for CP, 2.7 for 2-methylcyclopentanone and 8.7 for 2,2,5,5-tetramethylcyclopentanone.² The increase of fluorescence with α substitution is also seen in the cyclohexa-

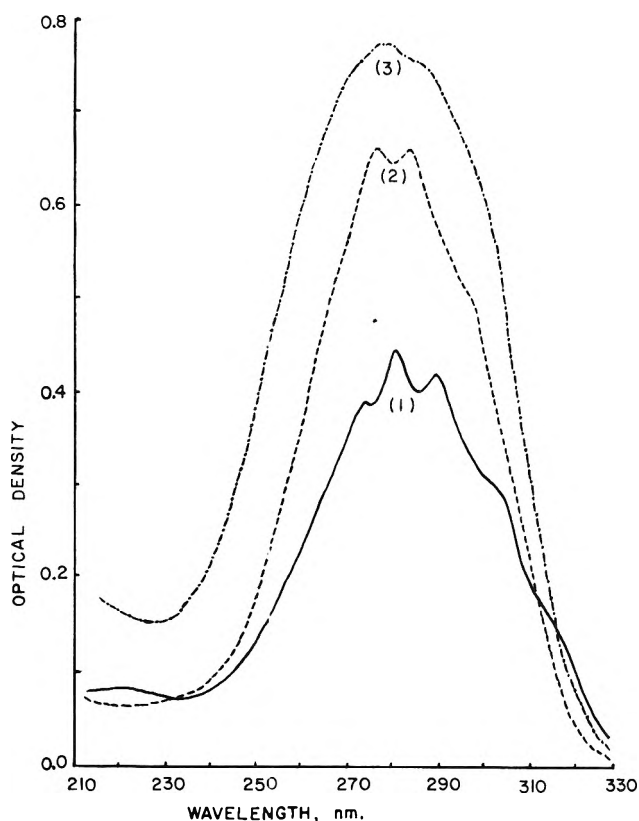


Figure 1. Absorption spectra of cyclobutanone at 25° (1-cm cell): (1) 0.023 *M* in *n*-hexane, (2) 0.029 *M* in acetonitrile, and (3) 0.035 *M* in methanol.

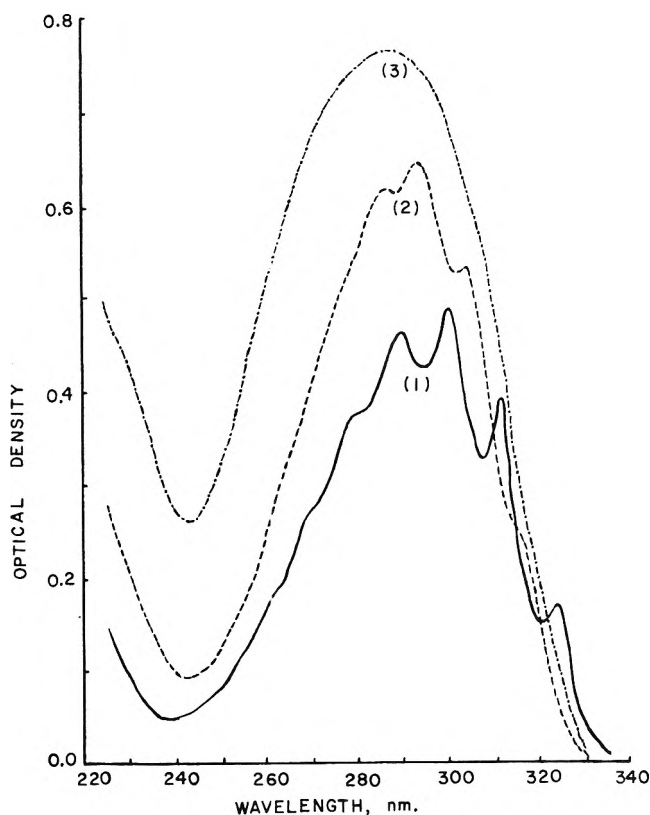


Figure 2. Absorption spectra of cyclopentanone at 25° (1-cm cell): (1) 0.027 *M* in *n*-hexane, (2) 0.030 *M* in acetonitrile, and (3) 0.033 *M* in methanol.

TABLE I: Absorption and Fluorescence Data for Cycloalkanones in *n*-Hexane

	ϵ_{\max}	λ_{\max}	$\tau_F^0 \times 10^6, \text{sec}^a$	$\phi_F \times 10^3^b$
Unsubstituted Ketones				
(1) Cyclobutanone	19 (15) ^c	281	1.9	~ 0.1 (0.1) ^d
(2) Cyclopentanone (CP) (1.9) ^e	18 (18)	300	2.3	1.6 (0.6)
(3) Cyclohexanone (CH) (2.6)	15 (14)	290	2.7	1.7 (0.9)
(4) Cycloheptanone	15 (16)	292	2.6	1.9
(5) Cyclooctanone	17	290	2.4	1.2
Substituted Ketones				
(6) 2-Methylcyclopentanone (2.7)	16	300	2.7	2.6
(7) 2,5-Dimethylcyclopentanone	19 (20)	300	2.2	5.4
(8) 2,2,4,4-Tetramethylcyclopentanone	18	300	2.3	5.8
(9) 3-Methylcyclopentanone	17	301	2.5	1.4
(10) <i>cis</i> -3,4-Dimethylcyclopentanone	20	301	2.2	1.4
(11) <i>trans</i> -3,4-Dimethylcyclopentanone	19	301	2.2	1.7
(12) 2-Methylcyclohexanone (2.9)	16	290	2.4	2.2
(13) 2,6-Dimethylcyclohexanone	18	291	2.2	2.7
(14) 3-Methylcyclohexanone	14	290	2.9	1.6
(15) 4-Methylcyclohexanone	16	290	2.4	1.6
(16) 3,5-Dimethylcyclohexanone	15	290	2.7	1.9
(17) 3,3,5,5-Tetramethylcyclohexanone (3.0)	17	288	2.3	2.0

^a τ_F^0 , radiative singlet lifetime, was calculated from integrated absorption spectrum using the following expression $\tau_F^0 = 3.5 \times 10^8 / \bar{\nu}_{\max}^2 \epsilon_{\max} \Delta \bar{\nu}_{1/2}$. ^b Relative fluorescence yield normalized to the value of 0.09 for tryptophan, 285-nm excitation. ^c Extinction coefficients from ref 8. ^d Fluorescence yields from ref 6; 313-nm excitation. ^e Fluorescence lifetime in nanoseconds; ref 2.

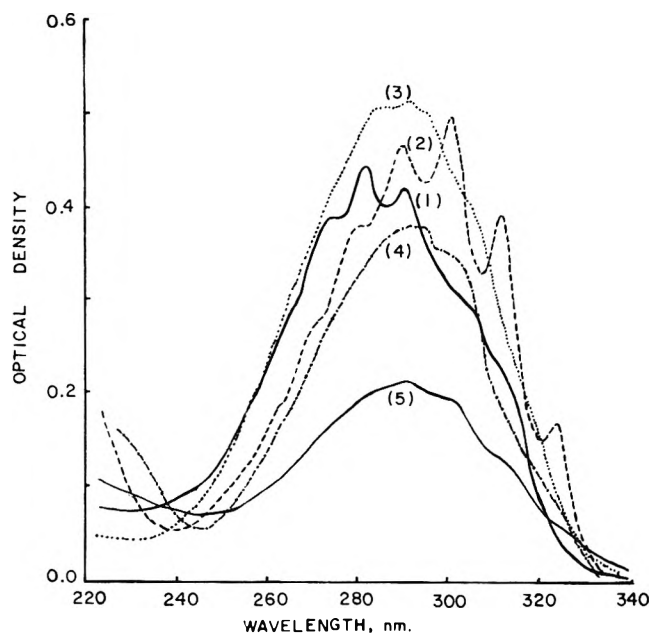


Figure 3. Absorption spectra of cycloalkanones in *n*-hexane at 25° (1-cm cell): (1) 0.023 *M* cyclobutanone, (2) 0.027 *M* cyclopentanone, (3) 0.034 *M* cyclohexanone, (4) 0.025 *M* cycloheptanone, and (5) 0.012 *M* cyclooctanone.

ones. The fluorescence yield of CH, 2-methylcyclohexanone and 2,6-dimethylcyclohexanone increases in the ratio 1.7:2.2:2.7. As is the case with β substitution in CP, substitution at the 3 and 4 position of CH has no effect on the fluorescence yield.

Discussion

The similarity of the fluorescence spectrum and the increasing fluorescence yield with α substitution observed with cycloalkanones confirms the effect previously demonstrated with alkyl ketones,⁹ *i.e.*, that the fluorescence is localized in the carbonyl group and that the α -CH bond is

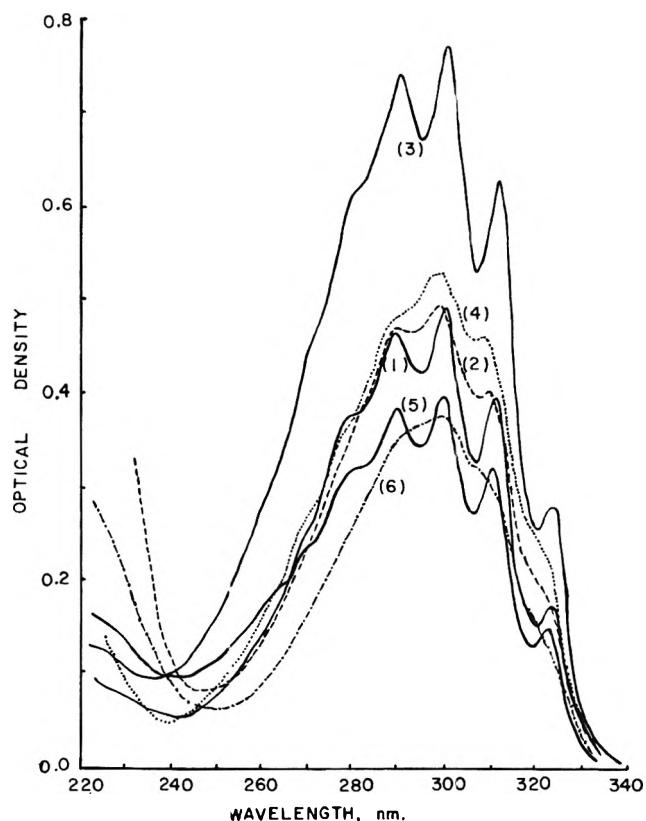


Figure 4. Absorption spectra of substituted cyclopentanones in *n*-hexane at 25° (1-cm cell): (1) 0.027 *M* cyclopentanone, (2) 0.031 *M* 2-methylcyclopentanone, (3) 0.045 *M* 3-methylcyclopentanone, (4) 0.028 *M* 2,5-dimethylcyclopentanone, (5) 0.021 *M* *trans*-3,4-dimethylcyclopentanone, and (6) 0.021 *M* 2,2,4,4-tetramethylcyclopentanone. (Spectra of *cis*-3,4-dimethylcyclopentanone was identical with that of the *trans* isomer.)

a factor in the radiationless deactivation of the lowest excited singlet state. Since the data in Table I indicate that the natural radiative singlet lifetime is approximately

constant for all the ketones investigated, it would appear, provided radiationless deactivation from the singlet is negligible, that intersystem crossing is faster for the weaker emitters, *i.e.*, $k_{isc} = (\phi_{FTF^0})^{-1}$. The photochemistry of cyclopentanones and cyclohexanones has been shown to proceed primarily through the triplet state and to involve α cleavage. In the unimolecular photodecomposition of cyclobutanone, however, the importance of triplets is not clear since no 1,3-pentadiene quenching is observed.² Although the effects reported here relate to the singlet state it is interesting to note that in those cases where intersystem crossing may be faster, namely, 2-substituted CP and CH, the photochemical quantum yields for the photoisomerization of cycloalkanones to enals are higher than in the unsubstituted ketone.² The photochemical quantum yield for 2,2,4,4-tetramethylcyclopentanone is larger than for CP and the corresponding value for 2-methylcyclohexanone and 2,6-dimethylcyclohexanone is larger than for cyclohexanone.

The effect of solvents and substitution on the vibrational structure of the ${}^1n,\pi^*$ band of CP and CH is unexpected. The same absorption band in alkyl ketones is diffuse and unstructured. A possible explanation for this behavior is vibronic coupling between the ring and carbonyl motions. In methanol the disappearance of vibrational structure may be due to hydrogen bonding of the lone pair on oxygen, while substitution at the α position affects radiationless processes and facilitates photocleavage, possibly from the singlet or triplet state. The quenching of the photoisomerization process in substituted CP and CH with 1,3-pentadiene is known to be less effective than in the unsubstituted compound.² In fact, the photochemistry of 2,2,5,5-tetramethylcyclopentanone is not quenched by 1,3-pentadiene.

In a recent report Furth¹² has suggested that the intersystem crossing efficiency, $S_1 \rightsquigarrow T_1$, and also $T_1 \rightsquigarrow S_0$ decrease as the internal strain of cyclic ketones increases. Available evidence indicates triplet yields of unity for CP

and CH; however, it appears that the triplet yield is significantly less than unity in CB. Lee, *et al.*,⁵ have indicated that the triplet yield is unity for CB, CP, and CH, and also that the intersystem crossing rate constant has a common value of $1-4 \times 10^8 \text{ sec}^{-1}$. On the other hand, Turro and Dalton² have suggested that the low yield (0.01) for photoreduction of CB's by tri-*n*-butylstannane may indicate a low intersystem crossing efficiency. The fluorescence results presented here for CB are inconsistent with the former conclusion since its low fluorescence yield indicates an inverse singlet lifetime of $\sim 10^{10} \text{ sec}^{-1}$. Since the intersystem crossing rate constant is believed to be $\sim 10^8 \text{ sec}^{-1}$, there must be a much more efficient singlet deactivation mode, probably photocleavage, in this molecule. A phosphorescence study of cycloalkanones should assist in elucidating the importance of triplets in these molecules.

References and Notes

- (1) J. G. Calvert and J. N. Pitts, Jr., "Photochemistry," Wiley, New York, N. Y., 1966, Chapter 5.
- (2) J. C. Dalton and N. J. Turro, *Annu. Rev. Phys. Chem.*, **21**, 499 (1970).
- (3) S. R. La Paglia and B. C. Roquette, *J. Phys. Chem.*, **66**, 1739 (1962).
- (4) G. L. Closs and C. E. Doubleday, *J. Amer. Chem. Soc.*, **94**, 9249 (1972).
- (5) R. G. Shorridge, Jr., C. F. Rusbult, and E. K. C. Lee, *J. Amer. Chem. Soc.*, **93**, 1863 (1971).
- (6) J. C. Hemminger, C. F. Rusbult, and E. K. C. Lee, *J. Amer. Chem. Soc.*, **93**, 1867 (1971).
- (7) J. Metcalfe and E. K. C. Lee, *J. Amer. Chem. Soc.*, **94**, 1 (1972).
- (8) W. D. Chandler and L. Goodman, *J. Mol. Spectrosc.*, **35**, 232 (1970).
- (9) M. O'Sullivan and A. C. Testa, *J. Amer. Chem. Soc.*, **92**, 5842 (1970).
- (10) V. G. Shore and A. B. Pardee, *Arch. Biochem. Biophys.*, **60**, 100 (1956). A recent value of 0.13 ± 0.01 has been determined by R. F. Chen, *Anal. Lett.*, **1**, 35 (1967); however, modification in the fluorescence yields affect only absolute values and do not alter the trends reported in this study.
- (11) J. C. P. Schwarz, Ed., "Physical Methods in Organic Chemistry," Holden-Day, San Francisco, Calif., 1964, pp 82 and 83.
- (12) B. Furth, Fourth IUPAC Symposium on Photochemistry, Baden-Baden, West Germany, July 16-22, 1972, Paper No. 19.

Pulse Radiolysis Studies of Nitrofurans. Radiation Chemistry of Nifuroxime

C. L. Greenstock* and I. Dunlop

Medical Biophysics Branch, Whiteshell Nuclear Research Establishment, Atomic Energy of Canada Limited, Pinawa, Manitoba, Canada (Received February 2, 1973)

Publication costs assisted by Atomic Energy of Canada Limited

Hydrated electrons, hydrogen atoms, and hydroxyl radicals react with nifuroxime with rate constants of 3.8×10^{10} , 3.0×10^9 , and $1.0 \times 10^{10} M^{-1} \text{sec}^{-1}$, respectively. There is little change in hydrated electron or hydroxyl radical reactivity from pH 4 to 10. The optical absorption spectra of the adduct species formed by e_{aq}^- , H, or OH addition to nifuroxime peak at 395, 400, and ≤ 375 nm and their molar extinction coefficients are 3900, 500, and $400 M^{-1} \text{cm}^{-1}$, respectively. The pK_a 's for protonation of the three primary species adducts are below 3.0. The nitrofurans have a high electron affinity and oxidize a variety of biochemical donor radicals and radical anions. However, oxygen reacts rapidly with both electron and hydroxyl radical adducts of nifuroxime with rate constants of 1.6×10^9 and $1.4 \times 10^9 M^{-1} \text{sec}^{-1}$, respectively.

Introduction

The nitrofurans, long known clinically for their antibiotic properties in the treatment of urinary tract infections,¹ have recently been shown to be excellent radiosensitizers both at the chemical^{2,3} and radiobiological^{4,5} level. Some derivatives have achieved the full oxygen effect in mammalian cells.⁵ Model systems of chemical radiosensitization have enabled us to screen potential radiosensitizers,⁶ and the nitrofurans have been shown to radiosensitize to a degree predicted by their electron affinity, which is midway between the nitrobenzenes and *p*-nitroacetophenone of low redox potential, and oxygen and certain quinones of high redox potential. It is clear from a comparison of the chemical and biological systems that at least two processes are occurring including electron transfer⁷ and radiation-induced binding.⁸

An understanding of the radiation chemistry of the nitrofurans was considered an important preliminary step in the study of the chemical mechanisms of radiosensitization. In view of their high electron affinity and excellent radiosensitizing ability as demonstrated in a variety of chemical and biological systems, the nitrofurans serve as ideal models for the study of radiation-induced chemical and biochemical redox processes and of chemical mechanisms of radiosensitization. The nitrofurans have characteristic narrow band intense electron-adduct spectra and this, combined with their high e_{aq}^- and OH reactivity, makes them extremely useful for studying relative redox potentials of both solutes and solute free radicals by pulse radiolysis.^{6,7}

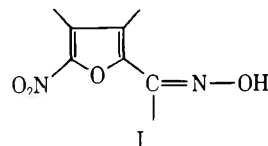
Experimental Section

The electronic and optical apparatus of the nanosecond pulse radiolysis equipment at Whiteshell Nuclear Research Establishment are similar to those previously described.⁹ Kinetic spectroscopy was used with a pulsed 450-W xenon lamp and transient spectra were determined with a Jarrel-Ash 0.25-m Ebert monochromator set to a bandwidth of 2 nm. Single 5–50-nsec pulses of 4-MeV electrons were used and the dose per pulse was monitored with a Faraday cup mounted behind the cell which was calibrated against air-saturated $10^{-2} M$ thiocyanate solu-

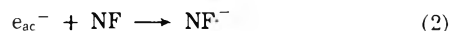
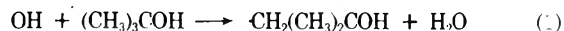
tions assuming $\epsilon_{\text{max}} 7100 M^{-1} \text{cm}^{-1}$ ¹⁰ and $G(\text{OH}) = 2.9$.¹¹ *N*-(5-Nitro-2-furfuraldehyde)semioxamazone was generously provided by Norwich Pharmacal. The other nitrofuran derivatives were obtained from Aldrich Chemical Co. and Pfaltz & Bauer, Inc.

Results and Discussion

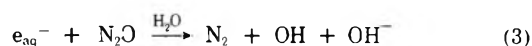
Transient Absorption Spectra. The transient absorption spectrum in deoxygenated solutions of nifuroxime (anti-5-nitro-2-furaldoxime, NF, I), with or without 0.5 *M tert*-



butyl alcohol, is characteristic of that found in all nitrofuran derivatives studied. Figure 1 shows the spectrum formed immediately after the pulse in the presence of *tert*-butyl alcohol as OH scavenger (reaction 1). The spectrum is due to a single species whose decay constant is independent of monitoring wavelength and whose kinetics of appearance is concomitant with the decay of the e_{aq}^- for a wide range of nifuroxime concentrations (reaction 2).



The spectrum peaking at 395 nm with a molar extinction coefficient at the absorption maximum of $3900 M^{-1} \text{cm}^{-1}$ is attributed to the electron adduct of nifuroxime ($\text{NF}^{\cdot-}$). This has recently been confirmed by the use of electron spin resonance.¹² The electron adduct spectrum is also formed by electron transfer from a variety of donor free radicals⁷ including the orotic acid OH adduct ($\cdot\text{OAOH}$) and the ribose radical (rib \cdot) (reaction 4), formed in N_2O -saturated solutions containing $10^{-3} M$ orotic acid or 0.1 *M* ribose, respectively, and $10^{-4} M$ nifuroxime. The transient spectra which build up after the pulse in the presence of excess orotic acid or ribose are identical with the nifuroxime electron adduct spectrum formed directly (Figure 1)



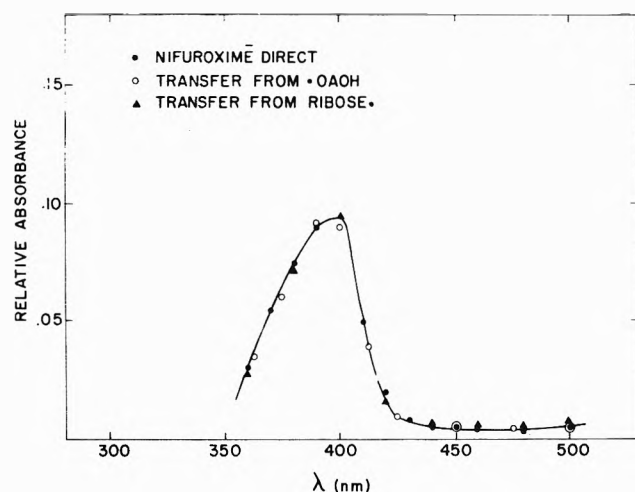
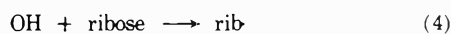
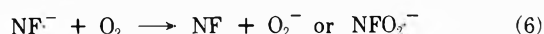


Figure 1. Transient absorption spectrum of the nifuroxime electron adduct: ●, direct electron attachment in deoxygenated $10^{-4} M$ solutions containing $0.5 M$ *tert*-butyl alcohol; ○, $10^{-3} M$ orotic acid (OA) present in N_2O -saturated solutions; ▲, $10^{-1} M$ ribose present in N_2O -saturated solutions.



The electron transfer reaction 5a is first order in nifuroxime concentration giving a rate constant $k_5 = 1.5 \times 10^9 M^{-1} \text{sec}^{-1}$. The reduced yield of $\text{NF}\cdot^-$ from such radical oxidation experiments indicates the presence of a competing reaction (5b).⁷ The *t*-BuOH radical formed in N_2O -saturated solutions is not oxidized by nitrofurans, a fact which enables us to determine the rate constant for the reaction of H atoms with nitrofurans at neutral pH in solutions containing both N_2O as an e_{aq}^- scavenger and *tert*-butyl alcohol to scavenge OH (see later section). Despite the high electron affinity of nitrofurans ($E_{1/2}$ vs. sce -0.25 for nifuroxime),¹³ which is an important factor in determining the radiosensitizing ability, the $\text{NF}\cdot^-$ reacts rapidly with oxygen ($E_{1/2}$ vs. sce -0.1)¹³ as expected. Using different N_2 - O_2 mixtures, the decay of $\text{NF}\cdot^-$ absorption was found to be first order in oxygen concentration giving a rate constant $k_6 = 1.6 \times 10^9 M^{-1} \text{sec}^{-1}$



Since the $O_2\cdot^-$ species absorbs at 240 nm in a region where both the nifuroxime and its radical anion both absorb strongly, it is not possible to determine whether the reaction with oxygen is an electron transfer or an addition reaction.

Attempts have been made to determine the pK_a for protonation of $\text{NF}\cdot^-$ (reaction 7) by monitoring the effect



of pH on λ_{max} and ϵ_{max} of the transient absorption formed in pulse irradiated deoxygenated solutions of 7 mM NF (limit of solubility) containing 0.5 M *tert*-butyl alcohol. There is very little change in the spectrum observed from 1 to 500 μsec after the pulse from pH 12 to 3, the lower limit for studying the reaction, because of the increasing competition for e_{aq}^- by H_{aq}^+ . Consequently, unless reaction 7 is slow compared with the time of observation, it may be assumed that the pK_a for protonation of the nifuroxime electron adduct is below pH 3.

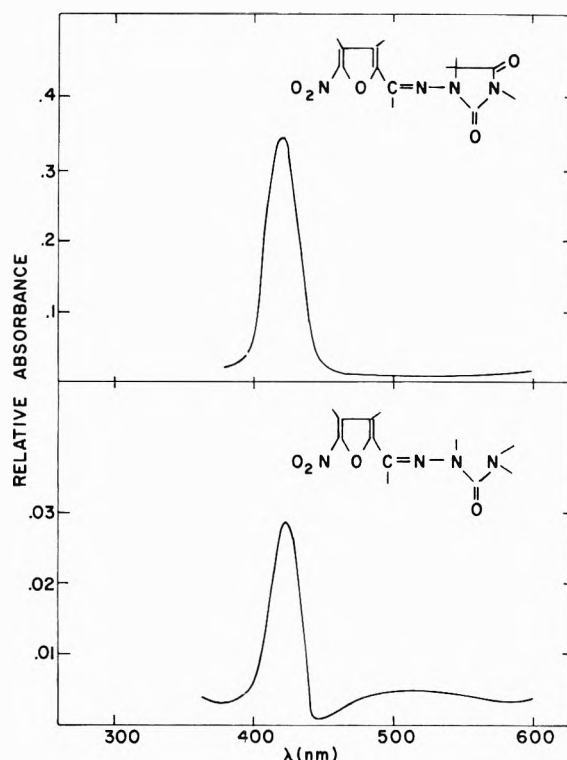
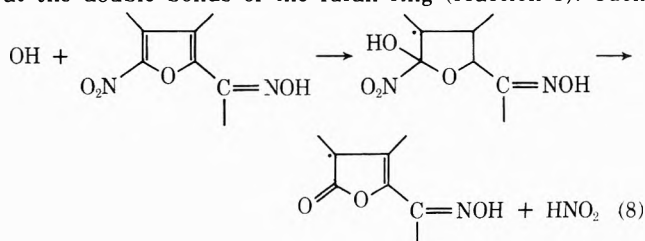


Figure 2. Electron adduct spectra of furadantin (upper) and nitrofurazone (lower) from pulse-irradiated oxygen-free solutions ($10^{-4} M$) in the presence of $0.5 M$ *tert*-butyl alcohol.

Figure 2 shows the transient absorption spectra of electron adducts of two other nitrofurans, furadantin and nitrofurazone. In the case of these strongly colored nitrofurans their absorption below 400 nm prevents observation of the electron adduct at high concentrations. However, by using low solute concentration or by resorting to electron transfer studies, the transient spectra can be determined and the extinction coefficients measured. All nitrofuran electron adducts studied have absorption spectra peaking around 400 nm.

The transient absorption spectrum observed in $10^{-3} M$ nifuroxime solutions saturated with N_2O is shown in Figure 3a. The spectrum peaks at 375 nm with an extinction coefficient at the peak absorption of $400 M^{-1} \text{cm}^{-1}$. The species is relatively long lived and decays by second-order kinetics with a rate constant $2k = 10^8 M^{-1} \text{sec}^{-1}$. The transient absorption spectra for other nitrofurans in solutions saturated with N_2O are very similar. This, together with the fact that the rate constants for OH attack are so high, suggests that the spectrum arises from an OH attack at the double bonds of the furan ring (reaction 8). Such



reactions have recently been reported for furan itself.¹⁴ It is believed, by analogy with the 5-nitouracils, that OH attack can lead to oxidative denitration of nitrofurans (reaction 8) with OH addition being the rate-limiting

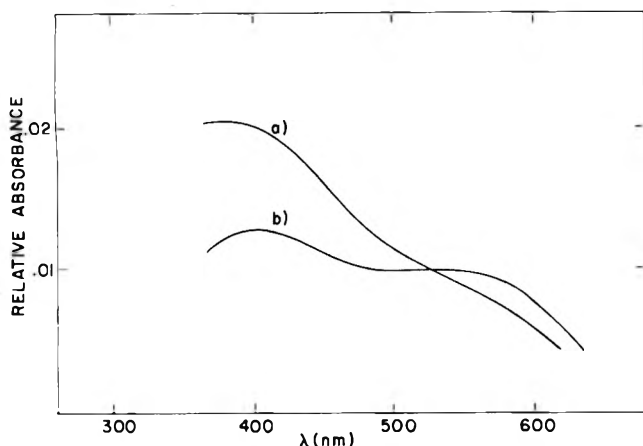


Figure 3. Transient absorption spectra formed by pulse radiolysis of 10^{-3} M nifuroxime solutions: (a) in N_2O -saturated solutions at neutral pH; (b) in oxygen-free solutions at pH 1 containing 0.5 M *tert*-butyl alcohol. The average dose per pulse was 7 krad.

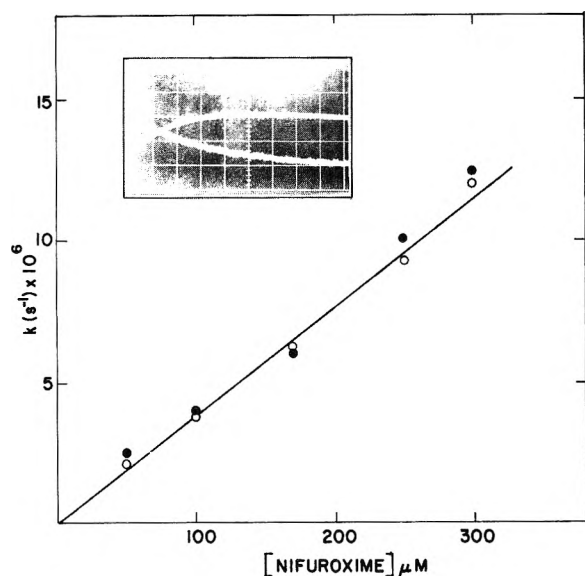
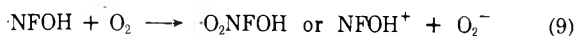


Figure 4. Effect of nifuroxime concentration on the rate of formation of nifuroxime $^{\cdot-}$ (●), or the rate of decay of the e_{aq}^- absorption (○). The oscillogram shows the build up of nifuroxime $^{\cdot-}$ absorption at 395 nm and the concomitant decay of e_{aq}^- absorption at 550 nm for a N_2 -saturated solution of 2.5×10^{-4} M nifuroxime containing *tert*-butyl alcohol. The sweep rate is 50 nsec/cm and the dose per pulse is ~ 1 krad.

step.¹⁵ No change is observed in the transient absorption spectrum (Figure 3a) from 1 μ sec to several milliseconds after the pulse, suggesting that oxidative denitration occurs prior to the earliest time of observation. In 5-nitrouacil the efficiency of oxidative denitration is $\sim 22\%$. Combined pulse radiolysis and esr studies with simple nitrofurans confirm this.¹²

The rate of oxygen quenching of the transient absorption following OH attack was determined directly using N_2O - O_2 mixtures from 1 to 10% O_2 , of known concentrations. The rate constant $k_9 = 1.4 \times 10^9 M^{-1} sec^{-1}$ is similar to those for peroxy radical formation in pyrimidines and amino acids.¹⁶



It cannot be determined by pulse radiolysis whether

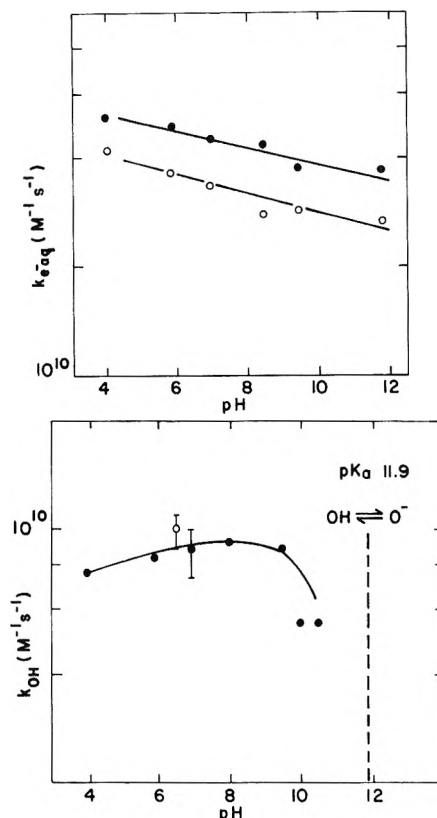


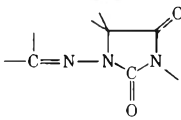
Figure 5. (a) A semilog plot of the variation in e_{aq}^- reactivity with pH: (●) build up of nifuroxime $^{\cdot-}$ absorption at 395 nm or decay of e_{aq}^- absorption at 550 nm; (○) bleaching of nifuroxime uv chromophore at 360 nm. (b) Variation in OH reactivity with pH: (●) build up of transient absorption at 500 nm; (○) bleaching of the uv chromophore at 360 nm.

reaction 9 is an electron transfer reaction or a radical addition because of the inability to observe $O_2^{\cdot-}$ directly.

The transient spectrum from solutions containing 10^{-3} M nifuroxime and 0.5 M *tert*-butyl alcohol at pH 1 is also shown in Figure 3. This spectrum is broad with a peak around 400 nm and is very weak ($\epsilon_{max} \sim 500 M^{-1} cm^{-1}$ using $G(H) = 3.25$). The low extinction may, in part, be due to partial scavenging of H atoms by *tert*-butyl alcohol.

Primary Species Reactivities. The rate constant for the reaction of e_{aq}^- with nifuroxime has been determined for different nifuroxime concentrations in the range 50–300 μM by monitoring both the e_{aq}^- decay at 550 nm and the electron adduct build up at 395 nm as shown in the oscillogram (Figure 4). Both methods give essentially the same rate constant. The data, which include corrections for the finite lifetime of the e_{aq}^- in the solution without nifuroxime,¹² are shown in Figure 4 for pH 6.8. From the slopes of such lines, which show the proportionality of the rates to nifuroxime concentration, the bimolecular rate constants were calculated for different pH values. Low doses were used to minimize radical-radical reactions. Data not shown in Figure 4 indicate that e_{aq}^- attack leads to loss of nifuroxime absorption at 360 nm. The rate constants calculated from this bleaching for different nifuroxime concentrations are close to but slightly lower than those obtained from the two methods illustrated in Figure 4. This result may indicate that there is some transient absorption at 360 nm due to the electron adduct which leads to a slight underestimate of the rate constant for e_{aq}^- in-

TABLE I: Absolute Rate Constants for the Reactions of e_{aq}^- and OH with Various Nitrofurans

Nitrofuran	Substituent	$k(e_{aq}^-) \times 10^{10}, M^{-1} \text{sec}^{-1}$	$k(\text{OH}) \times 10^9, M^{-1} \text{sec}^{-1}$
Nitrofurvaldehyde	-CHO	3.4	5.5
Nitrofuoroic acid	-COOH	2.2	5.3
Nifuroxime	-C=NOH	3.8	10.0
Nitrofurazone	-C=NNCONH ₂	2.8	10.6
Nitrofurvaldehyde diacetate	-C(OOCH ₃) ₂	3.0	
Furamazone	-C=NNCOCO NH ₂	3.25	10.3
Furadantin		3.35	9.3

duced bleaching of the nifuroxime uv chromophore. At pH 6.8 the rate constant for e_{aq}^- attack averaged over the three methods of determination is $3.8 \times 10^{10} M^{-1} \text{sec}^{-1}$. This is among the highest e_{aq}^- rate constants ever published. The effect of pH on this value is shown in Figure 5a. There is a slight decrease in reactivity with increasing pH. This may be due to ionization of the side group associated with a strong yellow color in solution.¹

The two methods of measuring OH reactivities directly by following the build up of OH adduct absorption at 500 nm or the bleaching of nifuroxime absorption at 360 nm, where the contribution of the OH adduct absorption is estimated to be less than 10%, are illustrated in Figure 6. The rates, determined for at least four nifuroxime concentrations, increase linearly with concentration, yielding average absolute rate constants of 9 and $10 \times 10^9 M^{-1} \text{sec}^{-1}$ respectively for the OH adduct build up and for the bleaching of nifuroxime absorption. Although rate constants of 5 and $7 \times 10^9 M^{-1} \text{sec}^{-1}$ were obtained by competition kinetics^{17,18} using ferricyanide and thiocyanate, in reasonable agreement with the more direct determinations, these cannot be considered accurate in view of the finite absorption of the nifuroxime OH adduct at 420 and 500 nm, the peaks of the ferricyanide and $(\text{CNS})_2 \cdot^-$ absorptions, which will tend to underestimate the true rate constant using competition kinetics.

There is no appreciable variation in OH reactivity with pH, except for a decrease around pH 10, the average value in the range pH 4-9 being $1 \times 10^{10} M^{-1} \text{sec}^{-1}$ (Figure 5b).

The rate of build up of the H adduct absorption at 500 nm was measured at pH 1 for deoxygenated solutions of $10^{-3} M$ nifuroxime in the presence of 0.5 M *tert*-butyl alcohol. The rate constant for the reaction of H with nifuroxime by this single estimate is $\sim 3 \times 10^9 M^{-1} \text{sec}^{-1}$. A similar determination at neutral pH in the presence of N_2O also gave a value of $3 \times 10^9 M^{-1} \text{sec}^{-1}$ which was independent of *tert*-butyl alcohol concentration, suggesting that the H scavenging by *tert*-butyl alcohol is not significant. The H adduct, formed in high yield at pH 1, reacts with oxygen and the rate constant determined from a single estimate in aerated solution is $1.0 \times 10^9 M^{-1} \text{sec}^{-1}$.

Table I shows rate constants for the reactions of OH and e_{aq}^- with various nitrofuran derivatives at neutral pH. Both the OH and e_{aq}^- rates are diffusion controlled for all the derivatives, with no real differences in rates being observed for the larger substituents. The simplest

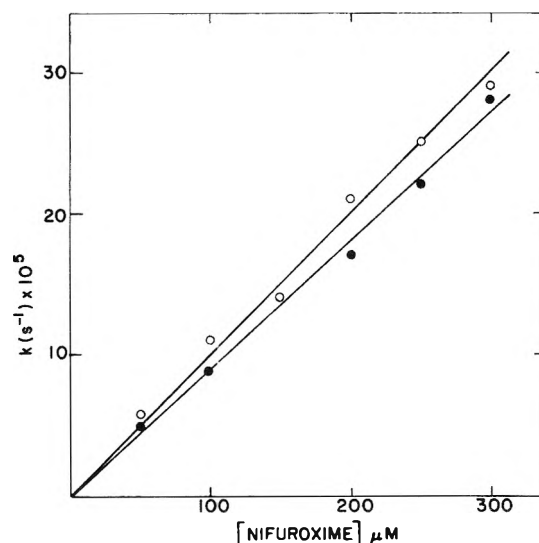


Figure 6. Effect of nifuroxime concentration on the rate of formation of the transient absorption at 500 nm (●) or the rate of bleaching of the nifuroxime uv chromophore (○). The solutions are N_2O saturated and at neutral pH.

derivative, nitrofurvaldehyde, has rate constants for e_{aq}^- and OH attack of 3.4×10^{10} and $0.55 \times 10^{10} M^{-1} \text{sec}^{-1}$, respectively, indicating that the nitrofuran ring confers the majority of the primary species reactivity, with the 2 substituents merely increasing the reactivity slightly, if at all, by increasing the cross section for primary species attack. The unsubstituted furan ring by comparison is very unreactive toward e_{aq}^- having a reactivity of $<10^6 M^{-1} \text{sec}^{-1}$.

Conclusion

The H, OH, and e_{aq}^- adducts of the nitrofurans studied all absorb in the uv region between 300 and 400 nm, as do those of other nitroaromatics. The electron adduct of nifuroxime has an intense, narrow band absorption spectrum peaking at 395 nm which is characteristic of all nitrofurans. The rate constant for e_{aq}^- addition to the nitro group is diffusion controlled and decreases only gradually with increase in pH over the range pH 4-12. Hydroxyl radicals are extremely reactive toward nifuroxime and this reactivity is independent of pH from pH 4 to 10. Oxidative denitration is believed to occur by analogy with 5-nitouracils.¹⁵

The nifuroxime electron adduct is formed by the oxidation of a variety of biochemical radicals and radical anions and can be oxidized by electron affinic compounds including oxygen as expected on the basis of electron affinity. These studies form part of a continuing program to investigate the mechanisms of electron affinic radiosensitization in biological systems.^{7,19}

Acknowledgments. We thank our colleagues in the Medical Biophysics Branch for their helpful discussions and acknowledge the technical assistance of Mr. L. Geofrey.

References and Notes

- (1) H. E. Paul and M. F. Paul, "Experimental Chemotherapy," R. J. Schnitzer and F. Hawking, Ed., Academic Press, London, 1964, p 307.
- (2) J. A. Raleigh, C. L. Greenstock, and W. Kremers, *Int. J. Radiat. Biol.*, in press.
- (3) C. L. Greenstock and C. Banerjee, *Radiat. Res.*, **47**, 217 (1971).

- (4) A. P. Reuvers, J. D. Chapman, and J. Borsa, *Nature (London)*, **237**, 402 (1972).
- (5) J. D. Chapman, A. P. Reuvers, J. Borsa, A. Petkau, and D. R. McCalla, *Cancer Res.*, **32**, 2616 (1972).
- (6) C. L. Greenstock, J. A. Raleigh, W. Kremers, and E. McDonald, *Int. J. Radiat. Biol.*, **22**, 401 (1972).
- (7) C. L. Greenstock and I. Dunlop, *Int. J. Radiat. Biol.*, **23**, 197 (1972).
- (8) J. D. Chapman, C. L. Greenstock, A. P. Reuvers, E. M. McDonald, and I. Dunlop, *Radiat. Res.*, **53**, 190 (1973).
- (9) J. W. Hunt, C. L. Greenstock, and M. J. Bronskill, *Int. J. Radiat. Phys. Chem.*, **4**, 87 (1972).
- (10) G. E. Adams, J. W. Boag, J. Currant, and B. D. Michael, "Pulse Radiolysis," M. Ebert, *et al.*, Ed., Academic Press, London, 1965, p. 77.
- (11) G. Czapski and B. H. J. Bielski, *J. Phys. Chem.*, **57**, 2180 (1963).
- (12) C. L. Greenstock, I. Dunlop, and P. Neta, *J. Phys. Chem.*, in press.
- (13) Half-wave potential measured against a saturated calomel reference electrode at pH 7 in 0.05 M tris buffer.
- (14) J. Lillie, *Z. Naturforsch.*, **266**, 197 (1971).
- (15) P. Neta and C. L. Greenstock, *Radiat. Res.*, in press.
- (16) R. L. Willson, *Int. J. Radiat. Biol.*, **17**, 349 (1970).
- (17) G. E. Adams, J. W. Boag, and B. D. Michael, *Trans. Faraday Soc.*, **61**, 1417 (1965).
- (18) R. L. Willson, C. L. Greenstock, G. E. Adams, L. M. Dorfman, and R. Wagemann, *Int. J. Radiat. Phys. Chem.*, **3**, 211 (1971).
- (19) G. E. Adams, C. L. Greenstock, J. J. vanHemmen, and R. L. Willson, *Radiat. Res.*, **49**, 85 (1972).

Yields and Decay of the Hydrated Electron at Times Greater Than 200 Picoseconds¹

C. D. Jonah,* E. J. Hart, and M. S. Matheson

Chemistry Division, Argonne National Laboratory, Argonne, Illinois 60439 (Received February 20, 1973)

Publication costs assisted by Argonne National Laboratory

We have measured the yield of the hydrated electron at times greater than 200 psec after irradiation with 19-MeV electrons as $4.1 \pm 0.1 e_{aq}^-/100$ eV of energy deposited. We have also measured the yield and the decay of e_{aq}^- in the presence of (a) 1 M CH₃OH, (b) 1 M NaOH, and (c) 1 M CH₃OH plus 1 M NaOH. The results confirm the concept of high local concentrations in the initial stages after energy deposition (the spur theory), but the time dependence of $[e_{aq}^-]$ differs from that predicted by published spur diffusion model calculations.

Introduction

It is a fundamental concept of the radiation chemistry of condensed phases that the energy of a charged particle is deposited inhomogeneously along its track in the absorbing medium, producing high local concentrations (spurs) of reactive intermediates. Samuel and Magee^{2a} developed the first theoretical model for the radiolysis of water, in which the transient species, initially at high local concentrations, participate in the competing processes of reaction with each other and diffusion into the bulk of the medium to form a homogeneous solution. This model with various refinements has been used quite successfully^{2b} to correlate yields of products obtained as a function of concentration of added scavenger (10^{-6} –1 M) and as a function of linear energy transfer (LET). (LET = energy deposited per unit path length.) For fast electrons with low LET the spurs are about 500 nm apart, while for protons or α particles of a few MeV the LET is high and the spurs overlap into a continuous track. In the past 20 years the following has been established: (1) the identity of the transient species escaping the spurs (e_{aq}^- , H, OH, H₃O⁺, and OH⁻); (2) the G values for these species that escape the spur (although there is disagreement for $G(\text{H}_3\text{O}^+)$ and $G(\text{OH}^-)$); (3) the rate constants for reaction among the intermediates; and (4) the diffusion constant of e_{aq}^- . This accumulation of data has aided in the formulation of the model but restricted the number of variable parameters.

Among the predictions of the spur-diffusion model are the initial yields of species at about 10^{-11} sec, and the time dependence of these yields as the spur expands. In the present work, we have measured the value of $G(e_{aq}^-)$ after 200 psec and followed the time dependence of $[e_{aq}^-]$ to 40 nsec in H₂O, 1 M CH₃OH, 1 M NaOH, and in 1 M NaOH + 1 M CH₃OH. A preliminary report of the measurement of the early $G(e_{aq}^-)$ has been published³ jointly with Hunt and his collaborators at the University of Toronto, who have independently measured $G(e_{aq}^-)$ at 30 psec. Our results confirm that e_{aq}^- initially is distributed inhomogeneously, but the time dependence of e_{aq}^- concentration is quite at variance with spur model predictions.^{4,5} Work such as that reported here can eventually restrict the choice of spur model parameters to (1) the radius of the spur, (2) the number of particles per spur, and (3) the percentage of spurs of a given radius and particle content, and thus define the inhomogeneity of the early stages of the radiation chemistry of water.

In this paper in addition to our results we describe some of the details of our apparatus, so that the reliability of these critical data can be judged, and so that an adequate experimental background for future papers in this series is provided.

Experimental Section

Linac. Irradiations were carried out using an Applied Radiation Corporation linear electron accelerator.⁶

Upgrading at Argonne includes the addition of a subharmonic prebuncher which enables the production of very short pulses of estimated duration ≤ 50 psec and with 7 nC of charge per pulse at 19 MeV.⁷ For experiments discussed in this paper the electron beam was pulsed 30 times a second and focussed to a cross sectional area ~ 5 mm² to give a dose per pulse of 2 krads in the irradiated volume.

Optical System. A schematic diagram of the experimental system is shown in Figure 1. Either an argon ion Model 71BR or krypton ion Model 71KR TRW pulsed gas ion laser with peak powers around 0.5 W was used for the analyzing light source.

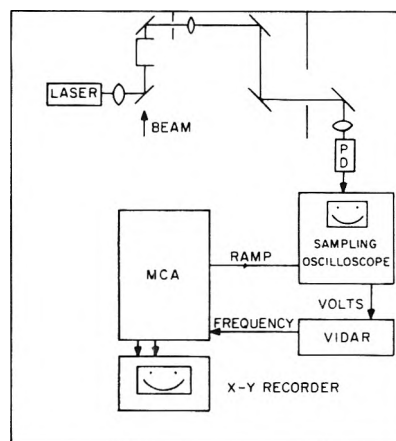
Since the laser and electron beam pulses were synchronized so that the electron pulse entered the cell at the peak of the much broader (5 or 50 μ sec) light pulse, the light pulse was flat on the reaction time scale. A Baird Atomic interference filter in front of the photodiode isolated either the 514.5- or 647.1-nm line and rejected essentially all Cerenkov radiation. The pulsed lasers produced an easily measurable output from the photodiode and simplified alignment. On the other hand, the number of wavelengths available from these lasers is limited, and their output includes much "high-frequency" noise which we attribute to mode beating in the laser.

A thin mirror of 0.5-mm fused silica front coated with aluminum reflected the light beam 90° to pass through the cell collinear with and in the same direction as the electron beam, and a similar mirror behind the cell reflected the light again perpendicular to the electron beam. Other mirrors directed the light beam out of the linac room through a hole in the wall and onto the active surface of the photodiode. The best signal-to-noise ratio was obtained by focussing the laser beam into the cell, making it parallel again after passage through the cell, and refocussing the light to fill the active surface of the photodiode.

Three ITT F 4014 photodiodes were used, two with S-20 photocathodes for detection at 647.1 nm, and the other with an S-5 active surface for measurement at 514.5 nm. Our two diodes with S-20 photocathodes lost all sensitivity after short usage, but, fortunately, no such problem was encountered with the S-5 photocathode. The diodes were operated at 1600 V, with risetimes which were measured to be less than 100 psec. There is, however, some overshoot and ringing lasts 400 to 500 psec.

Signal Sampling System. The photodiode output was sampled by a Tektronix S-4 sampling head with a rated risetime of 25 psec. As in all sampling oscilloscopes, the sampled signal voltage is held until the next trigger pulse. Since the sampling trigger is capacitively coupled to the pulse that fires the injector of the linear accelerator, the timing jitter between the sampling system and the electron pulse is less than 50 psec.

The signal from the sampling oscilloscope (Tektronix 7704) is biased so that the signal voltage is always positive (between 0 and 2 V for a signal on the scope face) and then is fed to a Model 241 Vidar voltage to frequency converter. The Vidar gives a pulsed output whose frequency is proportional to the input voltage. These pulses were counted by a multichannel analyzer used in a multiscaling mode. The analyzer was stepped from channel to channel at a fixed rate of 4 to 10 channels per second. An output signal which is linearly proportional to the number of the channel being counted in the analyzer was used to sweep the sampling oscilloscope. Thus each channel in the analyzer has a unique time (relative to the triggering



SUBNANOSECOND PULSE RADIOLYSIS APPARATUS

Figure 1. Schematic experimental set up for the picosecond pulse radiolysis experiments.

pulse) associated with it. A shutter in front of the photodiode automatically interrupts the analyzing light as the last 20 analyzer channels are swept to give a measurement of zero light.

After each sweep of the analyzer through all channels, the data from the analyzer channels are transferred to the Chemistry Division's Sigma 5 computer.⁸ The number of sweeps desired for a run are input by means of a teletype to the computer, which, at the end of a run, automatically transfers the data back into the analyzer one sweep at a time. Each sweep can be displayed on an oscilloscope and examined for experimental artifacts. Any sweep or sweeps showing experimental artifacts such as those caused by accelerator faulting can be rejected, without loss of the data of the whole run. The accepted sweeps of a run are summed and stored in disk storage. Ten sweeps were generally made to enhance signal-to-noise. The linearity of response of the overall system was confirmed by measuring a Cerenkov pulse with and without the analyzing laser light. The measured intensity of the Cerenkov was the same in both cases within 5%, which was the signal-to-noise limitation of that experiment. The peak Cerenkov light intensity was about one-sixth that of the analyzing light.

Three points should be made about the operation of the system: (1) the frequency of stepping channel-to-channel in the analyzer is not tied to the linac pulsing frequency; (2) the counting in the analyzer does the averaging and the analog to digital conversion; and (3) the system must spend the same length of time in each channel.

Irradiation Cell and Flow System. Since the experimental technique requires many electron pulses per run (20,000 pulses or 40 Mrads typically), a flow system was necessary to avoid overheating and buildup of radiolytic products. In each run 2 l. or more of fresh solution were circulated through a closed system at ~ 200 ml/min by a CRC vibrostaltic pump. The solution enters the bottom of the 2-cm long fused silica cell (windows of high-purity silica), is spread by a perforated plate for more uniform flow through the main body of the cell, and exits at the top of the cell. Total volume of the cell is about 3 cc. The solution can be purged continuously during a run by bubbling helium or other gas through the reservoir. At the end of a run in which such purging by helium had been done, analysis showed average concentrations of 2 μ M O₂ and <20 μ M H₂O₂ in the irradiated solution. On the time

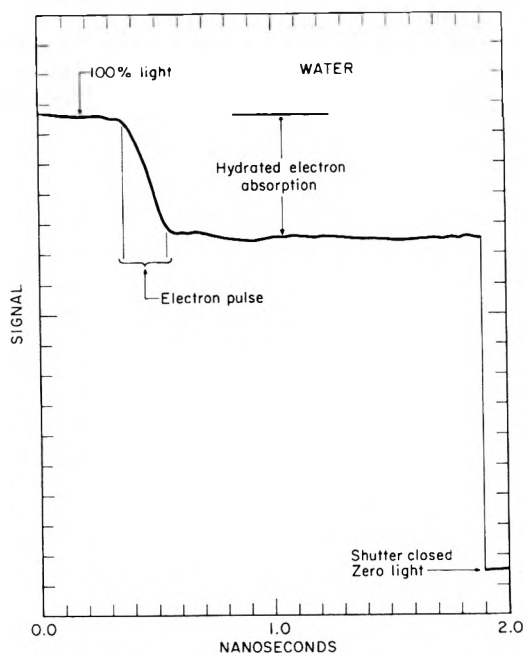


Figure 2. Transmission of irradiated water at 514.5 nm showing 100% light (far left), absorption by hydrated electron (center), and zero light (far right). Light signal intensity in arbitrary units.

scales used in these experiments the effects of such concentrations of O_2 and H_2O_2 are negligible.

G Value Measurements. The G value for the hydrated electron at less than 1 nsec after formation was determined by two methods: (1) directly, by measurement of both the dose deposited in the cell and the resulting hydrated electron concentration; and (2) indirectly, by measurement of the relative hydrated electron concentrations at <1 and at 30 nsec, since a lower limit for the G value is known for the latter time. The hydrated electron concentration was calculated from absorption signals such as that shown in Figure 2 using the extinction coefficients of Fielden and Hart,⁹ $\epsilon^{514.5}$ 7,100 and $\epsilon^{647.1}$ 16,900 $M^{-1} \text{cm}^{-1}$. When the 514.5- and 647.1-nm wavelengths were alternated for the analyzing light, the hydrated electron yields agreed within 1%, better than our experimental error. This supports the result of Bronskill, *et al.*,¹⁰ that the hydrated electron absorption is the same at these times and at microsecond or longer times. For G value determinations both the dose and the absorption must be measured in exactly the same volume. Two dosimeters were used and the results compared: the thiocyanate dosimeter¹¹ (0.01 M KCNS aerated) and the "Super Fricke" dosimeter¹² (0.01 M $FeSO_4$ in oxygen-saturated 0.8 M H_2SO_4 , no chloride).

With the thiocyanate dosimeter the same optical system and same wavelength (514.5 nm) were used when measuring either the absorption of the hydrated electron or that produced in the dosimeter. Since Fielden¹³ has previously measured $G\epsilon$ for the thiocyanate system at 500 nm, $G\epsilon$ at 514.5 nm could be obtained by determining the ratio of $G\epsilon^{514.5}/G\epsilon^{500}$. The ratio obtained was 0.96. To avoid interfering absorption by the hydrated electron the absorption in the thiocyanate dosimeter was measured after 1 μsec , at which time almost all the hydrated electrons had reacted with the oxygen present. The flow system described above was used and the accelerator pulsed at 30 pulses/sec to avoid problems which might arise from operating the accelerator in different modes for the e_{aq}^-

concentration and the dosimetry measurements. The photodiode was used with conventional trace recording on the oscilloscope to measure the absorption in this dosimeter, since the time is long, 1 μsec .

For determination of $G(e_{aq}^-)$ with the Fricke dosimeter a flow cell was made from a block of lucite similar in dimensions to our regular fused silica cell: 2 cm long, 1.2 cm wide, and about 3.9 cm high. A 3-mm cylindrical hole was drilled through the 2 cm length so as to be centered on the optical axis of the system. The capillary entrance and exit tubes drilled at each end were 1.6-mm diameter. Thin high-purity silica windows were cemented on the ends of the cell. The density of lucite is close to that of water and should scatter electrons similarly.

The concentration of hydrated electron at less than 1 nsec was determined by the time sampling method already described. The yield of ferric ion per pulse was measured by putting a known number of pulses, typically 2000, into the flowing Fricke dosimeter solution, and measuring the volume of solution and concentration of ferric ion afterwards. Ferric ion concentrations were determined on a Beckman DU spectrophotometer.

With this procedure it is necessary to estimate the irradiation volume in order to obtain an accurate G value. To do this hydrated electron concentrations and corresponding Super Fricke dosimetry were obtained with (1) the normal focussed beam and with (2) this beam scattered by a $\frac{1}{16}$ -in. thick sheet of aluminum. There is little energy loss by the beam in the aluminum, so that except for the larger beam diameter the process of energy deposition in the cell will be unchanged.

The height of the unscattered beam as it enters the cell is less than 3 mm, therefore using the volume of the cell (measured to be 0.175 cc) for the irradiated volume of the dosimeter underestimates the dose in the volume sampled by the laser beam and $G(e_{aq}^-)$ is overestimated. On the other hand, with the scattered beam the cylindrical cell volume is irradiated uniformly and in addition a portion of the entrance and exit tubes are irradiated so that use of only the cell volume for dosimetry calculations gives a lower limit to $G(e_{aq}^-)$. The hydrated electron concentrations for the two beams are proportional to the effective cross sectional areas of the beams. From this ratio the effective irradiated length of entrance and exit tubes was estimated and the appropriate volume added to the cell volume to obtain the effective volume for the Super Fricke dosimeter. This corrected dosimetry for the scattered beam combined with the corresponding hydrated electron concentration gave a corrected $G(e_{aq}^-)$ at less than 1 nsec of 4.05 ± 0.1 , only 5% higher than the uncorrected result. Indeed various assumptions about the beam spatial distribution affected the G value by less than 3%.

The relative yields at less than 1 and at 30 nsec were determined from decay curves for the hydrated electron in pure water. Such a curve is shown in Figure 2 of ref 3.

The pulses used in this work are quite short so that dose rates are tremendous. On the other hand, the dose per pulse is not large and therefore no overlap of "spurs" was expected. Nevertheless, it was deemed worthwhile to see if dose rate effects were present. Solutions containing 0.2 mM N_2O plus 2 mM ethanol were irradiated and the nitrogen yields measured. The dose per pulse was kept approximately constant for 50 psec, 4, 40, and 500-nsec pulses, and further, a similar solution was γ -irradiated to an equivalent dose. The results are listed in Table I. There seems to be no definite trend nor any large change in ni-

TABLE I: Lack of Effect of Dose Rate on Nitrogen Yields from Aqueous N₂O

Time	G value	Time	G value
1 psec ^a	2.46	500 nsec	2.30
4 nsec	2.48	Long time ^b	2.34
40 nsec	2.42		

^a Single fine structure pulse. ^b ⁶⁰Co γ radiolysis.

trogen yields over a dose rate variation of nine orders of magnitude (γ -radiation to 50-psec pulse).

Results and Discussion

Our G values for the hydrated electron after ~ 200 psec are listed in Table II. Further, we find within experimental error no decay of e_{aq}^- from 100 to 1000 psec (see Figure 2) which is comparable to the lack of decay reported by Hunt³ from 30 to 350 psec. Thus, it is to be expected that the average $G(e_{aq}^-) = 4.1 \pm 0.1$ that we measure after 200 psec should agree with the 30-psec value of 4.0 ± 0.2 found by Hunt.³ The excellent agreement among the different methods leads to some assurance that the results obtained are correct.

The relative optical densities (at 514.5 or 647.1 nm) produced in different aqueous solutions by equivalent electron pulses are summarized in Table III. The optical density of a solution relative to that of water was measured by alternately irradiating water and solution, obtaining for each alternate irradiation, data, such as that in Figure 2, although with fewer sweeps and therefore more noise. This alternation allowed us to correct fairly accurately for the small but consistent downward drift in electron pulse intensity. Three factors may change the relative optical density: (1) a change in the amount of energy deposited in the cell; (2) a change in the extinction coefficient of e_{aq}^- ; and (3) a change in the yield of e_{aq}^- . We assume that energy deposition is proportional to electron density since the electron beam loses less than half its energy in the 2-cm cell. Thus, dividing relative optical density by electron density corrects for energy deposition and gives the results in column 5.

Optical density changes which are due only to changes in e_{aq}^- extinction coefficients are not easy to estimate from available data. However, we have used the e_{aq}^- absorption curves in aqueous sodium chloride of Peled, *et al.*,¹⁴ and have also estimated in a few cases the shift in λ_{max} for e_{aq}^- for a given solution from the shift in λ_{max} for I^- in the same solution.¹⁵ In applying these data we have assumed the absorption curves are shifted in wavelength but unchanged in form and in the extinction coefficient at λ_{max} . For the shifts involved here this assumption should be a close approximation. The estimated relative optical densities due to changes in extinction coefficients at 514.5 nm are given in column 6 in Table III. We conclude that none of the salts tested increases the e_{aq}^- yield, but tentatively we conclude that 1 M NaOH increases the initial yield of $e_{aq}^- \sim 5\%$.

It is preferable to work nearer the peak of the hydrated electron absorption curve where small shifts in the curve will have little effect on the extinction coefficient. Unfortunately, already noted experimental difficulties limited the work at 647.1 nm. At this wavelength the (measured OD/electron density) for 1 M NaCl is quite small, while for 1 M NaOH this quantity is essentially the same as at

TABLE II: Initial Yields of Hydrated Electron at ~ 200 psec^a

Dosimetry		
Type	Krads	G
(SCN) ₂ ⁻	2.18	4.06 \pm 0.1
	2.40	4.16 \pm 0.1
Super Fricke		4.0 \pm 0.2
Hydrated electron ^b	0.3-3	4.1 \pm 0.2
		Av 4.1 \pm 0.1

^a Measured at 514.5 nm. ^b Relative to 2.9 at 30 nsec.

TABLE III: Relative Optical Densities Measured for e_{aq}^- in Various Solutions

Solute	Concn. M	Electron density	Relative optical density (514.5 nm)	(Optical density)/(electron density)	
				Measured	Estimated ^a
None		1.0	1.0	1.0	1.0
NaOH	1.0	1.038	1.13	1.09	1.04
	0.5	1.019	1.08	1.06	
	0.25	1.009	1.04	1.03	
NaCl	3.0	1.10	1.18	1.07	1.13
	1.0	1.035	1.11	1.07	1.08
KCl	3.0	1.11	1.22	1.10	
	1.0	1.04	1.14	1.10	
L ClO ₄	1.0	1.047	1.043	0.996	
KF	1.0	1.042	1.12	1.08	1.08
	0.25	1.01	1.03	1.02	
MeOH	1.0	0.994	1.03	1.036	
EtOH	1.0	0.992	1.01	1.018	
			647.1 nm		
NaOH	1.0	1.038	1.12	1.08	
NaCl	1.0	1.035	1.065	1.03	

^a Estimated change in optical density resulting from change in ϵ , the extinction coefficient of e_{aq}^- .

514.5 nm. These results at 647.1 nm confirm the conclusion above that NaOH slightly increases $G(e_{aq}^-)$ initial, while NaCl does not.

These results invalidate the proposal of Hamill,^{16,17} that high concentrations of chloride or fluoride ions will increase the initial yield of e_{aq}^- by scavenging H_2O^+ as in eq 1 and so preventing recapture of electrons by H_2O^+ or its successor H_3O^+ . Wolff, *et al.*,¹⁸ also find 1 M NaOH increases $G(e_{aq}^-)$ slightly at 30 psec ($2 \pm 3\%$) while 1 M NaCl does not. Further, from data based on less direct measurements Peled, *et al.*,¹⁴ similarly conclude Cl^- does not increase the yield of e_{aq}^- .



Methanol and ethanol have a minimal effect on the measured optical density. The peak of absorption for e_{aq}^- is shifted toward shorter wavelengths by methanol (1.97 eV) whereas λ_{max} (1.77 eV) for the solvated electron in ethanol is essentially the same as λ_{max} (1.72 eV) in water.¹⁹ This may account for the higher optical density observed in methanol solutions.

The observed decay of the hydrated electron is shown in Figures 2 and 3. The lack of decay from 200 to 1000 psec (Figure 2) has already been noted. Figure 3 shows the form of hydrated electron decay curves for water and three solutions. Although the exact intercept and the exact form at early times are difficult to determine be-

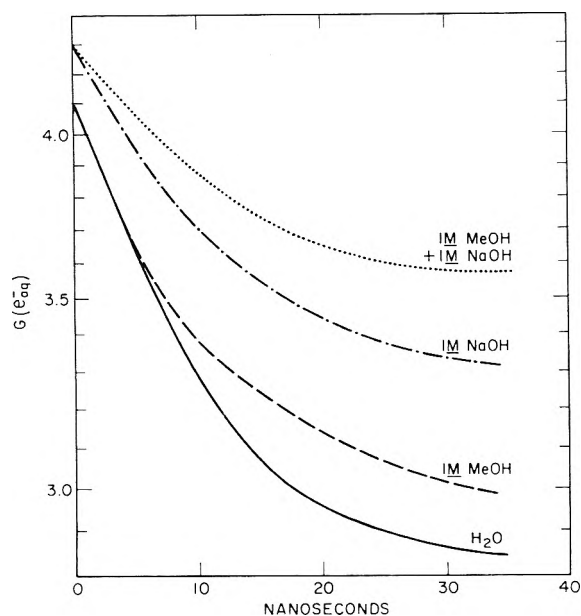
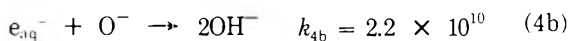
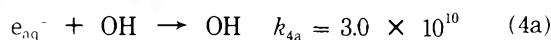
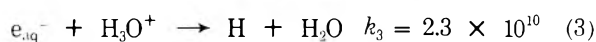
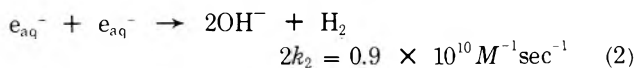


Figure 3. Hydrated electron yields as a function of time for several aqueous systems as indicated on curves. Note that the yield scale is logarithmic.

cause of the noise and the steepness of the slope, we believe these are close to the actual decay curves. The curves were obtained by plotting the natural log of the optical density for 200 points and passing a line through the center of the scatter of points. Scatter was at most $\pm 0.1 G$ value.

The principal spur reactions of the hydrated electron presumed to be involved in the interpretation of Figure 3 are the following

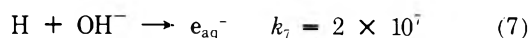


The rate constants given are dilute solution values. A more complete set of reactions can be found elsewhere.²⁰ In the presence of 1 M NaOH, H_3O^+ is scavenged



with a half-life of about 6 psec, so that reaction 3 is completely eliminated on our time scale. This accounts for the decreased slope in the presence of OH^- (Figure 3), and would account for the apparent 5% increase in $G(e_{aq}^-)$ from 4.1 to 4.3 at 200 psec.

The reaction



with a half-life of ~ 35 nsec could also decrease the apparent decay rate toward the end of the NaOH solution curve. The exact initial $G(H)$ in the spur for pure water is unknown, but is less than the 0.7 measured for H escaping the spur, since some H is formed in the spur by reaction 3.

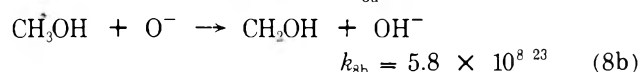
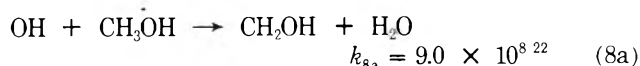
No compound scavenges OH with the efficiency that OH^- removes H_3O^+ . Methanol is about 100-fold less effective. Thus the water and methanol curves begin at the

TABLE IV: Comparison of Results of Buxton²⁵ and This Work

	Relative $G\epsilon (e_{aq}^-)^a$		$[G\epsilon(\text{Solute})/G\epsilon(H_2O)]^a$	
	Buxton (7 nsec/ 45 nsec)	This work (7 nsec/ 40 nsec)	Buxton (45 nsec)	This work (40 nsec)
H_2O	1.17	1.22	1.00	1.00
1 M NaOH	1.13	1.16	1.30	1.27
1 M MeOH	1.18	1.18	1.14	1.09
1 M NaOH } 1 M MeOH }	1.10	1.11	1.51	1.43

^a Measured optical densities have been corrected for changes in energy input by dividing by relative electron densities of solutions. $G\epsilon$ is not corrected for changes in extinction coefficients, ϵ .

same yield and with the same slope



diverging only after several nanoseconds when reaction 4 has been suppressed.

In comparing our results with previous experimental measurements, it must be remembered that our measurements span the time over which spur decay seems to occur using equipment with a risetime less than 1 nsec. At short times (200–1000 psec) we find little or no decay, which agrees with the lack of decay which Hunt has found at times from 20 to 350 psec,³ while at long times we qualitatively agree with conventional pulse radiolysis experiments.^{24,25} Others, limited to the time window of 20–350 psec,^{3,10} have seen only the beginning of the spur processes or, limited by experimental equipment, have seen only the end of the spur processes.^{24,25} The spur decay component we have observed is approximately twice as large as that previously observed,^{24,25} and the decay of the fast component is 10–15% faster than that reported by Buxton.²⁵ It is difficult to compare our results to those of Buxton at short times since much reaction and diffusion must go on during the 5-nsec van de Graaff pulse used by him. Nevertheless, we have attempted a crude comparison in Table IV. Buxton's results are calculated from his Table I in which the data are corrected for electron density. Our results are calculated from our Table III and Figure 3 correcting for electron density but not for changes in ϵ . At 7 nsec after the pulse the hydrated electrons in Buxton's work have an average age ~ 9.5 nsec, whereas in our work the average age at 7 nsec is 7 nsec. Thus, noting that the curves are fairly flat at 40 nsec, one would therefore expect the ratios of yields in column 3 to be slightly higher than those in column 2 as is found. For the relative yields in solute *vs.* those in water at 40 or 45 nsec, columns 4 and 5, our results are a few per cent lower. We conclude that Buxton's higher ratios (column 4) plus his neglect of the changes in extinction coefficients in solutions can largely account for the difference between his extrapolated yields and our measured values.

Both Kuppermann⁴ and Schwarz⁵ have calculated the time dependence of a reactive species in the spur model. They find considerable decay (Figure 1^{4a} and Figure 6⁵) between 10^{-10} and 10^{-9} sec where we find little (Figure 2), while at times longer than 10^{-9} sec we find greater decay than they do. It appears that spur parameters must be changed so that the spur model calculations yield the

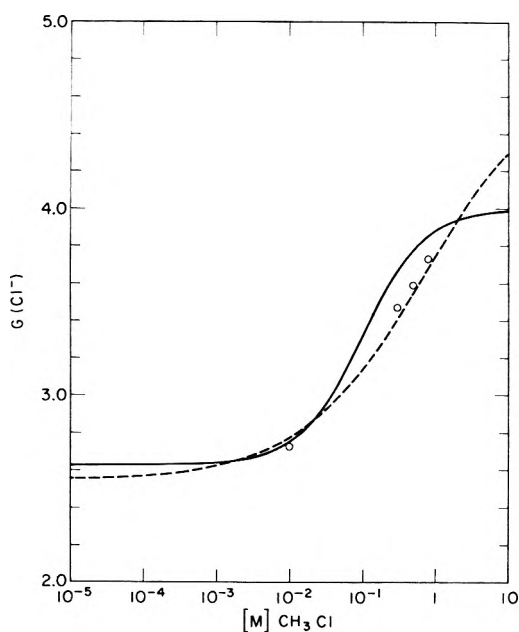
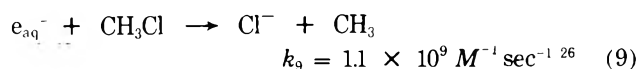


Figure 4. Dependence of $G(\text{Cl}^-)$ on molar concentration of methyl chloride in irradiated aqueous systems: O, experimental results from Table I ref 26; ---, empirical curve from Figure 6, ref 26; and —, curve predicted from the e_{aq}^- decays described in this paper.

same time dependence for $[e_{\text{aq}}^-]$ as is found experimentally.

Our experimental decay curve for e_{aq}^- may also be compared with the theoretical-experimental curve of Balkas, *et al.* In Figure 4 we have compared the experimental points and the empirical curve of these authors with the concentration dependence of $G(\text{Cl}^-)$ on methyl chloride concentration which would be predicted with the empirical time dependence of e_{aq}^- in the absence of scavenger which we have previously reported.³ Using similar assumptions to those Balkas, *et al.*, used for going from their eq II to III (actually identical reasoning with that required to go from eq III to II)²⁶ and using



we obtain

$$G(\text{Cl}^-) = 2.63 + \frac{1.37}{1 + 10^8/(1.1 \times 10^9[\text{CH}_3\text{Cl}])} \quad (10)$$

Since we are trying to fit the experimental results of Balkas, *et al.*, we use as a limiting value for electrons escaping the spur, 2.63, the yield measured by these authors in this system. The accord between our calculation and the experimental points listed in Table I of Balkas, *et al.*, is excellent. The highest concentration of CH_3Cl used was 0.8 M, so the extrapolation of the empirical curve²⁶ above 1 M is not significant. We conclude that our form of the decay curve of the hydrated electron adequately explains the aqueous methyl chloride system.

In summary, we have (1) measured the G value of the hydrated electron at short times, (2) given further experimental confirmation for the inhomogeneous distributions of the deposition of energy by fast electrons, and (3) found strong differences between the predicted and experimental time dependence of the hydrated electron concentration. We are presently carrying out theoretical calculations as well as further experiments to try to better understand early processes in water.

Acknowledgment. We would like to acknowledge the consultations with Dr. John Hunt on the design of the picosecond radiolysis system. We also would like to thank Gene Clift and Ken Johnson for being instrumental in designing and modifying the equipment and Don Ficht, Benno Naderer, and Lee Rawson for supplying us every week with such a fine electron beam. Finally we gratefully acknowledge the invaluable assistance of Robert Clarke throughout these experiments.

References and Notes

- (1) Work performed under the auspices of the U. S. Atomic Energy Commission.
- (2) (a) A. H. Samuel and J. L. Magee, *J. Chem. Phys.*, **21**, 1080 (1953); (b) I. G. Draganic and Z. D. Draganic, "The Radiation Chemistry of Water," Academic Press, New York, N. Y., 1971, Chapter 6.
- (3) J. W. Hunt, R. K. Wolff, M. J. Bronskill, C. D. Jonah, E. J. Hart, and M. S. Matheson, *J. Phys. Chem.*, **77**, 425 (1973).
- (4) (a) A. Kuppermann and G. G. Belford, *J. Chem. Phys.*, **36**, 1427 (1962); (b) A. Kuppermann in "Radiation Research," G. Silini, Ed., North Holland Publishing Co., Amsterdam, 1967.
- (5) H. A. Schwarz, *J. Phys. Chem.*, **73**, 1928 (1969).
- (6) W. Gallagher, K. Johnson, G. Mavrogenes, and W. Ramler, *IEEE Trans. Nucl. Sci.*, **18**, 584 (1971).
- (7) G. Mavrogenes, W. S. Ramler, W. A. Wesolowski, K. Johnson, and G. Clift, presented at The International Accelerator Conference, March 4, 1973, San Francisco, Calif.
- (8) P. Day and J. Hines, manuscript in preparation.
- (9) E. M. Fielden and E. J. Hart, *Trans. Faraday Soc.*, **63**, 2975 (1967).
- (10) M. J. Bronskill, R. K. Wolff, and J. W. Hunt, *J. Chem. Phys.*, **53**, 4201 (1970).
- (11) E. M. Fielden and N. W. Holm, "Manual on Radiation Dosimetry," N. W. Holm and R. J. Berry, Ed., Marcel Dekker, New York, N. Y., 1970, p 288.
- (12) K. Sehested, E. Bjergbaekke, O. L. Rasmussen, and H. Fricke, *J. Chem. Phys.*, **51**, 3159 (1969).
- (13) E. M. Fielden, private communication.
- (14) E. Peled, D. Meisel, and G. Czapski, *J. Phys. Chem.*, **76**, 3677 (1972).
- (15) M. Anbar and E. J. Hart, *J. Phys. Chem.*, **69**, 1244 (1965).
- (16) T. Sawai and W. H. Hamill, *J. Phys. Chem.*, **74**, 3914 (1970).
- (17) S. Khorana and W. H. Hamill, *J. Phys. Chem.*, **75**, 3081 (1971).
- (18) R. K. Wolff, J. E. Aldrich, T. L. Penner, L. Gilles, and J. W. Hunt, manuscript in preparation for *J. Phys. Chem.*, quoted by R. K. Wolff, Thesis, University of Toronto, Oct 1972.
- (19) S. Arai and M. C. Sauer, Jr., *J. Chem. Phys.*, **44**, 2297 (1966).
- (20) M. S. Matheson and L. M. Dorfman, "Pulse Radiolysis," The MIT Press, Cambridge, Mass., 1969, Chapter 6.
- (21) M. Eigen and L. DeMaeyer, *Z. Elektrochem.*, **59**, 986 (1955); see also K. H. Schmidt, *Int. J. Radiat. Phys. Chem.*, **4**, 439 (1972).
- (22) R. L. Willson, G. L. Greenstock, G. E. Adams, R. Wageman, and L. M. Dorfman, *Int. J. Radiat. Phys. Chem.*, **3**, 211 (1970).
- (23) R. Wander, B. L. Gall, and L. M. Dorfman, *J. Phys. Chem.*, **74**, 1879 (1970).
- (24) J. K. Thomas and R. V. Bensasson, *J. Chem. Phys.*, **46**, 4147 (1967).
- (25) G. V. Buxton, *Proc. Roy Soc., Sec. A*, **328**, 9 (1972).
- (26) T. I. Balkas, J. H. Fendler, and R. H. Schuler, *J. Phys. Chem.*, **74**, 4497 (1970).

Hydrogen Isotope Effects in the Reaction of Water Vapor with Alkali Metal Mirrors

R. O. Bremner and D. H. Volman*

Department of Chemistry, University of California, Davis, California 95616 (Received March 12, 1973)

Publication costs assisted by the University of California

The reaction of variable-composition-deuterated water vapor with alkali metal mirrors at 23° to yield hydrogen gas has been studied. From flow experiments it was determined that every collision of water with the surface results in removal of water. In static experiments, it was found that isotope fractionation and composition of molecular hydrogen produced was independent of the metal to water ratio for metal in excess. Under these conditions, the expression $([HD]^2/[H_2][D_2]) = Q$ yielded $Q = 12.0 \pm 2.6$, well above the equilibrium constant value of 3.85 at 298 K, independent of metal. These results are in accord with the following model: the reaction of metal with water results in the corresponding alkali hydroxide and a bound hydrogen atom; these adatoms transfer by quantum mechanical tunneling for which the relative probabilities for H and D are $(P_1/P_2) = 9.9$ and the calculated transfer energy based on an assumed rectangular barrier is approximately 6.0 kJ mol^{-1} ; molecular hydrogen is formed by the reaction of transfer atoms with adatoms. The order of effectiveness of the metals to yield H enrichment in the gas was $\text{Na} \cong \text{K} < \text{Li} < \text{Rb} \cong \text{Cs}$ but the differences were not large. Isotope fractionation is explained by assuming fractionation occurs only through $\text{HOD} + \text{M} \rightarrow \text{MOD} + \text{M} \cdot \text{H}$ (k_1), $\text{HOD} + \text{M} \rightarrow \text{MOH} + \text{M} \cdot \text{D}$ (k_2). Zero-point energy considerations yield $(k_1/k_2) = 14.0$, giving general agreement with the results.

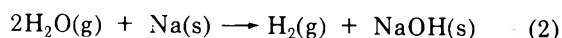
Introduction

Surprisingly few studies have been made of hydrogen isotope effects for the reaction of alkali metals in aqueous media to give hydrogen gas. Soon after the discovery of deuterium, fragmentary experiments of this nature directed at exploring the practicality of obtaining isotope enrichment were carried out. Farkas and Farkas¹ found that the reaction of sodium with 0.1 N H_2SO_4 (aq) containing 25 atom % D gave enrichment of H in the hydrogen gas evolved and enrichment of D in the aqueous media. Davis and Johnston² obtained analogous results for the reaction of sodium with natural liquid water. In more extended studies, Hughes, Ingold, and Wilson³ found the order $\text{Na} > \text{K} > \text{Li}$ for effectiveness of the metal in yielding H enrichment in the gas from the reaction with water containing 2.15–2.42% D. Finally, Johnston and Davis⁴ found the order $\text{Na} > \text{Li} > \text{K}$ for the reaction with liquid water containing 0.5% D.

Prior to a study made in this laboratory,⁵ only a single study had been made of fractionation by the reaction of water vapor with an alkali metal. Horiuti and Szabo⁶ using vapor from water liquid containing 1.8% D found a separation factor of $\alpha = 1.8$ where α is defined by

$$\alpha = (\text{H/D})_g / (\text{H/D})_l \quad (1)$$

In studies of reaction kinetics in this laboratory⁵ using D as a tracer, to analyze reaction products it was necessary to establish α over a wide range of D concentration. Consequently we determined hydrogen isotope fractionation in the reaction of water vapor with sodium mirrors, the sodium being in large excess, using liquid water with 0–90% D. The results of Horiuti and Szabo at 1.8% D were confirmed, but α was not constant over the entire composition range. The ratio of the total moles of gas formed to the moles of water used was found to be 0.51 ± 0.01 , establishing that the reaction



proceeded to completion. A further finding, which was not

reported because it was not germane to the purpose of the work at that time, was that the mass action expression

$$[\text{HD}]^2 / [\text{H}_2][\text{D}_2] = Q \quad (3)$$

for the molecular hydrogen formed was not the equilibrium constant for the reaction



From general considerations relating to isotope effects, isotope fractionation in the reaction is an expected result. However, the results reported^{3,4} for the order of effectiveness of Li, K, and Na in aqueous systems do not agree. Moreover, interpretation of results in liquid media is bound to be inherently difficult because of the possibility of both ionic and molecular initiation and the formation of a solution of the hydroxide product. A study of the gas-solid system seemed to us to offer the possibility of developing a reasonable model for the reaction provided results other than for sodium were known. Also in the earlier work, except for ours with sodium, because of analytical limitations, only total isotopic composition rather than composition of the molecular hydrogen was obtained. We have, therefore, in this work obtained results for all of the alkali metals and have developed models for both fractionation of the isotopes and composition of the gaseous product.

Experimental Section

Materials. D_2O , at least 99.8% D, was obtained from International Nuclear and Chemical Corp. The pure metals used were lithium, Fischer Scientific Co., and sodium and potassium, Malinkrodt. The azides used were sodium azide, Alfa Inorganics, and lithium, potassium, rubidium, and cesium azides, Eastman Organic Chemicals. Argon, 99.95% pure, was obtained from Liquid Carbonic.

Water Solutions. Solutions were prepared by mixing weighed amounts of pure D_2O and normal water. The compositions were determined from the masses used and also by measurements at 25° and 546 nm of the difference

between the refractive indexes of the solutions and normal water using a Brice-Phoenix differential refractometer and literature values of the refractive indices.⁷ The calculations by the two methods were in excellent agreement, and values of composition used below were those determined by refractive index.

Static Experiments. Most experiments were carried out by the method previously reported⁵ with minor modifications. The reaction chamber was a cylindrical Pyrex tube, 6 cm in diameter and 20 cm long. Mirrors of sodium and potassium were formed as described earlier. Because of the very rapid oxidation of rubidium and cesium in air, it was more convenient to obtain the metal from the azides, a method which could also be used for sodium and potassium. The azide was placed in a side tube attached at about a 45° angle below the alkali metal seal-off portion of the reaction vessel. After evacuating the system, the azide was heated by an external electric furnace to 500°. As the azide decomposed, the metal distilled out of the hot zone. Some 2.5 hr were required to complete the decomposition of sodium azide while the other azides required a longer period. In practice a minimum 6-hr period was used since after this length of time no additional metal was obtained from any of the azides. Subsequently, the tube containing the azide was sealed off from the reaction vessel and a metal mirror was formed in the reaction zone. Lithium mirrors could not be formed by either of the above methods: the bare metal on Pyrex because molten lithium reacts rapidly with glass; the azide because very little lithium was evolved presumably because of nitride formation. Consequently lithium was placed in a molybdenum boat which was inserted in the usual metal position and distillation under vacuum was accomplished by using the external resistance heater at 600°. The solid lithium film deposited on the glass walls could be deposited in the reaction zone in the same manner as for the other metals: gentle heating with a torch to yield a shiny cylindrical mirror about 10 cm in length.

Subsequent to formation of the metal mirror, water vapor was introduced by a different method from that used earlier. The inlet system consisted of a storage tube separated from the mirror vessel by a stopcock and having access to dry air and to water through stopcocks. With the inlet system closed off to the reaction vessel and filled with dry air, water was injected into the storage tube from a microsyringe through a stopcock and degassed by several freeze-pump-thaw cycles. The storage tube was surrounded by a 50° water bath and the stopcock to the reaction cell was opened whereupon the water flash evaporated into the cell. The amount of water used was never more than that which would yield 40% of the saturation vapor pressure in the reaction chamber. The product molecular hydrogens were collected through an aerosol-dispersal trap,⁸ necessary in experiments where excess water was used, measured in a gas buret, and analyzed by mass spectrometry.

Flow Experiments. The system used for these experiments was designed to allow passage of a stream of water vapor in argon at atmospheric pressure to pass through a cylindrical reaction tube containing an alkali metal mirror. The reaction tube, 16 mm in diameter, could be isolated and evacuated to permit the deposition of a uniform mirror, 13 cm long, in much the same manner as in the static experiments. Two flow-metered gas streams were used to establish the water composition and total flow rate

through the reaction tube: the first stream was dry argon; the second stream was argon which had been passed through constant-temperature water. After mixing the two streams, the gas was passed through the reaction tube. The initial water content of the gas mixture was determined gravimetrically by collecting the water vapor in Drierite.

Results

Isotope Fractionation and Molecular Hydrogen Composition. In our earlier work⁵ the sodium metal was always in excess of that necessary to react completely with water and no precautions to ensure a constant metal to water ratio were used. This method yielded reproducible results and it seemed that reproducibility would obtain if the metal were in excess, regardless of the extent of excess. For the present studies, however, in order to ensure consistency it was decided to obtain quantitative information on the effect of metal to water ratio on isotope fractionation and the composition of the molecular hydrogen. The results of experiments with sodium mirrors and 0.842 D atom fraction water are given in Figure 1.

The number of moles of sodium in the mirror was obtained by determining the number of moles of molecular hydrogen produced. When sodium was in excess, this was accomplished by treating unused sodium with an excess of water and summing the moles of hydrogen produced by the two injections of water. It may be concluded that for number of moles of sodium equal to or greater than the number of moles of water, isotope fractionation and gas composition are invariant.

For all the alkali metals the composition of the evolved molecular hydrogen and the separation factors, α , defined by eq 1 are shown in Table I. In all experiments, the

TABLE I: Composition of Molecular Hydrogen at Various Water Compositions

Metal	Water D, atom fraction	Molecular hydrogen, mol fraction			α $\frac{\{(H/D)_g\}}{(H/D)_l}$
		H ₂	HD	D ₂	
Li	0.228	0.718	0.275	0.007	1.76
	0.431	0.499	0.469	0.032	2.08
	0.616	0.278	0.626	0.095	2.33
	0.842	0.057	0.533	0.410	2.55
	0.904	0.023	0.378	0.599	2.50
Na	0.228	0.727	0.266	0.007	1.77
	0.431	0.450	0.499	0.051	1.77
	0.616	0.235	0.639	0.126	2.00
	0.616 (80°)	0.239	0.632	0.129	2.00
	0.814	0.119	0.490	0.391	2.10
K	0.842	0.056	0.469	0.475	2.19
	0.228	0.737	0.256	0.007	1.89
	0.431	0.483	0.485	0.032	2.00
	0.616	0.235	0.572	0.193	2.18
	0.814	0.084	0.512	0.404	2.01
Rb	0.814	0.084	0.512	0.404	2.01
	0.228	0.764	0.231	0.005	2.15
	0.329	0.650	0.338	0.012	2.22
	0.431	0.512	0.462	0.026	2.18
	0.616	0.337	0.602	0.061	2.83
Cs	0.814	0.092	0.615	0.293	2.91
	0.119	0.873	0.124	0.003	1.94
	0.431	0.530	0.438	0.032	2.26
	0.616	0.318	0.599	0.083	2.58
	0.814	0.095	0.622	0.283	2.98
	0.904	0.034	0.462	0.504	3.40

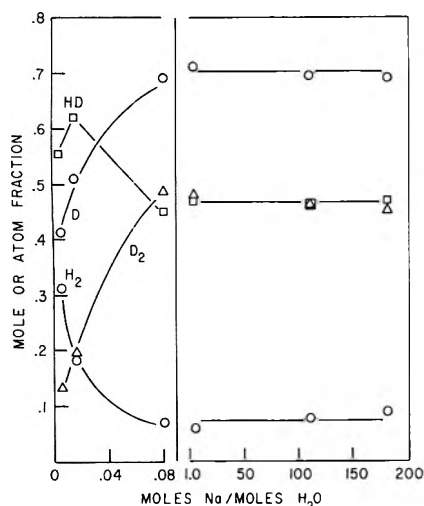


Figure 1. Atom fraction D and composition of molecular hydrogens as a function of the sodium to water ratio. Water with 0.842 D atom fraction.

amount of water used was 2.8×10^{-4} mol and the amount of metal mirror was about 8×10^{-4} mol. Except for a single experiment with sodium at 80° , results were obtained at ambient temperature, about 23° . The values of water composition, column 2, are accurate to about $\pm 0.5\%$. The higher values of mole fractions of molecular hydrogen, >0.5 , are accurate to $\pm 1\%$ while the lower values, <0.01 , are accurate to $\pm 30\%$. However, the low values contribute little to the $(H/D)_R$ ratio and, therefore, the maximum inaccuracy in α is about $\pm 10\%$.

Flow System Reaction. The extent of reaction of H_2O with sodium and rubidium mirrors in a flow system was determined and the results are given in Table II. The calculated values, last column, will be explained later. In each experiment the amount of water removed was determined by subtracting the amount of metal remaining from the original amount. The amount of metal remaining was found by measuring the quantity of molecular hydrogen produced on injection of an excess of water after the flow stream was stopped. For sodium, the original amount of metal was established by using a weighed quantity of the azide and calculating the mass of mirror from experiments which had established the metal yield from azide decomposition. For rubidium, the metal yield from the azide was not reproducible and the original amount of mirror was found by rinsing out the reaction tube with water and determining the base content. Thus the result with sodium at the low flow rate indicates complete removal of water within the experimental error of the procedure.

Discussion

Water Removal by Collision with Metal. The flow experiments provide information for the effectiveness of removal of water from the gas by interaction with the mirror. The development which follows is based on considerations of transport phenomena.⁹ Assume that every water molecule which reaches the surface is removed from the gas stream. The concentration of water vapor as a function of distance in the reaction zone for a tube of diameter d is given by

$$-dc/dz = \pi dK_m cF^{-1} \quad (5)$$

where K_m is the mass transfer coefficient and F is the vol-

TABLE II: Extent of Reaction of H_2O with Sodium and Rubidium in a Flow System in 180 sec

Metal	Metal, mol $\times 10^4$	Flow rate, $dm^3 sec^{-1}$	Initial H_2O , mol $\times 10^4$	Final H_2O , mol $\times 10^4$	
				Expt	Calcd
Na	3.00	0.0133	1.70	-0.07	0.15
Na	3.00	0.133	1.70	1.12	1.0
Rb	2.86	0.133	1.70	1.19	1.0

ume flow rate. For laminar flow and transforming heat-transfer correlations to mass-transfer correlations,¹⁰ the expression for K_m is

$$K_m = 1.86D(Re Sc)^{1/3}l^{-1/3}d^{-2/3} \quad (6)$$

where D is diffusivity of the pair, H_2O -Ar, Re and Sc are the Reynolds and Schmidt numbers, and l is the length of the reaction zone. The Reynolds numbers, given by $d\nu\rho/\eta$ where ν is the flow velocity, ρ is the density, and η is the coefficient of viscosity, are 79.1 and 791, respectively, for the low and high flow rates used. These values are within the laminar flow region. The Schmidt number is given by $Sc = \eta/\rho D$. Substitution of the expressions for Re and Sc and integration yields

$$c/c_0 = \exp[-1.86(4)^{1/3}(\pi l D/F)^{2/3}] \quad (7)$$

The diffusivity calculated from a developed expression for water with a nonpolar gas¹¹ yielded $D = 0.24 cm^2 sec^{-1}$ for the binary mixture H_2O -Ar. The calculated values of c/c_0 were 0.09 and 0.60 for the low and high flow rates employed. Using these values, the moles of water remaining in the flow stream after passing over the mirror were calculated and are given in the last column of Table II. Although eq 7 probably yields values accurate to only some $\pm 20\%$, a comparison of the experimental and calculated values makes it reasonable to conclude that a correct model was chosen and that every collision of water with the mirror surface results in removal of the water.

Static Experiments and the Mass Action Expression. Because of the difficulty of reproducing conditions which depend upon deposition of a metal mirror and introduction of water vapor, it might be expected that the results obtained would be greatly influenced by experimental parameters. However, it may be concluded that within wide limits this is not the case. The results shown in Figure 1 indicate that isotope fractionation and composition of the evolved gas are invariant with metal to water ratios from below unity to above 180. Further evidence that precise duplication of experimental conditions is not important is shown in Figure 2, a comparison of our current results for sodium with those obtained in previous experiments.⁵ The experimental points for both studies are shown, but the curve is based on the present work. The earlier results were obtained with a somewhat different geometry and a much different method of water vapor introduction. Further worth noting, but not so important, the analytical method in the earlier work was glpc while in the current work it was mass spectrometry.

Table I shows that there is a significant difference in separation factors among the metals, although not uniformly throughout. However, over most of the range, the order of fractionation effectiveness for production of protium in the evolved gas is $Na \cong K < Li < Rb \cong Cs$. Representations such as Figure 2 for the other metals yield similar curves with, however, different abscissa values for

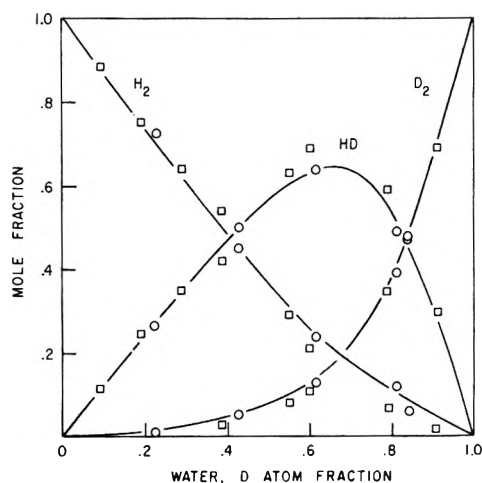


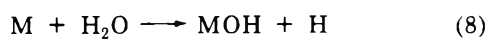
Figure 2. Composition of molecular hydrogen from sodium mirrors as a function of water composition: O, this study; □, Leyshon and Volman.⁵ Curves based on this study.

the maximum in the HD curve. The atom fraction of D in water corresponding to these positions are Li, 0.72; Na, 0.68; K, 0.67; Rb, 0.74; and Cs, 0.74.

Although plots of gas composition *vs.* atom fraction of D in water are not the same, if atom fraction D in the evolved gas rather than in water is chosen as the axis, the plots are the same within the error of reproducibility of the experiments. The experimental points for such a plot are shown in Figure 3. The curve drawn in this figure was, however, not constructed from the experimental points but instead has been calculated taking $Q = 12.0$ for the mass action expression of eq 3. The average value of Q using all the points in the diagram for calculation is 12.0 ± 2.6 with 80% of the experimental values within these limits. No identifiable trend was observed for the variation of Q with composition or among the metals.

The equilibrium constant for the expression calculated from the Gibbs energy of formation, $\Delta G_f^\circ_{298} = -1.46 \text{ kJ mol}^{-1}$, for HD^{12} is $K = 3.26$. Clearly the molecular hydrogens are not at equilibrium. Also, as will be shown below, the value of Q cannot be achieved by mixing the products formed from a succession of instantaneous equilibria.

Models for the Value of Q . From the results of the flow experiments it can be taken that every molecule which reaches the metal surface reacts, although adsorption of water vapor prior to reaction is not excluded. In the absence of other information, it seems valid to proceed from the simplest mechanistic premise which, using H_2O as an example, is



the proven gas-phase reaction.¹³ Now we may consider that the hydrogen atoms formed are freely mobile, either on the metal surface or in the gas phase adjacent, or are initially bound to the surface. The bound atoms may be considered to be either strongly bound, in which case ordinary kinetic interpretations will apply, or weakly bound, in which case quantum mechanical tunneling will be important.

Assuming steady-state concentrations, it is possible to consider the correspondence of the models with the experimental value of Q . However, it is more realistic to assume that steady-state conditions are not achieved, in which case the system may be treated as a succession of steady states. At each steady-state interval, the same

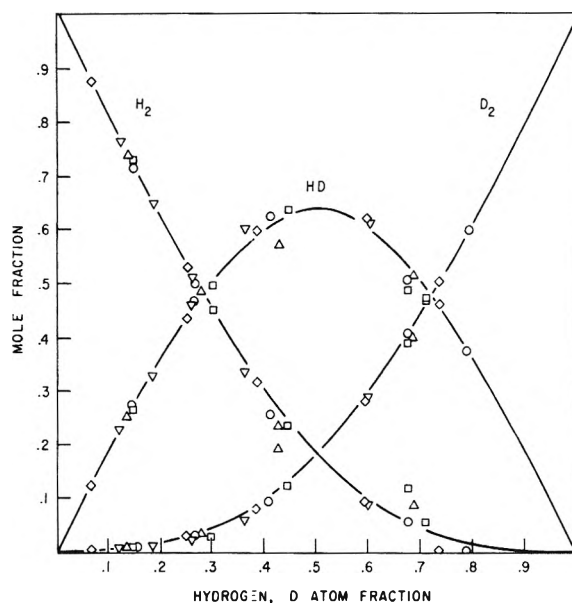


Figure 3. Composition of molecular hydrogen as a function of atom fraction D in the gas: O, Li; □, Na; Δ, K; ∇, Rb; ◇, Cs. Curve calculated with $Q = 12.0$.

value of Q will result for that portion of the product formed during the steady-state time interval; but summation of the products from the various steady-state intervals will not yield Q . That such a summation for this system will lead to a value $\leq Q$ may be seen from the following argument. Consider two time intervals, a and b , during which the system is in a steady state. Then

$$\frac{([\text{HD}]_a + [\text{HD}]_b)^2 / ([\text{H}_2]_a + [\text{H}_2]_b)([\text{D}_2]_a + [\text{D}_2]_b)}{[\text{D}_2]_b} = Q_{a+b} \quad (9)$$

which yields

$$\frac{\frac{1}{2} + f_{\text{H}_2}f_{\text{D}_2}/2 + (f_{\text{H}_2}f_{\text{D}_2})^{1/2}}{\frac{1}{2} + f_{\text{H}_2}f_{\text{D}_2}/2 + (f_{\text{H}_2} + f_{\text{D}_2})/2} = \frac{Q_{a+b}}{Q} \quad (10)$$

were $f_{\text{H}_2} = [\text{H}_2]_a/[\text{H}_2]_b$ and $f_{\text{D}_2} = [\text{D}_2]_a/[\text{D}_2]_b$. The first two terms in the numerator and denominator of the left-hand side are the same and the relative values of numerator and denominator are determined by a comparison of the third terms. The ratio of these quantities, $(f_{\text{H}_2}f_{\text{D}_2})^{1/2} / [(f_{\text{H}_2} + f_{\text{D}_2})/2]$, is just the ratio of the geometric mean to the arithmetic mean which for positive quantities is ≤ 1 . Therefore $Q_{a+b} \leq Q$. Inclusion of additional intervals, leads to the same conclusion, $Q_{\Sigma} \leq Q$.

We have considered some models which yield unsatisfactory conclusions. A model in which freely mobile hydrogen atoms on the surface combine to form molecular hydrogen yields $Q = 4.2$, much too low. The Rideal mechanism, reaction of a free atom with an adatom,¹⁴ does not yield a value of Q but, using the experimental value of Q , gives a difference in zero-point energies, $E^\circ_{(\text{M}-\text{H})} - E^\circ_{(\text{M}-\text{D})}$, of 4.8 kJ mol^{-1} considerably higher than the average difference in zero-point energies, $(E^\circ_{\text{M}-\text{H}} - E^\circ_{\text{M}-\text{D}}) = 1.94 \text{ kJ mol}^{-1}$, for the five alkali hydrides.¹⁵ Thus this model leads to adatom molecules $\text{M}-\text{H}$ and $\text{M}-\text{D}$ in which the binding is considerably stronger than in the true hydrides. Also, this model predicts $(Q_{353}/Q_{296}) < 0.8$, contrary to the experimental result. If single hydrogen atoms are considered bound to several metal atoms, the zero-point energy per bond would be reduced accordingly, but the predicted temperature effect on Q would not be

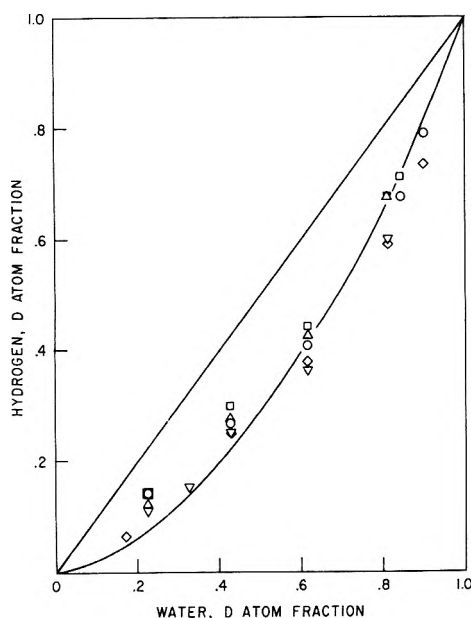
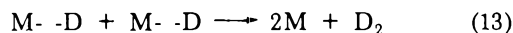
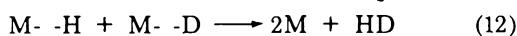
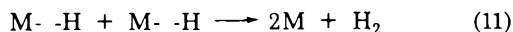


Figure 4. D in molecular hydrogen as a function of water composition. Curve calculated with $(k_1/k_2) = 14.0$. Straight line represents zero fractionation: O, Li; □, Na; △, K; ▽, Rb; ◇, Cs.

changed. Modification of the above to consider initial equilibrium between free atoms and adatoms leads to similar conclusions.

Having rejected the above models, we proceed now to consider atom tunneling. (It may be noted that Horiuti and Szabo stated that Polanyi suggested that atom tunneling would be important in the reaction of water vapor with sodium.) Consider that reaction occurs by tunneling of one adatom to a second adatom which may be represented by the equations



The corresponding relative rates of formation of molecular hydrogen are

$$\begin{aligned} d[H_2]/dt &= P_1[M\cdot -H]^2 \\ d[HD]/dt &= (P_1 + P_2)[M\cdot -H][M\cdot -D] \\ d[D_2]/dt &= P_2[M\cdot -D]^2 \end{aligned} \quad (14)$$

where P_1 and P_2 are the tunneling probabilities of H and D. These expressions yield

$$\frac{[d[HD]/dt]^2/[d[H_2]/dt][d[D_2]/dt]}{(P_1/P_2) + 2 + (P_2/P_1)} \quad (15)$$

For time intervals during which $[M\cdot -H]/[M\cdot -D]$ may be considered constant, eq 15 will also represent the mass action value Q for molecular hydrogen produced during the time interval. From the experimental value of Q , calculation yields $P_1/P_2 = 9.90$.

The simplest model for tunneling to consider is transfer of an adatom through a rectangular barrier. For this model the transmission coefficient is approximately given by $T_E = \exp[-(4\pi/h)(2mV)^{1/2}d]$ ¹⁶ where d is the thickness of barrier and V is the height (energy) of the barrier relative to the energy of the adatom, the effective energy barrier for transfer of an atom on the surface. Then for H and D

$$P_1/P_2 = \exp[(4\pi/h)(2V)^{1/2}(m_D^{1/2} - m_H^{1/2})d] \quad (16)$$

To calculate V it is necessary to assume a value for d . It seems not unreasonable to take a value of 0.5 Å, in the range of expectation for the difference in distance between separated atoms and the maximum extension in a vibrational state corresponding to a weakly bound molecule. This value of d yields $V = 6.0 \text{ kJ mol}^{-1}$.

Equation 16 indicates that the effect of temperature on P_1/P_2 depends on the value of V . The height of the barrier will not be affected by temperature but the energy of the adatom will be. The maximum effect would appear to be a change of $\frac{1}{2}k\Delta T$ associated with translational motion in the direction of the barrier. The only experimental result, Table I, we have on temperature variation is for sodium at 80°. Allowing V to diminish by $\frac{1}{2}k\Delta T$ yields $P_1/P_2 = 9.0$ and $(Q_{353}/Q_{296}) = 0.93$. For the single result we have $(Q_{353}/Q_{296}) = 0.94$. The only significance we attach to these values is that they predict a small temperature effect and that the experimental results are not inconsistent with the prediction.

From the above discussion, we conclude that tunneling is in reasonable accord with the experimental results. Thus we propose that reaction of water with the surface results in an adatom which in order to yield molecular hydrogen must transfer and react with an adatom. It should be noted that the calculated value of V is only a very rough approximation as it depends not only on a model for the barrier shape and thickness but also on the instantaneous Q values rather than Q_Σ which was used. As discussed earlier the instantaneous Q values is probably higher which would consequently lead to a higher value of V . Nevertheless, the value of V we have calculated seems reasonable.

Isotope Fractionation. In accordance with the above model, consider that every water molecule which reaches the surface reacts to yield a hydrogen atom. Consequently fractionation will occur only through the HOD molecule in accordance with



Since reactions 17 and 18 have the same reactants

$$E_2 - E_1 = [E_{0(MOH)} - E_{0(MOD)}] - [E_{0(M\cdot -H)} - E_{0(M\cdot -D)}] \quad (19)$$

The zero-point energy difference $E_{0(MOH)} - E_{0(MOD)}$ may reasonably be expected to be not far different from $E_{0(OH)} - E_{0(OD)}$, 6.5 kJ mol⁻¹. On the basis of our model, $E_{0(M\cdot -H)} - E_{0(M\cdot -D)}$ is probably negligible. With $E_2 - E_1$ taken as 6.5 the corresponding value of k_1/k_2 is 14.0. From the value of k_1/k_2 and the molecular composition of water vapor, the isotopic fractions in the evolved gas may be calculated. The composition of the water vapor was calculated from the constant, $K_{298} = 3.85$,¹⁷ for the equilibrium



From the foregoing, the atom fraction of D in the hydrogen gas is

$$N_D = (N_{HOD}/[1 + (k_1/k_2)]) + N_{D_2O} \quad (21)$$

where N_{HOD} and N_{D_2O} represent mole fractions. The atom fraction of D in the evolved gas as a function of water composition is shown in Figure 4. The straight line represents no fractionation, $\alpha = 1.0$. The curve is the calculated

ed value using $(k_1/k_2) = 14.0$. The calculated curve is in general agreement with the experimental results also shown in the figure.

Assignment of values to $E_{0(M-H)} - E_{0(M-D)}$ would yield increasing values of k_1/k_2 going from Cs to Na, in accord with the effectiveness of fractionation except for Li which would remain anomalous. However, any reasonable values for this difference in zero-point energies would not change the calculated curve appreciably. Also exchange of water vapor with hydroxide previously formed on the surface could play a role. It should be emphasized that we have considered only the systems with metal in excess. Where water is in large excess, Figure 1, fractionation may be considerably greater. Thus for $(Na/H_2O) = 0.005$, the corresponding fractionation factor is $\alpha = 7.6$ for 0.842 atom fraction D in water rather than $\alpha = 2.2$ for $(Na/H_2O) \cong 3$. A more complete model which can explain this difference as well as the differences among the metals remains for the future.

Acknowledgment. This research was supported, in part, by the National Science Foundation. We are grateful to Professors C. P. Nash and N. A. Dougharty for helpful discussions.

References and Notes

- (1) A. Farkas and L. Farkas, *Nature (London)*, **133**, 139 (1934).
- (2) C. D. Davis and H. L. Johnston, *J. Amer. Chem. Soc.*, **56**, 492 (1934).
- (3) E. D. Hughes, C. K. Ingold, and C. L. Wilson, *J. Chem. Soc.*, 492 (1934).
- (4) H. L. Johnston and C. D. Davis, *J. Amer. Chem. Soc.*, **64**, 2613 (1942).
- (5) L. J. Leyshon and D. H. Volman, *J. Amer. Chem. Soc.*, **87**, 5565 (1965).
- (6) J. Horiuti and A. L. Szabo, *Nature (London)*, **133**, 327 (1934).
- (7) I. Kirshenbaum, "Physical Properties and Analysis of Heavy Water," McGraw-Hill, New York, N. Y., 1951, p 348.
- (8) H. Melville and B. G. Gowenlock, "Experimental Methods in Gas Reactions," 2nd ed, Macmillan, London, 1964, p 165.
- (9) R. B. Bird, W. E. Stewart, and E. N. Lightfoot, "Transport Phenomena," Wiley, New York, N. Y., 1960.
- (10) Reference 9, pp 399 and 645.
- (11) Reference 9, p 505.
- (12) "Selected Values of Chemical Thermodynamic Properties," *Nat. Bur. Stand. (U.S.), Tech. Note*, No. 270-3, 12 (1968).
- (13) W. S. Cathro and J. C. Mackie, *Trans. Faraday Soc.*, **68**, 150 (1972).
- (14) A. Gelb and S. K. Kim, *J. Chem. Phys.*, **55**, 4935 (1971).
- (15) Values for this and all subsequent calculations based on spectroscopic values taken from G. H. Herzberg, "Molecular Spectra and Molecular Structure I. Spectra of Diatomic Molecules," 2nd ed, Van Nostrand, Princeton, N. J., 1950, Table 39, p 501, *et seq.*
- (16) V. Rojansky, "Introductory Quantum Mechanics," Prentice-Hall, New York, N. Y., 1938, p 221.
- (17) M. Wolfsberg, A. A. Massa, and J. W. Pyper, *J. Chem. Phys.*, **53**, 3138 (1970).

Adsorption of Gases on Gold Films

J. M. Saleh

Department of Chemistry, College of Science, Baghdad, Adamiya, Republic of Iraq (Received January 26, 1973)

The interaction of SO₂, CS₂, H₂S, and N₂O with evaporated Au films has been investigated in the temperature range -80 to 200°. Strong chemisorption as well as weak reversible adsorption occurred on Au film at -80° with SO₂ and N₂O. Adsorption of CS₂ and H₂S on the film at such a temperature was molecular but irreversible. Further chemisorption on Au took place only with H₂S above 100° and was accompanied by H₂ evolution. A mixed film of Au-Ni, prepared by deposition of Au on a film of Ni, was shown to be more reactive with gases (N₂O and SO₂) than Au film. This was attributed to the formation of a solid solution which had either a greater tendency for gas uptake than Au or through which the Ni atoms could move to the surface to interact with the gas molecules. Extensive SO₂ or CS₂ uptake was observed on Au at -80° when a W filament was heated in the gas to temperatures $\geq 1000^\circ$. An appreciable fraction of the adsorbed SO₂ or CS₂ was desorbed when the current of the W filament was switched off and the Au film was heated to $\geq 30^\circ$. Adsorption, with the formation of an unstable gas-solid solution, and incorporation were assumed to occur in Au at -80° on heating a W filament in SO₂ or CS₂. Tungsten sulfide which may be formed by circulating H₂S gas on a heated W filament is unstable above 1000° resulting probably in the desorption of sulfur atoms. These atoms are expected to be trapped ultimately by the film which is maintained at -80°.

Introduction

A metal film of Au tends to chemisorb, between -183 and 0°, such gases as CO, C₂H₄, and C₂H₂ but is inactive toward N₂, H₂ and O₂.^{1,2} The data available are generally qualitative as the results are only expressed as "gas chemisorbed" or "gas not chemisorbed." There is a need for more fundamental and quantitative studies on this metal over a wider range of temperatures. The present paper describes such an attempt using SO₂, CS₂, H₂S, and N₂O;

the interaction of these gases with other metals has been discussed elsewhere.³⁻⁶

Adsorption of these gases was also studied on Au films (mixed films) which had been deposited on films of Ni or Pd; it was thus possible to determine the effect of these substrates on the reactivity of Au films at various temperatures. The work was further extended by studying the effect of a heated tungsten filament on subsequent adsorption of gases on Au films.

Experimental Section

The apparatus, the materials, and the experimental techniques have been described.³⁻⁶ Gold films were prepared from 0.5-mm wire which was obtained from Johnson Matthey Chemicals Ltd. A known length (4 cm) of the wire was supported on a tungsten coil, prepared from 0.2-mm W wire, and the latter was heated electrically. The W coil was first degassed in the absence of the Au wire, and the same coil was used for up to five evaporations, thereby reducing contamination to a minimum. The evaporation current was 2.5 A and the reaction vessel was kept open to the pumps throughout the degassing of the filament and the subsequent preparation and sintering of the film. Each film was sintered at 70° for 20 min and, thereafter, its area was measured by krypton adsorption at -195°. A pirani gauge was calibrated^{7,8} for known pressures of each of the gases SO₂, CS₂, H₂S, N₂O, N₂, and H₂ and the gauge was used for the analysis of the gas phase.

Mixtures of H₂ + H₂S and N₂ + N₂O were also analyzed by condensing the latter gas of each couple in a cold glass finger which was immersed in liquid nitrogen. Mixed films (Au/Ni and Au/Pd) were prepared and sintered by similar procedures to those described before.^{6,9} Temperatures of the W filament, consisting of 0.2-mm diameter tungsten wire about 10 cm long which was used for thermal activation or dissociation of gases, were measured with an accuracy of ±20° using an optical pyrometer.

The extent of gas uptake was expressed as $\theta = V_g/V_{Kr}$, where V_g was the volume of gas adsorbed and V_{Kr} was the volume of krypton monolayer on the film surface. The volumes were expressed in units of μl (STP) and each unit of adsorbed krypton is equivalent to an area of 52.4 cm² assuming a cross-sectional area of 0.195 nm² for the krypton atom.

Results and Discussion

Adsorption of Gases between -80 and 200° SO₂. There was an instantaneous rapid SO₂ adsorption on Au film at -80°; the amount adsorbed under a gas pressure of 5 Nm⁻² corresponded to $\theta \simeq 3.2$. About 2/3 of the adsorbed gas was desorbed within ~2 min at the same temperature, hence decreasing the value of θ to about 1.2. No further SO₂ desorption occurred even when the film was heated to about 200°.

Confirmation that desorption is likely to take place even at -80° can be obtained from the relation

$$\tau = \tau_0 \exp(Q/RT) \quad (1)$$

relating the lifetime (τ) of an adsorbed molecule to both the latent heat of adsorption (Q) and the time of the oscillation of the molecules in the adsorbed state which could be taken as 10⁻³ sec. If Q is taken to be equal to the latent heat of liquefaction (*i.e.*, 25 kJ mol⁻¹) and $T = 195$ K, then τ would be about 10⁻⁷ sec.

CS₂. Fast irreversible adsorption of CS₂ occurred on Au film at -80°, at an initial pressure of 6 Nm⁻², until the value of θ was 1.0; the rate of uptake at this coverage became 10⁻⁴ $\mu\text{l sec}^{-1} \text{cm}^{-2}$. Further CS₂ uptake was not observed at any temperature below 200°. Thus, with CS₂ no weak reversible adsorption was possible at -80° unlike the behavior of SO₂; the latter gas has a considerably lower boiling point (SO₂, -10°) than the former (CS₂, 46.25°).

H₂S. There was an initial fast H₂S uptake on Au film at -80° by which θ became 1.2, and this was followed by a

rate process. At $\theta = 1.5$ the rate of H₂S adsorption decreased to below 10⁻⁴ $\mu\text{l sec}^{-1} \text{cm}^{-2}$. No H₂ was desorbed at -80° or even on warming the film to 30° suggesting molecular chemisorption of H₂S on Au at -80°, the molecules being coordinated to the surface through sulfur atoms.¹⁰ The Au film does not tend to chemisorb hydrogen in the temperature range -80 to 30°^{1,2} and if H₂S adsorption on this metal was associated with dissociation the evolution of H₂ would have been expected. Further, but very slow, adsorption of H₂S began at temperatures >100° with an activation energy of 25 kJ mol⁻¹ and the process was accompanied by H₂ evolution. The complete breakdown of H₂S on Au is assumed to take place at such temperatures because the total gas pressure remained constant and for each H₂S molecule which was adsorbed one molecule of H₂ appeared in the gas phase. The slowness of the sulfidation process, despite the low energy of activation, may be accounted for on the basis of a low preexponential factor resulting mainly from a low concentration of special sites on the film surface.

When a mixture of SO₂ + H₂S (50% each) with a total pressure of 8 Nm⁻² was admitted to an Au film at -80°, the gas adsorbed involved about 80% H₂S and 20% SO₂; the final value of θ was 1.2, taking into consideration the adsorbed volumes of both gases. This result may suggest a greater activity of Au film toward H₂S than for SO₂; adsorption of H₂S is likely to be accompanied with a higher heat than of SO₂. Similar results were obtained with CS₂ + H₂S mixtures although the percentage of the latter (H₂S) gas in the adsorbate was comparatively less (about 70%) than that given for former mixture (SO₂ + H₂S).

N₂O. The uptake of N₂O on Au at -80° and $P(\text{N}_2\text{O}) = 6$ Nm⁻² was rapid and took place only to the extent $\theta = 0.85$; the change in coverage with time at this value became negligible. About 60% of the adsorption was weak and reversible and could be removed either by pumping down to 10⁻² Nm⁻² or on warming the film to 30°, and a similar amount of N₂O could be re-adsorbed on the film at the former temperature. The small amount of N₂O chemisorption on Au film may be a consequence of the rapid decrease in the heat of N₂O adsorption with coverage. Also, Au film does not tend to adsorb N₂ or O₂¹ and this probably accounts for the absence of dissociation on Au despite the low dissociation energy of the N=O bond in N₂O (159 kJ mol⁻¹).

Mixed Films. Surface Area. An Au film which was deposited on the surface of a glass reaction vessel (area = 200 cm² = 4 μl of krypton) at -195° and subsequently heated *in vacuo* (10⁻⁴ Nm⁻²) to 70° for 20 min was found to acquire almost twice the geometric area of the glass substrate. When the substrate, on which the Au film was deposited, was a metal film of Pd or Ni the area of the former film (Au) was substantially greater than the geometric area of the reaction vessel. This is indicated for two typical experiments in Table I. Films of Au with much larger areas ($V_{Kr} > 30 \mu\text{l}$) could be obtained provided the area of the underlying Pd or Ni film was greater than $V_{Kr} = 40 \mu\text{l}$ (Table I). Each Pd or Ni film was sintered (at 70° for 20 min) before the deposition of the Au film. Such films of Au on Pd or on Ni are described as mixed films and represented in this paper as Au/Pd and Au/Ni, respectively.

Adsorption on Mixed Films. N₂O adsorption at -80° and a pressure of 6 Nm⁻² on Au/Pd or Au/Ni was molecular and occurred to the extent $\theta = 0.8$; most of the adsorbate could be removed by warming the film to 30°C. This

TABLE I: The Weight and the Area of Au Films Which Were Deposited on Pd or Ni Films^a

Metal substrate		Au film				
Metal	Wt. mg	(area) ₂ , μl of Kr	Wt. mg	(area) ₃ , μl of Kr	(area) ₃ / (area) ₂	(area) ₃ / (area) ₁
Pd	43	30	61	21	0.7	5.25
Ni	40.5	42	60	30	0.71	7.50

^a The area of the glass reaction vessel is represented (area)₁.

behavior is identical with that observed with Au film at such temperatures. No further adsorption took place on Au/Pd film at any temperature below 200°. This is expected because the Au film does not chemisorb N₂O or O₂ at similar temperatures and the tendency of Pd film for taking up these gases is also small and very limited.^{6,9}

Slow N₂O uptake, with complete dissociation and subsequent N₂ evolution, occurred on the Au/Ni film above 50° and the rate increased with temperature; an activation energy of 40 kJ mol⁻¹ was determined for N₂O adsorption, in the temperature range 60–160°, which was independent of the values of θ in the range 1.5–3.1. These results probably reflect the difference in activity between Ni and Pd toward N₂O; the former metal is known⁶ to be far more active for interaction with the gas than the latter metal. Because of the close similarity between the atomic diameters of Pd (0.274 nm) and Au (0.288 nm) there is little possibility for the formation of a solid solution or an alloy by the Au/Pd system at temperatures <200°. On the other hand, such possibility is greater with the Au/Ni system due to the smaller diameter of Ni (0.248 nm), and also Ni is a slightly lower melting metal than Pd; the melting points of Ni and Pd are 1455 and 1554°, respectively. Ni atoms are likely to diffuse into the Au phase at temperatures >60° forming a solid solution which may be more active toward N₂O than Au. Moreover, the outward diffusion of Ni atoms through the Au–Ni phase may result in a direct contact of these atoms with the gas. A factor which may facilitate the latter process is the high tendency of Ni atoms for oxygen and consequently the large electric field that arises from the chemisorbed oxygen layer on the metal surface; such an electric field may play an important role in bringing out Ni atoms to interact with the gas.^{6,9}

At –80° and $P(\text{SO}_2) = 5 \text{ Nm}^{-2}$, SO₂ gas was rapidly adsorbed on Au/Pd and Au/Ni films until θ was 1.1–1.2. About 50% of the adsorption on each film at this temperature was reversible. Desorption of SO₂ continued on raising the temperature of the Au/Pd film to 100°; at this temperature the value of θ became about 0.5 within 30 min. The remainder of the adsorbed SO₂ on Au/Pd was stable up to 200° and further SO₂ adsorption in the temperature range 100 to 200° was extremely slow; the value of θ increased at 150° to 0.54 in about 60 min. With the Au/Ni system, SO₂ desorption was observed at 30° and the value of θ decreased to 0.6. Above 50°C, there was a slow adsorption of SO₂ on the Au/Ni film and the rate increased with temperature. An activation energy of 50 kJ mol⁻¹ was determined from the rates of SO₂ uptake at two different temperatures in the range 80–150°, but virtually the same value of θ ; the energy of activation was the same for values of θ from 1.0 to 2.7.

The interaction of the mixed films with SO₂ at –80° was in general similar to that of Au film. The difference in behavior of the two films Au/Pd and Au/Ni toward the

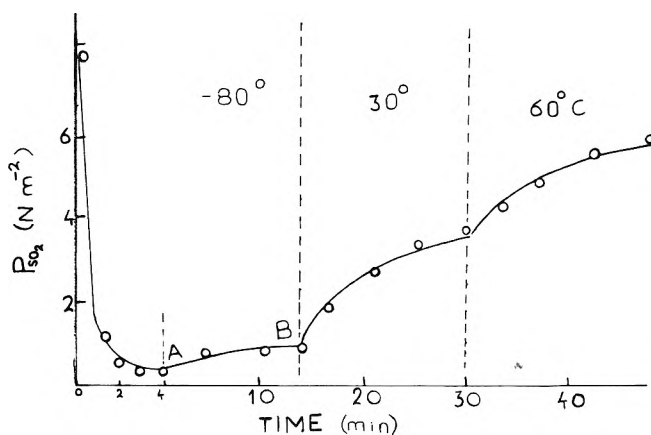


Figure 1. Uptake of SO₂ in one dose on an Au film which was kept at –80° on heating a W filament in the gas to 1300°. At point A on the graph the current of the filament was switched off and at B the film was warmed to temperatures greater than –80°.

TABLE II: Activation Energies (E) for Gas Uptake at Various Filament Temperatures While Au Film Was Kept at –80°

Gas	Temp range, °C	E, kJ mol ⁻¹
SO ₂	1000–1300	60
CS ₂	1000–1250	40
H ₂ S	1000–1270	20

gas began at temperatures >50° owing, as discussed above, to the contribution of Ni atoms to the activity of the latter system throughout its interaction with SO₂. It has been found¹¹ that Ni atoms react to a much higher extent with SO₂ than of Pd; the reaction of the gas with the latter is only limited to the surface phase.¹¹

Effect of the Heated W Filament on Gas Uptake. Further gas adsorption (SO₂, CS₂, and H₂S) on Au film, which was maintained at –80°, was only observed when a W filament was heated in the gas to the temperatures ≥1000°. The rate of uptake increased with an increase of both the filament temperature and the gas pressure. From the rates of gas uptake at two filament temperatures in the range 1000–1300° but the same film temperature (–80°), activation energies were obtained and the values which are given in Table II were shown to be independent of temperature in this range. Extensive gas uptake occurred at a constant rate provided the filament temperature and the gas pressure were kept constant. The extent of adsorption, at a filament temperature of 1300° and a gas pressure of 8 Nm⁻², in a period of 5 min corresponded to θ values which ranged from 8 to 10.

SO₂ and CS₂. At the same filament temperature, the Au film tended to take up in a given time more SO₂ than CS₂; at a filament temperature of 1300° the rates of SO₂ and CS₂ uptake, in the presence of an Au film which was cooled to –80°, were 0.1 and 0.034 μl sec⁻¹ cm⁻² when other conditions were almost identical. When the current of the W filament was switched off, desorption was observed in the case of SO₂ and CS₂. The rate of desorption increased considerably when the Au film was heated to higher temperatures (30–100°), and the results for a typical experiment with SO₂ are shown in Figure 1. Activation energies of 40 and 30 kJ mol⁻¹ were determined from desorption rates at 30 and 60° for SO₂ and CS₂, respectively, for values of θ in the range 10–7.0. The lower energy of activation with CS₂ as compared with that of SO₂

suggests probably a weaker attachment of CS₂ molecules to Au surface than of SO₂. About 50–60% of the adsorbed gas, due to filament heating, was desorbed on heating the Au film in the absence of the filament current to 100° for 30 min. Analysis of the gas phase subsequent to desorption experiments by a precalibrated pirani gauge^{7,8} showed that the desorbed gas was entirely SO₂ or CS₂ depending on the nature of the adsorbed gas; no other products were ever observed in these experiments.

The amount of gas adsorbed by this technique was sufficiently large and continued to be larger than $\theta = 20$ so long as the W filament was kept hot (at $\geq 1000^\circ$) and the gas supply was maintained. To account for such large gas uptake, the following may be relevant.

1. Since the amount adsorbed was far in excess of the quantity which could possibly be adsorbed on the film surface at any temperature, it is likely that the process involved *absorption* associated probably with the formation of a comparatively unstable compound in the bulk of the solid. The W filament seems to provide thermally activated SO₂ or CS₂ molecules which can diffuse into the solid Au similar probably to the diffusion of certain gases in Pd, Ag, and other metals.¹²

2. A fraction of the molecules which were desorbed may involve those which were weakly chemisorbed in addition to physically adsorbed molecules.

3. Some incorporation of SO₂ or CS₂ in Au is also possible because the amount of the gas that was retained by the solid, when the desorption rate at 100° became negligibly small, was appreciable and corresponded in most cases to $\theta = 6-8$.

A fraction of the gas molecules may undergo dissociation by the heated W filament and the resulting species are likely to be adsorbed on the film of Au. This may account for the observed irreversible adsorption and the subsequent incorporation of SO₂ and CS₂ on the metal.

H₂S. A W filament heated to $\sim 1000^\circ$ in H₂S gas caused further ($\theta > 1.5$) gas uptake on an Au film which was kept at -80° . The initial adsorption was rapid and occurred without H₂ evolution. This was followed by a slower process in which the volume of the desorbed hydrogen was equivalent to that of the adsorbed H₂S. At a filament temperature of 1300° and an initial pressure of 8 Nm⁻², the rate of uptake was 0.16 $\mu\text{l sec}^{-1} \text{cm}^{-2}$, which is slightly greater than that of SO₂ (0.1 $\mu\text{l sec}^{-1} \text{cm}^{-2}$). The activation energy which was obtained from the uptake rates at filament temperatures of 1000 and 1300°, but the film temperature of -80° , is given in Table II. The only product observed by careful analysis of the gas phase was H₂.

With the heated W filament mainly the breakdown of H₂S molecules on the filament surface is expected. In addition, some thermally activated H₂S molecules may also be produced by the action of the hot wire on the gas. The

initial rapid H₂S uptake with little H₂ evolution may be ascribed to the existence of the latter type of H₂S which may undergo molecular adsorption on the Au film at -80° . When the current of the W filament was turned off and the film was warmed from -80 to 30° there was some H₂S desorption, the amount being 20% of that adsorbed in the dose.

It has been found from field emission studies¹³ that hydrogen atoms, resulting from H₂S adsorption on a tungsten tip, were unstable on the tungsten surface at temperatures $\geq 1000^\circ$ and the observed desorption patterns above this temperature were very similar to those obtained when sulfur was initially adsorbed on the clean tip and the latter was subsequently heated to similar temperatures. Moreover, the vapor pressure of tungsten sulfide is 10⁻² Nm⁻² at 1000°¹⁴ so that if the chemisorbed layer behaves like bulk sulfide one would expect to observe sulfur desorption at such temperatures, and at higher temperatures more desorption and sulfur removal are expected. In the same field emission work¹³ an activated energy of 380 kJ mol⁻¹ was obtained from the desorption of sulfur from tungsten; with such values of energy the lifetime of an adsorbed sulfur atom (eq 1) on tungsten was estimated to be just under 1 sec.

It appears that sulfur atoms, resulting from H₂S dissociation on W filament, are probably captured by the Au film while H₂ enters the gas phase. The high tendency of the Au film for sulfur adsorption may account for a substantially greater rate of H₂S adsorption in presence of an Au film than when the film was absent; the latter was about 25% of the former. The ease of sulfur removal from the W filament and the continuous regeneration of tungsten sites for subsequent H₂S dissociation may account for the higher rate of H₂S uptake by this technique.

References and Notes

- (1) B. M. W. Trapnell, *Proc. Roy. Soc., Ser. A*, **218**, 566 (1953).
- (2) A. Couper and D. D. Eley, *Discuss. Faraday Soc.*, **8**, 172 (1950).
- (3) J. M. Saleh, *Trans. Faraday Soc.*, **64**, 796 (1968).
- (4) J. M. Saleh, *Trans. Faraday Soc.*, **65**, 259 (1969).
- (5) J. M. Saleh, *Trans. Faraday Soc.*, **67**, 1830 (1971).
- (6) S. A. Isa and J. M. Saleh, *J. Phys. Chem.*, **76**, 2530 (1972).
- (7) J. M. Saleh, C. Kemball, and M. W. Roberts, *Trans. Faraday Soc.*, **57**, 1771 (1961).
- (8) J. M. Saleh, M. W. Roberts, and C. Kemball, *Trans. Faraday Soc.*, **58**, 1642 (1962).
- (9) Y. M. Dadiza and J. M. Saleh, *J. Chem. Soc., Faraday Trans. 1*, **68**, 1513 (1972).
- (10) M. H. Dilke, D. D. Eley, and E. B. Maxted, *Nature*, **161**, 804 (1948).
- (11) J. M. Saleh, *Trans. Faraday Soc.*, **66**, 242 (1970).
- (12) B. M. W. Trapnell, "Chemisorption," Butterworths, London, 1955, p 6.
- (13) J. M. Saleh, M. W. Roberts, and C. Kemball, *J. Catal.*, **2**, 189 (1963).
- (14) J. W. Mellor, "A Comprehensive Treatise on Inorganic and Theoretical Chemistry," Vol. 11. Longmans, Green and Co., London, 1931, p 853.

Temperature-Dependent Splitting Constants in the Electron Spin Resonance Spectra of Cation Radicals. IV.¹ The Ethoxy Group

Paul D. Sullivan

Department of Chemistry, Ohio University, Athens, Ohio 45701 (Received March 8, 1973)

Publication costs assisted by the Petroleum Research Fund and the Ohio University Research Institute

The temperature dependence of the proton splitting constants of a series of ethoxy substituted cation radicals has been measured. Particular attention has been paid to the magnitude and temperature coefficients of the splittings from the β - and γ -ethoxy protons. Qualitative conclusions regarding the molecular conformation of the ethoxy group have been drawn from the β -ethoxy proton splitting constants. INDO calculations on the ethoxymethyl radical and ethanol cation radical have been used to rationalize the β - and γ -ethoxy proton splittings. The averaged β -alkoxy proton splittings are given by $a_{\beta^H} = Q_{O^{\beta-H}}\rho_{O^\pi} + Q_{C^{\beta-H}}\rho_{C^\pi}$, where $Q_{O^{\beta-H}} = +33.4$ G and $Q_{C^{\beta-H}} = -4.99$ G. Similarly the γ -alkoxy proton splitting is given by $a_{\gamma^H} = Q_{O^{\gamma-H}}\rho_{O^\pi} + Q_{C^{\gamma-H}}\rho_{C^\pi}$ where $Q_{O^{\gamma-H}}$ and $Q_{C^{\gamma-H}}$ depend on the dihedral angle about the O-C (alkyl) bond. Good agreement for the freely rotating γ proton is found between the experimental and calculated splitting constants.

Introduction

Previous papers in this series have studied the temperature dependence of the methoxyl and hydroxyl proton splitting constants¹⁻³ in a number of cation radicals in an effort to obtain potential barriers to rotation. It is the purpose of this paper to extend these studies to the temperature dependence of the ethoxy proton splitting constants. Our object in this paper is not, however, to obtain quantitative information on the potential barriers to rotation but rather to give an explanation of the magnitude and temperature dependence of the β - and γ -ethoxy proton splitting constants⁴ in terms of specific molecular motions and conformations and with reference to INDO calculations.

Experimental Section

p-Diethoxybenzene was a commercially available compound and was recrystallized before use; 1,4-diethoxy-2,5-dimethylbenzene, 1,4-diethoxy-2,5-di-*tert*-butylbenzene, and 4,4'-diethoxybiphenyl were prepared by allowing ethyl iodide to react with the appropriate phenol following a method outlined by Ristow.⁵ 1,2,4,5-Tetraethoxybenzene is found as a \sim 1% impurity in commercially available 1,2,4-triethoxybenzene and can be prepared as the cation radical from this source. 1,4-Diethoxy-2,5-dimethylthiobenzene and 1,4-diethoxy-2,5-diethylthiobenzene were a gift from Dr. Z. I. Ariyan. The cation radicals were prepared by treating the neutral compounds with aluminum chloride or concentrated sulfuric acid in nitromethane or nitroethane.⁶ The esr spectra were measured on a Varian E-15 spectrometer in a dual cavity using a sample of the perylene radical anion as a secondary standard. The least-squares analyses of the experimental spectra were carried out as previously described.³

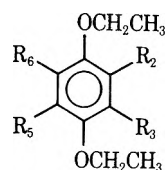
Results

p-Diethoxybenzene (DEB). The cation radical derived from this compound in $AlCl_3-CH_3NO_2$ has been previously investigated rather extensively.⁷ The radical was shown to exist as *cis* and *trans* isomers at room temperature and below. The averaged values of the splitting constants and the temperature coefficients obtained from the previous

study are shown in Table I. The important points to note are that the methylene (β) protons⁸ of the ethoxy group have a splitting constant of 3.80 G (at -40°) compared to 3.35 G for the methoxyl protons of *p*-dimethoxybenzene (DMB)⁷ and that their temperature coefficient is -3.72 mG/deg (cf. 0.09 mG/deg for DMB). Also, a splitting of 0.144 G is detected from the γ -ethoxy protons.

1,4-Diethoxy-2,5-dimethylbenzene (DEDMB). The cation radical of DEDMB was formed in $AlCl_3-CH_3NO_2$ and gave well-resolved spectra (line width ca. 0.040 G) over the temperature range from 0 to -50° . The spectra are readily analyzed in terms of only one isomer, presumably the *trans* form, and the splitting constants (see Table I) account for all the protons in the molecule. Again a large temperature dependence is found for the β -ethoxy protons (-3.46 ± 0.3 mG/deg) and splittings from the γ -ethoxy protons are observed which are also temperature dependent (-0.29 ± 0.03 mG/deg). The methyl splittings are not measurably temperature dependent whereas the ring proton splittings do show a significant dependence (-0.62 ± 0.06 mG/deg).

1,4-Diethoxy-2,5-di-*tert*-butylbenzene (DEDDB). The esr spectrum of the cation radical of DEDDB produced in $AlCl_3-CH_3NO_2$ was obtained over the temperature range from -40 to $+20^\circ$. The spectrum is again analyzed in terms of only one species. The major splittings are a quintet from the β -ethoxy protons which shows a large temperature dependence (-5.2 mG/deg) and a triplet from the ring protons which has a small but significant temperature coefficient (-0.76 mG/deg). Each of these 15 major lines is split further by small splittings from the γ -*tert*-butyl protons and the γ -ethoxy protons. The overall pattern of this additional splitting changes markedly with temperature. By using expanded field sweeps these small splittings were investigated and computer simulations indicated that the splittings were made up of two components. First, a temperature-independent splitting of 0.100 G which could be attributed to the γ -*tert*-butyl protons. This assignment was made on the basis of expected intensity ratios for 18 equivalent protons and by analogy to the same splitting in 1,4-dimethoxy-2,5-di-*tert*-butylbenzene

TABLE I: Summary of ESR Results for Substituted *p*-Diethoxybenzenes

Substituents		Splitting constants, G, and temperature coefficients, ^e mG/°C					
R ₂ = R ₅	R ₃ = R ₆	a ₂ = a ₅	a ₃ = a ₆	a _{OCH₂H}	a _{OCH₂CH₃} ^{CH₃}	g factor ^a	a _β ^b /a _γ
H	H	2.272 c	2.272 c	3.802 (-3.72)	0.144 c	2.00371	26.40
CH ₃	H	4.113 ± 0.001 c	0.6032 ± 0.0007 (-0.62 ± 0.06) ^f	3.636 ± 0.002 (-3.46 ± 0.3)	0.1365 ± 0.0005 (-0.29 ± 0.03)	2.00363	26.63
(CH ₃) ₃ C	H	0.1002 ± 0.0011 c	1.0536 ± 0.0009 (-0.76 ± 0.11)	4.0000 ± 0.0008 (-5.21 ± 0.24)	0.1552 ± 0.0011 (-0.25)	2.00366	25.77
CH ₃ CH ₂ O	H	2.6556 ± 0.0008 (-2.90 ± 0.03)	0.8579 ± 0.0008 (+0.27 ± 0.03)	2.6556 ± 0.0008 (-2.90 ± 0.03)	0.1138 ± 0.0008 (-0.16 ± 0.02)	2.00401	23.33
CH ₃ S	H	3.457 ± 0.001 c	0.789 ± 0.001 (+0.37 ± 0.05)	1.967 ± 0.001 (-2.56 ± 0.06)	0.0775 ± 0.0013 (-0.25 ± 0.02)	2.00690	25.35
CH ₃ CH ₂ S	H	3.194 ± 0.004 (-0.75 ± 0.10)	0.770 ± 0.006 (0.52 ± 0.11)	1.964 ± 0.006 (-2.52 ± 0.16)	c	2.00690	
4,4'-Diethoxybiphenyl		d	d	2.0796 ± 0.0008 (-2.30 ± 0.10)	0.0819 ± 0.0006 (-0.12 ± 0.02)	2.00323	25.24

^a Estimated errors ± 0.00302. ^b The ratio of the splittings of the β and γ protons of the ethoxy group. ^c Not measured. ^d Not applicable. ^e Given in parentheses immediately below the approximate splitting constant. ^f The signs of the temperature coefficients for the ring protons are related to the sign of their coupling constant. It is planned to discuss this point in more detail in a future publication.

TABLE II: Least-Squares Analysis of the Splitting Constants for the 1,2,4,5-Tetraethoxybenzene Cation Radical

Temp. °C	a _{OCH₂H}	a _{CH} ^H	a _{γ-CH} ^H
-30	2.6821 ± 0.0012	0.8569 ± 0.0012	0.1141 ± 0.0012
-20	2.6556 ± 0.0008	0.8579 ± 0.0008	0.1138 ± 0.0008
-10	2.6250 ± 0.0009	0.8623 ± 0.0010	0.1109 ± 0.0010
0	2.5951 ± 0.0009	0.8650 ± 0.0009	0.1096 ± 0.0009
+10	2.5684 ± 0.0008	0.8685 ± 0.0008	0.1072 ± 0.0008
+20	2.5373 ± 0.0018	0.8691 ± 0.0018	0.1069 ± 0.0017

cation radical (a^H_{t-Bu} = 0.103 G).⁹ Second, a temperature-dependent splitting of ca. 0.150 G with a temperature coefficient of ca. -0.25 mG/deg was assigned to the γ-ethoxy protons.

1,2,4,5-Tetraethoxybenzene (TEB). The cation radical of TEB can be produced by the reaction of commercial samples of 1,2,4-triethoxybenzene with either H₂SO₄ or AlCl₃ in nitromethane or nitroethane. The TEB is believed to be present as an impurity to about 1% and the 1,2,4-triethoxybenzene is apparently not oxidized under the conditions employed. The esr spectrum of TEB is readily interpreted in terms of a nonet of triplets from the β-ethoxy and ring protons with additional hyperfine splittings from γ-ethoxy protons. In order to indicate the precision of our results the least-squares analysis of the splitting constants for TEB over the range from -30 to +20° is given in Table II. From these results one finds temperature coefficients of -2.90 ± 0.03, +0.27 ± 0.03, and -0.16 ± 0.02 mG/deg for the β-ethoxy, ring, and γ-ethoxy protons, respectively.

1,4-Diethoxy-2,5-dimethylthiobenzene (DEDMTB). The cation radical of DEDMTB was obtained in AlCl₃-

CH₃NO₂ and was analyzed in the temperature range from -40 to +10°. The esr spectrum consists of a septet from the β-methylthio protons (3.457 G), a quintet from the β-ethoxy protons (1.967 G), a triplet from the ring protons (0.789 G), plus a small splitting from the γ-ethoxy protons (0.0775 G). The g factor is significantly larger than the radicals containing only oxygen atoms and the line widths are also significantly increased. Temperature coefficients were obtained for the β-ethoxy, the ring, and the γ-ethoxy protons of -2.56 ± 0.06, +0.37 ± 0.05, and -0.25 ± 0.02 mG/deg, respectively.

1,4-Diethoxy-2,5-diethylthiobenzene (DEDETb). The esr spectrum of the DEDETb cation radical in AlCl₃-CH₃NO₂ is entirely analogous to the previous compound DEDMTB. The major difference is the substitution of a major quintet splitting of 3.19 G from the β-ethylthio protons. Another difference between the two compounds was the failure to resolve any splittings from either the γ-ethoxy or the γ-ethylthio protons in the DEDETb spectrum. Temperature coefficients were obtained for the β-ethylthio, β-ethoxy, and ring protons of -0.75 ± 0.10, -2.52 ± 0.16, and +0.52 ± 0.11 mG/deg, respectively.

4,4'-Diethoxybiphenyl (DEBP). The cation radical was produced in AlCl₃-CH₃NO₂ over the temperature range from -30 to +10°. The analysis of the esr spectrum was complicated by the fact that rotational motions about the C(aryl)-O bond are occurring. This results in a line width alternation of the lines associated with the ring protons. The ethoxy group splitting constants are unaffected by this cis-trans isomerism and since these are our main concern in this paper only the splitting constants for the β- and γ-ethoxy protons are shown in Table I. Temperature coefficients were measured as -2.30 ± 0.10 and -0.12 ± 0.02 mG/deg for the β and γ-ethoxy protons.

Discussion

The Ethoxy Group. In order to explain the temperature dependence of the ethoxy group protons one should consider the various torsional oscillations which can occur in the alkoxy group and also the mechanism by which the hyperfine splitting is produced. Previous studies on methoxy-substituted compounds have led us to believe that the primary mechanism responsible for the hyperfine splitting of the β -alkoxy protons is *via* a hyperconjugative interaction with the spin density on the oxygen atom. In addition, there is likely to be a small long-range contribution to the splitting from spin density on the adjacent carbon atom; this contribution should be small and has been ignored for the moment (see INDO Calculations). Two torsional oscillations can effect the magnitude of the hyperfine interaction. First, oscillations about the C(aryl)-O bond would change the conjugation and hence the spin density on the oxygen atom (*i.e.*, a change in θ , see Figure 1). Second, oscillations about the O-C(alkyl) bond (change in Φ) can alter the hyperconjugative interaction between the β protons and the spin density on the oxygen p_z orbital. Both of these oscillations can in principle lead to a temperature dependence of the hyperfine splitting constant. Our studies on methoxyl compounds have indicated that the oscillation about the C(aryl)-O bond has a large potential barrier to rotation associated with it (*ca.* 16 kcal/mol for *p*-dimethoxybenzene), when the methoxyl groups are not sterically hindered, and hence leads to only a very small temperature dependence of the methoxyl splitting constants. The oscillation about the O-C(alkyl) bond is thought to have a very small barrier to rotation associated with it and for the methoxyl compounds essentially free rotation occurs around this bond. In the light of these results it is proposed that torsional oscillations about the C(aryl)-O bond are of little importance to the ethoxy group and contribute only slightly to the temperature dependence of the β protons. Restricted rotation about the O-C(alkyl) bond is considered to be the major origin of the temperature dependence. Since this is so, the results can be interpreted by analogy with previous work on β -alkyl protons.^{10,11} Assuming that the β -ethoxy proton coupling is given by eq 1, where Φ is the dihedral

$$a_{\beta}^{\text{H}} = Q_{\text{O}}^{\beta-\text{H}}(\cos^2 \Phi) \rho_{\text{O}}^{\pi} \quad (1)$$

angle between the C-H bond and the oxygen p_z orbital and $(\cos^2 \Phi)$ represents the time-averaged value of $\cos^2 \Phi$. For a freely rotating methoxyl group $(\cos^2 \Phi) = \frac{1}{2}$. If the other alkoxy groups were freely rotating one would expect no change in the β -alkoxy proton coupling constant. Deviations from the methoxy proton splitting constant can, however, be regarded as evidence for a preferred orientation of the alkyl group. These deviations are most easily compared by calculating the ratio of the β -alkoxy proton splitting to the methoxyl splitting in a similar compound ($R = a_{\beta-\text{OCH}_2\text{H}}/a_{\text{OCH}_3\text{H}}$). This ratio is given in Table III for the compounds studied in this paper and for two neutral radicals containing alkoxy groups studied by other workers.^{12,13} As can be seen, the ratio for the β -ethoxy protons is >1.0 . This can be compared to the same ratio for β -ethyl protons in a variety of ethyl-substituted aromatic compounds, which is consistently <1.0 . This result implies a different preferred conformation in similarly substituted compounds for the ethoxy group as compared to the ethyl group. A ratio of >1.0 implies that the β pro-

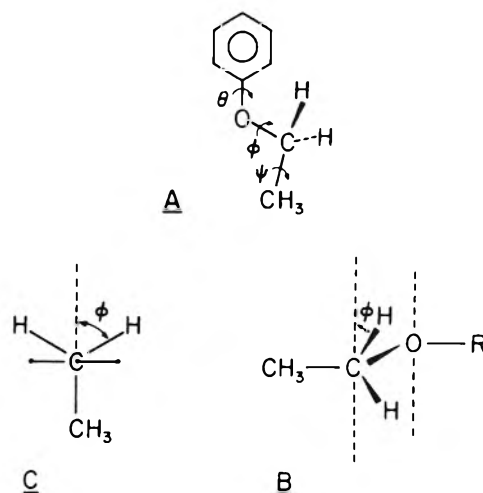


Figure 1. Definition of angles θ , Φ , and ψ .

TABLE III: Calculated R Values for Some Dialkoxy Compounds

	$a_{\text{OCH}_3\text{H}}$	$a_{\text{OCH}_2\text{CH}_3\text{H}}$	R
Cation Radicals			
1,4-Dialkoxybenzene	3.36	3.802	1.13
1,4-Dialkoxy-2,5-dimethylbenzene	3.153 ^a	3.636	1.15
1,4-Dialkoxy-2,5-di- <i>tert</i> -butylbenzene	3.242 ^a	4.000	1.23
1,2,4,5-Tetraalkoxybenzene	2.208 ^b	2.655	1.20
4,4'-Dialkoxybiphenyl	1.78 ^c	2.079	1.17
Neutral Radicals			
2,6-Dimethyl-4-alkoxyphenoxy	1.58 ^d	1.85 ^d	1.17
2,6-Di- <i>tert</i> -butyl-4-alkoxyphenoxy	1.51 ^e	1.82 ^e	1.20

^a Reference 27. ^b Reference 9. ^c Reference 21. ^d Reference 12. ^e Reference 13.

tons spend more of their time in configurations for which $\Phi < 45^\circ$; for a ratio of <1.0 the β protons must spend more of their time in configurations with $\Phi > 45^\circ$. The reasons for the different configurations of the ethoxy and ethyl groups are probably steric in origin. Thus, in order to minimize steric interactions between the methyl group and the ortho ring protons the ethoxy group would be expected to have a minimum energy conformation as shown in Figure 1B ($\Phi = 30^\circ$). In the same way for an ethyl group substituted on a benzene ring the minimum energy conformation should be one in which the methyl group is out of the benzene plane, $\Phi = 60^\circ$ for the β -CH₂ protons (Figure 1C). In both cases temperature-dependent torsional oscillations about the equilibrium position will result in temperature-dependent splitting constants. It should be noted that the temperature coefficients are predicted to be of opposite sign for the two cases. For the ethoxy group with an equilibrium configuration of $\Phi = 30^\circ$ an increasing splitting with decreasing temperature is predicted, whereas for an ethyl group with an equilibrium configuration of $\Phi = 60^\circ$ a decreased splitting with decreasing temperature is predicted. Experimentally Vincow, *et al.*^{14,15} have found temperature coefficients of +1.80 and +2.10 mG/°C, for the 9-ethylxanthyl radical and the hexaethylbenzene cation radical, respectively, as compared to our results for the ethoxy protons which show negative temperature coefficients.

Previous workers have used the temperature dependencies of the β -alkyl protons to evaluate the potential bar-

riers to rotation by fitting the experimental splitting constants to calculated values using various models for the torsional oscillations.^{10,14-19} All of these calculations have used a symmetric periodic potential function in their calculations. Unfortunately in the case of the ethoxy group the periodic potential is expected to be far from symmetric and it was decided not to pursue further calculations since the significance of the barriers obtained would be, at best, doubtful. It can be noted, for comparison purposes, that another series of radicals which are believed to have the same $\Phi = 30^\circ$ equilibrium conformation as the ethoxy group are the *n*-alkyl radicals (propyl, butyl, etc).²⁰ For example, the *n*-propyl radical has a β -proton splitting constant of 33.2 G at -180° , an *R* value of 1.23, and a temperature coefficient of -24 mG/deg, representing a 0.78%/deg change. This compared with changes of ca. 1.2%/deg for the ethoxyl compounds studied. This result certainly suggests that the barriers to rotation in the two systems are of the same order of magnitude.

Another aspect of our results concerning β -proton splittings which is worth comment is related to the β -alkylthio protons. The *R* value for the β -alkylthio protons of DEDMTB and DEDETB is found to be $3.194/3.457 = 0.92$. This compares with *R* values of 0.83, 0.74, and 0.72 for 1,4-bis(alkylthio)benzenes²¹ and tetrakis(alkylthio)ethylene²² radical cations and 4-alkylthio-2,6-di-*tert*-butylphenoxy²³ radicals, respectively. Assuming, as has been suggested,^{21,22} that the mechanism of the β -alkylthio splittings is similar to the β -alkoxy splittings (*i.e.*, hyperconjugative coupling to the spin density on sulfur) then, these *R* values < 1.0 suggest a different equilibrium conformation of the alkylthio group as compared to the ethoxy group. The *R* values are similar to many ethyl-substituted compounds and therefore suggest a similar equilibrium conformation with $\Phi = 60^\circ$. Unfortunately the measured temperature coefficient of the β -ethylthio protons in the DEDETB cation radical, although small (-0.75 ± 0.10), does not have the same sign as would be predicted assuming an equilibrium conformation with $\Phi = 60^\circ$. Therefore, although the results suggest differences in conformation between ethoxy and ethylthio groups the exact nature of this difference may be more complex than the simple model above suggests. An additional difference between ethoxy and ethylthio groups which has been noted is the inability to resolve splittings from β -ethylthio protons suggesting that these protons have much smaller values than the corresponding β -ethoxy protons.

γ -Proton Splittings. Hyperfine splittings from distant protons, as exemplified by γ protons, are an area of considerable current interest, particularly with regard to the signs and mechanisms of the hyperfine splittings. However, most of the recent work has concerned itself with rigid rather than rotating systems (see ref 24 and references therein). These results have emphasized the conformational dependence of the sign and magnitude of the γ -proton interaction. Hyperfine splittings from freely rotating or partially restricted γ -protons, on the other hand, have received much less attention. Hyperfine splittings from freely rotating γ -protons occur most frequently in *tert*-butyl-substituted compounds, the protons of the *tert*-butyl group being γ to the adjacent carbon atom. Splitting of the *tert*-butyl protons have been reported in several anion,^{25,26} neutral,¹² and cation²⁷ radicals and INDO calculations have been used to rationalize these splittings.²⁸ Hyperfine splittings from γ protons of other alkyl

groups have also been noted and those of the ethyl group (ref 14, 15, 25, 29-32) are of particular relevance to this paper.

The hyperfine splitting patterns of the γ -ethoxy protons lead us to conclude that the CH_3 group is freely rotating, since no line width effects are observed and the relative intensities are consistent with the numbers of γ -ethoxy protons. The magnitude of the γ -ethoxy proton splittings are indicated in Table I. The ratio of the β - to γ -proton splittings a_{β^H}/a_{γ^H} is found to be approximately constant at 24.9 ± 1.6 . The only other documented example of a splitting from the γ protons of an ethoxy group occurs in the neutral 2,6-dimethyl-4-ethoxyphenoxy radical,¹² where the a_{β}/a_{γ} ratio is found to be 20.5. This almost constant a_{β}/a_{γ} ratio is to be contrasted with the same ratio found for ethyl groups where considerable variation is found (*e.g.*, for hexaethylbenzene¹⁵ cation radical $a_{\beta}/a_{\gamma} = 7.16$, for tetraethylbenzene cation radical³² $a_{\beta}/a_{\gamma} = 34.0$, and for 9-ethylxanthyl¹⁴ radical $a_{\beta}/a_{\gamma} = 46.8$).

The mechanism leading to the hyperfine splitting of the γ -ethoxy protons is undoubtedly complex. Qualitative considerations of this splitting usually consider spin polarization, hyperconjugation, and homohyperconjugation as possible mechanisms. In order to obtain quantitative agreement it appears that the best method presently available is a molecular orbital calculation in the INDO approximation. These calculations were therefore carried out in order to further understand the splittings of the β - and γ -ethoxy protons.

INDO Calculations. Space and time limitations of our computer prohibited INDO calculations on any of the actual molecules shown in Table I. Instead calculations were carried out on smaller molecules which model the ethoxy group interaction. The simplest model compounds of interest are the ethoxymethyl radical ($\text{CH}_3\text{CH}_2\text{O}\dot{\text{C}}\text{H}_2$) and the ethanol cation radical ($\text{CH}_3\text{CH}_2\text{OH}^+$). Although hyperfine splittings for the ethoxymethyl radical are not available, those of the hydroxymethyl and methoxymethyl radicals are.¹⁷ Therefore, our initial calculations were intended to provide a set of molecular parameters which would give good agreement with the experimental splitting constants. For the planar conformation, standard bond lengths and angles³³ gave reasonable agreement for hydroxymethyl (see Table IV) and also for the CH protons of methoxymethyl, but the averaged methoxyl proton splitting constant (averaged for rotation about the O-C(alkyl) bond) of $+0.70$ G is in poor agreement with the measured value of $+2.09$ G. This could be improved considerably if the COC angle were allowed to increase to 130° and the O- CH_2 bond length decreased to 1.30 Å. The averaged methoxyl splitting is then $+1.90$ G. Since the alkoxy splitting is our primary concern these molecular parameters were used in all further calculations. Calculations for the ethoxymethyl radical were made for various values of Φ (rotation about O-C(alkyl) bond) and ψ (rotation about C- CH_3 bond) where the angles are shown in Figure 1A. The dependence of the γ -ethoxy protons on ψ are shown in Figure 2 for the conformation shown in Figure 1B where $\Phi = 30$ and 150° for the two β -ethoxy protons. Since the γ protons are thought to be freely rotating a simple average over ψ was taken to represent the γ splitting. The calculated splittings for the conformation shown in Figure 1B are $a_{\beta^H} = 3.52$ G and $a_{\gamma^H} = -0.261$ G, giving $a_{\beta}/a_{\gamma} = 8.2$. Calculations were then performed to observe the effect of a rotation about the O-C(alkyl) bond, *i.e.*, a change in Φ . These re-

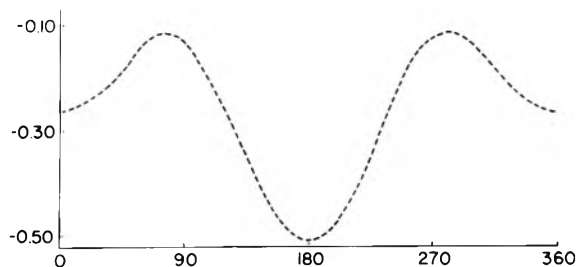


Figure 2. The calculated dependence of the γ -ethoxy proton splitting (G) of the ethoxymethyl radical as a function of the angle ψ for the fixed conformation shown in Figure 1B.

TABLE IV: Hyperfine Splittings Calculated by the INDO Method

		a_{OR^H}	$a_{CH^H} (1)$	$a_{CH^H} (2)$
Hydroxymethyl	Exptl ^a	-2.16	-18.53	-17.65
	Calcd ^b	-2.58	-19.67	-20.85
Methoxymethyl	Exptl ^a	+2.09	-18.43	-17.13
	Calcd ^b	+0.70	-19.93	-20.44
	Calcd ^c	+1.93	-19.98	-18.93

^a Reference 17. ^b Standard bond lengths and angles. ^c C-O-C = 130°, O-CH₂ = 1.30 Å.

sults are shown in Figure 3, where the Φ dependence of a_{β^H} is plotted as well as the Φ dependence of the average γ -proton splitting. The results indicate that the $\cos^2 \Phi$ dependence of the β protons is a reasonably good approximation, therefore, our previous qualitative comments on the origin of the temperature dependence seem justified. The averaged β coupling is 2.16 G, which with an R value of 1.18 would correspond to 2.54 G, a value which is in close agreement with the β -ethoxy proton splitting of TEB (i.e., $a_{\beta^H} = 2.65$ G). The calculated γ splittings are in the range from -0.21 to -0.31 G (giving ratios of a_{β}/a_{γ} of ~ 8.0) which is not in such good agreement with the experimental value of ± 0.114 G for TEB. However, considering that the spin distribution in the C-O bond is quite different for ethoxymethyl ($\rho_{O^\pi} = 0.185$ and $\rho_{C^\pi} = 0.805$, respectively) as compared to tetraethoxybenzene, perhaps the results are better than might be realized. It should be noted that although the ethoxymethyl radical has not been reported, a related radical ((CH₃)₂CHO \dot{C} (CH₃)₂) has been observed³⁴ and γ -alkoxy splittings of 0.26 G were measured, in excellent agreement with the INDO predictions.

Another model compound which will allow us to interpret the ethoxy group splittings is the cation radical of ethanol (CH₃CH₂ $\dot{O}H$)⁺. The advantage of this compound is that it is a cation radical and that the spin density can be considered as being almost completely localized on the p_z orbital of the oxygen atom. The dependence of the splitting constants on the oxygen spin density in the absence of large spin densities on adjacent carbon atoms can, therefore, be investigated with this compound. The molecular parameters were the same as those used above for the ethoxymethyl radical. The INDO calculated splittings for the β protons and their dependence on Φ are indicated in Figure 4. Figure 5 shows the ψ and Φ dependency of the γ -ethoxy proton splittings. The β splittings are found to fit eq 1 quite well with a $Q_{O^{\beta-H}}$ value of +66.4 G, again justifying our qualitative arguments concerning the temperature dependence of the β splittings. From the methoxyl splitting of 3.36 G for 1,4-dimethoxy-

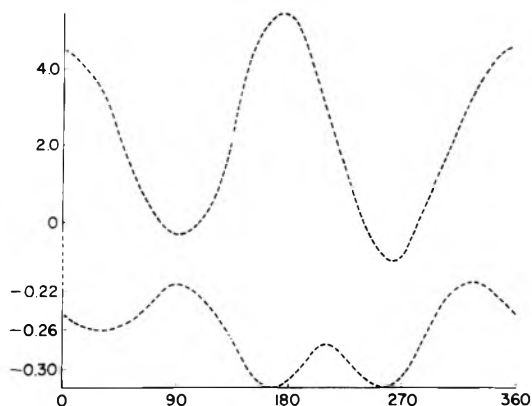


Figure 3. The upper curve shows the calculated β -ethoxy splitting (G) of the ethoxymethyl radical as a function of the angle Φ . The lower curve shows the calculated average (over ψ) γ -ethoxy splitting (G) of the ethoxymethyl radical also as a function of Φ . Note the change in scale for the two curves.

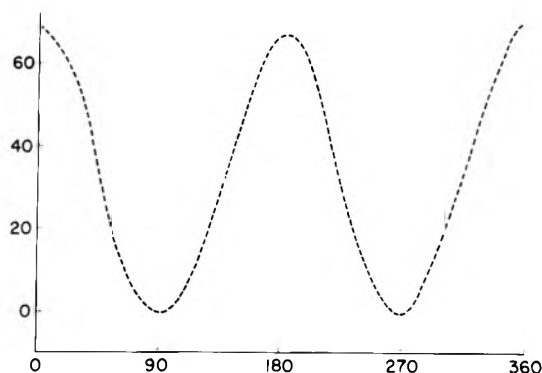


Figure 4. The calculated β -ethoxy splitting (G) of the ethanol cation radical as a function of the angle Φ .

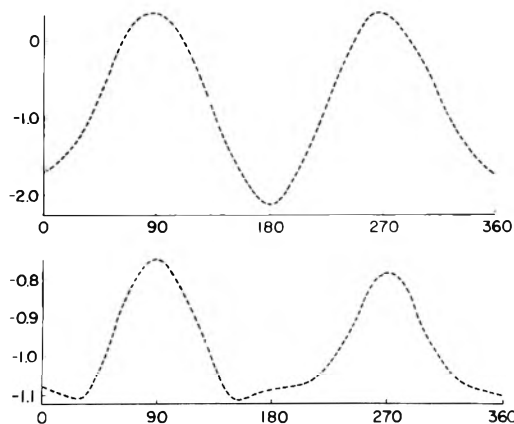


Figure 5. The upper curve shows the calculated γ -ethoxy splitting (G) of the ethanol cation radical as a function of the angle ψ for a fixed conformation as shown in Figure 1B. The lower curve shows the calculated average γ -ethoxy splitting (G) of the ethanol cation radical as a function of the angle ψ .

benzene the value of $\rho_{O^\pi} = 0.1012$ can be estimated from eq 1. This compares with values of $\rho_{O^\pi} = 0.170$ and 0.101 for 1,4-dimethoxybenzene and hydroquinone previously calculated using McLachlan modified HMO theory.^{3,35} Since the value for p -dimethoxybenzene was only estimated from proton splitting constants while the value for hydroquinone was based on splittings from all nuclei in the molecule, the agreement can be considered quite good. If it is assumed that ρ_{O^π} does not change appreciably be-

TABLE V: Calculated values of $Q_O^{\gamma-H}$, $Q_C^{\gamma-H}$, and a_{γ}^H as a function of Φ

Φ , degree	a_{γ}^H ^a	$Q_O^{\gamma-H}$ ^b	$Q_C^{\gamma-H}$ ^c	a_{γ}^H (for DEB)
0	-0.261	-0.780	-0.145	-0.131
30	-0.246	-0.938	-0.090	-0.140
60	-0.214	-1.062	-0.022	-0.143
90	-0.241	-1.082	-0.051	-0.151
120	-0.309	-1.109	-0.129	-0.170
150	-0.309	-0.893	-0.179	-0.152
180	-0.276	-0.747	-0.171	-0.131

^a As calculated for ethoxymethyl, plotted in Figure 3. ^b As calculated for $\text{CH}_3\text{CH}_2\text{OH}^+$. ^c Evaluated from eq 7 with $\rho_O^\pi = 0.185$ and $\rho_C^\pi = 0.805$.

tween dimethoxybenzene and diethoxybenzene and if it is further assumed that the magnitude of the γ splittings is directly proportional to ρ_O^π , then the magnitude of the γ splitting in DEB is calculated to be in the range from -0.079 to -0.112 G. These values are somewhat lower than the experimental value of 0.144 G.

The results for the ethoxymethyl and ethanol radicals probably represent extreme situations for an ethoxy group. In one case there is a very large spin density on the adjacent carbon atom, and in the other almost all the spin density is on the oxygen atom. Certainly for the ethoxy-substituted compounds investigated the real situation is an intermediate one in which there is a finite spin density on the adjacent carbon atom. It seems possible, therefore, that some sort of linear combination of the results for ethoxymethyl and ethanol might give better agreement with experiment. On the assumption that an alkoxy-substituted compound containing appreciable spin density on the adjacent carbon atom should have a term in the expression for the β splitting proportional to the carbon spin density, one can replace eq 1 by eq 2, where $Q_C^{\beta-H}$ may be some function of the angle Φ .

$$a_{\beta}^H = Q_O^{\beta-H}(\cos^2 \Phi)\rho_O^\pi + Q_C^{\beta-H}\rho_C^\pi \quad (2)$$

For ethoxymethyl the INDO calculations gave $a_{\beta}^H(\text{av}) = 2.16$ G (corresponding to $\langle \cos^2 \Phi \rangle = 1/2$), $\rho_O^\pi = 0.185$, and $\rho_C^\pi = 0.805$ and if $Q_C^{\beta-H}$ as calculated for ethanol is used (66.8 G), $Q_C^{\beta-H}$ can be evaluated as -4.992 G. Therefore, for averaged β splittings eq 3 is indicated. Cer-

$$a_{\beta}^H(\text{av}) = 33.4\rho_O^\pi - 4.992\rho_C^\pi \quad (3)$$

tainly the negative contribution due to the adjacent spin density on carbon is what would have been expected when one considers that the β -ethoxy protons are γ to the spin density on the carbon atom.³⁶ Applying eq 3 to the methoxyl splittings of dimethoxybenzene one obtains eq 4. This

$$3.36 = 33.4\rho_O^\pi - 4.992\rho_C^\pi \quad (4)$$

may be combined with the fact that the normalization condition of spin densities gives $\rho_C^\pi + \rho_O^\pi = 0.33$ for dimethoxybenzene if $Q_{\text{CH}}^H = -27$ G. Solving gives $\rho_O^\pi = 0.1304$ and $\rho_C^\pi = 0.1996$, again in fairly good agreement with previous HMO calculations.^{3,35}

If one now further assumes that the γ -ethoxy proton splittings consist of two contributions, one from the spin density on oxygen and one from the carbon spin density, eq 5 can be proposed. Again taking $Q_O^{\gamma-H}$ from the ethanol calculations, and ρ_O^π , ρ_C^π , and a_{γ}^H from the ethoxymethyl calculations, $Q_C^{\gamma-H}$ can be evaluated. The results are shown in Table V as a function of the angle Φ .³⁷ Fi-

TABLE VI: Calculated and Experimental a_{γ}^H splittings

Compd	Exptl ^a a_{γ}^H	Calcd ^b a_{γ}^H
DEB	0.144	-0.143
DEDMB	0.136	-0.134
DEDBB	0.155	-0.138
DEBP	0.082	-0.076
TEB ^c	0.114	-0.093
TEB ^d	0.114	-0.105

^a Measured at -20° . ^b Calculated for $\Phi = 60^\circ$. ^c Calculated assuming a constant ρ_O^π/ρ_C^π ratio. ^d Calculated assuming spin density normalization.

nally, on the assumption that one can apply the calculated spin densities for DMB to DEB the γ splittings for DEB can be evaluated as a function of Φ using eq 5 and the results are also given in Table V. The experimental γ splitting of 0.144 G is in excellent agreement with these predictions. The sign of the γ splitting is not directly determinable experimentally, however, indirect evidence from line width variations suggest that the sign of the splitting is negative in agreement with the calculated results. The only remaining problem to rationalize is the experimental temperature dependence of the γ -proton splittings. The dependence of a_{γ}^H on Φ is not large and it seems likely that small changes in the time-averaged value of Φ would be unlikely to change a_{γ}^H sufficiently to explain the measured temperature dependence (*i.e.*, -0.25 mG/deg). One should note, that the a_{γ}^H values are simple averages over the angle ψ and, as shown in Figure 5, the variation with ψ is quite large. It is certainly possible that rather than free rotation about ψ there could exist a rapid equilibrium between several possible conformations which could also in principle lead to a temperature dependence of the γ splittings.

$$a_{\gamma}^H = Q_O^{\gamma-H}\rho_O^\pi + Q_C^{\gamma-H}\rho_C^\pi \quad (5)$$

Finally, the γ splittings for some of the other compounds studied were estimated. Since the values of ρ_O^π and ρ_C^π are not known with certainty for the other compounds it was assumed that the ratio (ρ_O^π/ρ_C^π) would be the same as that found for DMB. Then, combining eq 3 with the known splitting of the related methoxyl compound (see Table III) one can evaluate ρ_C^π and ρ_O^π ; substitution into eq 5 then leads to a value for a_{γ}^H . In the case of TEB it is possible to solve directly for ρ_C^π and ρ_O^π if one assumes the normalization condition holds for the spin densities. The results are shown in Table VI, where the calculated values for a_{γ}^H are tabulated for $\Phi = 60^\circ$. The relative magnitudes are seen to be in excellent agreement with the experimental values.

Conclusion

These studies have indicated that INDO calculations give a good rationalization of the β - and γ -ethoxy proton splittings in a series of ethoxy-substituted cation radicals. The results lend credence to the qualitative conclusions regarding molecular conformations that can be drawn from the magnitude and the temperature coefficients of the β -alkoxy proton splitting constants. The INDO calculations also indicate that both the β and γ splittings have contributions from the spin density on the adjacent carbon atom as well as from the oxygen atom although by far the largest contribution arises from the oxygen spin density.

Acknowledgments. Acknowledgment is made to the donors of the Petroleum Research Fund, administered by the American Chemical Society, and to the Research Corporation for partial support of this research. I would also like to thank Dr. Z. I. Ariyan for his gift of two of the compounds used in this work. Acknowledgment is also made to Donna M. Olson and William S. Mullane, NSF undergraduate research participants, for technical assistance with certain parts of this study.

References and Notes

- (1) Part III; P. D. Sullivan, *J. Phys. Chem.* **75**, 2195 (1971).
- (2) P. D. Sullivan, *J. Phys. Chem.* **73**, 2790 (1969).
- (3) P. D. Sullivan, *J. Phys. Chem.* **74**, 2563 (1970).
- (4) Nomenclature follows the usual esr spectroscopists notation

$$\begin{array}{ccccccc} & \cdot & \text{C} & - & \text{C} & - & \text{C} & - & \text{C} & - & \text{C} & \cdot \\ & & | & & | & & | & & | & & | & \\ & & \text{H} & & \text{H} & & \text{H} & & \text{H} & & \text{H} & \\ & & \alpha & & \beta & & \gamma & & \delta & & \epsilon & \end{array}$$
- (5) B. W. Ristow, Thesis, Cornell University, 1966.
- (6) W. F. Forbes and P. D. Sullivan, *J. Amer. Chem. Soc.* **88**, 2862 (1966).
- (7) W. F. Forbes, P. D. Sullivan, and H. M. Wang, *J. Amer. Chem. Soc.* **89**, 2705 (1967).
- (8) That is, β to the oxygen atom.
- (9) W. F. Forbes and P. D. Sullivan, *J. Chem. Phys.* **48**, 1411 (1968).
- (10) E. W. Stone and A. H. Maki, *J. Chem. Phys.* **37**, 1326 (1962); **38**, 1254 (1963).
- (11) D. M. Geske, *Progr. Phys. Org. Chem.*, **4**, 125 (1967).
- (12) W. J. Van den Hoek, Thesis, Technische Hogeschool Delft, Holland, 1972.
- (13) N. M. Atherton, A. J. Blackhurst, and I. P. Cook, *Trans. Faraday Soc.* **67**, 2510 (1971).
- (14) M. D. Sevilla and G. Vincow, *J. Phys. Chem.* **72**, 3647 (1968).
- (15) M. K. Carter and G. Vincow, *J. Chem. Phys.* **47**, 302 (1967).
- (16) R. W. Fessenden, *J. Chim. Phys.* **61**, 1570 (1964).
- (17) P. J. Krusic, P. Meakin, and J. P. Jesson, *J. Phys. Chem.* **75**, 3438 (1971).
- (18) P. J. Krusic and J. K. Kochi, *J. Amer. Chem. Soc.* **93**, 846 (1971).
- (19) N. L. Bauld, J. D. McDermid, C. E. Hudson, Y. S. Rim, J. Zoeller, R. D. Gordon, and J. S. Hyde, *J. Amer. Chem. Soc.* **91**, 6666 (1969).
- (20) D. J. Edge and J. K. Kochi, *J. Amer. Chem. Soc.* **94**, 7695 (1972).
- (21) W. F. Forbes and P. D. Sullivan, *Can. J. Chem.* **46**, 317 (1968).
- (22) D. M. Geske and M. V. Merritt, *J. Amer. Chem. Soc.* **91**, 6921 (1969).
- (23) K. Scheffler, *Ber. Bunsenges. Phys. Chem.* **65**, 439 (1961).
- (24) L. M. Stock and P. E. Young, *J. Amer. Chem. Soc.* **94**, 7686 (1972).
- (25) J. Pilar, *J. Phys. Chem.* **74**, 4029 (1970).
- (26) C. Trapp, C. A. Tyson, and G. Giacometti, *J. Amer. Chem. Soc.* **90**, 1394 (1968).
- (27) P. D. Sullivan, *J. Phys. Chem.* **76**, 3943 (1972).
- (28) P. D. Sullivan, unpublished results.
- (29) J. K. Kochi and P. J. Krusic, *J. Amer. Chem. Soc.* **91**, 3940 (1969).
- (30) B. C. Gilbert, R. H. Schlossel, and W. M. Gulick, *J. Amer. Chem. Soc.* **92**, 2974 (1970).
- (31) D. Bachmann, *Z. Phys. Chem.* **43**, 198 (1964).
- (32) R. M. Dessau and S. Shih, *J. Chem. Phys.* **57**, 1200 (1972).
- (33) C-H = 1.08 Å, C-O = 1.36 Å, O-H = 0.98 Å, $\angle\text{COC} = 120^\circ$, C-C = 1.54 Å.
- (34) A. Hudson and K. D. J. Root, *Tetrahedron*, **25**, 5311 (1969).
- (35) P. D. Sullivan, J. R. Bolton, and W. E. Geiger, *J. Amer. Chem. Soc.* **92**, 4176 (1970).
- (36) This contribution is also probably angular dependent, but since only averaged values of the β splittings are being considered we have not calculated this angular dependence.
- (37) The values of $Q_{\text{C}-\text{Y}-\text{H}}$ are, perhaps, somewhat surprisingly negative. The γ -ethoxy protons are of course β to the carbon atom and calculations on simple hydrocarbons would have indicated a small positive value for a δ proton. Therefore, the influence of the intervening oxygen atom must be sufficient to change the sign of this interaction.

Raman Spectra of Sulfur Dissolved in Primary Amines

Francis P. Daly and Chris W. Brown*

Department of Chemistry, University of Rhode Island, Kingston, Rhode Island 02881 (Received April 16, 1973)

Raman spectra of rhombic sulfur dissolved in ethylenediamine, *n*-propylamine, and monomethylamine have been measured. Bands due to new species are observed at 400, 440, 462, \sim 510, and 535 cm^{-1} . The band at 535 cm^{-1} is assigned to the symmetric stretching vibration of S_3^- . The antisymmetric stretching vibration of S_3^- is observed at 585 cm^{-1} in the infrared spectrum of sulfur dissolved in ethylenediamine. The other new bands in the Raman spectra are attributed to polysulfides. The Raman spectrum of the ethylenediamine solution changed considerably during a 24-hr time dependence study, whereas the spectra of the other solutions changed only slightly.

Introduction

Solutions of alkali metals and sulfur in liquid ammonia and amines have been the subject of numerous investigations for the better part of this century.¹ The solutions are characterized by unusual colors and high conductivities; however, the exact nature of the solvent or solute is far from being understood. Recently, Smith and Koehler² investigated the Raman spectra of alkali metals dissolved in liquid ammonia. We have been performing similar experiments using sulfur as a solute and herein we report on the Raman spectra of sulfur dissolved in three primary amines.

Experimental Section

Rhombic sulfur (Alfa Inorganics, 99.999%) and monoethylamine (Matheson) were used without further purification. Ethylenediamine (EDA) and *n*-propylamine (both from Matheson Coleman and Bell) were distilled under atmospheric conditions and then under vacuum prior to being used.

Raman spectra were measured using a Spex Industries Model 1401 double monochromator with photon counting detection and a C.R.L. Model 52-A argon ion laser emitting at 5145 Å (≤ 150 mW power at the sample). All spectra were measured with a spectral slitwidth < 8 cm^{-1} .

EDA and *n*-propylamine solutions were contained, at $24 \pm 1^\circ$, in sealed Pyrex capillary tubes with an inner diameter greater than 1.2 mm. Monomethylamine was liquified under vacuum in a Raman cell designed for low-temperature liquids³ using a Dry Ice-acetone slush bath. A measured amount of sulfur was added to this solvent without breaking the vacuum. Infrared spectra were measured using a Perkin-Elmer Model 521 spectrometer. Samples were contained between CsBr windows with a polyethylene spacer ~ 1.0 mm thick.

Results and Discussion

Dilute solutions of sulfur in EDA are emerald green in color and, as the concentration is increased, the color changes from green to dark orange. The more concentrated solutions vaporized in the laser beam; thus, we confined this study to dilute solutions in the range 1×10^{-3} – 3×10^{-2} *M*. The Raman spectrum of a 3×10^{-3} *M* solution of sulfur in EDA is shown in Figure 1, where it is compared with the spectrum of pure EDA. Spectra are shown only for the 200–600- cm^{-1} region, since all of the new bands were in this region. Four new bands are observed at 400, 438, 510, and 535 cm^{-1} .

Previously, it was observed that the esr spectrum of sulfur in EDA changed after 24 hr,⁴ and it has also been found that the conductivity of the solution changes with time;⁵ therefore, we measured the Raman spectrum as a function of time. After 24 hr the bands at 400 and 510 cm^{-1} almost disappear, whereas the other bands remain about the same. The resulting spectrum is shown in Figure 1b. Using control samples we found the same changes in samples exposed to the laser light as those kept in a light-tight container; thus, the changes are not induced by the laser. In addition, we first observed changes in the spectrum within 1 hr after the solution was prepared, and we found that the spectrum continued to change for approximately 24 hr.

The Raman spectrum of 3×10^{-2} *M* solution of sulfur in *n*-propylamine (light orange color) is shown in Figure 2, where it is compared with the spectrum of pure *n*-propylamine. New bands are observed at 400, ~ 440 , 505, and 535 cm^{-1} . After 24 hr the band at 535 cm^{-1} increased slightly in intensity, but the other bands remained about the same (Figure 2b).

The Raman spectrum of a $\sim 3 \times 10^{-2}$ *M* solution of sulfur in monomethylamine (straw-yellow color) is shown in Figure 3. Monomethylamine was selected as the third solvent because, unlike the other two solvents, it does not have any Raman bands in the 200–600- cm^{-1} region. Five new bands are observed at 400, 440, 462, 505, and 535 cm^{-1} . There were no significant changes in the spectrum after 24 hr.

The observed frequencies and relative intensities of rhombic sulfur, and of sulfur dissolved in the three amines and in CS_2 , are listed in Table I. Sulfur in a rhombic crystal and in CS_2 exists as S_8 rings. Comparison of the frequencies and relative intensities indicates that S_8 rings are not present in the amine solutions; however, the bands observed in the amine solutions between 400 and 600 cm^{-1} are undoubtedly due to sulfur-containing species.

There is a close similarity between the spectra of the three amine solutions. All three solutions have bands at about 400, 440, 510, and 535 cm^{-1} . The band observed at 462 cm^{-1} in monomethylamine could be masked by solvent bands in the spectra of the other two amines. Since the bands at 400 and 510 cm^{-1} in the EDA solution al-

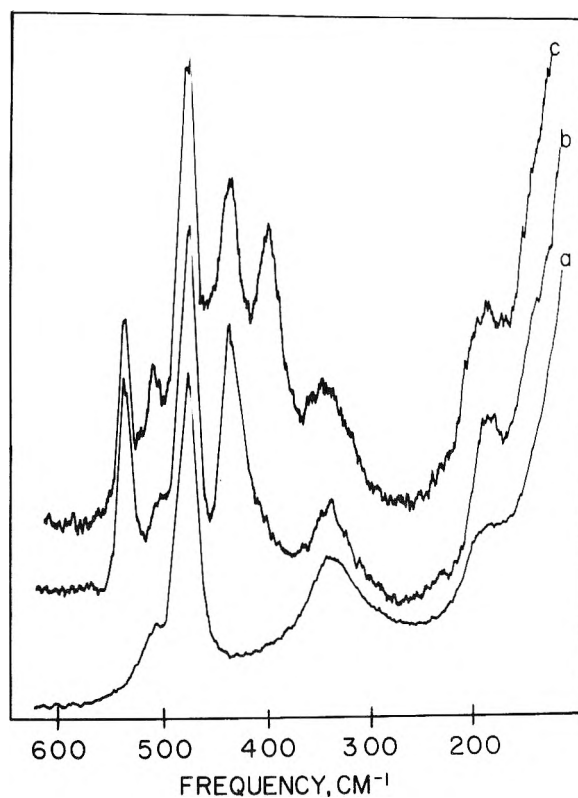


Figure 1. Raman spectra of (a) EDA, (b) 3×10^{-3} *M* sulfur in EDA after 24 hr, and (c) 3×10^{-3} *M* sulfur in EDA immediately after mixing.

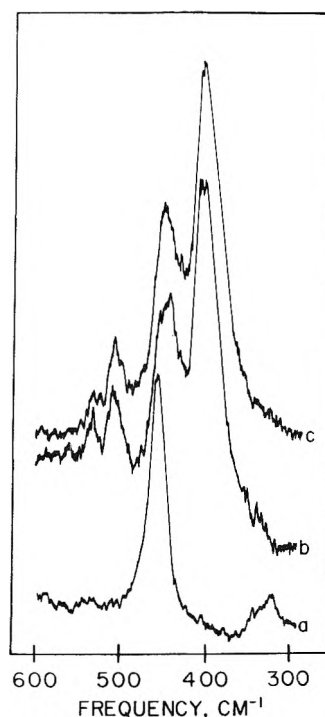


Figure 2. Raman spectra of (a) *n*-propylamine, (b) 3×10^{-2} *M* sulfur in *n*-propylamine after 24 hr, and (c) 3×10^{-2} *M* sulfur in *n*-propylamine immediately after mixing.

most disappear after 24 hr, we suspect that they belong to the same species. As mentioned above, the esr spectrum of sulfur in EDA changes considerably after 24 hr suggesting the disappearance of a free radical. It is possible that the 400- and 510- cm^{-1} bands in the EDA solution are also

TABLE I: Frequencies (cm^{-1}) and Relative Intensities of Bands in the Raman Spectra of Rhombic Sulfur, Rhombic Sulfur Dissolved in CS_2 , and Rhombic Sulfur Dissolved in the Primary Amines

Rhombic sulfur ^a	Sulfur in CS_2 ^b	Sulfur in EDA	Sulfur in $\text{C}_3\text{H}_7\text{NH}_2$	Sulfur in CH_3NH_2
152 s	152 s			
186 vw		188 ^c m		
215 w				
218 vs	218 s			
246 vw	245 vw			
			333 ^c w	
		345 ^c m		
		400 s	400 s	400 s
		438 m	438 s	440 m
441 w	440 vw			
				462 sh
			465 ^c m	
474 s	475 m			
		475 ^c vs		
		505 ^c w-sh		
		510 w	505 w	505 w
		535 m	535 w	535 m

^a R. E. Barletta and C. W. Brown, *J. Phys. Chem.*, **75**, 4059 (1971). ^b A. Anderson and Y. T. Yah, *Can. J. Chem.*, **47**, 879 (1969). ^c Solvent bands.

associated with the disappearance of the free radical, *i.e.*, they may be due to a species that reacts with the free radical or to a precursor of the free radical.

Davis and Nakshbendi⁵ suggested that open chain polysulfides could be responsible for the unusual colors and conductivities of the sulfur-amine solutions. This is consistent with our observations, *i.e.*, Raman bands between 400 and 550 cm^{-1} could be due to S-S stretching modes in polysulfides. Recently, infrared and Raman spectra of S_3^- in hexamethylphosphoramide were reported.⁶ Raman bands at 533 and 232 cm^{-1} were assigned to the symmetric stretching and bending vibrations, respectively, and an infrared band at 580 cm^{-1} was assigned to the antisymmetric stretching vibration. Alkali halides doped with sulfur also give evidence of S_3^- with a Raman band between 523 and 544 cm^{-1} , and an infrared band at 585 cm^{-1} .⁷ In EDA and monomethylamine a relatively strong, sharp Raman band is observed at 535 cm^{-1} , and in *n*-propylamine a weak, broad band is observed at 535 cm^{-1} . We recorded the infrared spectrum of an EDA solution and found a weak, sharp band at 585 cm^{-1} which is consistent with the antisymmetric stretching mode of S_3^- . Thus, we feel that S_3^- is present in the EDA solution. We were unable to obtain the infrared spectrum of a monomethylamine solution due to the problem of liquifying the solvent in an infrared cell; however, the fact that the band at 535 cm^{-1} in the Raman spectrum is the same as in EDA indicates that S_3^- is also formed in monomethylamine. It is possible that S_3^- is present in *n*-propylamine; however, the increase in the intensity of the

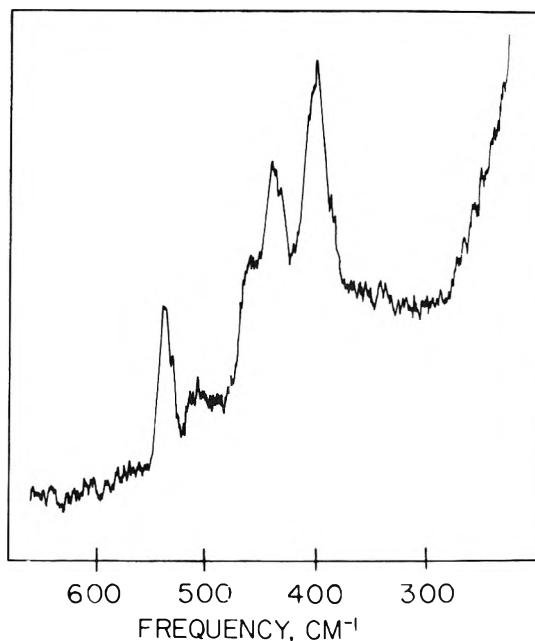


Figure 3. Raman spectrum of $\sim 3 \times 10^{-2}$ M sulfur in monomethylamine immediately after mixing.

band at 535 cm^{-1} after 24 hr suggests that S_3^- is slow to form in this solvent.

Conclusion

The present study demonstrates the feasibility of using Raman spectroscopy to elucidate the nature of sulfur dissolved in amines. There is good evidence that S_3^- and other polysulfides are present in the solutions. It should be emphasized that sulfur species are strong Raman scatterers and can be detected at low concentrations. Undoubtedly there are other species such as thioamides or ammonium ions present in the solution, but their Raman bands are too weak to be detected at such low concentrations.

Acknowledgments. We wish to express our appreciation to the National Science Foundation and to the University of Rhode Island for a grant which made possible the purchase of the Raman instrumentation. One of us (F. P. D.) gratefully acknowledges financial aid in the form of a NDEA Title IV Fellowship.

References and Notes

- (1) A. P. Zipp and S. G. Zipp, *Sulfur Inst. J.*, **4**, 2 (1968); J. J. Lagowski and M. J. Sienko, Ed., "Metal-Ammonia Solutions," Butterworths, London, 1970.
- (2) B. L. Smith and W. H. Koehler, *J. Phys. Chem.*, **76**, 2481 (1972).
- (3) A. G. Hopkins, F. P. Daly, and C. W. Brown, to be submitted for publication.
- (4) W. G. Hodgson, S. A. Buckler, and G. Peters, *J. Amer. Chem. Soc.*, **85**, 543 (1963).
- (5) R. E. Davis and H. F. Nakshbendi, *J. Amer. Chem. Soc.*, **84**, 2085 (1962).
- (6) T. Chivers and I. Drummond, *Inorg. Chem.*, **11**, 2525 (1972).
- (7) W. Holzer, W. F. Murphy, and H. J. Berstein, *J. Mol. Spectrosc.*, **32**, 13 (1969).

The Tetrathiotetracene Cation Radical

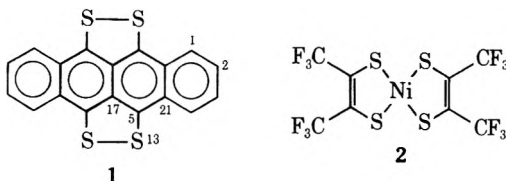
William E. Geiger, Jr.

Department of Chemistry and Biochemistry, Southern Illinois University, Carbondale, Illinois 62901 (Received March 14, 1973)

The anodic oxidation of tetrathiotetracene has been studied by voltammetry at the rotating platinum electrode, by cyclic voltammetry, and by controlled potential electrolysis. Two reversible one-electron oxidations are observed. The rose-colored solutions of the cation radical produced by electrolysis are extremely stable in the absence of added water. ESR data and HMO calculations are consistent with the conclusion that most of spin density in the cation radical resides in the C-S-S-C bridges. Tetrathiotetracene forms a one-to-one molecular complex with nickel thiete in an ionic ground state, as determined by optical spectroscopy and by esr. The complex shows no charge-transfer transitions in the infrared-to-ultraviolet region and has a high resistivity.

Introduction

Remarkably low resistivities have been reported¹ for cation radical salts of tetrathiotetracene (TTT, 1) and for tetrathiotetracene-quinone complexes with ionic ground states.² In spite of the fact that this potentially useful cation radical has been known for a long time, virtually no data has appeared on its physical properties. In this paper we discuss the anodic oxidation of tetrathiotetracene and report electron spin resonance measurements on its cation radical. In addition, we report the properties of a complex between tetrathiotetracene and bis-*cis*(1,2-perfluoromethylene-1,2-dithiolato)nickel (nickel thiete, 2). Nickel



thiete is an extremely strong acceptor which has been shown to form π molecular complexes in ionic ground states (Weiss-type complexes³) with easily oxidized compounds such as amines (*N,N,N',N'*-tetramethylphenylenediamine)⁴ and heterocyclic polynuclear aromatics (such as phenothiazine).⁵ Nickel thiete possesses several advantages over organic acceptors in the study of such complexes, including high stability in both neutral and the paramagnetic monoanionic forms, which have been discussed in an earlier paper.⁵

Experimental Section

The purple nickel thiete and the green tetrathiotetracene were prepared using literature procedures^{6,7} and were purified by sublimation *in vacuo*. Solutions containing neutral nickel thiete must be relatively water free and nonbasic to retard spurious reduction to the monoanion. For these reasons the nickel thiete-TTT complex was prepared by mixing equimolar solutions of the components in toluene or dried dichloromethane. The resulting rose-colored solutions gradually deposited the complex as a deeply colored powder, which was filtered and washed with pure solvent. The complex displayed very limited solubility in nonpolar solvents, but solubility in acetone or acetonitrile was sufficient to allow spectroscopic or esr measurements to be made.

Spectrograde solvents from Matheson Coleman and Bell were employed. Acetonitrile and dichloromethane were distilled from calcium hydride and acetone, toluene, and benzonitrile were used as received. The supporting electrolyte for electrochemical experiments in dichloromethane was tetrabutylammonium hexafluorophosphate, which was obtained from the metathetical reaction of tetrabutylammonium iodide (Ozark-Mahoning) in ethanol with 65% hexafluorophosphoric acid, recrystallized three times from 95% ethanol and dried under vacuum at 100°. Tetrabutylammonium perchlorate, recrystallized three times from anhydrous ethyl acetate, was employed as supporting electrolyte in benzonitrile. Approximately 0.1 M solutions of supporting electrolytes were employed in the electrochemical experiments. Voltammetry at the rotating platinum electrode was accomplished using conventional three-electrode cell design with an aqueous saturated calomel reference electrode separated from the solution by an agar salt bridge and a fine frit. A Sargent synchronous rotator drove the working electrode at 1800 rpm. Controlled potential electrolysis was accomplished using a normal two-compartment cell with the anodic and cathodic compartments separated by a 20-mm medium frit. A platinum gauze anode was used and the anodic compartment purged with argon throughout the experiment. All electrochemical experiments were performed with the Princeton Applied Research Model 173 potentiostat. Cyclic voltammetry experiments were performed at a stationary platinum microelectrode. Triangular waveforms were generated by a Hewlett-Packard Model 3300A function generator with Model 3302A trigger. Potentials were monitored by a Simpson Model 2700 digital voltmeter and data were read out with the Hewlett-Packard Model 7001A x-y recorder or Tektronix Model 502A oscilloscope and camera. Optical and infrared spectra were obtained with the Beckman DK-1A and IR-10 spectrophotometers, respectively. ESR experiments were performed using the Varian V-4502 spectrometer system employing 100-kHz field modulation and a 12-in. magnet. Diphenylpicrylhydrazyl was used as a *g* value reference. Molecular orbital calculations were performed on the IBM 370/155 computer. Resistivity of the solid complex was measured on a pressed pellet by Dr. M. G. Miles.

Results and Discussion

I. The Tetrathiotetracene Cation Radical. Although

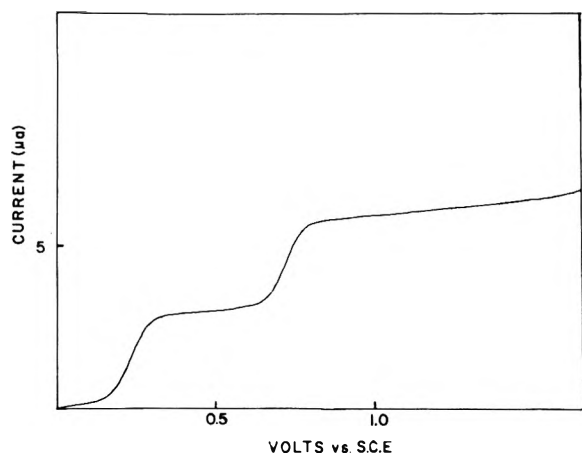


Figure 1. Voltammogram at the rotating platinum electrode for tetrathiotetracene in dichloromethane containing 0.1 M tetrabutylammonium hexafluorophosphate.

Marschalk and Niederhauser oxidized tetrathiotetracene to form its cation radical salts over 20 years ago,⁸ no data have appeared on the oxidation potentials of these compounds. Accurate electrochemical measurements are somewhat difficult because of the limited solubility of TTT in the solvents popularly employed for anodic oxidations (e.g., TTT is virtually insoluble in acetonitrile). A nearly saturated solution of the compound in dichloromethane (~ 0.1 mM) was investigated by voltammetry at the rotating platinum electrode and two well-developed oxidation waves were obtained (Figure 1) having half-wave potentials of +0.24 and +0.73 V *vs.* the aqueous sce and approximately equal limiting currents. The ratio of limiting current to concentration of electroactive species for each wave corresponded roughly to those obtained for systems undergoing known one-electron oxidations at the same electrode. The limited solubility of TTT resulted in a low ratio of faradaic current to charging current in cyclic voltammetry experiments at a platinum bead electrode, prohibiting quantitative measurements of anodic and cathodic peak currents, but at least some qualitative conclusions may be drawn from the data. At a scan rate of approximately 200 mV/sec, both oxidations were apparently quasi-reversible, each showing a cathodic current peak separated by about 100 mV from the anodic peak. It was later shown in controlled potential electrolysis experiments that over a longer time scale filming of the electrode occurs at the second oxidation wave, but no clear evidence of this occurs in the more rapid cyclic experiments.

Electrolysis of a 4.7×10^{-5} M solution of TTT in dichloromethane at a platinum gauze anode at +0.40 V (on the first oxidation plateau) resulted in a brilliant rose-colored solution. This solution was extremely stable in the absence of added water and could be withdrawn *via* syringe for purposes of obtaining esr and optical spectra. Exclusion of the atmosphere was not required. The total number of coulombs passed corresponded to a one-electron process and the solution could be reduced quantitatively back to the green starting solution by electrolysis at 0 V. The optical and esr spectra proved unequivocally that the rose-colored species is TTT cation radical (*vide infra*). If the rose-colored solution was further oxidized at +0.85 V, the solution gradually became colorless and the platinum gauze appeared to be coated with a yellowish material. Again, about one electron was passed. If the po-

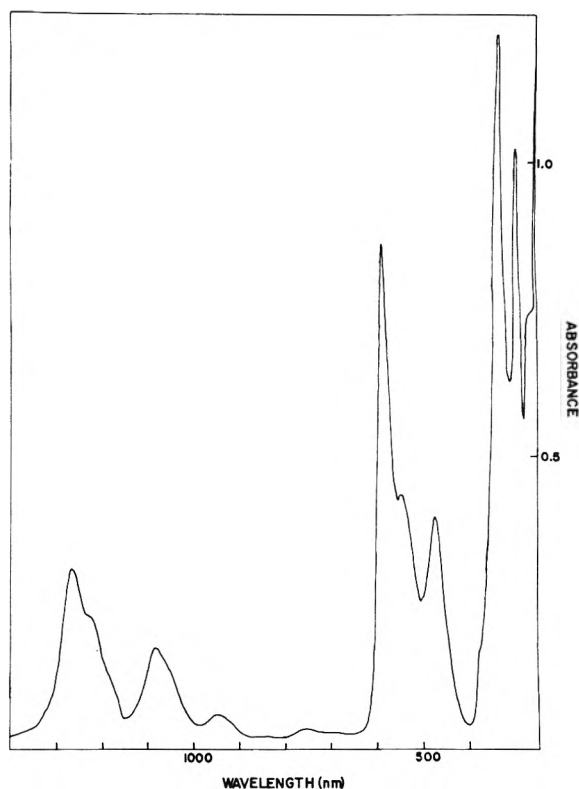


Figure 2. Optical absorption spectrum in a 1-cm cell of the tetrathiotetracene cation radical produced by electrolysis of a 4.7×10^{-5} M solution of the neutral compound in dichloromethane.

tential was then again made +0.40 V, small cathodic currents were observed and the rose color slowly regenerated, implying that the product of the second oxidation was the TTT dication, TTT^{2+} , largely insoluble in dichloromethane, which was then slowly re-reduced to the monocation.

The optical absorption spectrum of the electrolytically produced cation radical (Figure 2) is rich in features and matches well in band positions and intensities with the spectrum obtained for tetrathiotetracene chloride in methanol.² The latter authors reported that spectra of TTT salts changed with temperature and solvent variations and warned that the spectrum reported in methanol at 25° may not have been due to the monomeric cation radical. In view of our observations that the rose-colored species may be assigned *via* its esr spectrum to the cation radical, it now appears certain that their spectrum is indeed that of the monomer. The solution produced after electrolysis to the dication contained a band at 317 nm, apparently the most intense band of the largely insoluble dication, and other features too weak to confidently assign to the dication.

The esr spectrum of the electrolytically produced solution of the cation radical showed only a single line with a peak-to-peak line width of 2.7 G and a *g* value of 2.0064. The lack of observed hyperfine splittings from the ring protons is readily explained by molecular orbital calculations (using the parameters of Sullivan⁹) which predict the spin densities given in Table I for the cation radical. Note that almost 80% of the unpaired spin density is found in the C-S-S-C bridges and that nearly 90% of the spin is at positions which show no hyperfine splittings because of the low natural abundance of ¹³C and ³³S. These observations are consistent with the observed stability of the cation radical, because the C-5 type carbons, which hold the

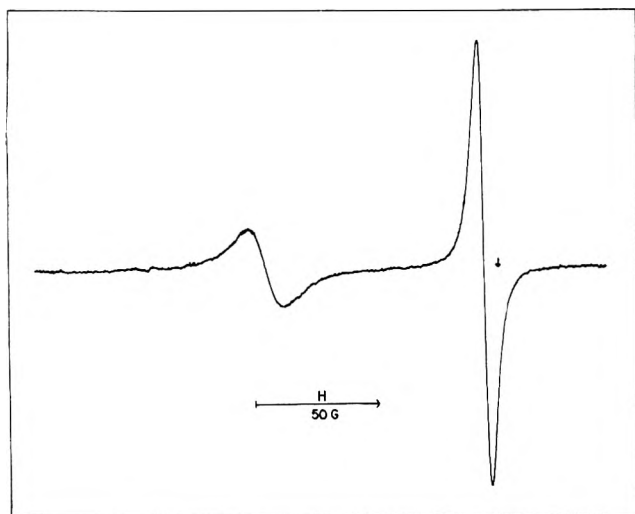


Figure 3. The X-band esr spectrum of the nickel thiete-tetrathiotetracene complex in acetone. The arrow marks the g value of DPPH ($g = 2.0037$).

TABLE I: Spin Densities Calculated By the McLachlan Method^a for the Tetrathiotetracene Cation Radical^b

Position	1 (C)	2 (C)	5 (C)	13 (S)	17 (C)	21 (C)
Spin density	0.022	0.024	0.129	0.067	0.023	-0.028

^a A. D. McLachlan, *Mol. Phys.*, **3**, 233 (1960). A value of $\lambda = 1.2$ was employed. ^b The parameters used in this calculation were⁹ $\alpha_S = 1.2\alpha_C$, $\beta_{CS} = 0.65\beta_{CC}$, and $\beta_{SS} = 0.42\beta_{CC}$.

highest spin density, are protected by the disulfide bridges from nucleophilic attack. This argument was previously used by Marcoux, *et al.*, to explain the enormously enhanced stability of the rubrene (5,6,11,12-tetraphenyltetracene) cation radical over that of the unsubstituted tetracene cation.¹⁰

No electrochemical reduction of tetrathiotetracene was observed in dichloromethane, but reduction waves were observed when benzonitrile was employed as solvent. On a platinum electrode two irreversible waves were noted with cathodic peak potentials at -1.01 and -1.38 V. On mercury these waves were observed along with an adsorption-controlled reduction at -1.14 V and a further irreversible reduction at -1.84 V. These experiments were not pursued.

II. The Molecular Complex of Tetrathiotetracene with Nickel Thiete. Tetrathiotetracene reacts with neutral nickel thiete to give a slightly soluble molecular complex which shows a visible near-ir absorption spectrum in a KBr disk having major bands at (in nm) 1265, 1225, 1080, 820, 590 (sh), 550, and 465. All of these bands are assigned to the tetrathiotetracene cation radical except the 820-nm

band, which is assigned to the nickel thiete monoanion.⁵ Strong bands at 1600, 1470, 1370, and 512 cm^{-1} in the infrared spectrum of the solid in KBr confirmed the presence of the cation radical.² Thus the solid is ionic (*i.e.*, composed of TTT^- and Ni^{th}^+ , as expected from the high reduction potential of neutral nickel thiete (we measure $E^\circ = +0.822$ V *vs.* sce in dichloromethane with 0.1 M tetrabutylammonium hexafluorophosphate). The esr spectrum of this powder showed a single broad line reminiscent of those obtained for the ionic complexes of nickel thiete with phenothiazine and phenoxazine.⁵ If the solid was dissolved in acetone, the resulting optical spectrum was a superposition of those of TTT^- and the nickel thiete monoanion at equimolar concentrations. The esr spectrum of this solution (Figure 3) shows lines at $g = 2.0610$ (nickel thiete monoanion⁶) and $g = 2.0064$ (TTT^+). The integrated intensities of these lines were obtained by measuring the peak-to-peak line width squared times the signal height and yielded an anion-to-cation ratio of 1.0 to 1.0.

It is noteworthy that no charge transfer band has been detected for the complex in the ultraviolet-to-infrared spectral range ($\sim 40,000$ – 250 cm^{-1}), in contrast to the strong charge-transfer interactions found for simple tetrathiotetracene salts¹ and TTT -quinone complexes.² This fact appears to correlate well with the enormously increased resistivity of our TTT -nickel thiete complex which has been measured on a pressed pellet as greater than 10^{10} ohm cm .¹¹ There is apparently no low-activation pathway for conduction in the absence of charge-transfer interactions.

Acknowledgments The author is grateful to Dr. Malcolm Miles for performing the resistivity measurement on the complex and for pointing out that tetrathiotetracene could be reduced in benzonitrile. We are also indebted to Mr. Ronald Turner for performing some of the experiments. Partial support of the work was given by Research Corporation and the Southern Illinois University Office of Research and Projects.

References and Notes

- (1) Y. Matsunaga, *J. Chem. Phys.*, **42**, 2248 (1965).
- (2) E. A. Perez-Albuera, H. Johnson, and D. J. Trevoy, *J. Chem. Phys.*, **55**, 1547 (1971).
- (3) F. H. Herbststein, *Perspect. Struct. Chem.*, **4**, 166 (1971).
- (4) R. D. Schmitt, Ph.D. Thesis, University of California at Riverside, 1969.
- (5) W. E. Geiger, Jr., and A. H. Maki, *J. Phys. Chem.*, **75**, 2387 (1971).
- (6) A. Davison, N. Edelstein, R. H. Holm, and A. H. Maki, *Inorg. Chem.*, **2**, 1227 (1963).
- (7) C. Marschalk and C. Stumm, *Bull. Soc. Chim. Fr.*, 418 (1948).
- (8) C. Marschalk and J. P. Niederhauser, *Bull. Soc. Chim. Fr.*, 147 (1952).
- (9) P. D. Sullivan, *J. Amer. Chem. Soc.*, **90**, 3618 (1968).
- (10) L. S. Marcoux, J. M. Fritsch, and R. N. Adams, *J. Amer. Chem. Soc.*, **89**, 5766 (1967).
- (11) This result was obtained by Dr. M. G. Miles, Monsanto Co.

Carbon-13 Chemical Shifts of Benzocycloalkenes¹

Edwin L. Motell,^{2a} Dieter Lauer, and Gary E. Maciel*^{2b}

Department of Chemistry, Colorado State University, Fort Collins, Colorado 80521 and Department of Chemistry, University of California, Davis, California 95616 (Received March 22, 1973;

Publication costs assisted by the Petroleum Research Fund

Carbon-13 chemical shifts have been determined for all carbons in five benzocycloalkenes, with one to five methylene groups, and in *o*-xylene, *o*-diethylbenzene, and *o*-di-*tert*-butylbenzene. The otherwise ambiguous peak assignments were clarified on the basis of the spectra of deuterium-labeled species and coherent proton decoupling experiments. With one exception, the ¹³C shieldings were found to follow the order $C_{\beta} > C_{\alpha} > C(4,5) > C(1,2)$. The ranges of ¹³C chemical shifts of the aromatic carbons are in the order $C(1,2) > C(4,5) > C(3,6)$. Additivity relationships are explored. The results are discussed in terms of crowding and strain.

Introduction

Hydrocarbons have occupied a place of importance in ¹³C magnetic resonance spectroscopy since the earliest ¹³C nmr studies.³⁻²⁰ Data on alkylbenzenes (ref 3, 5, 6, 10-12, 17, 20) and other aromatic hydrocarbons (ref 3, 4, 13, 14, 17) have been reported. Cycloalkanes were investigated by Burke and Lauterbur.⁷ Aromatic hydrocarbons, cycloalkanes, and polycyclic hydrocarbons^{15,16} are of great importance in the development of ¹³C nmr spectroscopy, because they demonstrate the order of *structural* effects on shielding in the absence of substituent effects (*i.e.*, heteroatoms). As such, they serve as especially valuable models for testing qualitative concepts^{4,7,12,15} as well as more sophisticated theories of shielding and have played an important role in establishing the scope of applicability of early theories of ¹³C chemical shifts.²¹⁻²³ It also seems likely that hydrocarbons will play an important role in gauging the reliability of emerging theories of ¹³C shielding.²⁴⁻²⁷

The present paper reports the ¹³C chemical shifts of a series of benzocycloalkenes and certain related dialkylbenzenes. The ¹H nmr data of these compounds have been reported previously by Cooper and Manatt²⁸ and others.²⁹⁻³¹ Benzocycloalkenes have received considerable attention in recent years in both chemical reactivity studies and spectroscopic investigations, especially from the point of view of the Mills-Nixon effect.³²

Experimental Section

Nmr Measurements. Natural abundance ¹³C nmr measurements were made on two spectrometer systems, both employing time averaging: (1) a synthesizer-based, center band-sweep modification of a Varian HA-100 spectrometer, operating at 25.142 MHz, and described elsewhere,³³ and (2) a Bruker HFX-90 spectrometer, equipped with a Digilab pulse and data system (FTS/NMR-3), and operating at 22.635 MHz. All samples were run in either 8- or 10-mm (o.d.) tubes, except for the benzocyclopropene and the deuterium-labeled samples; these were studied in 5-mm tubes. Field/frequency lock was accomplished with an inner capillary containing either CF₃CO₂H (25.1 MHz system) or C₆F₆ (22.6 MHz system), except for the 5-mm sample tubes, which were held concentrically inside a 8- or 10-mm tube with the outer annulus containing the lock substance.

Pseudorandom proton noise decoupling was employed with both spectrometer systems. The coherent-decoupling experiments and the experiments with deuterium-labeled compounds were all carried out in the Fourier transform mode. All FT spectra were obtained in the phase-corrected absorption mode, using 8K or 16K transforms. Off-resonance proton decoupling was employed for each compound. Except for benzocyclopropene, which was studied at 0 and 25°, all spectra were obtained at ambient probe temperatures, 45° for the 25.1 MHz system and 39° for the 22.6 MHz system. Chemical shift determinations were based on 10% internal cyclohexane as a reference (except for benzocyclopropene, see Table I).

Materials. All of the samples on which the chemical shift determinations were based were at least 99% chemically (not necessarily isotopically) pure, as obtained either commercially, synthetically, or after distillation. The criteria for purity were ¹H nmr and gas chromatography. The *o*-xylene sample was Eastman White Label. Indan and *o*-diethylbenzene were obtained from Aldrich. Tetralin was Eastman Practical, redistilled on a spinning-band column (bp 108.5-109.0°, 45 mm). The *o*-di-*tert*-butylbenzene sample was kindly provided by Professor A. W. Burgstahler (University of Kansas). The benzocyclopropene sample was kindly provided by Professor E. Vogel (Universität Koln).

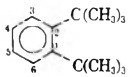
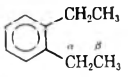
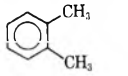
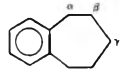
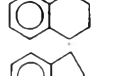
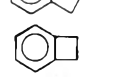

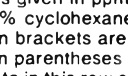
Benzocyclobutene was prepared from $\alpha,\alpha,\alpha',\alpha'$ -tetrabromo-*o*-xylene (Aldrich) according to the procedure of Coleman and Jensen.³⁴

Benzosuberone was prepared by a standard Wolf-Kischner reduction of benzosuberone (Aldrich).

3-Deuterio-*o*-xylene. 3-Lithio-*o*-xylene, prepared at 0° in anhydrous ether from 3-bromo-*o*-xylene (Aldrich) and *n*-butyllithium (Foote), was allowed to react with deuterioacetic acid, according to the procedure of Mowery and Streitwieser,³⁵ giving 3-deuterio-*o*-xylene. The center cut of a spinning-band distillation was employed as the nmr sample.

2-Deuterio-1,2,3,4-tetrahydronaphthalene. The 2 hydrogens of 1-tetralone (Aldrich) were exchanged with deuterium in a mixture of D₂O, diglyme, and sodium methoxide at 70-80°. The resulting α -deuterio ketone (55% 2 hydrogen replacement by ¹H nmr, *i.e.*, mainly monodeuterio ketone) was converted to the thioketal by treatment with ethanedithiol, according to a procedure similar to that reported by Djerassi and Gorman.³⁶ 2-Deuterio-1,2,3,4-te-

TABLE I: ^{13}C Chemical Shifts of Benzocycloalkenes and 1,2-Dialkylbenzenes^a

	Aromatic carbons			Aliphatic carbons		
	$\delta_{\text{C}(1,2)}$	$\delta_{\text{C}(3,6)}$	$\delta_{\text{C}(4,5)}$	$\delta_{\text{C}\alpha}$	$\delta_{\text{C}\beta}$	$\delta_{\text{C}\gamma}$
	148.56 [147.12] ^b	129.59 [124.67]	125.82 [125.02]	37.75	35.27	
	141.54 [143.58]	128.46 [127.95]	126.21 [125.85]	25.81	15.39	
	136.21 [138.45]	129.84 [129.22]	126.11 [125.60]	19.44		
	143.19	(129.15) ^c	(126.19)	37.04	28.83	33.06
	136.89	129.28	125.76	29.85	23.88	
	143.91	126.24	124.44	33.16	25.64	
	145.68	126.90	122.46	29.67		
	126.92 ^d 125.58 ^e	130.30 130.27	116.05 114.84	18.61 18.27		

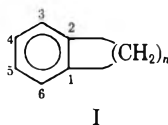
^a Values given in ppm with respect to TMS. More positive values correspond to lower shielding. Shifts accurate to ± 0.03 ppm. Unless otherwise indicated, 10% cyclohexane was used as an internal reference, and the data converted to the TMS scale by the formula $\delta_{\text{C}} = \delta_{\text{(wrt to C}_6\text{H}_{12})} + 27.36$. ^b Values in brackets are the chemical shifts calculated from data on the corresponding monoalkylbenzenes,²⁰ using the additivity model embodied in eq 1. ^c Values in parentheses are based on arbitrary assignments of the C(3,6) and C(4,5) resonances, made tentatively on the basis of apparent trends in the data. ^d Data in this row obtained at 25°, using 10% TMS as reference. ^e Data in this row obtained at 0°, using 20% TMS as reference.

tetrahydronaphthalene was obtained from the thioketal by hydrogen/Raney nickel reduction. The ^1H nmr spectrum and gas chromatography confirmed the purity and structure of the product. The ^1H nmr analysis indicated the possibility of some scrambling of deuterium to the aromatic ring; but in the aliphatic ring only one type of carbon was found by ^1H and ^{13}C nmr to have deuterium attached.

1-Deuterio-5,6,7,8-tetrahydronaphthalene. 1-Amino-5,6,7,8-tetrahydronaphthalene (Aldrich) was converted to the corresponding bromide by the Sandmeyer method.³⁷ The 1-bromo-5,6,7,8-tetrahydronaphthalene was converted to 1-deuterio-5,6,7,8-tetrahydronaphthalene, *via* the 1-lithio derivative, by the same procedure described above for 3-deuterio-*o*-xylene.

Results and Discussion

Carbon-13 chemical shifts were obtained for all of the carbons in compounds of the type shown in structure I where $n = 1, 2, 3, 4,$ and 5. For comparison purposes, ^{13}C chemical shifts were also obtained for *o*-xylene, *o*-diethylbenzene, and *o*-di-*tert*-butylbenzene. The results are summarized in Table I.



Assignments. The assignments of the aliphatic carbons were made as follows: For *o*-diethylbenzene, off-resonance proton decoupling distinguished the CH_2 and CH_3 resonances. For di-*tert*-butylbenzene the relative peak intensities, together with off-resonance decoupling experiments, were conclusive. For tetralin two methods were employed. The ^1H nmr spectrum, in which the α and β aliphatic hy-

drogens are separated by 1.0 ppm, had been assigned previously,³¹ so that coherent proton decoupling ^{13}C experiments give unequivocal ^{13}C assignments; the ^{13}C results so obtained agreed with assignments based upon observation of the 1:1:1 C-D splitting pattern of 2-deuterio-1,2,3,4-tetrahydronaphthalene. For the aliphatic carbons in benzosuberane, the γ carbon was identified by relative intensities. The α and β carbon resonances of benzosuberane were clearly distinguishable by the coherent proton decoupling approach, as the CH_2 proton resonances for the α position (previously assigned by Kabuss, Friebolin, and Schmid)³⁰ are clearly separated by substantial chemical shift differences (about 1 ppm) from the β and γ hydrogens. For indan, relative peak intensities and the coherent decoupling approach provided unequivocal assignments; the latter approach was possible because of the 0.8-ppm ^1H chemical shift difference between the previously assigned α and β proton resonances.³¹

For the aromatic carbon atoms, off-resonance proton decoupling experiments provide unequivocal identification of the substituted carbon atoms, C(1) and C(2). For *o*-xylene, the C(3) resonance was assigned unequivocally by noting the 1:1:1 triplet C-D splitting in 3-deuterio-*o*-xylene. This assignment is in agreement with an earlier assignment for *o*-xylene made by Lauterbur³ on the basis of a partially deuterated sample, but limited by the uncertainties inherent in the broad lines of the rapid-passage dispersion-mode method employed. The deuterium substitution approach was also employed to identify the C(3) resonance of tetralin.

In the cases of indan, *o*-di-*tert*-butylbenzene, benzocyclopropene, and benzocyclobutene, previous work^{28,29} on the ^1H nmr parameters of the aromatic hydrogens had displayed sufficiently large chemical shift differences between H(3) and H(4) that the coherent ^1H decoupling

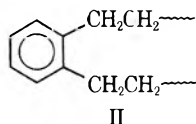
method was practicable. The smallest H(3)–H(4) shift difference among these four compounds is 0.04 ppm, and C(4) assignments are therefore determined relative to the reported proton assignments.

The assignments of C(3) and C(4) in *o*-diethylbenzene were made on the basis of the homonuclear ^{13}C – ^{13}C double resonance method reported recently by Dorn and Maciel.³⁸ The weak satellites resulting from ^{13}C – ^{13}C splittings due to neighboring ^{13}C atoms in natural abundance were monitored as the satellites of the ^{13}C resonances of the neighboring ^{13}C atoms were selectively irradiated *via* adiabatic rapid passage. In this manner it was possible to establish which peaks in the aromatic region correspond to directly bonded carbons. As the C(1),C(2) resonance is assigned unequivocally by the off-resonance method, it was possible to distinguish which ^{13}C peak corresponds to C(3),C(6).

The C(3) and C(4) assignments for benzosuberane are listed within parentheses in Table I. This reflects the fact that they were not based upon experimental data; the indicated assignments have been inferred from what appear to be regular patterns of chemical shifts displayed in the table.

For the aromatic carbons of all of the compounds of this study except benzocyclopropene the ^{13}C shieldings are found to follow the order C(4,5) > C(3,6) > C(1,2). In benzocyclopropene the relative order of the shifts of C(1,2) and C(3,6) is reversed. The C(1,2) resonances of all of the compounds are found within a 23-ppm range; eliminating the two extreme values of $\delta_{\text{C}(1,2)}$ from consideration (*o*-di-*tert*-butylbenzene and benzocyclopropene) would reduce this range to 9.5 ppm. There is no regular trend of $\delta_{\text{C}(1,2)}$ throughout the benzocycloalkene series. The $\delta_{\text{C}(3,6)}$ values all fall within a range of \pm ppm; there is no regular trend throughout the benzocycloalkene series. The $\delta_{\text{C}(4,5)}$ values cover a span of 11.8 ppm, and there is a regular trend of increasing shielding with decreasing *n* value (structure I) in the benzocycloalkene series.

Comparison of the data for the aromatic carbons of benzosuberane and *o*-diethylbenzene reveals a pattern of very close similarity. The $\delta_{\text{C}(1,2)}$ values differ by only 1.7 ppm, and the $\delta_{\text{C}(3,6)}$ and $\delta_{\text{C}(4,5)}$ comparisons are even closer. This is consistent with what one might expect if *o*-diethylbenzene is considered a good model of an unstrained system of the general structure II, and if one views benzo-



suberane as a relatively unstrained *cyclic* system of type II. There is also a very close correspondence between the ^{13}C shieldings of the aromatic carbons of tetralin and *o*-xylene. We make no attempt here to explore the detailed relationships between ^{13}C shieldings and electronic distribution; nevertheless, if one accepts the basic premise that ^{13}C shieldings are governed mainly by local atomic distributions (*e.g.*, $\sigma_{\text{d}}^{\text{AA}}$ and $\sigma_{\text{p}}^{\text{AA}}$ terms of the Pople–Karplus treatment^{21,22}), then this close correspondence suggests that the electronic distributions in the aromatic rings of *o*-xylene and tetralin (or in *o*-diethylbenzene and benzosuberane) are very similar.

It is of interest to compare the experimentally determined ^{13}C shifts of the aromatic carbons of the *o*-dialkylbenzenes with those obtained by additivity predictions

TABLE II: Miscellaneous ^{13}C Data on Deuterium-Substituted Compounds^a

Compound	$(^*\delta_{\text{D}}^* - ^*\delta_{\text{H}}^*)^b$	$(\ddagger\delta_{\text{D}}^* - \ddagger\delta_{\text{H}}^*)^c$	$(^{**}\delta_{\text{D}}^* - ^{**}\delta_{\text{H}}^*)^d$	$ J_{\text{CD}}^* ^e$
	–0.31	0.08	0.10	23.9
	–0.32			18.2
	–0.28	0.09	0.07	21.9

^a Chemical shift differences in ppm, accuracy ± 0.02 ppm; negative values correspond to higher shielding of the deuterium-substituted carbon. ^b Chemical shift difference, for the carbon indicated by a single asterisk, between the species with deuterium attached to that carbon and the corresponding species with no deuterium. ^c Magnitude of the chemical shift difference, for the carbon indicated by a dagger, between the species with deuterium attached to the carbon indicated by a single asterisk and the corresponding species with no deuterium. Sign not determined. ^d Magnitude of the chemical shift difference, for the carbon indicated by a double asterisk, between the species with deuterium attached to the carbon indicated by a single asterisk and the corresponding species with no deuterium. Sign not determined. ^e Absolute value of the directly bonded C–D coupling constant of the carbon indicated by a single asterisk.

based upon the equation

$${}^{R(1)R(2)}\delta_{\text{C}(i)} = R^{(1)}\delta_{\text{C}(i)} + R^{(2)}\delta_{\text{C}(i)} + \delta_{\text{C}(B)} \quad (1)$$

In this equation ${}^{R(1)R(2)}\delta_{\text{C}(i)}$ represents the ^{13}C chemical shift of the *i*th carbon in a dialkyl benzene ring that has the alkyl group R at positions 1 and 2, $R^{(2)}\delta_{\text{C}(i)}$ is the chemical shift (relative to benzene) of the *i*th carbon in a monoalkylbenzene with the alkyl group at position 2, and $\delta_{\text{C}(B)}$ is the chemical shift of benzene relative to the chosen standard (in this case TMS). This type of approach has been explored previously for disubstituted benzenes.^{10,39} The numbers derived from this equation, and from data on monoalkylbenzenes reported previously,²⁰ are given in brackets in Table I. It can be noted that the experimentally determined $\delta_{\text{C}(4,5)}$ values and those given by additivity are in fairly close agreement for all three *o*-dialkylbenzenes (within 0.8 ppm). For *o*-xylene and for *o*-diethylbenzene the predicted $\delta_{\text{C}(3,6)}$ values are in agreement with the experimental results within 0.6 ppm, but for *o*-di-*tert*-butylbenzene the deviation is nearly 5 ppm, the largest deviation found for any carbon position on these three compounds. For $\delta_{\text{C}(1,2)}$ the deviations range in magnitude from 1.4 to 2.2 ppm, with *o*-xylene giving the largest deviation. If one accepts the intuitive view that steric crowding and strain would be greatest for *o*-di-*tert*-butylbenzene among the three dialkylbenzenes, then it appears that the C(3,6) position, rather than the C(1,2) position, is more sensitive to the crowding, at least as far as ^{13}C shieldings are concerned. The fact that the additivity model is more successful for *o*-di-*tert*-butylbenzene than for *o*-xylene or *o*-diethylbenzene at C(1,2) may indicate that there are important limitations of the additivity approach for *o*-dialkylbenzenes, for which strain effects just happen to compensate in the *tert*-butyl case.

Also of interest in this regard are comparisons of the chemical shifts of the alkyl carbons of the *o*-dialkylbenzenes with those reported earlier for the monoalkylbenzenes.²⁰ Such comparisons reveal a 1.9-ppm increase in shielding of the methyl carbon in *o*-xylene relative to that in toluene; a 3.4-ppm increase and a 0.4-ppm increase in shielding for the α and β carbons, respectively, of *o*-diethylbenzene relative to ethylbenzene; and a 3.3-ppm *de*-

crease and 3.8-ppm decrease in shielding for the α and β carbons, respectively, of *o*-di-*tert*-butylbenzene relative to *tert*-butylbenzene. Considerable attention has been given previously, especially by Grant and Cheney,¹² to the small increases in shielding observed in sterically perturbed methyl groups such as those in *o*-xylene. However, the present results indicate that *negative* effects on the shielding may arise when the steric crowding is more acute. Negative ¹³C shielding effects have previously been attributed to 1,5 steric interactions.⁴⁰

From the deuterium-labeled compounds of this study, both isotope effects on the ¹³C shieldings and ¹³C-D coupling constants were measured. These are summarized in Table II. The results for both aromatic and aliphatic C-D moieties are very similar to what was reported earlier for monoalkylbenzenes²⁰ and analogous systems.⁴¹

Conclusions

The data presented here demonstrate that the aromatic carbons in benzocycloalkanes and *o*-dialkylbenzenes are sensitive to the geometrical constraints of the attached alkyl groups. The patterns of chemical shifts and the relationships to additivity predictions are consistent with the view that benzocyclopropene and *o*-di-*tert*-butylbenzene are the most highly strained systems in this study. The great similarity between the patterns of aromatic carbon shifts for benzosuberane and *o*-diethylbenzene imply that the former compound exhibits the least amount of strain in the five members of the benzocycloalkene series of the present investigation.

Acknowledgment. The authors wish to thank the National Science Foundation, the Research Corporation, and the Petroleum Research Fund, administered by the American Chemical Society, for financial support of this work. They gratefully acknowledge the help of Mr. Harry Dorn, Dr. Thomas Nakashima, and Mr. Jerry Dallas. D. L. wishes to thank the Deutsche Forschungsgemeinschaft for a fellowship. Acknowledgment of National Science Foundation equipment grants toward the purchases of the Bruker spectrometer and the Digilab data system is gratefully made.

References and Notes

- (1) Supported in part by a grant from the Petroleum Research Fund, administered by the American Chemical Society, by National Science Foundation Grant No. GP-7072, and by a grant from the Research Corporation.
- (2) (a) On leave to U. C., Davis (1969-1970) from San Francisco State College. (b) To whom correspondence should be sent at Department of Chemistry, Colorado State University, Fort Collins, Colorado 80521.
- (3) P. C. Lauterbur, *J. Amer. Chem. Soc.*, **83**, 1838 (1961).
- (4) H. Spiessbeck and W. G. Schneider, *Tetrahedron Lett.*, 468 (1961).
- (5) R. A. Friedel and H. L. Retcofsky, *J. Amer. Chem. Soc.*, **85**, 1300 (1963).
- (6) G. B. Savitsky and K. Namikawa, *J. Phys. Chem.*, **68**, 1956 (1964).
- (7) J. J. Burke and P. C. Lauterbur, *J. Amer. Chem. Soc.*, **86**, 1870 (1964).
- (8) D. M. Grant and E. G. Paul, *J. Amer. Chem. Soc.*, **86**, 2984 (1964).
- (9) D. D. Traficante and G. E. Maciel, *J. Phys. Chem.*, **69**, 1348 (1965).
- (10) G. E. Maciel and J. J. Natterstad, *J. Chem. Phys.*, **42**, 2427 (1965).
- (11) W. R. Woolfenden and D. M. Grant, *J. Amer. Chem. Soc.*, **88**, 1496 (1966).
- (12) D. M. Grant and V. B. Cheney, *J. Amer. Chem. Soc.*, **89**, 5315 (1967).
- (13) H. L. Retcofsky, J. M. Hoffman, Jr., and R. A. Friedel, *J. Chem. Phys.*, **46**, 4545 (1967).
- (14) A. J. Jones, D. M. Grant, and K. F. Kuhlmann, *J. Amer. Chem. Soc.*, **91**, 5014 (1969).
- (15) J. D. Roberts, J. B. Grutzner, M. Jautelat, J. B. Dence, and R. A. Smith, *J. Amer. Chem. Soc.*, **92**, 7107 (1970).
- (16) E. Lippma, T. Pehk, J. Paasivirta, N. Belikova, and A. Plate, *Org. Magn. Resonance*, **2**, 481 (1970).
- (17) C. S. Yannoni and H. E. Bleich, *J. Chem. Phys.*, **55**, 5406 (1971).
- (18) D. K. Dalling, D. M. Grant, and L. F. Jonson, *J. Amer. Chem. Soc.*, **93**, 3678 (1971).
- (19) M. Christl, H. J. Reich, and J. D. Roberts, *J. Amer. Chem. Soc.*, **93**, 3463 (1971).
- (20) D. Lauer, E. L. Motell, D. D. Traficante, and G. E. Maciel, *J. Amer. Chem. Soc.*, **94**, 5335 (1972).
- (21) M. Karplus and J. A. Pople, *J. Chem. Phys.*, **38**, 2803 (1963).
- (22) J. A. Pople, *Mol. Phys.*, **4**, 301 (1964).
- (23) B. V. Cheney and D. M. Grant, *J. Amer. Chem. Soc.*, **89**, 5319 (1967).
- (24) R. Ditchfield, D. P. Miller, and J. A. Pople, *J. Chem. Phys.*, **34**, 4186 (1971).
- (25) P. D. Ellis, G. E. Maciel, and J. W. McIver, Jr., *J. Amer. Chem. Soc.*, in press.
- (26) T. Tokuhira and G. Fraenkel, *J. Amer. Chem. Soc.*, **91**, 5005 (1969).
- (27) A. Velenik and R. M. Lynden-Bell, *Mol. Phys.*, **19**, 371 (1970).
- (28) M. A. Cooper and S. L. Manatt, *J. Amer. Chem. Soc.*, **92**, 1605 (1970).
- (29) S. Castellano and R. Kostelnik, *Tetrahedron Lett.*, 5511 (1967).
- (30) S. Kabuss, H. Friebolin, and H. Schmid, *Tetrahedron Lett.*, 469 (1965).
- (31) N. S. Bhacca, L. F. Johnson, and J. N. Shoolery, "Varian High Resolution NMR Spectra Catalog," Varian Associates, Palo Alto, Calif., 1962.
- (32) V. H. Meier, J. Heiss, H. Suhr, and E. Müller, *Tetrahedron*, **24**, 2307 (1968), and references therein.
- (33) V. J. Bartuska, T. T. Nakashima, and G. E. Maciel, *Rev. Sci. Instrum.*, **41**, 1458 (1970).
- (34) W. E. Coleman, Ph.D. Thesis, University of California, Berkeley, June 1960.
- (35) P. Mowery, Ph.D. Thesis, University of California, Berkeley, Dec 1970.
- (36) C. Djerassi and M. Gorman, *J. Amer. Chem. Soc.*, **75**, 3704 (1953).
- (37) G. Eigenmann and H. Zollinger, *Helv. Chim. Acta*, **48**, 1795 (1965).
- (38) H. C. Dorn and G. E. Maciel, *J. Phys. Chem.*, **76**, 2972 (1972).
- (39) G. B. Savitsky, *J. Phys. Chem.*, **67**, 2723 (1963).
- (40) J. I. Kroschwitz, M. Winokur, H. J. Reich, and J. D. Roberts, *J. Amer. Chem. Soc.*, **91**, 5927 (1969).
- (41) R. A. Bell, C. L. Chan, and B. G. Sayer, *J. Chem. Soc., Chem. Commun.*, 67 (1972).

Proton Magnetic Resonance Chemical Shifts and the Hydrogen Bond in Concentrated Aqueous Electrolyte Solutions

E. J. Sare, C. T. Moynihan, and C. A. Angell*

Department of Chemistry, Purdue University, Lafayette, Indiana 47907 (Received August 3, 1972)

Publication costs assisted by the Office of Saline Water, Department of the Interior

Proton chemical shifts have been measured over the temperature range 0–100° for concentrated solutions in 28 salt-water systems. A wide variety of cation charge/radius ratios and anion basicities are included. For salts of a given cation, correlations of the magnitude of the downfield shift, and especially of the temperature dependence of the shift, are found with the anion basicity. This is attributed to the importance in these solutions of hydrogen bonds between cation-solvated water molecules and nearest neighbor anions. The interpretation is consistent with the further finding that, for constant anion and salt/water ratio (R), shifts may be correlated with the hydrolysis constant of the various cations. The magnitude of the downfield shift for $R = 10 \text{ Al}(\text{NO}_3)_3$ is striking. Solutions of thiocyanate ions are anomalous. The relation of the temperature dependence of the shift to temperature-induced hydrogen bond rupturing, to solution configurational heat capacities, to solution glass transition temperatures, and to hydration number assessments, is considered.

Concentrated aqueous solutions, frequently avoided by physical chemists in the past because of their apparent complexity, are currently being given considerable attention.¹⁻⁹ In a number of cases, interest is directly related to the ability of these solutions to supercool, thus opening the long-relaxation time domain to investigation. In a broad front effort to determine the range of systems available for study in this significant and interesting region of behavior, Sare² determined the glass-forming composition regions and glass-transition temperatures for some 50 salt-water systems. This study, which established the glass temperature as a useful new structure-indicating probe, led to the conclusion that differences in the viscous behavior of solutions of a given concentration in the high concentration range are largely determined by the nature of the hydrogen bond acting between anions and the water molecules of the first or second hydration shell of the cation.

The present study, initially intended only to elucidate some observations on the temperature dependence of the proton chemical shift made during a proton magnetic resonance (pmr) study of cation hydration in molten hydrates,³ has been greatly extended because of the information it has provided on hydrogen bonding in these solutions, and the correlations with the viscous behavior which it has consequently made possible. We report chemical shift and shift temperature dependence data for 15 salt-water systems for which glass temperatures were previously determined² and 13 additional systems deemed of value for purposes of interpretation. Some of our conclusions were foreshadowed in a publication by Ellis and Hester,⁷ who measured δ relative to tetramethylammonium ion (TMA^+) as internal standard at 90° for solutions selected from five salt-water systems. In the present study, in which TMA^+ internal standard is also adopted, the temperature dependence of the shift is made the focus of attention. For this purpose the otherwise preferable but more time-consuming method of external referencing with directly measured susceptibility corrections¹⁰ offers no advantages.

Experimental Section

The pmr measurements were performed using a Varian A-60 nmr spectrophotometer which was equipped with a Varian V-6040 variable temperature system. Samples of the solutions of interest, which had been prepared by weight using distilled and deionized water, were contained in sealed, standard 5-mm o.d. nmr tubes. Approximately the lower 3.5 cm of each tube was filled with solution, while the remainder of the tube was blocked off with a close fitting Pyrex rod in order to minimize any distillation of water from the solution to upper portions of the tube during measurements at elevated temperatures.

All chemical shifts were measured relative to the proton signal from (TMA^+), which was included in the solution as an internal reference at a concentration of 0.005 cation mole fraction. A minimum of four spectra were run at each of the temperatures, which in general were spaced at approximately 20° intervals between 0 and 100° for each solution. Probe temperatures were measured prior to and immediately after the spectra were recorded by a substitution technique in which an nmr tube containing a copper-constantan thermocouple immersed in the center of a volume of inert liquid equal to that of the electrolyte solution was inserted into the probe. The temperature was found to be constant to within $\pm 1^\circ$ over the ~ 15 -min period required for the recording of each solution spectrum. Samples were preheated to a few degrees above the desired temperature in an external Temp-Blok module heater before insertion into the probe, in order to reduce the thermal equilibration period to 2–3 min.

The proton magnetic resonance spectra of all solutions studied were found to consist of two unsplit peaks corresponding to the water protons and the tetramethylammonium ion protons, respectively. A typical spectrum is shown as an inset to Figure 1. The reproducibility of the spectra and the uncertainty in the sample temperature indicate an accuracy of within $\pm 0.5 \text{ Hz}$ ($\pm 0.01 \text{ ppm}$) for the chemical shift of the water proton resonance referred to the internal standard proton resonance.

The problem of a reference standard for the proton reso-

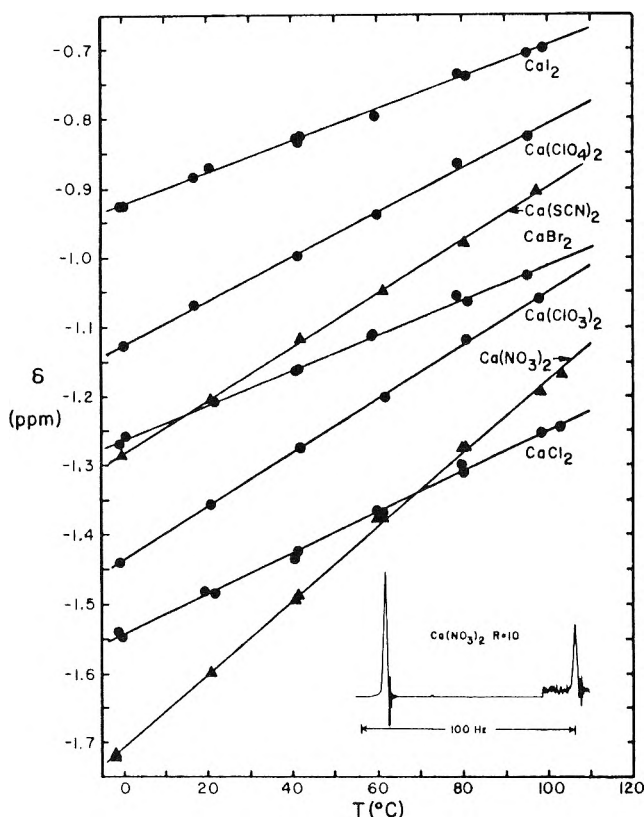


Figure 1. Proton chemical shift δ relative to TMA^+ as a function of temperature for solutions of calcium salts in water at a water/salt mole ratio of $R = 10$. Inset: typical proton magnetic resonance spectrum with both the water proton and tetramethyl ammonium ion (TMA^+) proton signals shown. TMA^+ signal is recorded at $200\times$ sensitivity increase over that used for solution protons.

nance has been given considerable attention in the present study. As frequently stated,^{7,11} the use of an internal standard renders somewhat unreliable the comparison of δ values between solutions of different salts and different concentrations of the same salt. This problem may be avoided by use of external standards if component susceptibilities are known or if the solution susceptibility is directly determined, *e.g.*, as described by in ref 10. The latter procedure, however, is technically demanding and the former, in view of the different sets of susceptibilities recommended,^{12,13} may lead to errors in δ as large as those associated with the use of internal standards. Since our concern in this work is mainly with the elucidation of the differences in temperature dependence of the chemical shifts between different solution types, and since this interest has required the recording of a great many spectra, experimental efficiency has been a prime consideration and has led us to adopt the internal standard. The value of the temperature dependence of the shift is neither expected nor found experimentally (see below) to depend on the choice of external *vs.* internal reference.

The value of δ itself at constant temperature will be seen to show a variation with solution anion which is large compared with any expected solvent effects on the reference frequency. While caution is warranted, these shifts can be given a natural interpretation. Comparisons of δ in this study are always made at constant water/cation mole ratio, hence almost constant ionic strength. Therefore, medium effects on the reference proton magnetic environment should derive principally from the anion-reference proton interactions, but these would tend to shift the sig-

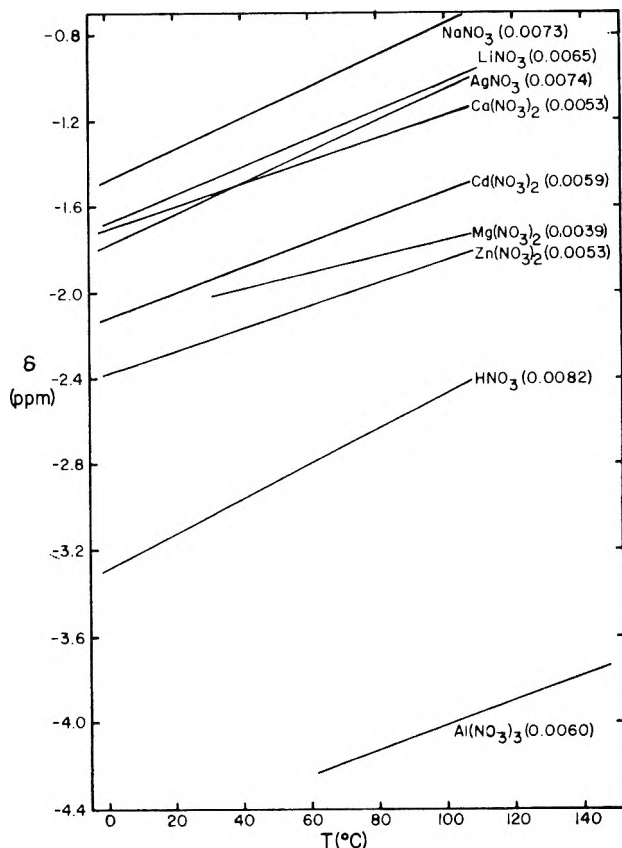


Figure 2. Proton chemical shift δ relative to TMA^+ as a function of temperature for various aqueous nitrate solutions of composition $R = 10$.

nal downfield from an external reference resonance and hence would, if anything, lead to an underestimate of the true magnitude of the anion effects we observe. The latter are thus in all probability reflecting a significant property of the solutions. Confidence in the significance of the observed shifts, and the correlations we will make, is raised by the observation that in the case of acetate solutions a second, and in this case anionic, internal reference was available. The shift of tetramethylammonium protons relative to the acetate protons was found to be constant, independent of temperature, cation type, and composition.

Results

Where practical, shifts were determined at two standard compositions, defined by R values of 10 and 6 (divalent cations) and 10 and 4 (monovalent cations), where

$$R = \text{moles of water/moles of salt}$$

In Figures 1 and 2 characteristic results are shown for the series of salt solutions of composition $R = 10$ (14.3 mol %, 9.2 *m*). In these figures the chemical shift relative to TMA^+ , δ (ppm), is plotted as a function of temperature. In Figure 2 the individual experimental points are omitted for the sake of clarity. In this latter case the chemical shift scale has been considerably reduced in order to accommodate the extraordinarily large downfield shift of the aluminum nitrate solutions, the implications of which will be discussed further below. For all solutions studied the chemical shift was found to be a linear function of temperature within experimental error and could be expressed by an equation of the form

$$\delta(\text{ppm}) = a + bt(^{\circ}\text{C})$$

Our experimental results are summarized in this form in Table I, where the a and b parameters for each solution were obtained from least-squares computer fits. Table I includes data from several solutions in which a tetramethylsilane vapor external reference was used. Note that the b parameters of eq 1 are independent of the type of reference used.

The only previous results of measurements of the TMA⁺-referenced proton chemical shift in solutions as concentrated as the present have been by Moynihan and coworkers³ and by Ellis and Hester.⁷ Only the points for Mg(NO₃)₂·6H₂O and Zn(NO₃)₂·6H₂O by the latter authors and Ca(NO₃)₂·4H₂O by the former are common to our study. For the Mg and Ca salts results agree within experimental error, while for the Zn salt a discrepancy of 0.04 ppm, slightly outside experimental uncertainties, exists.

Discussion

Cation and Anion Dependence of δ . Values of the proton chemical shift in dilute aqueous solutions have been intensively studied, and the results have been analyzed in terms of proton deshielding due to polarization of the oxygen by adjacent cations^{14,15} and of the attraction for the water protons exercised by anions of differing basicity.¹⁶ The present "solutions" differ from those studied by the latter authors insofar as there is no solvent water in the sense of a bulk water continuum, separating the hydrated cations from the anions; their chemical and physical properties may, for this reason, be distinctive.^{1,2} Nevertheless, cation and anion effects related to the above, and exceeding those attributable to medium effects on the internal reference, were found by Ellis and Hester⁷ in their hydrated nitrate, chlorate, and acetate "solutions." The anion effect was particularly marked, a finding they attributed to the direct manner in which the anions can act to deshield the protons due to the particular orientation of water molecules in the strong cation field. This interaction can be viewed as a tendency for the proton to vacate its position on the water oxygen in favor of residence on the anion.

Taking advantage of the additional systems investigated in this study, a correlation of the anion deshielding effect with known physical constants may be attempted by recognizing the relation between the latter proton transfer process and that which determines the strength of weak acids. Gurney¹⁷ has shown that the pK_a value attributed to a given acid is related to the electrical work of proton transfer from the anion in question to a particular reference energy state, *viz.*, a remote solvent molecule, by the relation

$$J = kT \cdot pK_a + kT \ln M \quad (1)$$

the second term being a constant for a given solvent of molecular weight M . For a remote water molecule reference state, data for the determination of J are available for a great many anions. These data have been assembled by Gurney in the useful form of a proton energy level diagram, shown in Figure 3a.

In the presence of cation polarization, the water levels are shifted up in proportion to the log (cation hydrolysis constant), pK_H , as represented by the levels Mg(II)-(H₂O):Mg(II)(OH)⁻ and Mg(II)H₃O⁺:Mg(II)H₂O which we have entered in Figure 3a.¹⁸

In both acid dissociation and cation hydrolysis processes most of the work of transfer is done in the region immedi-

ately adjacent to the anion or polarized water molecule where the dielectric constant is much lower than the bulk water value and the electrical field therefore very large. The net energy of proton transfer from polarized water to anion, which for dilute solutions is accurately obtained from Figure 3a, need therefore not be greatly altered in the absence of bulk water. Accordingly, the ordering of energy levels seen in Figure 3a should apply approximately to the concentrated solutions of this study. When hydrated cation and anion are near neighbors the nature of the proton transfer will depend on the potential function for the proton between the two electronegative centers. If this is of the single minimum type associated with strong hydrogen bonds then the "transfer" will in fact amount to a displacement of the proton equilibrium position in the lower (polarized water) level toward the anion, the displacement increasing with decreasing Figure 3a energy level separation. Since displacement away from the H₂O oxygen implies a deshielding of the proton, hence a downfield shift in δ , δ for solutions of a given cation should move downfield with increasing anion pK_a . For different cations, correlation lines should be displaced along the pK_a axis by intervals related to pK_H .

These (partly after the fact) notions are tested in Figure 3b. Although there are glaring discrepancies in the cases of ClO₃⁻, BrO₃⁻, and SCN⁻ anions, it appears that a useful degree of order among the results of Table I may be achieved. The cation effects are shown more broadly in Figure 2 where the order of δ is seen to be the order of the hydrolysis constants¹⁸ (at 25°) with the exception of Cd²⁺ for which δ falls above rather than below that of Mg²⁺. This would evidently be rectified at lower temperatures, (Figure 2).

There are a number of reasons, apart from the use of an internal standard, why the correlation should be imperfect. For reasons given above, the most obvious one, *viz.* the effect of removal of bulk water on the pK_a - and pK_H -based proton level ordering, may not be the most important. Differences in local ionic electrical environment between dilute and concentrated solutions, such as those associated with the substitution of anion for water in the first coordination sheath of the cation, should have a more pronounced effect. There is evidence that such substitution occurs in some⁴ but not all⁸ of the present solutions in our concentration range. Its effect should be to increase the average water-to-anion energy separation, hence to decrease the downfield shift observed (*cf.* BrO₃⁻, ClO₃⁻, and SCN⁻ in Figure 3b). A discrepancy for Ca(NO₃)₂ solution would also be expected on this basis⁴ but is only found in the temperature dependence (see below).

Temperature Dependence of δ . Because of current interest in the temperature dependence of charge migration and mechanical relaxation processes in concentrated solutions,^{6-9,19} and its correlation with thermodynamic properties, information on the temperature dependence of hydrogen bonding made possible by these studies is of importance. Before examining the data, however, we should first note that it has been assumed, in some discussions of the proton chemical shift in dilute aqueous solutions, that the temperature dependence of a proton shift for water molecules immediately coordinated to cations should have a value sufficiently small to be neglected in comparison with the temperature dependence of the shift for pure water. Further, this assumption has been made the basis of a means of determining hydration numbers from the temperature dependence of the chemical shift in dilute

TABLE I: Least-Squares Fits of Water Proton Chemical Shifts with Respect to $(\text{CH}_3)_4\text{N}^+$ Ion Internal Reference^a for Aqueous Electrolyte Solutions to the Equation $\delta(\text{ppm}) = a + bT(^{\circ}\text{C})$. Solution Compositions Given in Terms of R (= moles of water/moles of salt). (Molality = $55.1/R$, mol % salt = $100/(R + 1)$)

Salt	R	a	10^3b	10^3 std dev	Temp range, $^{\circ}\text{C}$
CaCl ₂	6 (i)	-1.54	2.3	4	19-103
	(ii) (TMS external ref)	-5.14	2.7	3	35-96
	10	-1.54	3.0	6	-1-103
CaBr ₂	6	-1.26	1.8	5	41-95
	10	-1.26	2.5	5	-1-96
CaI ₂	6	-0.86	1.3	3	49-105
	10	-0.92	2.3	4	-1-99
Ca(NO ₃) ₂	4	-1.66	4.0	3	18-99
	6 (i)	-1.70	4.7	4	-1-99
	(ii)	-1.70	4.7	4	-1-79
	(iii) (TMS external ref)	-5.06	4.4	6	-2-104
	10	-1.71	5.3	8	-2-104
Ca(ClO ₄) ₂	14	-1.72	5.8	15	0-99
	6	-0.92	1.5	6	76-138
	10	-1.13	3.2	6	0-96
Ca(ClO ₃) ₂	6	-1.37	3.0	3	-1-98
	10	-1.44	3.9	2	-1-98
Ca(SCN) ₂	6	-1.25	2.9	5	-1-98
	10	-1.28	3.9	4	0-98
MgCl ₂	10	-2.00	3.0	7	-3-98
MgBr ₂	10	-1.73	2.9	7	1-98
MgI ₂	10	-1.39	2.9	5	-2-89
Mg(NO ₃) ₂	6	-2.32	3.9	3	92-137
	10	-2.14	3.9	4	49-101
Mg(SCN) ₂	10	-1.67	4.6	4	-5-94
Mg(CH ₃ CO ₂) ₂	10	-2.69	7.8	13	36-95
Mg(CHCl ₂ CO ₂) ₂	10	-2.38	6.7	11	-5-88
LiCl	3	-1.48	3.4	5	5-97
	4	-1.47	3.7	5	1-96
	6	-1.52	4.7	8	1-91
	10	-1.62	5.9	8	2-91
LiBr	3				
	4	-1.17	3.4	8	-3-96
	6				
LiI	10	-1.42	5.7	7	-3-95
	4	-0.77	3.3	1	63-94
	9	-1.2	5.9	7	-5-94
LiNO ₃	4	-1.61	5.4	6	11-101
	10	-1.67	6.5	11	10-102
LiClO ₄	9	-1.29	5.7	10	12-101
LiSCN	4	-1.12	4.7	6	11-101
	10	-1.42	6.9	6	-1.5-88
LiCH ₃ CO ₂	4	-2.23	6.5	7	34-102
	10	-2.10	7.3	16	12-102
LiBrO ₃	4	-1.5	5.2	1	3-86
	10	-1.63	6.8	6	3-86
AgNO ₃	6	-1.80	7.1	6	3-86
	10	-1.79	7.3	8	-2-84
HNO ₃	6	-4.00	9.3	6	3-86
	10	-3.29	8.2	7	3-86
NaNO ₃	6	-1.37	6.6	4	3-85
	10	-1.48	7.3	9	4-84
Cd(NO ₃) ₂	4	-2.22	5.2	8	33-88
	6 (i)	-2.18	5.3	6	30-96
	(ii) (TMS external ref)	-5.57	5.0	5	35-92
Zn(NO ₃) ₂	10	-2.12	5.9	5	36-100
	6	-2.54	3.9	9	36-94
	10	-2.38	5.3	2	3-85
Al(NO ₃) ₃	10	-4.60	6.0	4	68-142

^a In three cases CaCl₂ $R = 6$, Ca(NO₃)₂ $R = 6$, and Cd(NO₃)₂ $R = 6$, chemical shifts measured vs. a tetramethylsilane vapor external reference are entered in the table. Note that the difference in a parameters, Δa , which represents the shift of internal vs. external reference in each case, is almost constant at 3.60, 3.37, and 3.39 ppm, respectively. Estimated susceptibility corrections to externally referenced shifts are large, and variations in Δa are expected. In three cases, LiCH₃CO₂ $R = 4$ and $R = 10$, and MgCH₃CO₂ $R = 10$, the shift of the acetate ion C-H proton relative to TMA⁺ was observed at 1.23, 1.23, and 1.26 ppm, respectively.

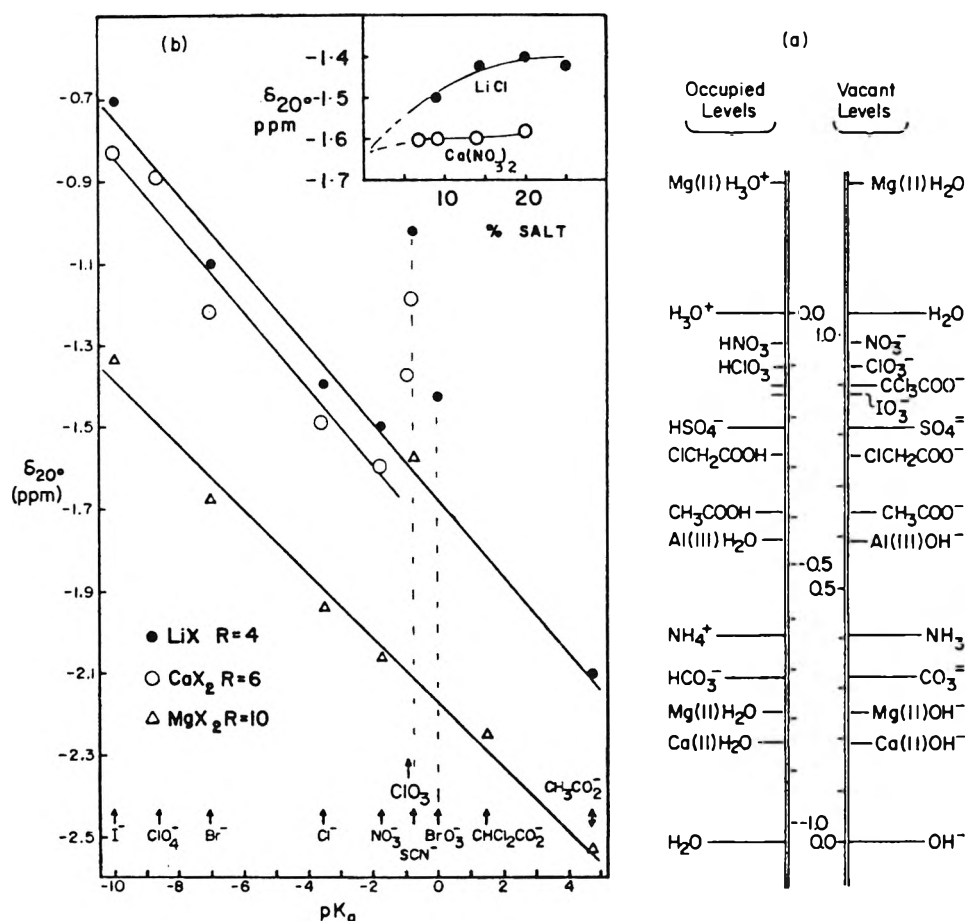


Figure 3. (a) Proton energy level diagram after Gurney,¹⁷ including cation-polarized water and hydronium ion levels. Energy units are electron volts. (b) Approximate correlation of proton chemical shifts relative to TMA⁺ with anion pK_a for lithium, calcium, and magnesium solutions of selected compositions at 25°. Inset: δ vs. composition for representative systems, LiCl-H₂O and Ca(NO₃)₂-H₂O.

solutions.²⁰⁻²⁶ Although it may be argued (neutron inelastic scattering data²⁷ notwithstanding) that the structure of water in the vicinity of cations in dilute solutions is not necessarily the same as that in the solutions studied in the present work, the position is at very least uncertain, and hydration numbers assigned on this basis should be treated with caution. (In the most recent paper on shift-based hydration numbers,²⁶ some highly concentrated solutions, *e.g.*, 17.8 *m* LiBr, have been studied, and the residual temperature dependence of δ has been noted and attributed to the onset of ion-pairing interactions.) On the basis of our findings, detailed below, we believe the standing of such calculations could be much improved (and the "hydration numbers" often increased) by at least taking into account the anion-water interaction which will certainly influence the proton shift in dilute solutions.

The temperature dependence of δ in these solutions in relation to those in dilute solutions can be emphasized with the data presented in Figure 4. In this figure, values of $d\delta/dT$ are plotted as a function of solution composition for solutions of both lithium and calcium cations. The data of the present study have been combined with those from previous investigations^{23,26} in which external reference standards were used to yield a clear overall picture of the composition dependence of $d\delta/dT$ over the composition region from infinite dilution to molten hydrate values. The excellent agreement of internally and externally referenced data is to be emphasized.

Not surprisingly, the region of most rapid change in the composition dependence of $d\delta/dT$ corresponds approxi-

mately to the composition region in which cohesive energy indicating properties, such as the glass transition temperature, also show most rapid changes in composition dependence.² Figures 4 and 5 show that where sufficiently basic anions are chosen, the values of $d\delta/dT$ observed for the concentrated solutions may not be greatly different from that in pure bulk water (0.0096 ppm/deg).²⁶ Whereas the large value of $d\delta/dT$ for pure water may be attributed to the breakup of the hydrogen-bonded bulk water structure with increasing temperature, the $d\delta/dT$ values for concentrated solutions must be attributed to processes which allow a temperature dependence of the proton chemical shift for water in a strictly ionic environment. A number of possible sources of the upfield shift with increase in temperature for such hydrate melts have been suggested:^{3,7,23} (1) weakening or breaking of hydrogen bonds between anions and the water molecules in the cation hydration sheath;⁷ (2) changes in the relative configuration of the waters of the hydrated cationic entity itself;³ (3) changes in the magnetic anisotropy effects due to the onset of rotation of asymmetric anions;^{23,28} (4) a temperature-dependent equilibrium involving anion-water exchange in the primary hydration sheaths of the cation.⁷

Detailed consideration of each of these effects²¹ leads to the conclusion that only effect (1) is sufficiently general to account for the observed behavior. In this case, a correlation should again exist between the magnitude of the temperature dependence of δ and the hydrogen bond-strength-indicating pK_a value for the anion. This is confirmed by the data shown in Figure 5, except for a "levelling" of the

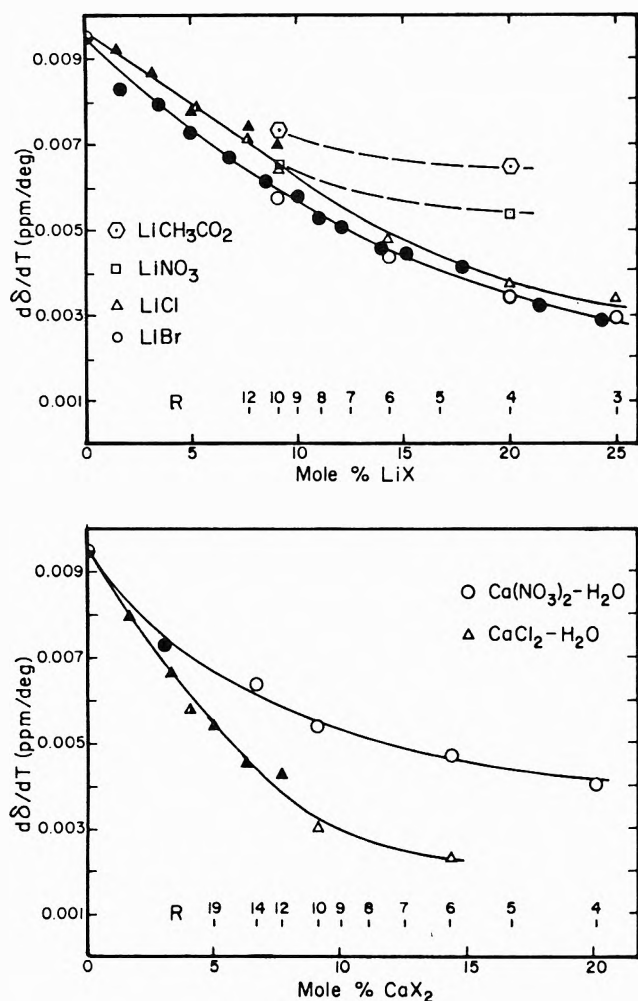


Figure 4. Temperature dependence of the proton chemical shift, $d\delta/dT$, as a function of composition for various lithium and calcium aqueous solutions. Open symbols, this work; closed symbols, data from ref 23 and 26, obtained using external standards.

$R = 10$ "strong acid" anion solutions. Data on additional solutions in which the cation pK_H and R values are varied widely will be reported separately.²⁹

The levelling effect for $R = 10$ solutions in Figure 6 we suppose to be due to the fact that in each of the strong acid anion solutions the temperature dependence of δ is determined by the breaking of H_2O-H_2O bonds. The reason is that when $pK_a < 1$ and when more than one hydration sheath of water molecules is present, the H bonds between first and second hydration sheath water molecules will be the strongest H bonds in the system and may be expected therefore to determine the $d\delta/dT$ value of the solution.

The actual value of $d\delta/dT$ exhibited by a given concentrated solution will depend both on the proton deshielding accompanying the rupture (or bending)^{30,31} of an H bond between water and an anion, and on the rate per $^{\circ}C$ at which H bonds are broken (or bent through some fixed angle—we will assume bond-breaking in the ensuing discussion). Large downfield values of δ will, therefore, only yield large values of $d\delta/dT$ if the bond-breaking rates (dN_{bb}/dT) are about the same for solutions being compared. Since, as seen above, $d\delta/dT$ at constant R correlates with pK_a as well as or better than δ itself, it appears that the dN_{bb}/dT values are either the same for all solutions or vary systematically with pK_a .

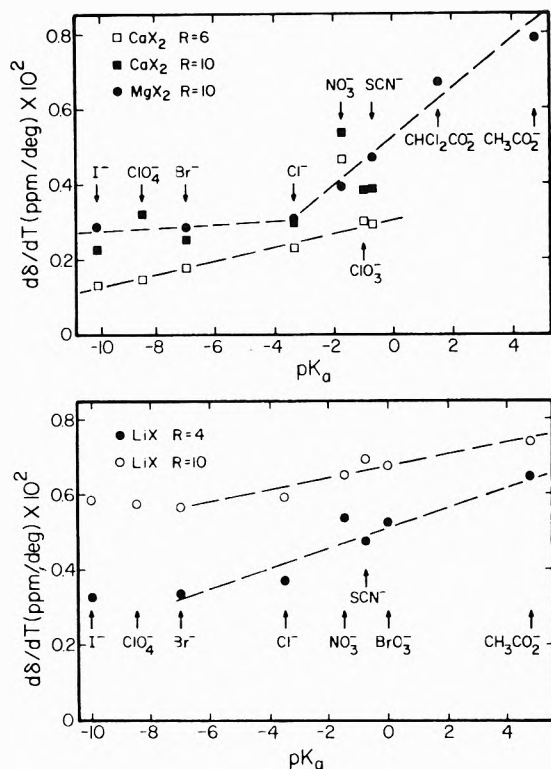


Figure 5. Correlation of the proton chemical shift temperature dependence, $d\delta/dT$, with anion basicity at specified compositions ($R = 4, 6, \text{ or } 10$) for various solutions of lithium, calcium and magnesium salts.

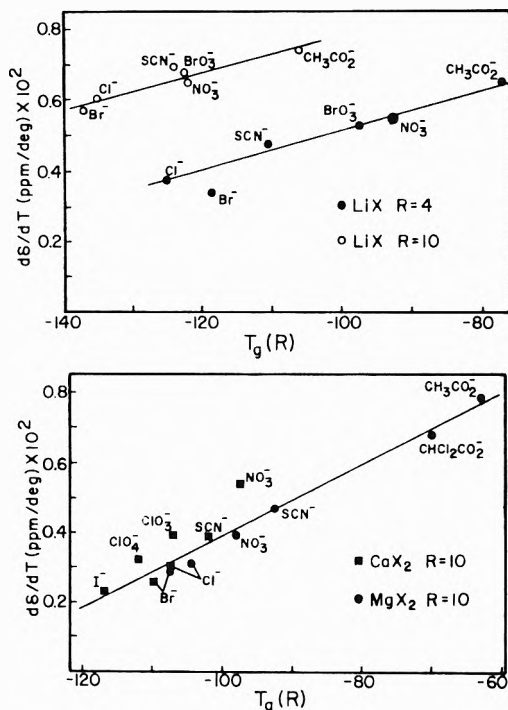


Figure 6. Correlation of the proton chemical shift temperature dependence, $d\delta/dT$, with the glass transition temperature for various fixed R value solutions of lithium, calcium, and magnesium cations.

Because the combination of bond strength and dN_{bb}/dT must determine, or strongly influence, such important solution properties as solution heat capacities and viscosities, we should consider what factors determine the bond-breaking rate. The importance of this is underlined when

it is noted, from Figures 4 and 5, that despite the fact that water-anion H bonds in basic anion solutions are much stronger than water-water H bonds, $d\delta/dT$ for pure water is larger than that observed for any of these solutions.

The temperature dependence of the bond-breaking process in water has been discussed by a number of authors.³¹⁻³⁴ In particular, Angell,³⁴ treating the broken hydrogen bond as a sort of quasi-lattice defect, showed that the fraction N_{bb} of possible bonds broken at the temperature T depended on temperature according to

$$N_{bb}(T) = \left[1 + \exp\left(\frac{\Delta H - T\Delta S}{RT}\right) \right]^{-1} \quad (2)$$

where ΔH and ΔS are respectively the molar changes of enthalpy and entropy associated with the bond-breaking process. ΔH is a direct measure of bond strength. Over wide ranges of temperature this expression requires that N_{bb} varies almost linearly with T ;³⁵ hence the linearity of the $d\delta/dT$ plots can be understood. The slope depends on both ΔS and ΔH . From analysis of the configurational³⁶ heat capacity, which is related to dN_{bb}/dT by

$$C_{p(\text{conf})} = \Delta H dN_{bb}/dT \quad (3)$$

it is found that the value of ΔS for water is exceptionally high. The difference between the $d\delta/dT$ values for the concentrated solutions and water is, therefore, to be understood in terms of the more normal values of the entropy change associated with hydrogen bond breaking in the former cases.

From this discussion it would appear that since δ ($\propto \Delta H$) and $d\delta/dT$ ($\propto \delta dN_{bb}/dT$) are appropriately weighted averages over all H bonds in the solution, $d\delta/dT$ for different solutions should, according to eq 3, be correlated to the solution "configurational" heat capacities, at least when other factors (such as hindered rotations of NO_3^-) are held constant. Appropriate data to investigate this possibility are currently being acquired.

Chemical Shift and the Glass Temperature. The glass-forming properties of these solutions and the interpretation of the glass temperature in terms of anion-to-solvated water H bonding were referred to in the introduction. The experimental glass temperature, T_g , as measured by dta experiments,² occurs when the structural relaxation, or equilibration, time reaches values of about 1 sec. To the extent that the viscous behavior is determined by the degree of H bonding,^{9,34} T_g may be related conceptually to the temperature at which the great majority of the possible H bonds have been formed [$\sim 96\%$ according to zeroth order theory³⁵].

It seems that a good correlation, Figure 6, exists between $d\delta/dT$ and T_g even though the former quantity is influenced by bond breaking entropy as well as bond strength factors. In this correlation only $\text{Ca}(\text{NO}_3)_2$ is exceptional, exhibiting a high $d\delta/dT$ value which might be accounted for by the occurrence of the NO_3^- - H_2O exchange process⁴ mentioned earlier for the case of this salt. The strong acid anions fall on the plot because, unlike pK_a , neither T_g nor $d\delta/dT$ changes much in the series Cl^- , Br^- , ClO_4^- , I^- .

Chemical Aspects. One of the more striking findings of this work is the magnitude of the downfield shift for the $\text{Al}(\text{NO}_3)_3$ $R = 10$ solution. Unlike their behavior in dilute solution Al salts in ultraconcentrated solutions do not hydrolyze to yield insoluble basic products. This is explained most simply by observing that, at these concentrations,

there is no bulk solvent from which basic products can precipitate. This behavior is also true of other normally hydrolyzing solutions such as those of Bi(III) and Sn(IV).^{2a} Under high concentration conditions, the $\text{Al}-\text{H}_2\text{O}$ interactions responsible for hydrolysis in dilute solutions produce solutions in which the protons on the water molecules are very loosely bound. This is manifested in the value of δ . Figure 3 shows the shift is much greater than for HNO_3 at the same R value, although this is partly because the Al^{3+} ion directly contacts six of the ten H_2O molecules present, whereas HNO_3 transfers its proton primarily to a single H_2O molecule leaving nine relatively unaffected which average the signal to more upfield values. Nevertheless, Figure 2 suggests that highly concentrated solutions of $\text{Al}(\text{NO}_3)_3$ and related salts must be regarded as forming an interesting class of strong protonic acids, stronger than the $\text{Al}(\text{III})\text{H}_2\text{O}$ -to- NO_3^- occupied-to-vacant proton energy level gap in Figure 3a would suggest. Experiments to be reported separately³⁷ will show that mixtures of $R = 10$ $\text{Al}(\text{NO}_3)_3$ and AlCl_3 solutions can be used to dissolve noble metals at a much greater rate than can be achieved with boiling aqua regia.

Acknowledgments. The authors gratefully acknowledge partial support of this work by a grant from the Department of the Interior, Office of Saline Water.

References and Notes

- (1) J. Braunstein in "Ionic Interactions: From Dilute Solutions to Fused Salts," I. Petrucci, Ed., Academic Press, New York, N. Y., 1971, p 53; *Inorg. Chim. Acta*, **2**, 19 (1968).
- (2) (a) C. A. Angell and E. J. Sare, *J. Chem. Phys.*, **52**, 1058 (1970); (b) E. J. Sare Ph.D. Thesis, Purdue University, Lafayette, Ind., 1971.
- (3) C. T. Moynihan and A. Fratiello, *J. Amer. Chem. Soc.*, **89**, 5546 (1967); C. T. Moynihan, C. R. Smalley, C. A. Angell, and E. J. Sare, *J. Phys. Chem.*, **73**, 2287 (1969).
- (4) (a) R. E. Hester and R. A. Plane, *Inorg. Chem.*, **3**, 769 (1965); *J. Chem. Phys.*, **40**, 411, (1960); (b) R. E. Hester and C. W. J. Scaife, *ibid.*, **54**, 654 (1971).
- (5) A. R. Davis and D. E. Irish, *Inorg. Chem.*, **7**, 1699 (1968); D. E. Irish, D. L. Nelson, and M. H. Brooker, *J. Chem. Phys.*, **54**, 654 (1971).
- (6) C. T. Moynihan, R. D. Bressel, and C. A. Angell, *J. Chem. Phys.*, **55**, 4414 (1971).
- (7) V. S. Ellis and R. E. Hester, *J. Chem. Soc. A*, 411 (1969).
- (8) M. Peleg, *J. Phys. Chem.*, **76**, 1019 (1972).
- (9) C. A. Angell and R. D. Bressel, *J. Phys. Chem.*, **76**, 3244 (1972).
- (10) (a) C. A. Reilly, H. M. McConnell, and R. G. Meisenheimer, *Phys. Rev.*, **98**, 264A (1955); (b) D. C. Douglass and A. Fratiello, *J. Chem. Phys.*, **39**, 3163 (1963); (c) K. Frei and H. J. Bernstein, *ibid.*, **37**, 1891 (1962).
- (11) (a) R. E. Glick, W. E. Stewart, and K. C. Tewari, *J. Chem. Phys.*, **45**, 4049 (1965); (b) J. E. Gordon and R. L. Thorne, *J. Phys. Chem.*, **73**, 3643 (1969); (c) N. C. Deno, H. G. Richey, Jr., N. Friedman, J. D. Hodge, J. J. Houser, and C. U. Pittman, Jr., *J. Amer. Chem. Soc.*, **85**, 299 (1963).
- (12) B. P. Fabricand and S. Goldberg, *J. Chem. Phys.*, **34**, 1624 (1961).
- (13) C. Franconi and F. Conti "NMR in Chemistry," B. Pesce, Ed., Academic Press, New York, N. Y., 1965.
- (14) J. C. Hindman, *J. Chem. Phys.*, **36**, 1000 (1962); **44**, 4582 (1966).
- (15) R. C. Axtmann, *J. Chem. Phys.*, **30**, 340 (1959).
- (16) K. A. Hartman, Jr., *J. Phys. Chem.*, **70**, 270 (1966).
- (17) R. W. Gurney, "Ionic Process in Solution," Dover Publications, New York, N. Y., 1953.
- (18) pK_H values for cations and estimated pK_a values for the halo-acids and perchloric acid used in Figures 3 and 5 are taken from F. Basolo and R. G. Pearson, "Mechanisms of Inorganic Reactions," 2nd ed, Wiley, New York, N. Y., 1968.
- (19) (a) J. H. Ambrus, C. T. Moynihan, and P. B. Macedo, *J. Phys. Chem.*, **76**, 3287 (1972); (b) J. H. Ambrus, H. Dardy, and C. T. Moynihan, *ibid.*, **76**, 3495 (1972); (c) C. T. Moynihan, N. Balitactac, L. Boone, and T. A. Litovitz, *J. Chem. Phys.*, **55**, 3013 (1971).
- (20) E. R. Malinowski, P. S. Knapp, and B. Beuer, *J. Chem. Phys.*, **45**, 4274 (1966).
- (21) E. R. Malinowski and P. S. Knapp, *J. Chem. Phys.*, **48**, 4989 (1968).
- (22) P. S. Knapp, R. O. Waite, and E. R. Malinowski, *J. Chem. Phys.*, **49**, 5459 (1968).
- (23) R. W. Creekmore and C. N. Reilly, *J. Phys. Chem.*, **73**, 1563 (1969).

- (24) R. W. Creekmore and C. N. Reilly, *Anal. Chem.*, **42**, 570 (1970).
 (25) T. E. Gough, H. D. Sharma, and N. Subramanian, *Can. J. Chem.*, **48**, 917 (1970).
 (26) Br. F. J. Vogrin, P. S. Knapp, W. L. Flint, A. Anton, G. Highberger, and E. R. Malinowski, *J. Chem. Phys.*, **54**, 178 (1971).
 (27) G. J. Safford, P. S. Leung, A. W. Naumann, and P. C. Schaffer, *J. Chem. Phys.*, **50**, 4444 (1969).
 (28) J. A. Pople, W. G. Schneider, and H. J. Bernstein, "High-Resolution Nuclear Magnetic Resonance," McGraw-Hill, New York, N. Y., 1959.
 (29) J. C. Tucker and C. A. Angell, to be published.
 (30) N. Muller and R. C. Reiter, *J. Chem. Phys.*, **42**, 3265 (1965).
 (31) J. C. Hindman, *J. Chem. Phys.*, **44**, 4582 (1966).
 (32) G. E. Walrafen in "Water, a Comprehensive Treatise," F. Franks, Ed., Plenum Press, New York, N. Y., 1971, Chapter 6.
 (33) J. D. Worley and I. M. Klotz, *J. Chem. Phys.*, **45**, 2868 (1966).
 (34) C. A. Angell, *J. Phys. Chem.*, **75**, 3698 (1971).
 (35) C. A. Angell and K. J. Rao, *J. Chem. Phys.*, **57**, 470 (1972).
 (36) E. Eisenberg and W. Kauzmann, "The Structure and Properties of Water," Oxford University Press, New York, 1969.
 (37) E. J. Sare and C. A. Angell, unpublished results.

Proton Magnetic Resonance Investigations of Alkylammonium Carboxylate Micelles in Nonaqueous Solvents. III.¹ Effects of Solvents

O. A. El Seoud, E. J. Fendler, J. H. Fendler,* and R. T. Medary

Department of Chemistry, Texas A & M University, College Station, Texas 77843 (Received January 18, 1973)

Changes in the chemical shifts of the magnetically discrete protons of butyl- (BAP), hexyl- (HAP), octyl- (OAP), and dodecyl- (DAP) ammonium propionates in CDCl_3 , CH_2Cl_2 , $\text{C}_6\text{H}_5\text{Cl}$, and DMAC as functions of their concentrations have established the formation of micelles with aggregation numbers in the range of 3–8. The critical micelle concentrations, cmc values, in CDCl_3 are: BAP = $(8\text{--}10)10^{-2} M$, HAP = $(5\text{--}6.35)10^{-2} M$, OAP = $(3.35\text{--}4.65)10^{-2} M$, DAP = $(2.0\text{--}2.7)10^{-2} M$; in CH_2Cl_2 are: BAP = $(10.7\text{--}12.0)10^{-2} M$, HAP = $(8.0\text{--}8.5)10^{-2} M$, OAP = $(5.0\text{--}5.7)10^{-2} M$, DAP = $(2.7\text{--}4.0)10^{-2} M$; in $\text{C}_6\text{H}_5\text{Cl}$ are: BAP = $(11.0\text{--}13.4)10^{-2} M$, HAP = $(8\text{--}10)10^{-2} M$, OAP = $(5.0\text{--}5.5)10^{-2} M$; and in DMAC are: BAP = $(15\text{--}17)10^{-2} M$, HAP = $(12\text{--}13)10^{-2} M$, OAP = $(9\text{--}11)10^{-2} M$, DAP = $(4\text{--}6)10^{-2} M$. The cmc values in each solvent decrease with increasing number of carbon atoms in the alkyl chain and for each surfactant they increase with increasing solvent polarity. With the exception of $\text{C}_5\text{H}_5\text{Cl}$, good relationships have been obtained between $\log \text{cmc}$ and both the reciprocal dielectric constant and solvent polarity parameter E_T . Structures of these micelles are discussed.

Introduction

Previous parts of this series reported the proton magnetic resonance spectroscopic investigation of the aggregation properties of alkylammonium carboxylate surfactants in benzene and in carbon tetrachloride.^{1,2} The data obtained indicated the formation of rather small aggregates, each containing three–seven monomers, in which the polar headgroups are located in the interior while the hydrophobic hydrocarbon chains are in contact with the nonpolar solvent. These aggregates have been termed reversed or inverted micelles.^{3,4} Critical micelle concentrations of alkylammonium carboxylates in carbon tetrachloride were found to be independent of the length of both the carboxylate and alkylammonium groups. In benzene, on the other hand, the critical micelle concentration decreases with an increasing number of carbon atoms in the alkylammonium group but it increases with an increasing number of carbon atoms in the carboxylate group.^{1,2} In order to obtain a better understanding of the effects of nonaqueous solvents on micellar parameters, a necessary requirement for the interpretation of the observed dramatic rate enhancements by reversed micelles,^{5–8} we have investigated the ^1H nmr behavior of alkylammonium propionates in deuteriochloroform (CDCl_3), dichloromethane (CH_2Cl_2), chlorobenzene ($\text{C}_6\text{H}_5\text{Cl}$), and *N,N*-dimethylacetamide (DMAC).

Experimental Section

The preparation and purification of butyl- (BAP), hexyl- (HAP), octyl- (OAP), and dodecyl- (DAP) ammonium propionate have been described previously.^{2,4,9} Reagent grade *n*-alkylamines, fractionally distilled from calcium hydride, and reagent grade propionic acid were used as starting materials. The purity of each surfactant was established by its melting or boiling point and by its infrared and proton magnetic resonance spectra. The following uncorrected melting and boiling points were obtained: BAP (60°, 0.25 Torr), HAP (68–69°, 0.80 Torr), OAP (70°, 0.25 Torr), DAP (56.0–56.5°).

Since water is solubilized in reversed micelles and seriously affects the chemical shifts in many cases, particularly that of the ammonium protons, special care has been taken to remove it from the surfactants and solvents used and to exclude inadvertent moisture from the solutions (any stock solutions for which the chemical shifts deviated more than 5.0 Hz at 100 Mz for the ammonium protons were not used). The solvents used were treated as follows: CDCl_3 (Thompson-Packard, 99.8% deuterated) was distilled from CaH_2 onto freshly activated Linde Type 4A molecular sieve; CH_2Cl_2 (Fisher spectrophotometric grade) was dried over freshly activated Linde Type 4A molecular sieve; $\text{C}_6\text{H}_5\text{Cl}$ (Fisher reagent grade) was dried with anhydrous CaSO_4 , filtered, and distilled from CaH_2 .

TABLE I: ^1H Nmr Parameters^a for Alkylammonium Propionates in Various Solvents^b

Solvent		Surfactant ^c				
		BAP	HAP	OAP	DAP	
CDCl_3	$\delta \text{CH}_3(\text{CH}_2)_{x-1}\text{N}^+$	1.456	1.411	1.395	1.409	
	$\delta \text{CH}_3\text{CH}_2\text{CO}_2^-$	1.606	1.602	1.595	1.591	
	$\delta \text{CH}_3(\text{CH}_2)_{x-2}\text{CH}_2\text{N}^+$		1.829	1.791	1.789	
	$\delta \text{CH}_3\text{CH}_2\text{CO}_2^-$	2.756	2.739	2.716	2.702	
	$\delta \text{CH}_3(\text{CH}_2)_{x-2}\text{CH}_2\text{N}^+$	3.363	3.342	3.317	3.308	
	δNH_3^+	8.893	8.726	8.613	8.409	
	$J(\text{CH}_3(\text{CH}_2)_x\text{N}^+)$					5.5
	$J(\text{CH}_3\text{CH}_2\text{CO}_2^-)$	7.4	7.5	7.7	7.4	
	$J(\text{CH}_2\text{CH}_2\text{N}^+)$	7.6		7.3	7.5	
	CH_2Cl_2	$\delta \text{CH}_3(\text{CH}_2)_{x-1}\text{N}^+$	1.433	1.399	1.389	1.372
$\delta \text{CH}_3\text{CH}_2\text{CO}_2^-$		1.565	1.554	1.554	1.525	
$\delta \text{CH}_3(\text{CH}_2)_{x-2}\text{CH}_2\text{N}^+$			1.832	1.795	1.763	
$\delta \text{CH}_3\text{CH}_2\text{CO}_2^-$		2.712	2.687	2.670	2.635	
$\delta \text{CH}_3(\text{CH}_2)_{x-2}\text{CH}_2\text{N}^+$		3.323	3.301	3.274	3.247	
δNH_3^+		8.894	8.753	8.384	8.360	
$J(\text{CH}_3(\text{CH}_2)_x\text{N}^+)$		6.0	5.7		6.9	
$J(\text{CH}_3\text{CH}_2\text{CO}_2^-)$		7.4	7.5	7.6	7.8	
$J(\text{CH}_3\text{CH}_2\text{N}^+)$		7.4	7.3	7.9	7.7	
$\text{C}_6\text{H}_5\text{Cl}$		$\delta \text{CH}_3(\text{CH}_2)_{x-1}\text{N}^+$	0.842	0.870	0.919	
	$\delta \text{CH}_3\text{CH}_2\text{CO}_2^-$	1.173	1.211	1.252		
	$\delta \text{CH}_3(\text{CH}_2)_{x-2}\text{CH}_2\text{N}^+$		1.223	1.280		
			1.441 ^d	1.450 ^d		
	$\delta \text{CH}_3\text{CH}_2\text{CO}_2^-$	2.348	2.377	2.407		
	$\delta \text{CH}_3(\text{CH}_2)_{x-2}\text{CH}_2\text{N}^+$	2.857	2.860	2.854		
	δNH_3^+	9.068	8.820	8.709		
	$J(\text{CH}_3(\text{CH}_2)_x\text{N}^+)$	6.8	5.0			
	$J(\text{CH}_3\text{CH}_2\text{CO}_2^-)$	7.5	7.5	7.3		
	$J(\text{CH}_2\text{CH}_2\text{N}^+)$	7.9	7.8	7.7		
DMAC ^e	δCH_3	0.648	0.641	0.633	0.628	
	δNH_3^+	6.353	6.498	6.175	5.984	

^a δ in ppm, J in Hz. ^b At 100 MHz and 30° unless specified otherwise (see Experimental Section). ^c [Surfactant] = 0.10 M. ^d See Results and Discussion. ^e At 60 MHz and 36° (see Experimental Section).

onto freshly activated Linde Type 4A molecular sieve; and DMAC (Aldrich gold label and J. T. Baker reagent grade) was distilled onto freshly activated Linde Type 4A molecular sieve. The Linde Type 4A molecular sieve used was activated by heating to 320°, cooled in a vacuum desiccator, and saturated with dry nitrogen. The solid surfactants were pulverized and dried under high vacuum (10^{-5} Torr) for at least 12 hr prior to preparation of solutions.

The 100-MHz proton magnetic resonance spectra were obtained on a modified Varian Associates HA-100 spectrometer with a Hewlett-Packard Model 200 ABR audio oscillator and frequency counter; those at 60 MHz were obtained on a Varian Associates T-60 spectrometer. Each spectrum was recorded after equilibration to ambient probe temperature (HA-100, 30°; T-60, 36°). All spectra were determined on freshly prepared solutions in the dried solvents and were measured relative to neat TMS in a Wilmad 520-2 internal coaxial capillary tube (at 100 MHz) or to a 10% solution of TMS in chloroform which was contained in a sealed capillary inserted in the tube (at 60 MHz). No difference between the capillary and coaxial tube containing the same reference could be detected. However, a downfield chemical shift difference of 47.5 Hz at 100 MHz was observed for the CHCl_3 resonance between the "external" neat TMS in the coaxial tube and internal 10% by volume TMS using a solution of CHCl_3 in CCl_4 (10% v/v). Chemical shifts, with the exception of downfield resonances, were generally obtained from the spectra recorded at 250 (T-60) and 500 Hz (HA-100) sweep

widths and are given on the δ scale in ppm relative to the external TMS ($\delta = 0$ ppm). Individual measurements are accurate to ± 0.002 at 100 MHz and ± 0.01 at 60 MHz. Coupling constants were measured from the spectra obtained at 500-Hz sweep widths at 100 MHz and at 250-Hz sweep widths at 60 MHz and are accurate to ± 0.2 Hz. Bulk susceptibility corrections were not applied; however, they are predictably small and would not affect the obtained results appreciably.

Results and Discussion

As typical of systems which equilibrate rapidly on the nmr timescale,^{1,2,10-15} these surfactants exhibit single weight-averaged resonance frequencies for the monomeric and aggregated species in each solvent over the range of concentrations employed above the cmc. The spectra of 0.10 M surfactant solutions generally consists of fairly well-resolved triplets for the terminal methyl protons of the alkylammonium and propionate ions, a broad singlet for the intermediate methylene protons of the ammonium ion, a quartet for those of the propionate ion, an apparent triplet for the methylene protons adjacent to the ammonium ion, and a relatively sharp singlet for the ammonium protons. Notable exceptions are the intermediate methylene protons of the ammonium ion in chlorobenzene. For HAP the middle and lower field portion of the $\text{CH}_3\text{CH}_2\text{CO}_2^-$ resonance appears as broad lines with part of the unresolved methylene singlet underneath and another part of it still further downfield. The resonance

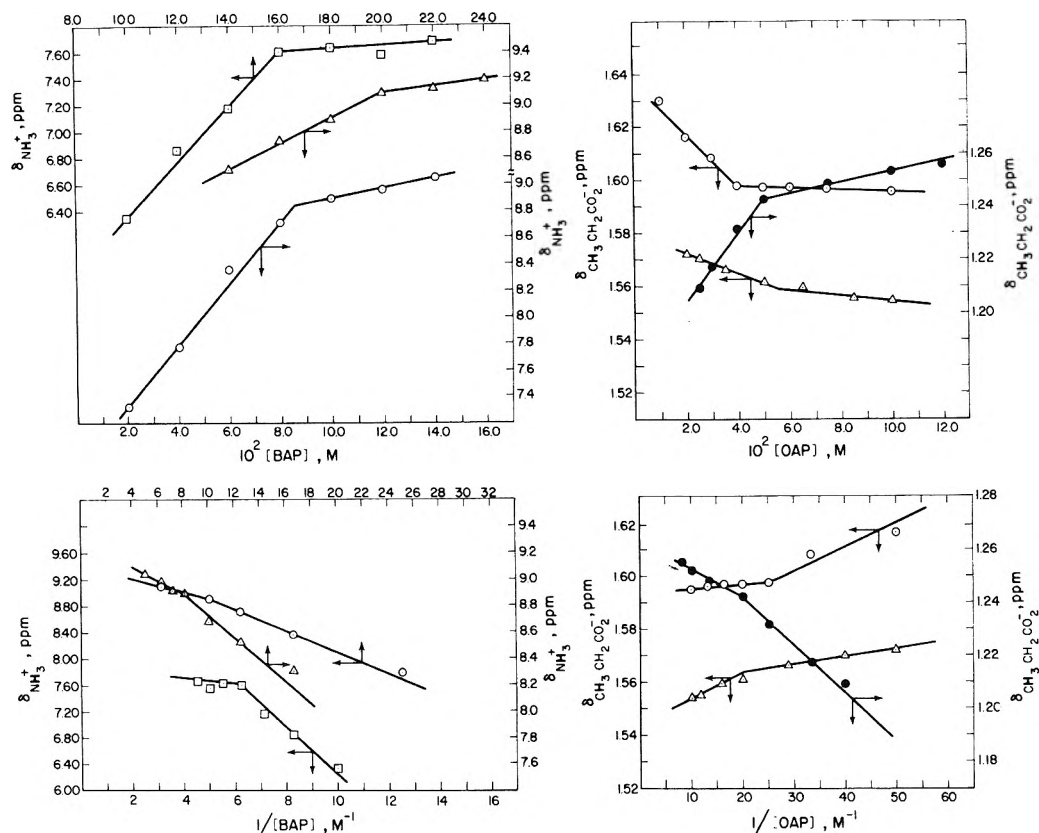


Figure 1. Observed chemical shifts for the ammonium protons of butylammonium propionate (BAP) and for the propionate methyl protons of octylammonium propionate (OAP) as functions of the stoichiometric surfactant concentration and its reciprocal in CDCl_3 (O), CH_2Cl_2 (Δ), $\text{C}_6\text{H}_5\text{Cl}$ (\bullet), and DMAC (\square).

frequencies for the $(\text{CH}_2)_4\text{CH}_2\text{N}^+$ protons lie between 1.223 and 1.441 ppm. For OAP the $\text{CH}_3\text{CH}_2\text{CO}_2^-$ triplet is broad. Part of the $(\text{CH}_2)_6\text{CH}_2\text{N}^+$ resonance appears under the center and lower field portions of the triplet and extends to lower field. The methylene resonances in this case appear between 1.280 and 1.450 ppm. The observed chemical shifts at 0.10 M stoichiometric surfactant concentrations have been measured on solutions in which the concentration is in the region of the cmc for BAP in all solvents investigated, with the exception of DMAC; in the region of the cmc for HAP in CH_2Cl_2 , $\text{C}_6\text{H}_5\text{Cl}$, and DMAC and for OAP in DMAC. The concentration is well above the cmc for HAP in CDCl_3 , OAP in CDCl_3 , CH_2Cl_2 , and $\text{C}_6\text{H}_5\text{Cl}$, for DAP in all four solvents, and for all the surfactants investigated in benzene and in carbon tetrachloride.²

In general, the observed resonance frequencies of the same surfactant protons shift downfield with an increase in the number of carbon atoms (x) in the alkylammonium ion and with an increase in the polarity of the solvent. The aromatic solvents, benzene and chlorobenzene, and DMAC are dissimilar, and the solvent-solute interactions in these cases are discussed separately. The chemical shifts and coupling constants for the alkylammonium propionates in CDCl_3 , CH_2Cl_2 , $\text{C}_6\text{H}_5\text{Cl}$, and DMAC are given in Table I. Those in benzene and carbon tetrachloride were reported in part I of this series.² As postulated previously, based only on results obtained in benzene and carbon tetrachloride,^{1,2} the coupling constants for the micellar alkylammonium carboxylates are essentially independent of solvent within experimental error.

Chemical shifts of the different protons as functions of

stoichiometric surfactant concentration generally show pronounced discontinuities at the same concentration indicating aggregation of the monomeric surfactant. The point of the linearly extrapolated intersection is considered to be an "operational critical micelle concentration." The rationale for using these breaks for obtaining critical micelle concentrations has been detailed in part II of this series (see footnote 19 in ref 1). It can be seen in Figure 1 that the discontinuities in plots of the chemical shifts *vs.* surfactant concentration give values which agree well with those obtained from plots of the chemical shifts *vs.* the reciprocal surfactant concentration. Table II gives the ranges of the critical micelle concentration obtained from the different protons in each solvent system.

Critical micelle concentrations for these alkylammonium propionate surfactants in CDCl_3 , CH_2Cl_2 , $\text{C}_6\text{H}_5\text{Cl}$, and DMAC decrease with an increasing number of carbon atoms (x) in the alkyl chain and for a given surfactant they increase with increasing solvent polarity. In the case of ionic surfactants in nonaqueous solvents the primary driving forces for aggregation include the interactions both of the polar groups with each other and with the solvent and of the hydrocarbon chain with the solvent;³ the contribution of the former, however, is undoubtedly far greater than that of the latter. The greater the interaction between the polar groups and the solvent, the less is the tendency to form micelles (*i.e.*, the cmc is higher). Changes in the cmc values as a function of x have been correlated by eq 1 (where a is related to the electrostatic free energy

$$\log \text{cmc} = a - bx \quad (1)$$

per molecule and b to the van der Waals energy of inter-

TABLE II: Micellar Parameters for Alkylammonium Propionates

Solvent ^a	Surfactant chemical shifts utilized	10 ² cmc, M	n	K, M ¹⁻ⁿ
CDCl ₃ (0.213, 39.0)	BAP CH ₃ CH ₂ CO ₂ ⁻ , CH ₂ CO ₂ ⁻ , CH ₂ NH ₃ ⁺ , NH ₃ ⁺	8.0-10.0	3.5 ± 1	(2-8)10 ²
	HAP CH ₃ (CH ₂) ₅ NH ₃ ⁺ , CH ₃ CH ₂ CO ₂ ⁻ , (CH ₂) ₄ , CH ₂ CO ₂ ⁻ , NH ₃ ⁺	5.0-6.35	4.5 ± 1	(3-4)10 ⁴
	OAP CH ₃ (CH ₂) ₇ NH ₃ ⁺ , CH ₃ CH ₂ CO ₂ ⁻ , (CH ₂) ₆ , CH ₂ CO ₂ ⁻ , NH ₃ ⁺	3.35-4.65	6.0 ± 1	(1-2)10 ⁸
	DAP CH ₃ CH ₂ CO ₂ ⁻ , CH ₂ CO ₂ ⁻ , NH ₃ ⁺	2.0-2.7	7.0 ± 1	(3-10)10 ⁹
CH ₂ Cl ₂ (0.112, 41.1)	BAP CH ₂ CO ₂ ⁻ , NH ₃ ⁺	10.7-12.0	5.0 ± 1	(1-3)10 ³
	HAP CH ₃ CH ₂ CO ₂ ⁻ , CH ₂ CO ₂ ⁻ , NH ₃ ⁺	8.0-8.5	6.0 ± 1	(3-8)10 ⁶
	OAP CH ₃ (CH ₂) ₇ NH ₃ ⁺ , CH ₃ CH ₂ CO ₂ ⁻ , (CH ₂) ₆ , CH ₂ CO ₂ ⁻ , CH ₂ NH ₃ ⁺ , NH ₃ ⁺	5.0-5.7	6.5 ± 1	(2-5)10 ⁸
	DAP CH ₃ CH ₂ CO ₂ ⁻ , CH ₂ CO ₂ ⁻ , NH ₃ ⁺	2.7-4.0	6.0 ± 1	(1-2)10 ⁸
DMAC (0.0264, 43.7)	BAP NH ₃ ⁺	15-17		
	HAP NH ₃ ⁺	12-13	5.0 ± 1	(3-8)10 ³
	OAP NH ₃ ⁺	9-11	8.0 ± 1	(7-10)10 ⁷
	DAP NH ₃ ⁺	4-6	5.0 ± 2	(1-3)10 ⁵
C ₆ H ₅ Cl (0.179, 37.5)	BAP CH ₃ (CH ₂) ₃ NH ₃ ⁺ , CH ₃ CH ₂ CO ₂ ⁻ , CH ₂ CO ₂ ⁻ , CH ₂ NH ₃ ⁺ , NH ₃ ⁺	11-13.4	6.0 ± 1	(4-9)10 ⁴
	HAP CH ₃ (CH ₂) ₅ NH ₃ ⁺ , CH ₂ CO ₂ ⁻ , CH ₂ NH ₂ ⁺ , NH ₃ ⁺	8.0-10.0	4.0 ± 1	(2-8)10 ²
	OAP CH ₃ (CH ₂) ₇ NH ₃ ⁺ , CH ₃ CH ₂ CO ₂ ⁻ , CH ₂ CO ₂ ⁻	5.0-5.5	6.5 ± 1	(2-5)10 ⁹
C ₆ H ₆ ^b (0.435, 34.5)	BAP CH ₃ CH ₂ CO ₂ ⁻	4.5-5.5	4.0 ± 1	10 ⁴
	HAP CH ₃ CH ₂ CO ₂ ⁻	2.2-3.2	7.0 ± 1	10 ¹²
	OAP CH ₃ CH ₂ CO ₂ ⁻	1.5-1.7	5.0 ± 1	10 ⁸
	DeAP CH ₃ CH ₂ CO ₂ ⁻	0.8-1.0		
CCl ₄ ^b (0.455, 32.5)	BAP CH ₃ CH ₂ CO ₂ ⁻	2.3-2.6	3.0 ± 1	9 × 10 ²
	HAP CH ₃ CH ₂ CO ₂ ⁻	2.1-2.4	7.0 ± 1	7 × 10 ¹¹
	OAP CH ₃ CH ₂ CO ₂ ⁻	2.6-3.1	5.0 ± 1	5 × 10 ⁷
	DAP CH ₃ CH ₂ CO ₂ ⁻	2.1-2.5	4.0 ± 1	5 × 10 ⁴

^a Values in parentheses are the reciprocal dielectric constant and E_T value, respectively (C. Reichart, *Ann. Chem.*, 752, 64 (1971), and ref 17). ^b Taken from ref 2.

action per CH₂ group per molecule and x is the number of carbon atoms in the chain) and are illustrated in Figure 2. In each solvent satisfactory straight lines are obtained although the slopes of these lines differ and are considerably smaller than those generally obtained for homologous series of surfactants in aqueous solutions.¹⁶ Within the limits of experimental error, values for b in CDCl₃, CH₂Cl₂, and DMAC are identical but they are smaller than those in C₆H₅Cl and C₆H₆. The complete invariance of cmc values for the different alkylammonium propionates in CCl₄, the least polar solvent investigated, substantiates the interaction between the polar headgroups of the surfactants with each other and with the solvent as the predominating force for aggregation.

The effects of solvents on the cmc can be discussed in terms of macroscopic and microscopic parameters.¹⁷ The former is based on direct measurements of bulk properties, such as the dielectric constants, while the latter relies on the introduction of probes, such as alkyl betaines whose transition energies give E_T values, or on kinetic measurements of the rates of model systems.¹⁷ The range of solvents investigated in the present and previous work^{1,2} represents changes in the dielectric constants, the hydrogen bonding abilities (e.g., CDCl₃ and CH₂Cl₂), and polarities (E_T value of the solvent). For C₆H₆, CDCl₃, CH₂Cl₂, and DMAC a good relationship has been obtained between the cmc values and both the dielectric constant and the E_T value of the solvent (Figure 3). Although the observed dependence on both macroscopic and microscopic solvent polarity parameters may be fortuitous, it appears that the predominant solvent-surfactant

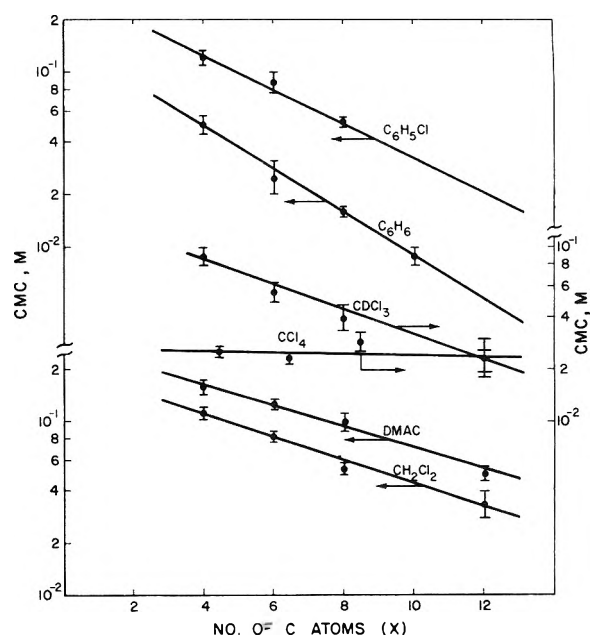


Figure 2. Plots of the cmc of alkylammonium propionates in nonaqueous solvents as a function of the number of carbon atoms (x) in the alkyl chain.

headgroup interactions are likely to be explicable in terms of bulk solvent polarity. Consequently the greater the interaction of the ionic surfactant monomers with the solvent, the less is the tendency to form micelles (as mani-

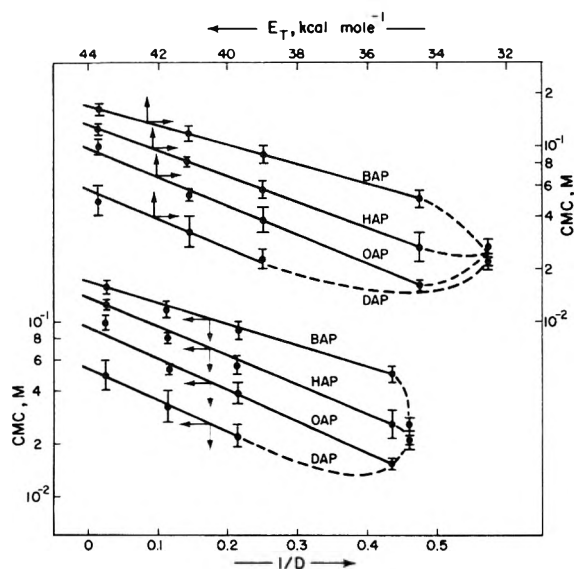


Figure 3. Plots of the logarithm of the cmc of alkylammonium propionates vs. the reciprocal of the dielectric constant and the polarity parameter E_T of the solvent.

fest by higher cmc values). Nmr data on the chemical shifts is consistent with this interpretation (*vide infra*). The anomalous behavior of CCl_4 is also apparent in the solvent polarity plots (Figure 3).

Aggregation numbers, n , and equilibrium constants for micelle formation, K , have been calculated from linear plots of the data treated according to eq 2,¹ where $[\text{C}_D]$

$$\log ([\text{C}_D] - [\text{S}]) = \log (nK) + n \log [\text{S}] \quad (2)$$

and $[\text{S}]$ are the stoichiometric and monomeric concentrations of the surfactant, respectively. Concentrations of monomeric surfactant, $[\text{S}]$, in the different systems have been calculated from eq 3 and 4 as described previously,^{1,2}

$$[\text{S}] = [\text{C}_D](\delta_M - \delta)/(\delta_M - \delta_m) \quad (3)$$

$$\delta = \delta_M + (\text{cmc}/[\text{C}_D])(\delta_m - \delta_M) \quad (4)$$

where δ , δ_M , and δ_m are the observed, micellar, and monomeric chemical shifts of the respective protons. The monomeric chemical shifts, δ_m , were obtained from extrapolations of the δ vs. $[\text{C}_D]$ plots to zero surfactant concentration below the cmc whereas the micellar chemical shifts, δ_M , were obtained from the intercept of plots of δ vs. $1/[\text{C}_D]$ (eq 4). It should be re-emphasized that eq 2-4 have been derived assuming that the concentration of monomers remain essentially constant above the cmc, that n is fairly large, and that there is an ideal monomer- n mer equilibrium between monomeric and micellar surfactant species.^{12,13} At least partial justification for the use of these equations is the internally self-consistent information obtained therefrom.

The values of n and K given in Table II are the mean values obtained from the data for the magnetically discrete and observable surfactant protons. Since these values for n and K depend upon errors in δ_m and δ_M , they are considered to be accurate within ± 1 and ± 50 , respectively. For each solvent there is a tendency for an increase in aggregation number with increasing number of carbon atoms (x) in the alkyl chain. Additionally for a given surfactant there is a slight, but distinct, increase in n with increasing solvent polarity (Table II). Values for the equilibrium constant for micelle formation also reflect, of

course, these trends. The significance of aggregation number changes as functions of x and solvent polarity will be fully appreciated subsequent to obtaining precise information on the geometry of these reversed micelles.

Due to the association equilibria involved, the proton magnetic resonance data, *i.e.*, the observed chemical shifts, can be discussed more meaningfully in terms of the calculated chemical shifts for the protons of the monomeric (δ_m) and micellar (δ_M) species. The values of δ_m and δ_M are given in Table III. It should be noted initially that δ_m necessarily reflects the polar effects within the monomeric surfactant molecule and the monomer-solvent effects whereas δ_M gives the change in these polar effects and in the solvent-solute interactions accompanying aggregation. As a consequence of the differences in sign of the chemical shifts for the discrete surfactant protons as a function of surfactant concentration, δ_m and δ_M do not behave in the same fashion. Thus $\delta_m > \delta_M$ in CDCl_3 and CH_2Cl_2 for all protons with the exception of NH_3^+ and $\delta_M > \delta_m$ for all protons in $\text{C}_6\text{H}_5\text{Cl}$ and for NH_3^+ in all solvents. For the methylene protons in the alkylammonium group (or in the carboxylate group) δ_m predictably would increase slowly as a function of alkyl chain length (x) due to greater interactions with the solvent for each additional CH_2 group (*i.e.*, ΔG of solvation would increase). δ_M , on the other hand, is expected to decrease with an increase in x since micellization would result in exclusion of part of the solvent originally surrounding the monomers thereby decreasing solute-solvent interactions and causing an up-field shift. An increase in the solvent polarity will result in still lower δ_M values since the more polar the solvent the greater the difference in solvent-solute interactions accompanying aggregation. The resultant of these two factors satisfactorily explains the observed greater slopes of the lines in plots of δ_M vs. x as compared to those for δ_m vs. x , as illustrated in Figure 4 for the ammonium protons in DMAC. For the NH_3^+ protons which exhibit anomalous behavior ($\delta_M > \delta_m$) in all solvents, one factor of primary importance here is the high sensitivity of these protons to changes in polar effects. δ_m decreases as a function of increasing chain length while δ_M decreases to a greater extent. Solvent interactions with the monomeric ion pair relative to that with the interior of the reversed micelle may be a primary contributing factor since the effect of an increase in x on the tightness of the ion pairs is expected to operate to a lesser extent in the micellar aggregate. Additionally, with an increase in x the micelles may become more compact thereby contributing to the increase in δ_M .

Two additional points are apparent from considering the monomeric and micellar NH_3^+ protons (Table III). δ_M is far less sensitive to changes in solvent polarity than δ_m and it is always greater than δ_m . These results are compatible with an aggregate structure in which the polar headgroups are oriented around an interior "cavity" from which the nonpolar solvent is largely excluded while the hydrophobic chains extend outward into the bulk nonpolar solvent pseudophase.

In the aromatic solvents, benzene and chlorobenzene, however, the observed chemical shifts, δ , are smaller for all the protons, with the exception of NH_3^+ , as compared to those in the hydrocarbon solvents. Additionally, the chemical shifts, in all cases, are smaller in benzene than in chlorobenzene. The difference between the micellar and monomeric chemical shifts ($\delta_M - \delta_m$) increases as a function of increasing number of carbon atoms (x) in the alkyl

TABLE III: Chemical Shifts of the Monomeric and Micellar Protons of Alkylammonium Propionates^a

Solvent	Proton	BAP		HAP		OAP		DAP	
		δ_M , ppm	δ_m , ppm	δ_M , ppm	δ_m , ppm	δ_M , ppm	δ_m , ppm	δ_M , ppm	δ_m , ppm
CDCl ₃	CH ₃ (CH ₂) _{x-1} N ⁺			1.405	1.427	1.391	1.419		
	CH ₃ CH ₂ CO ₂ ⁻	1.593	1.633	1.598	1.625	1.593	1.637	1.583	1.651
	CH ₃ (CH ₂) _{x-2} CH ₂ N ⁺			1.826	1.863	1.789	1.808		
	CH ₃ CH ₂ CO ₂ ⁻	2.713	2.765	2.686	2.749	2.671	2.775	2.637	2.778
	CH ₃ (CH ₂) _{x-2} CH ₂ N ⁺	3.368	3.320						
CH ₂ Cl ₂	NH ₃ ⁺	9.280	6.900	9.200		9.160	4.400	9.000	4.000
	CH ₃ (CH ₂) _{x-1} N ⁺					1.385	1.412		
	CH ₃ CH ₂ CO ₂ ⁻				1.567	1.544	1.580	1.511	1.574
	CH ₃ (CH ₂) _{x-2} CH ₂ N ⁺					1.786	1.814		
	CH ₃ CH ₂ CO ₂ ⁻	2.656	2.695	2.641	2.682	2.617	2.709	2.575	2.716
C ₆ H ₅ Cl	CH ₃ (CH ₂) _{x-2} CH ₂ N ⁺					3.283	3.232		
	NH ₃ ⁺	9.520	7.920	9.380	7.080	8.680	5.620	8.940	5.200
	CH ₃ (CH ₂) _{x-1} N ⁺	0.864	0.820	0.899	0.865	0.924	0.882		
	CH ₃ CH ₂ CO ₂ ⁻	1.188	1.155			1.262	1.180		
	CH ₃ CH ₂ CO ₂ ⁻	2.320	2.293	2.364	2.321	2.379	2.303		
DMAC	CH ₃ (CH ₂) _{x-2} CH ₂ N ⁺	2.884	2.823	2.905	2.805				
	NH ₃ ⁺	9.640	8.510	9.360	7.940	9.500	7.340	6.280	4.050

^a At 100 MHz and 30° (see Experimental Section).

group. The smaller chemical shifts values observed in benzene and chlorobenzene result from the relatively greater shielding by these solvents than those in the non-aromatic chlorohydrocarbons. This behavior is well recognized and is ascribed to diamagnetic anisotropy.¹⁸ Moreover, since the diamagnetic anisotropy is believed to be largely due to the π -electron system¹⁸ such shielding is expected to be the most pronounced for benzene.

Based on the calculated δ_M and δ_m values in the different solvents several structural features of these reversed micelles emerge. At concentrations below the cmc (*i.e.*, for monomeric species) interactions exist between the alkyl groups of the surfactant and the solvent, between the polar headgroups of the surfactant, and between these and the solvent. The last two factors are (*vide supra*) the predominating force for micellization. On aggregation, the polar groups pull together forming a cavity from which the solvent molecules are essentially excluded, while the hydrocarbon tails remain in contact with the solvent. Solvent penetration through the hydrocarbon chains of the micelle will depend on its volume and shape, and on the number of carbon atoms (x) in the alkyl chain. The bulkier the solvent and the longer the hydrocarbon chain, the shorter distance the solvent can penetrate. Due to the planar structure of benzene and chlorobenzene¹⁸ they can fit better between the hydrocarbon chains than the bulkier solvents such as CDCl₃. However, it appears that in no case is there any appreciable direct interaction between these nonpolar solvents and the ammonium or the methylene protons adjacent to the carboxyl group subsequent to micelle formation. Interaction of the functional groups with the solvent increases, of course, with decreasing distance from the outer surface of the micelle. Such a picture is amply substantiated by the experimental results. It is evident from Table III and Figure 4 that (a) the outer group CH₃(CH₂)_xN⁺ is affected the least by changes of x since it is probably in contact with the solvent both in monomeric and aggregated forms; (b) for a given surfactant and solvent the order of $\delta_M - \delta_m$ (CH₃(CH₂)_xN⁺ < (CH₂)_n < CH₃CH₂CO₂⁻ < CH₂CO₂⁻ < CH₂N+H₃ < NH₃⁺) paral-

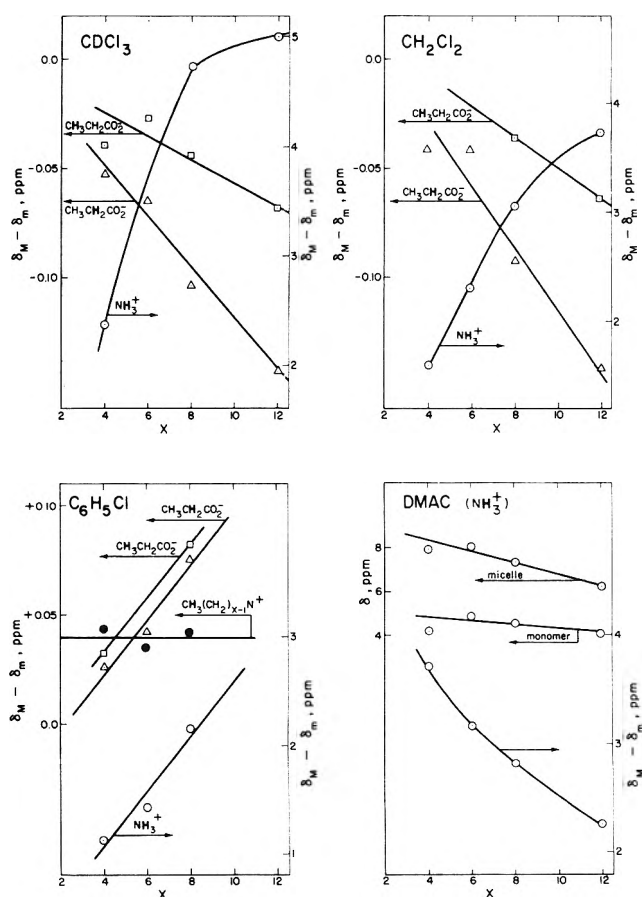
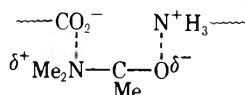


Figure 4. Dependence of the monomeric (δ_m) and micellar (δ_M) chemical shifts on the number of carbon atoms (x) in alkylammonium propionates in nonaqueous solvents.

els the distance of these groups from the micellar core and represents the ease of solvent penetration into the micelle; and (c) δ_M for NH₃⁺ for a given surfactant is not appreciably solvent dependent.

Chlorobenzene shows somewhat different behavior. Plots of $\delta_M - \delta_m$ vs. x for $\text{CH}_3\text{CH}_2\text{CO}_2^-$ and CH_2CO_2^- have similar slopes and those for $\text{CH}_3(\text{CH}_2)\text{N}^+$ are essentially invariant with x . These results might imply a somewhat deeper penetration by chlorobenzene into a given alkylammonium propionate micelle than by the aliphatic hydrocarbon solvents.

The considerably higher dielectric constant, stronger dipole character, and ordered structure of dipolar aprotic DMAC merits separate discussion. Indeed the monomeric and micellar chemical shift data for the alkylammonium propionate surfactants in this solvent possess unique features (Table III and Figure 4). Most striking is the behavior of the NH_3^+ protons; a plot of $\delta_M - \delta_m$ vs. x has a negative slope! This behavior can be more profitably discussed in terms of comparing changes of δ_m and δ_M as functions of the alkyl chain length (x) in DMAC with those in the other solvents. It is evident that an increase in chain length of the surfactant affects the monomeric chemical shifts considerably more in CDCl_3 , CH_2Cl_2 , and $\text{C}_6\text{H}_5\text{Cl}$ than in DMAC while the converse is true for δ_M . It is tempting to rationalize these results in terms *dipole-dipole interactions in the monomeric species*



which are only slightly affected by changes in x . Formation of micelles requires, however, strong desolvation of the monomers and values of values for δ_M will change rapidly as x increases due to the formation of more compact micelles.

Changes in the polarity of the solvent are likely to alter the structure of the micelles. A transition from a spherical or ellipsoidal structure to a lamellar or "staggered" one is not improbable with a relatively large increase in solvent polarity. There may be, of course, a solvent polarity range in which micelle formation is not observable. In summary, formation and structures of micelles in nonaqueous solvents are delicately balanced between the interaction of functional groups of the surfactants with each other

and with the solvent both in the monomer and in the aggregate. Alterations in the size and geometry of the surfactant functional groups and polarizability as well as such properties of the solvent as polarity, bulk, and geometry are the many factors which may be responsible for the ultimate arrangement of solvent molecules in and around the aggregated surfactant. Efforts in our laboratories are directed toward the systematic elucidation of these factors.

Acknowledgments. Support for this work from the Robert A. Welch Foundation and from the Research Corporation is gratefully acknowledged. E. J. F. is a Research Career Development Awardee of the National Institutes of Health, U. S. Public Health Service.

References and Notes

- (1) Part II: E. J. Fendler, J. H. Fendler, R. T. Medary, and O. A. El Seoud, *J. Phys. Chem.*, **76**, 1432 (1973).
- (2) J. H. Fendler, E. J. Fendler, R. T. Medary, and O. A. El Seoud, *J. Chem. Soc., Faraday Trans. 1*, **69**, 280 (1973).
- (3) F. M. Fowkes in "Solvent Properties of Surfactant Solutions," K. Shinoda, Ed., Marcel Dekker, New York, N. Y., 1967, p 65.
- (4) A. Kitahara in "Cationic Surfactants," E. Jungermann, Ed., Marcel Dekker, New York, N. Y., 1970, p 289, and references cited therein.
- (5) E. J. Fendler, J. H. Fendler, R. T. Medary, and V. A. Woods, *J. Chem. Soc. D*, 1497 (1971).
- (6) J. H. Fendler, *J. Chem. Soc., Chem. Commun.*, 269 (1972).
- (7) J. H. Fendler, E. J. Fendler, R. T. Medary, and V. A. Woods, *J. Amer. Chem. Soc.*, **94**, 7288 (1972).
- (8) C. J. O'Connor, E. J. Fendler, and J. H. Fendler, *J. Amer. Chem. Soc.*, **95**, 600 (1973).
- (9) A. Kitahara, *Bull. Chem. Soc. Jap.*, **28**, 234 (1955); A. Kitahara, *ibid.*, **30**, 586 (1957).
- (10) H. Inoue and T. Nakagawa, *J. Phys. Chem.*, **70**, 1108 (1966).
- (11) J. C. Eriksson, *Acta Chem. Scand.*, **17**, 1478 (1963).
- (12) N. Muller and R. H. Birkhahn, *J. Phys. Chem.*, **71**, 957 (1967).
- (13) N. Muller and R. H. Birkhahn, *J. Phys. Chem.*, **72**, 583 (1968).
- (14) R. Haque, *J. Phys. Chem.*, **72**, 3056 (1968).
- (15) R. E. Bailey and G. H. Cady, *J. Phys. Chem.*, **73**, 1612 (1969).
- (16) I. J. Lin and P. Somasundaran, *J. Colloid Interface Sci.*, **37**, 731 (1971), and references cited therein.
- (17) E. M. Kosower, "An Introduction to Physical Organic Chemistry," Wiley, New York, N. Y., 1968.
- (18) L. M. Jackman and S. Sternhell, "Applications of Nmr Spectroscopy in Organic Chemistry," Pergamon Press, Elmsford, N. Y., 1969; A. D. Buckingham, T. Schaefer, and W. G. Schneider, *J. Chem. Phys.*, **32**, 1227 (1960).

Spectroscopic Studies of Solvation in Sulfolane

T. L. Buxton and J. A. Caruso*

Department of Chemistry, University of Cincinnati, Cincinnati, Ohio 45221 (Received October 30, 1972)

Infrared spectroscopy has been used to study ion solvation in sulfolane, a dipolar aprotic solvent of high (44) dielectric constant. Lithium, sodium, potassium, rubidium, and cesium salts were investigated. The solute absorption bands appear to be independent of anion. The spectral data indicate that solvation takes place in a manner similar to that observed for dimethyl sulfoxide solutions and that sulfolane is a far weaker donor. It is proposed that solvent-separated ion pairs may be formed in sulfolane solutions.

In the past few years there have been a number of spectroscopic studies of solvation in nonaqueous solvents.¹⁻¹¹ The solvents studied have varied from those with low dielectric constants such as tetrahydrofuran,^{1,9} benzene,¹¹

and pyridine⁸ to moderate dielectric constants such as dimethylformamide¹⁰ and the pyrrolidones⁶ to those of moderately high dielectric constants such as dimethyl sulfoxide.³⁻⁵

TABLE I

Salt	Concn, <i>M</i>	$\nu(\text{max})$, cm^{-1}
NaClO ₄	0.50	187 ± 2
NaI	0.50	186 ± 2
NaB(Ph) ₄	0.50	186 ± 2
KI	0.50	156 ± 5
KClO ₄	0.25	152 ± 5
KB(Ph) ₄	0.25	156 ± 5
NH ₄ I	0.25	197 ± 2
NH ₄ B(Ph) ₄	0.25	197 ± 2
NH ₄ ClO ₄	0.25	195 ± 2
RbClO ₄	≈ 0.25 (satd)	
CsClO ₄	≈ 0.25 (satd)	
LiBr	0.50	
LiCl	0.50	

Sulfolane is a dipolar aprotic solvent with a moderately high dielectric constant (44).¹² It has been shown to dissolve chlorides and perchlorates to a reasonable extent.¹³ Conductance studies have indicated that ions are slightly associated and have led to solvation numbers at 2.0, 1.5, 1.4, 1.3, and 0.9 for Na⁺, K⁺, Li⁺, Rb⁺, Cs⁺, and NH₄⁺, respectively.^{14,15}

In these laboratories, sulfolane has been investigated as a medium for the study of weak acids¹⁶ and for the analysis of drugs.¹⁷ This study was undertaken to gain further insight into ionic solvation in sulfolane.

Experimental Section

Sulfolane (Phillips Petroleum Co.) was purified as previously described.¹⁶

Sodium and ammonium iodide (Baker Analyzed Reagents) and sodium perchlorate (G. Frederick Smith) were recrystallized from acetone with ether and vacuum dried. Sodium tetraphenylborate and potassium iodide (Fisher) and potassium perchlorate (G. Frederick Smith) were vacuum dried and used without further purification. Potassium and ammonium tetraphenylborates were synthesized by adding an aqueous solution of the respective iodide to one of sodium tetraphenylborate and washing until iodine free. They were then vacuum dried. Ammonium perchlorate was synthesized by adding perchloric acid to an aqueous solution of the iodide; the precipitate was vacuum dried. Rubidium perchlorate, cesium perchlorate, lithium bromide, and lithium chloride were all the purest grade available from Alpha Ventron and were vacuum dried and used without further purification.

Infrared spectra were recorded between 4000 and 200 cm^{-1} using a Beckman Model IR-12 spectrophotometer. Infrared spectra between 400 and 20 cm^{-1} were recorded on an R.I.I.C. (Beckman) FS-720 Fourier spectrometer equipped with FTC 300 Fourier transform electronics. All spectra on the IR-12 were run using a Beckman demountable cell with 0.05-mm Teflon spacers and KBr windows to 400 cm^{-1} ; polyethylene windows were used from 400 to 200 cm^{-1} . All spectra on the FS-720 were run with R.I.I.C. FS-03 vacuum-tight cells with polyethylene windows and 0.075-mm Teflon spacers. A Du Pont Model 310 curve analyzer was used to help resolve some of the far-ir spectra.

Results and Discussion

Katon and Fearheller have described the structure of sulfolane and made infrared band assignments.¹⁸ Our spectra agree reasonably well with theirs with two excep-

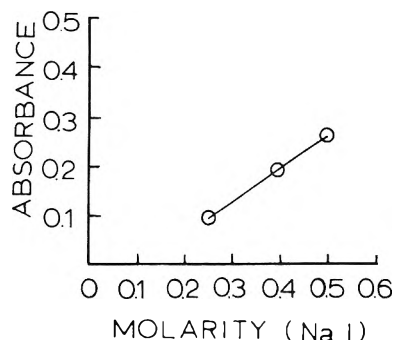


Figure 1. Relationship of absorbance to concentration for solute-solvent band using NaI.

tions. They report no bands below 242 cm^{-1} although the spectra were run to 80 cm^{-1} . Below 100 cm^{-1} we find a strong band that is probably due to dipole-dipole interactions as noted for other polar solvents.¹⁹ A second extremely weak band was seen with a center about 140 cm^{-1} and was partly overlapped by the dipole-dipole band. This may be the band due to C-S-C ring puckering which Katon and Fearheller predicted but did not observe.¹⁸

The spectral tabulation for salt solutions is given in Table I. It was originally anticipated that all solutions would be run at 0.5 *M*; however, solubility difficulties precluded this for some salts.

The theoretical reproducibility of the band maxima for the FS-720 is $\pm 0.5 \text{ cm}^{-1}$, but because the bands are broad and often overlap the dipole-dipole band, the best that could be achieved was $\pm 2 \text{ cm}^{-1}$. The potassium peak is almost totally overlapped by the dipole-dipole band and is therefore much more difficult to locate accurately.

No bands are seen for rubidium or cesium salts, probably because they fall at lower energy and are hidden by the dipole-dipole band. Neither is a band seen for lithium salts. This band maximum would probably come at about 400 cm^{-1} as in other solvents.^{5-8,10} Unfortunately, sulfolane has strong absorption bands between 440 and 310 cm^{-1} . Attempts to find an absorption band for the lithium solutions up to 1.0 *M* were made. No bands were found and no change could be found for any of the other bands in the sulfolane spectra.

The solute absorption bands observed have a linear relationship between absorbance and concentration. Figure 1 is an example with NaI as solute.

The bands seem to be independent of the anion, which would be expected in a polar solvent like sulfolane.³ There was no shift in the peak location at different salt concentrations.

Sulfolane and dimethyl sulfoxide have been compared previously as solvents.^{20,21} In spite of similar dielectric constants, 44.0 for sulfolane¹² and 46.4 for dimethyl sulfoxide⁶ and the S=O group through which the molecule probably interacts with solute, sulfolane has consistently shown weaker interactions with ionic species.^{20,21} The Gutmann donor numbers also reflect this order, 14.8 for sulfolane²² and 29.8 for DMSO.²³ Sulfolane's far infrared solvent-cation bands were at lower energy and weaker than those in DMSO.^{3,5} This indicates that solvation takes place in a similar manner in both solvents but that sulfolane is a far weaker donor. Previous studies have shown evidence for ion pair formation in sulfolane.^{14,15,20} The anion independence of the far-ir band shows that it does not enter into the inner solvation shell and therefore

probably does not form contact ion pairs. This does not rule out the formation of solvent-separated ion pairs as has been postulated for other solvents.²⁴ It seems probable that in sulfolane this type of pairing occurs.

References and Notes

- (1) W. F. Edgell, J. Lyford, IV, R. Wright, W. Risen, Jr., and A. Watts, *J. Amer. Chem. Soc.*, **92**, 2240 (1970).
- (2) E. G. Hohn, J. A. Olander, and M. C. Day, *J. Phys. Chem.*, **73**, 3880 (1969).
- (3) B. W. Maxey and A. I. Popov, *J. Amer. Chem. Soc.*, **89**, 2230 (1967).
- (4) B. W. Maxey and A. I. Popov, *J. Amer. Chem. Soc.*, **90**, 4470 (1968).
- (5) B. W. Maxey and A. I. Popov, *J. Amer. Chem. Soc.*, **91**, 20 (1969).
- (6) J. L. Wuepper and A. I. Popov, *J. Amer. Chem. Soc.*, **91**, 4352 (1969).
- (7) J. L. Wuepper and A. I. Popov, *J. Amer. Chem. Soc.*, **92**, 1493 (1970).
- (8) W. M. McKinney and A. I. Popov, *J. Phys. Chem.*, **74**, 535 (1970).
- (9) W. F. Edgell, A. J. Watts, John Lyford, IV, and W. M. Risen, Jr., *J. Amer. Chem. Soc.*, **88**, 1815 (1966).
- (10) C. Lassigne and P. Baine, *J. Phys. Chem.*, **75**, 3188 (1971).
- (11) J. C. Evans and R. Y. Lo, *J. Phys. Chem.*, **69**, 3223 (1965).
- (12) E. M. Arnett and C. F. Douty, *J. Amer. Chem. Soc.*, **86**, 409 (1964).
- (13) J. A. Starkovich and M. Janghorbani, *J. Inorg. Nucl. Chem.*, **34**, 789 (1972).
- (14) M. Della Monica, U. Lamanna, and L. Senatore, *J. Phys. Chem.*, **72**, 2124 (1968).
- (15) M. Della Monica and U. Lamanna, *J. Phys. Chem.*, **72**, 4329 (1968).
- (16) P. M. P. Eller and J. Caruso, *Anal. Lett.*, **4**, 13 (1971).
- (17) T. Buxton and J. Caruso, *Talanta*, **20**, 254 (1973).
- (18) J. E. Katon and W. R. Fearheller, Jr., *Spectrochim. Acta*, **21**, 199 (1965).
- (19) R. J. Jakobsen and J. W. Brasch, *J. Amer. Chem. Soc.*, **86**, 3571 (1964).
- (20) R. Garnsy and J. E. Prue, *Trans. Faraday Soc.*, **64**, 1206 (1968).
- (21) C. Agami and P. Gondouin, *Bull. Soc. Chim. Fr.*, 3930 (1969).
- (22) V. Gütman and A. Scherhauser, *Monatsh. Chem.*, **101**, 3930 (1970); **99**, 335 (1968).
- (23) V. Gütman and U. Mayer, *Monatsh. Chem.*, **101**, 3930 (1970).
- (24) R. H. Ehrlich and A. I. Popov, *J. Amer. Chem. Soc.*, **93**, 5620 (1971).

Transport Property Investigation of Ammonium and Tetraalkylammonium Salts in 1,1,3,3-Tetramethylurea¹

Barbara J. Barker and Joseph A. Caruso*

Department of Chemistry, University of Cincinnati, Cincinnati, Ohio 45221 (Received October 30, 1972)

The behavior of ammonium and a series of tetraalkylammonium salts in a relatively new, aprotic solvent of moderate dielectric constant, tetramethylurea (TMU), was studied by conductance and viscosity techniques. Conductance data for all salts were evaluated both by the Fuoss-Shedlovsky method of analysis and by the Fuoss-Onsager equations for unassociated and associated electrolytes. The effect of tetraalkylammonium salts on the viscosity of TMU was determined by experimentally evaluating viscosity B coefficients of the Jones-Dole equation; the effect of solution viscosity on the electrolyte size parameter α_j of the Fuoss-Onsager theory was determined by including viscosity corrections in the conductance data evaluation. Tetraalkylammonium perchlorates and bromides were found to be associated electrolytes in TMU. Ionic limiting equivalent conductances in TMU were obtained indirectly by using triisomybutylammonium tetraphenylborate as a reference electrolyte. The order of decreasing relative cationic limiting equivalent conductances which was observed in tetramethylurea also has been noted in several other nonaqueous solvents.

Introduction

Frequent use of nonaqueous solvents as media for organic and inorganic reactions has led to increasing interest in the transport properties of electrolytes in solution. Electrolyte behavior in solution is revealed by fundamental viscosity and conductance investigations which elucidate directly from experimental measurement the nature of ion-ion and ion-solvent interactions. Recently there have been a number of transport property investigations in polar nonaqueous solvents such as propylene carbonate (PC),² dimethyl sulfoxide (DMSO),³⁻⁵ sulfolane,⁶ acetonitrile (ACN),⁷⁻⁹ acetone,^{10,11} methyl ethyl ketone,¹² and aliphatic alcohols.¹³⁻¹⁵ Tetramethylurea (TMU), a relatively new aprotic solvent of moderate dielectric constant (23.45) and wide liquid range (from -1 to 176.5°), proved to be an interesting nonaqueous medium for a recent conductance investigation¹⁶ of alkali metal salts.

Quaternary ammonium salts often are studied as theoretical models in solution chemistry since they form systematic electrolyte series containing cations of relatively large crystallographic size and low charge density. Since tetramethylurea promises to be a solvent of considerable interest and since no transport property investigations of tetraalkylammonium salts in TMU have been reported, the present investigation was undertaken.

Experimental Section

The purification of tetramethylurea has been described previously.¹⁶ Ammonium tetraphenylborate was prepared by mixing equimolar aqueous solutions of ammonium bromide (Fisher Certified Reagent) and sodium tetraphenylborate (Baker Analyzed Reagent). The precipitate was recrystallized from an acetone-ether mixture. Tetramethylammonium perchlorate was prepared by adding an ap-

proximately 1.5 *M* perchloric acid solution to an aqueous solution of tetramethylammonium bromide (Eastman chemical). The salt was washed well with water to remove excess acid. Conductivity water, obtained by passing laboratory distilled water through a Deeminizer ion-exchange resin (Crystalab Inc.), was used in the salt preparations. Tetraethyl-, tetra-*n*-propyl-, and tetra-*n*-butylammonium perchlorate and tetra-*n*-butyl-, tetra-*n*-pentyl-, tetra-*n*-hexyl-, and tetra-*n*-heptylammonium bromide (all Eastman chemicals) were recrystallized several times from acetone-ether mixtures. All salts were ground finely and dried *in vacuo* prior to use.

Procedures and Apparatus. All solution preparations were performed under normal laboratory conditions since most tetraalkylammonium salts used were not appreciably hygroscopic. All salt solutions were prepared by weight; all weighings were corrected to vacuum. Since salt solutions ranging in concentration from $0.4\text{--}40 \times 10^{-4}$ *M* were used in the conductance studies, molar concentrations were determined by assuming that solution densities were equal to the solvent density. Since solutions ranging in concentration from 0.01 to 0.15 *M* were used in the viscosity investigations, molar concentrations of the most concentrated salt solutions were evaluated from densities determined in 10-cm³ modified Ostwald-Sprengel type pycnometers; molar concentrations of moderately concentrated solutions were determined from calculated densities.

The procedures and apparatus used in the present conductance study have been described in detail in the previous investigation.¹⁶ In all conductance experiments a solvent correction was applied to the solution resistances by subtracting the specific conductance of the solvent ($2\text{--}8 \times 10^{-8}$ ohm⁻¹ cm⁻¹) from the specific conductance of the solution. Viscosities of solutions ranging in concentration from 0.01 to 0.15 *M* were determined with sizes 25 and 50 Cannon Fenske viscometers (manufactured and calibrated by Cannon Instrument Co.). The viscometers were supported by modified Ostwald viscometer holders (Sargent Model S-67432) in a viscometer bath assembly (Sargent Model S-67424) filled with water and maintained at $25.00 \pm 0.01^\circ$. (The bath also was used for density determinations.) With viscometers of the chosen sizes flow times were sufficiently large that kinetic energy corrections were assumed to be negligible. Approximately four measurements of flow time (Time-It, Precision Scientific Co., Model 69230) resulted in values with a precision of 0.2 sec. The viscosity of freshly distilled tetramethylurea differed from that of TMU which had been stored under a nitrogen atmosphere for several weeks; therefore, the solvent viscosity was determined for each investigated set of solutions.

Results and Discussion

All conductance data were evaluated with computer programs^{17,18} written in Fortran IV for an IBM 360/65 computer system. Values¹⁶ of the density, viscosity, and dielectric constant of tetramethylurea at 25° which were used in all calculations were 0.9619 g/ml, 0.01401 P, and 23.45, respectively.

Conductance data for all salts were evaluated both by the Fuoss-Shedlovsky method¹⁹ of analysis and by the Fuoss-Onsager equations^{20,21} for unassociated and associated electrolytes.

The Fuoss-Shedlovsky method of evaluation yielded values of Λ_0 and K_A from least-squares analyses of the

functions Λ_0' vs. *C* and *y* vs. *x*. The symbols have their usual meaning

$$\Lambda_0' = (\Lambda + \beta C^{1/2}) / (1 - \alpha C^{1/2}) \quad (1)$$

$$1/\Lambda S_z = 1/\Lambda_0 + C \Lambda S_z f^2 K_A / \Lambda_0^2 \quad (2)$$

in which $y = 1/\Lambda S_z$ and $x = C \Lambda S_z f^2$.

The Fuoss-Onsager method of evaluation yielded values of Λ_0 , K_A , and a_j from the equation

$$\Lambda = \Lambda_0 - S(C\gamma)^{1/2} + [E \log C\gamma + (J - F\Lambda_0) - K_A \Lambda f^2] C\gamma \quad (3)$$

Again, the symbols have their usual meaning, $S = \alpha \Lambda_0 + \beta$ and $E = E_1 \Lambda_0 - E_2$. The physical properties of TMU at 25° lead to values of 1.403, 70.42, 19.82, and 145.7 for the coefficients α , β , E_1 and E_2 , respectively. For unassociated electrolytes $\gamma = 1$ and $K_A = 0$; for associated electrolytes $\gamma < 1$ and $K_A > 0$. For graphical representation of data the preceding equation is rearranged to the form²²

$$\Lambda' \equiv \Lambda + SC^{1/2} - EC \log C = \Lambda_0 + (J - F\Lambda_0)C \quad (4)$$

Initial Λ_0 values used in the Fuoss-Onsager evaluation were those obtained from the Shedlovsky *y* - *x* least-squares analysis of original data. For all salts except NH_4BPh_4 unweighted values of Λ were used for the determination of conductance parameters in the Fuoss-Onsager method of evaluation. For the associated electrolytes unweighted data led to a smaller standard deviation $\sigma\Lambda$ for individual conductance values than did data weighted by the factor $C\gamma$.

Although the necessity^{23,24} of viscosity corrections in the Fuoss-Onsager evaluation of conductance data has been questioned,¹⁷ such corrections frequently are included in the analysis of data for quaternary ammonium salts since the size of these electrolytes often approaches or exceeds that of solvent molecules. Therefore, the effect of solution viscosity on the a_j parameter of the Fuoss-Onsager theory was determined for selected tetraalkylammonium salts in TMU.

Salt solutions which are more concentrated than those generally used in conductance investigations are needed for viscosity studies in order that the solution viscosity differ significantly from the solvent viscosity. Therefore, the *F* coefficient in the Fuoss-Onsager equations is obtained from independent viscosity studies. The *F* coefficient is considered²⁰ equal to the experimentally determined *B* coefficient in the Jones-Dole viscosity equation²⁵

$$\eta/\eta_0 = 1 + AC^{1/2} + BC \quad (5)$$

Including viscosity corrections in conductance data analyses leads to increased a_j values, unchanged Λ_0 values, and slightly increased K_A values.

In the Jones-Dole equation η and η_0 are solution and solvent viscosities, respectively, and *C* is the molar concentration of the solution. Since $[(\eta/\eta_0) - 1]/C^{1/2}$ is a linear function of $C^{1/2}$ for concentrations up to approximately 0.1 *M*, the *B* coefficient, which represents ion-solvent interactions, can be obtained as the slope from a least-squares analysis of viscosity data. The Falkenhagen coefficient *A*,²⁶ which represents ion-ion interactions, either can be obtained as the intercept from a least-squares analysis of data or can be calculated²⁷ from electrolyte limiting equivalent conductances and solvent physical properties.

TABLE I: Conductance Values of the Fuoss–Onsager Equations for Ammonium and Tetraalkylammonium Salts in Tetramethylurea at 25^a_{a-c}

Salt	$\sigma\Lambda$	Λ_0	a_J	K_A	S	E	J
NH ₄ BPh ₄	0.01	31.20 ± 0.024	5.53 ± 0.07		114.2	472.6	1464
	0.03	31.35 ± 0.065	5.16 ± 0.12		114.4	475.6	1407
Me ₄ NClO ₄	0.01	50.93 ± 0.016	4.31 ± 0.18	41.4 ± 2.5	141.9	863.7	2015
	0.02	50.86 ± 0.026	4.14 ± 0.21	37.3 ± 3.3	141.8	862.4	1959
Et ₄ NClO ₄	0.02	50.33 ± 0.026	4.20 ± 0.14	26.9 ± 2.5	141.1	851.8	1958
	0.03	50.46 ± 0.028	4.04 ± 0.15	23.4 ± 2.7	141.2	854.4	1914
Pr ₄ NClO ₄	0.03	45.28 ± 0.024	4.11 ± 0.24	21.3 ± 3.6	134.0	751.6	1737
(1.50 ± 0.04)	0.02	45.41 ± 0.031	3.87 ± 0.15	18.5 ± 2.9	134.2	754.3	1673
Bu ₄ NClO ₄	0.06	43.94 ± 0.051	6.76 ± 1.13	61.8 ± 12.7	132.1	725.0	2333
(1.70 ± 0.04)	0.03	43.70 ± 0.028	3.96 ± 0.27	20.3 ± 4.5	131.8	720.4	1637
Pen ₄ NBr	0.04	44.18 ± 0.047	3.97 ± 0.48	194 ± 8	132.4	729.9	1658
(2.12 ± 0.01)	0.02	44.18 ± 0.020	3.84 ± 0.13	192 ± 2	132.4	730.0	1621
Hex ₄ NBr	0.02	41.86 ± 0.032	3.04 ± 0.22	127 ± 4	129.2	683.9	1306
	0.01	41.84 ± 0.036	3.21 ± 0.14	130 ± 3	129.1	683.5	1358
Hept ₄ NBr	0.02	41.65 ± 0.039	3.12 ± 0.30	127 ± 6	128.9	679.8	1325
	0.01	41.64 ± 0.022	3.11 ± 0.07	127 ± 2	128.8	679.4	1319

^a No viscosity correction applied. ^b Me = methyl, Et = ethyl, Pr = *n*-propyl, Bu = *n*-butyl, Pen = *n*-pentyl, Hex = *n*-hexyl, Hept = *n*-heptyl. ^c Number in parentheses indicates viscosity *B* coefficient.

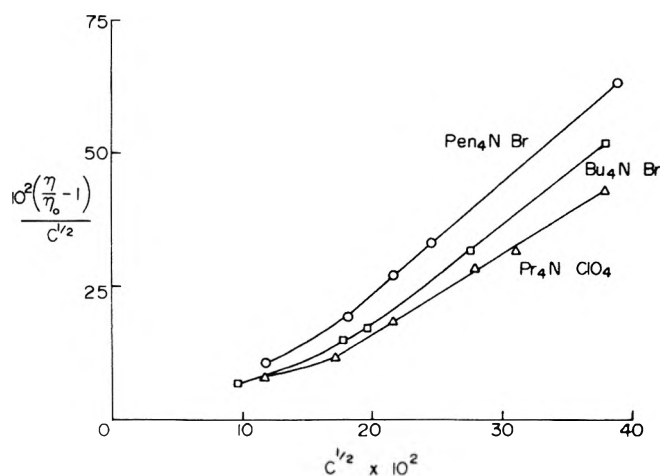


Figure 1. Plot of the Jones–Dole equation for tetraalkylammonium salts in tetramethylurea.

The effect of selected tetraalkylammonium salts on the viscosity of TMU was determined by experimentally evaluating viscosity *B* coefficients of the Jones–Dole equation. Since solutions were prepared by weight, molar concentrations were determined with densities obtained from the equation

$$d = d_0 + A_d \bar{m} \quad (6)$$

in which *d* and *d*₀ are solution and solvent densities, respectively, *A*_{*d*} is the density coefficient, and \bar{m} is the concentration in moles of solute per kilogram of solution. Experimentally determined densities of the most concentrated salt solutions led to *A*_{*d*} values which were used in the calculation of densities of moderately concentrated solutions.

The viscosity data and the density *A* coefficients of the salts studied in tetramethylurea appear in the microfilm edition of this volume of the journal.²⁸ As Figure 1 illustrates, the function $[(\eta/\eta_0) - 1]/C^{1/2}$ vs. $C^{1/2}$ is linear over a 0.03–0.15 *M* concentration range. A computer least-squares analysis of the data within this concentration range yielded the viscosity *B* coefficients listed in Table I.

The precision of the viscosity data in this investigation is comparable to that obtained in viscosity studies of tetraalkylammonium salts in other nonaqueous solvents, such as propylene carbonate² and aliphatic alcohols.²⁹ The curvature below 0.03 *M* concentration indicates that, as expected^{27,30} in a Jones–Dole plot for associated electrolytes, the linear region at high concentrations cannot be extrapolated to zero concentration to obtain the Falkenhagen coefficient. Extrapolation of viscosity data for tetraalkylammonium salts in TMU led to negative values of the Falkenhagen coefficient, similar to those obtained for salts in other nonaqueous solvents such as dimethyl sulfoxide³ and aliphatic alcohols.³¹ Comparison of the viscosity *B* coefficient of tetra-*n*-butylammonium bromide in TMU (1.91 ± 0.05) with values obtained for the same salt in other nonaqueous solvents, such as methanol,^{29,32} acetonitrile,^{29,32} propylene carbonate,^{2a} and methyl ethyl ketone,³² indicated that the *B* coefficient of Bu₄NBr increases with increasing solvent molecular volume.

The molar concentrations and the equivalent conductances of the salts studied in tetramethylurea appear in the microfilm edition of this volume of the journal.²⁸ The conductance values obtained from the Fuoss–Onsager equations are listed in Table I. For all salts two independent sets of conductance data were combined and treated as one set of data. The average conductance values for all salts are presented in Table II.

Table II reveals that consideration of solution viscosity in the Fuoss–Onsager conductance data analysis increases the *a*_{*J*} parameter value by 0.3 unit for the perchlorate salts and 0.7 unit for the bromide salt. The assumption that $F = B_\eta$ for quaternary ammonium halides frequently has led^{13,15} to *a*_{*J*} values 0.2 unit higher than if no viscosity correction were considered.

The sum of the crystallographic radii of all tetraalkylammonium salts is much greater than the *a*_{*J*} parameter. Values of *a*_{*J*} which are small compared to the sum of cationic and anionic crystallographic radii frequently have been obtained^{2a,8,10,13,33} for electrolytes in nonaqueous solvents. Small *a*_{*J*} values are to be expected¹⁰ since the Fuoss–Onsager equations predict ionic separations which are too small to be physically realistic. In many non-

TABLE II: Average Conductance Values of the Fuoss-Onsager Equations for Ammonium and Tetraalkylammonium Salts and Ions in Tetramethylurea

Salt	(Cation)	Λ_0	$(\lambda_0^+)^a$	$a_J(F=0)$	$a_J(F=B_J)$	K_A
NH ₄ BPh ₄	(NH ₄ ⁺)	31.29	(17.57)	5.25		
Me ₄ NCIO ₄	(Me ₄ N ⁺)	50.90	(22.19)	4.24		39.7
Et ₄ NCIO ₄	(Et ₄ N ⁺)	50.40	(21.69)	4.15		25.6
Pr ₄ NCIO ₄	(Pr ₄ N ⁺)	45.31	(16.60)	3.88	4.14	17.5
Bu ₄ NCIO ₄	(Bu ₄ N ⁺)	43.82	(15.11)	4.89	5.27	37.0
Pen ₄ NBr	(Pen ₄ N ⁺)	44.18	(13.80)	3.84	4.50	192
Hex ₄ NBr	(Hex ₄ N ⁺)	41.87	(11.49)	3.19		130
Hept ₄ NBr	(Hept ₄ N ⁺)	41.64	(11.26)	3.07		126

^a Determined at 25° with TABBPh₄ as a reference electrolyte.

aqueous solvents a_J values do not correlate with crystallographic radii; therefore, there is difficulty in interpreting a_J as an ion size parameter.³⁴

In Shedlovsky $\Lambda_0' - C$ plots (as in Figure 1) increasing curvature indicated increasing association within the salt series Pen₄NBr > Me₄NCIO₄ > TABBPh₄; the increasing slope of the straight lines in Shedlovsky $y - x$ plots indicated increasing association within the series. Since the Shedlovsky function Λ_0' is almost linear in concentration for unassociated electrolytes,³⁵ both Shedlovsky analyses ($y - x$ and $\Lambda_0' - C$) yielded the same values for the limiting equivalent conductance of tetraphenylborate salts in TMU. Values of Λ_0 for the tetraalkylammonium perchlorates determined from the Shedlovsky $y - x$ analysis were essentially the same as those Λ_0 values listed in Table II; the Shedlovsky Λ_0 values for the tetraalkylammonium bromides ranged from 0.6 to 1.2% higher than the values calculated from the Fuoss-Onsager equation for associated electrolytes. (See Figure 2.)

Table II indicates that (with the exception of Bu₄NCIO₄ in TMU) association within the two salt series decreases as the crystallographic size of the cations increases. This same trend in association behavior has been observed for tetraalkylammonium salts in other polar nonaqueous solvents such as dimethyl sulfoxide,⁵ acetonitrile,^{7,9} acetone,¹¹ and methanol.¹³

The limiting equivalent conductances of the ammonium and tetraalkylammonium ions, which are listed in Table II, were calculated by subtracting $\lambda_0(\text{BPh}_4^-) = 13.72$, $\lambda_0(\text{ClO}_4^-) = 28.71$, or $\lambda_0(\text{Br}^-) = 30.38$ from the limiting equivalent conductance of the ammonium and tetraalkylammonium salts. The previously determined¹⁶ tetraphenylborate, perchlorate, and bromide limiting equivalent conductances were obtained by assuming that the limiting equivalent conductance of the triisooamylbutylammonium ion (TAB⁺), shown to be equal to that of the tetraphenylborate ion (BPh₄⁻) in methanol,³⁶ is the same as that of the BPh₄⁻ ion in tetramethylurea. Since the purpose of the present investigation is the determination of relative solvation effects within tetraalkylammonium salt series, the validity of the use of TABBPh₄ as a reference electrolyte in TMU is not of primary concern in this study. Future transference number investigations in TMU will assess the validity of the assumption $\lambda_0(\text{TAB}^+) = \lambda_0(\text{BPh}_4^-)$ in this solvent. As expected, the limiting equivalent conductances of the tetraalkylammonium ions decrease as the crystallographic radii of these ions increase.

Since the order of decreasing relative cationic limiting equivalent conductances which is observed in tetramethyl-

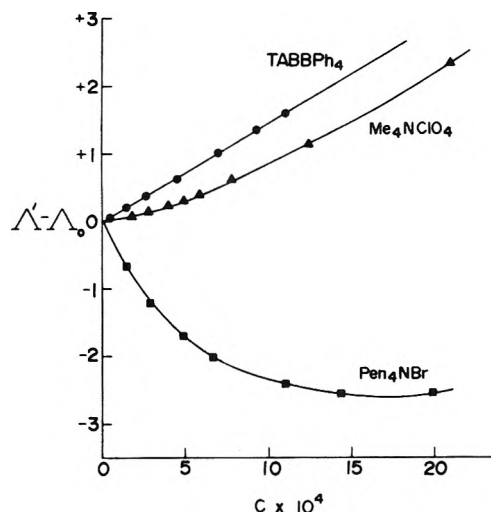


Figure 2. Fuoss-Onsager $\Lambda' - \Lambda_0$ vs. C plots for quaternary ammonium salts in tetramethylurea.

urea, Me₄N⁺ > Et₄N⁺ > NH₄⁺ > Pr₄N⁺ > Na⁺ > K⁺ > Bu₄N⁺, also is noted in dimethylacetamide³⁷ and dimethylpropionamide,³⁸ similar behavior of electrolytes exists in the three solvents. The λ_0^+ order indicates that the "effective" size of the solvated alkali metal ions is comparable to that of the large tetraalkylammonium ions in these solvents. Also of interest in TMU is the order of decreasing λ_0^+ values within the series Bu₄N⁺ > Pen₄N⁺ > TAB⁺. In other nonaqueous solvents such as methyl ethyl ketone¹² and aliphatic alcohols,^{13-15,39} λ_0^+ values decrease in the order Bu₄N⁺ > TAB⁺ > Pen₄N⁺.

Since tetramethylurea has been found to be an interesting medium for study of the transport property behavior of tetraalkylammonium salts, this solvent should be of interest for future investigations of electrolyte behavior in solution.

Acknowledgment. B. J. Barker gratefully acknowledges financial support of these research investigations. This work was supported, in part, by an American Chemical Society, Division of Analytical Chemistry Summer Fellowship, sponsored by the Olin Corporation.

References and Notes

- (1) This study was presented, in part, at the Third Central Regional Meeting of the American Chemical Society, Cincinnati, Ohio, June 1971.
- (2) (a) L. M. Mukherjee and D. P. Boden, *J. Phys. Chem.*, **73**, 3965 (1969); (b) L. M. Mukherjee, D. P. Boden, and R. Lindauer, *ibid.*, **74**, 1942 (1970).

- (3) N. P. Yao and D. N. Bennion, *J. Phys. Chem.*, **75**, 1727 (1971).
 (4) N. P. Yao and D. N. Bennion, *J. Electrochem. Soc.*, **118**, 1097 (1971).
 (5) D. E. Arrington and E. Griswold, *J. Phys. Chem.*, **74**, 123 (1970).
 (6) M. Della Monica and U. Lamanna, *J. Phys. Chem.*, **72**, 4329 (1968).
 (7) D. F. Evans, C. Zawoyski, and R. L. Kay, *J. Phys. Chem.*, **69**, 3878 (1965).
 (8) C. Treiner and R. M. Fuoss, *Z. Phys. Chem.*, **228**, 343 (1965).
 (9) A. C. Harkness and H. M. Daggett, Jr., *Can. J. Chem.*, **43**, 1215 (1965).
 (10) W. A. Adams and K. J. Laidler, *Can. J. Chem.*, **46**, 2005 (1968).
 (11) D. F. Evans, J. Thomas, J. A. Nadas, and M. A. Matesich, *J. Phys. Chem.*, **75**, 1714 (1971).
 (12) S. R. C. Hughes and D. H. Price, *J. Chem. Soc. A*, 1093 (1967).
 (13) R. L. Kay, C. Zawoyski, and D. F. Evans, *J. Phys. Chem.*, **69**, 4208 (1965).
 (14) D. F. Evans and P. Gardam, *J. Phys. Chem.*, **72**, 3281 (1968).
 (15) D. F. Evans and P. Gardam, *J. Phys. Chem.*, **73**, 158 (1969).
 (16) B. J. Barker and J. A. Caruso, *J. Amer. Chem. Soc.*, **93**, 1341 (1971).
 (17) R. L. Kay, *J. Amer. Chem. Soc.*, **82**, 2099 (1960).
 (18) J. L. Hawes and R. L. Kay, *J. Phys. Chem.*, **69**, 2420 (1965).
 (19) (a) T. Shedlovsky, *J. Franklin Inst.*, **225**, 739 (1938); (b) R. M. Fuoss and T. Shedlovsky, *J. Amer. Chem. Soc.*, **71**, 1496 (1949).
 (20) R. M. Fuoss and F. Accascina, "Electrolytic Conductance," Interscience, New York, N. Y., 1959.
 (21) R. M. Fuoss and L. Onsager, *J. Phys. Chem.*, **61**, 668 (1957).
 (22) R. M. Fuoss and E. Hirsch, *J. Amer. Chem. Soc.*, **82**, 1013 (1960).
 (23) Reference 20, p 242.
 (24) R. M. Fuoss, *J. Amer. Chem. Soc.*, **79**, 3301 (1957).
 (25) G. Jones and M. Dole, *J. Amer. Chem. Soc.*, **51**, 2950 (1929).
 (26) (a) H. Falkenhagen and M. Dole, *Phys. Z.*, **30**, 611 (1929); (b) H. Falkenhagen and E. L. Vernon, *ibid.*, **33**, 140 (1932).
 (27) H. S. Harned and B. B. Owen, "The Physical Chemistry of Electrolytic Solutions," 3rd ed, Reinhold, New York, N. Y., 1958, p 240.
 (28) The viscosity and conductance data of the salts studied in tetramethylurea will appear following these pages in the microfilm edition of this volume of the journal. Single copies may be obtained from the Journals Department, American Chemical Society, 1155 Sixteenth St., N.W., Washington, D. C. 20036. Remit check or money order for \$3.00 for photocopy or \$2.00 for microfiche, referring to code number JPC-73-1884.
 (29) R. L. Kay, T. Vituccio, C. Zawoyski, and D. F. Evans, *J. Phys. Chem.*, **70**, 2336 (1966).
 (30) M. Kaminsky, *Disc. Faraday Soc.*, **24**, 175 (1957).
 (31) J. P. Bare and J. F. Skinner, *J. Phys. Chem.*, **76**, 434 (1972).
 (32) D. F. T. Tuan and R. M. Fuoss, *J. Phys. Chem.*, **67**, 1343 (1963).
 (33) P. Bruno and M. Della Monica, *J. Phys. Chem.*, **76**, 1049 (1972).
 (34) M. A. Matesich, J. A. Nadas, and D. F. Evans, *J. Phys. Chem.*, **74**, 4568 (1970). Larger values of the ion size parameter (and larger K_A values) for the salts in TMU would have been obtained if the data had been evaluated by the procedures of Justice or by the Fernandez-Prini expanded form of the Fuoss-Hsia and the Pitts equations. In these relatively recent methods of data evaluation a $C^{3/2}$ term is included in the conductance equations and the ion size parameter is given a new interpretation.
 (35) Reference 20, p 157.
 (36) M. A. Coplan and R. M. Fuoss, *J. Phys. Chem.*, **68**, 1177 (1964).
 (37) G. R. Lester, T. A. Gover, and P. G. Sears, *J. Phys. Chem.*, **60**, 1076 (1956).
 (38) E. D. Wilhoit and P. G. Sears, *Trans. Ky. Acad. Sci.*, **17**, 123 (1956).
 (39) E. C. Evers and A. G. Knox, *J. Amer. Chem. Soc.*, **73**, 1739 (1951).

Uracilyl Radical Production in the Radiolysis of Aqueous Solutions of the 5-Halouracils¹

Kishan Bhatia and Robert H. Schuler*

Radiation Research Laboratories, Center for Special Studies and Department of Chemistry, Mellon Institute of Science, Carnegie-Mellon University, Pittsburgh, Pennsylvania 15213 (Received March 19, 1973)

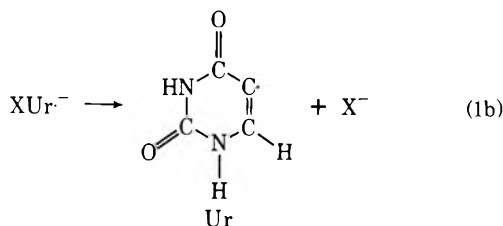
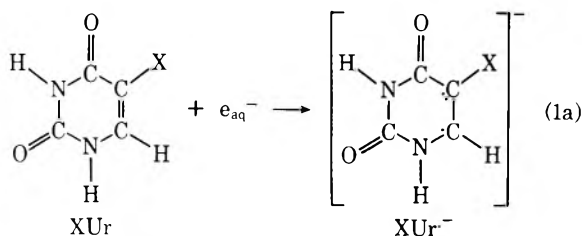
Publication costs assisted by the U. S. Atomic Energy Commission and Carnegie-Mellon University

The radiolysis of dilute aqueous solutions of 5-bromo-, 5-chloro-, and 5-fluorouracil has been investigated by liquid chromatographic and by pulse radiolysis conductometric methods with attention being focussed on determining the importance of the production of 5-uracilyl radical as an intermediate. In the chromatographic study both the consumption of the starting material and formation of uracil have been examined in the presence of a suitable H atom donor. It is concluded that at pH 7 the reaction of hydrated electrons with 5-bromo- and 5-chlorouracil yields 5-uracilyl radical essentially quantitatively. From the conductometric study it is apparent that the loss of chloride from the anion radical initially produced by reaction of e_{aq}^- with 5-chlorouracil is sufficiently slow that in acidic solutions protonation is important and as a result 5-uracilyl radical is produced only in reduced yield. It is estimated that in this case protonation competes with dissociation on equal terms at pH 5.2. For 5-bromouracil protonation of the intermediate anion radical is unimportant even at pH 3 indicating that in this case the anion intermediate has a lifetime $<10^{-7}$ sec. The hydrated electron reacts rapidly with 5-fluorouracil but does not give any appreciable yield of 5-uracilyl radical. In neutral solution the anion radical formed by reaction of e_{aq}^- with uracil is shown to transfer electrons to each of the halouracils and result in their reaction even when they are present as only a minor component in the system. With 5-bromouracil $>10^{-5}$ M this transfer reaction is 100% efficient. Auxiliary results are presented on other aspects of the radiolysis of the halouracils.

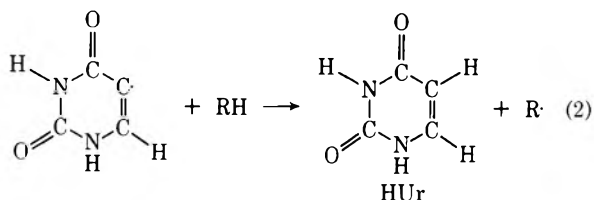
The radiation chemistry of aqueous solutions of 5-bromouracil (BrUr) has been the subject of a large number of investigations because of the importance of this compound as a sensitizer in radiobiological studies.² Comparative

studies of the radiolysis of 5-bromouracil and of 5-chlorouracil (ClUr) and 5-fluorouracil (FUr) have recently been carried out³ and it appears that the rate constants for the reaction of H, OH, and e_{aq}^- with these compounds are known

sufficiently accurately^{3b} that effects of processes which compete with the initial reactions can be taken into account quite well. It has also been known for some time that attack of e_{aq}^- on 5-bromouracil produces a large yield of bromide ion^{4,5} and it has been suggested⁴ that 5-uracilyl radical (Ur \cdot ; referred to in the following as uracilyl radical) is formed by reaction 1. Measurements of ha-



lide ion production indicate that in the cases where X is Br or Cl reaction 1 is a major contributor to the overall radiation chemical process.^{3a,4,5} Electron transfer from other radicals present in the system can, however, be important and it was found experimentally that secondary reactions complicated the detailed interpretation of the results from the halide measurements.^{3a} Conductometric pulse radiolysis studies^{3a} indicated that approximately 80, 50, and 15% of e_{aq}^- react with BrUr, ClUr, and FUr, respectively, *via* reaction 1. In the presence of a source of abstractable hydrogen the uracilyl radical is expected to react to produce uracil (HUr) (reaction 2). Zimbrick,



Ward, and Myers⁶ measured both the loss of bromouracil and the production of uracil by spectrophotometric techniques and found similar yields although detailed studies were not possible because of the high similarity of the absorption spectra of the product and the starting material. The recent development of high-speed liquid chromatographic methods suitable for measurements on dilute aqueous solutions⁷ provides a means of examining the radiation chemistry of the 5-halouracil systems in considerable detail. We wish to report here the results of investigations of the importance of reaction 1 in solutions to which *tert*-butyl alcohol has been added to suppress contributions from OH radical reactions. These results indicate that in neutral solution e_{aq}^- reacts with 5-bromo- and 5-chlorouracil to produce uracilyl radical and halide ion with near unit efficiency. Reaction with 5-fluorouracil produces a radical anion which, however, does not dissociate to the uracilyl radical. These conclusions are corroborated by further conductometric studies using an ac method. Both the product analysis and conductometric

studies show that in acidic solutions of 5-chlorouracil, protonation of the radical anion initially produced competes with its dissociation so that uracilyl radical is produced only in reduced yield. With 5-bromouracil protonation appears to be unimportant down to pH values below 4. Auxiliary measurements on a number of other aspects of the radiolysis of the 5-halouracil systems are also reported.

Experimental Section

Samples of 5-bromouracil and 5-fluorouracil were obtained from Sigma Chemical Co. and 5-chlorouracil from Calbiochem. These samples were the same as used in previous studies.³ Chromatographic analysis showed that the chlorouracil had ~0.5% of uracil as an impurity and this background to a considerable extent placed a lower limit on the doses that could be studied. A correction for this background was made in all cases. The bromo- and fluorouracil samples contained 0.05 and 0.01% uracil impurity.

Studies of product formation at pH 7 were carried out on solutions containing appropriate concentrations of phosphate buffer. Perchloric acid and potassium hydroxide were used to adjust the pH in the other steady-state studies and also in the conductometric measurements. Cupric sulfate was used as a radical oxidant in certain studies where it was desired to suppress secondary radical reactions. Samples were purged of oxygen by bubbling with either N₂ or N₂O.

Steady-state irradiations were carried out in cobalt sources at dose rates of 6×10^{16} or 8×10^{17} eV g⁻¹ min⁻¹. Absorbed doses were generally in the range 3×10^{16} – 4×10^{18} eV/g. Samples were analyzed immediately after the irradiation using the high-speed liquid chromatographic apparatus described previously.⁷ The methods employed were essentially the same as used in the previously reported study of the radiolysis of *p*-bromophenol solutes with absorption spectrophotometry at 254 nm being used to examine the column effluent.⁸ Short-term reproducibility of the chromatographic peak heights is ~1% and in most cases the analyses are believed to be good to a few per cent or better. In the present study 2.1-mm i.d. columns 1–2 m long packed with Du Pont Anion Exchange Column Packing Material were used. The chromatographic conditions were such that there was complete separation of uracil, 5- and 6-hydroxyuracil, and the 5-halouracils. Typical relative retention times were 1, 1.50, 1.60, 1.25, 2.3, and 3.0 for uracil, 5-hydroxyuracil, 6-hydroxyuracil, 5-fluorouracil, 5-chlorouracil, and 5-bromouracil. All of these compounds have high extinction coefficients (4000–30,000 M⁻¹ cm⁻¹) at 254 nm and are readily detected at concentrations greater than 10⁻⁷ M. The sensitivity of the detector toward products such as 5,6-dihydrouracil and its hydroxylated analogs is low because of their low extinction coefficients (*e.g.*, ≈ 35 M⁻¹ cm⁻¹ for 5,6-dihydrouracil).

Conductometric experiments were carried out by an ac method using the 10-MHz bridge developed by Lilie and Fessenden.⁹ With the cell used the sensitivity of the apparatus is essentially constant for ionic concentrations <10⁻³ M (*i.e.*, over the pH range of 3–11). Yields were determined by reference to the production of HCl from CH₃Cl solutions saturated at atmospheric pressure (0.1 M; $G(\text{HCl}) = 3.15$).¹⁰ Doses in these experiments were such as to produce from 10⁻⁶ to 10⁻⁵ M HX.

TABLE I: Initial Yields for Halouracil Consumption and Uracil Production at pH 7 for Solutions 0.1 M in *tert*-Butyl Alcohol

	[XUr]	FUr	ClUr	BrUr
G(-XUr)	10^{-4}	2.1	2.9	3.0
G(-XUr) N ₂ O _{sat} ^a	10^{-4}	0.41	0.43	0.45
G(-XUr) trans ^b	10^{-4}	1.3	2.5	3.0
G(HUr)	10^{-4}	0.25	2.7	2.7
	10^{-3}	0.40	3.15	3.15
G(HUr) N ₂ O _{sat} ^{c,d}	10^{-4}	0.18	0.15	0.30

^a Approximately 1% of the electrons and 1% of the OH radicals are not scavenged in these solutions so that the net yields assignable to H atom reactions are 0.05–0.10 lower. The *tert*-butyl alcohol will remove ~30% of the H atoms initially produced. ^b Yields from electron transfer reactions as observed from solutions also containing 10^{-3} M uracil where ~90% of both e_{aq}^- and H atoms react with the uracil. ^c Essentially the same values were observed for N₂O-saturated solution in the absence of *tert*-butyl alcohol. ^d For the most part these yields appear to be attributable to H atom reactions and the yields at 10^{-3} M, where essentially all H atoms react with the halouracil, are expected to be ~50% greater.

Results and Discussion

Consumption of the 5-Halouracils. The consumption of the starting material as a function of dose for 10^{-4} M solutions of each of the halouracils also containing 0.1 M *tert*-butyl alcohol is indicated by the solid points in Figure 1. Since the rate constants for reaction of OH with the halouracils ($\sim 5 \times 10^9$ M⁻¹ sec⁻¹)^{3b} are only one order of magnitude greater than that for their reaction with *tert*-butyl alcohol, the alcohol will remove ~99% of the OH radicals. The alcohol also serves to prevent secondary reaction of the uracil radical with the halouracil. Presumably the loss of halouracil is principally attributable to attack by e_{aq}^- although there will be a component from H atom reactions since the *tert*-butyl alcohol present will remove only about 30% of the H atoms. Experiments on solutions also saturated with N₂O (where 99% of e_{aq}^- is converted to OH) show net yields for consumption of each of the halouracils of 0.3–0.4 (see Table I) or about the contribution expected from H atom attack, *i.e.*, ~70% of the independent H atom yield of 0.6.¹¹ The observed yields (*G* values) for consumption of the halouracils for 10^{-4} M solutions of FUr, ClUr, and BrUr measured at a dose of 10¹⁸ eV/g are respectively 2.1, 2.6, and 2.7. At this dose ~40% of the starting material is consumed so that the errors involved in determining the slope correspond to errors in yield ~0.1. These observed yields are, however, expected to be somewhat lower than the initial yields because of reaction of e_{aq}^- with radiation-produced product. Corrections for this latter effect can be made only after first considering the importance of secondary processes involving electron transfer. From the raw data of Figure 1 lower limits to consumption of FUr, ClUr, and BrUr which result from attack of e_{aq}^- in 10^{-4} M solutions are 1.6, 2.2, and 2.3.

Electron Transfer from Uracil Radical Anion. One notes in Figure 1 that loss of the starting material is reasonably linear with dose even down to concentrations ~50% of the initial solution. Since e_{aq}^- reacts with uracil (which in the presence of *tert*-butyl alcohol is both the expected and observed product from both BrUr and ClUr, see below) about as rapidly as it does with the halouracils^{3b} one expects the yield for consumption of the starting material to decrease appreciably as the irradiation progresses (as it does, for example, in the case of *p*-bromophenol).⁸ The linearity of the plots of Figure 1, therefore, immediately indicates that the anion radical produced by the

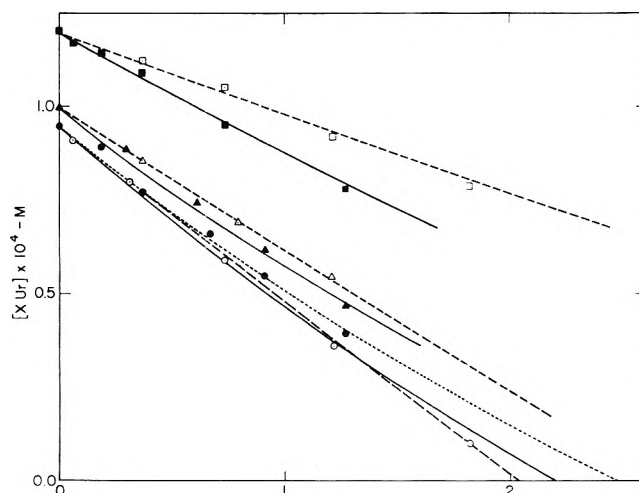
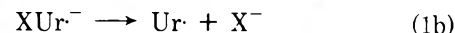


Figure 1. Consumption of (●,○) 5-bromouracil, (▲,△) 5-chlorouracil, and (■,□) 5-fluorouracil as a function of dose. Closed symbols are for neat solutions, open symbols are with 10^{-3} M uracil added. Curves are calculated by integration of the sum of eq 6 and 7. For bromouracil the solid and dashed curves assume that both direct reaction of e_{aq}^- and transfer from uracil anion radical consume the bromouracil with unit efficiency. The dotted curve assumes that 90% of e_{aq}^- consume the halouracil. The other curves are similarly calculated with appropriately reduced efficiencies (see text).

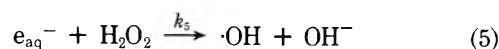
reaction of e_{aq}^- with product uracil must undergo an efficient electron transfer reaction and result, ultimately, in consumption of the halouracil. Electron transfer from thymine anion radical to bromouracil is known to occur rapidly ($k_{trans} = 1.1 \times 10^9$ M⁻¹ sec⁻¹) and appears to account for the high yields of bromide ion produced from bromouracil solutions containing relatively higher concentrations of thymine.² In the present work experiments were carried out on solutions containing 10^{-3} M uracil in addition to 10^{-4} M halouracil and the results are also given in Figure 1. It is seen that the yields for consumption of both BrUr and ClUr are not significantly affected by the presence of uracil in spite of the fact that ~90% of the reaction of e_{aq}^- is with the latter material. It is clear that for BrUr and ClUr electron transfer contributes to the ultimate consumption of the halouracil, *e.g.*



with an efficiency (ϵ_T) very near to unity. With FUr the observed yield from the uracil-containing solutions is somewhat lower and it appears that in this case the transfer reaction is only about 45% efficient. Uracil, when present by itself, is not consumed as the result of electron attack ($G(-\text{HUr})$ was measured to be only 0.04 for a solution 10^{-4} M in HUr) so that it is not possible to examine directly the effect of adding bromouracil to uracil solutions.

Kinetic Treatment of the Yield-Dose Curves. Within the above framework one can proceed to treat the halouracil consumption curves quantitatively. The rate constants for reaction of e_{aq}^- with XUr is $1-2 \times 10^{10}$ M⁻¹ sec⁻¹ and the rate constant ratio k_3/k_1 is ~ 1 .^{3b} However, since ϵ_T is obviously very near to unity the buildup of uracil makes little difference to the course of the overall reaction. The principal additional complication in these ex-

periments is the removal of e_{aq}^- by reaction with the radiation-produced peroxide



The rate constant for reaction 5 ($1.23 \times 10^{10} M^{-1} sec^{-1}$)¹² and the molecular peroxide yield ($G = 0.8$)¹¹ are both sufficiently high that loss of e_{aq}^- via this path is appreciable at doses where consumption of the halouracil is measured. The appropriate differential equation which describes the rate of consumption of XUr resulting from reactions 1-5 is

$$-\left[\frac{d(XUr)}{dD}\right]_{e_{aq}^-} = \frac{10G(e_{aq}^-)}{N} \frac{\epsilon + \epsilon_T \frac{k_3 [HUr]}{k_1 [XUr]}}{1 + \frac{k_3 [HUr]}{k_1 [XUr]} + \frac{k_5 [H_2O_2]}{k_1 [XUr]}} \quad (6)$$

where D is the dose in eV/g, ϵ is the efficiency for consumption of XUr by the reaction of e_{aq}^- , ϵ_T is the efficiency of the electron transfer reaction, and $10G(e_{aq}^-)/N$ is the production rate of electrons in units of $M/eV/g$. If it is assumed that the halouracil is removed by the reaction of H atoms with an efficiency ϵ_H then this contribution is

$$-\left[\frac{d(XUr)}{dD}\right]_H = \frac{10G(H)}{N} \frac{\epsilon_H}{1 + \frac{k_7 [UrH]}{k_6 [XUr]} + \frac{k_8 [BrOH]}{k_6 [XUr]}} \quad (7)$$

In eq 7 $G(H)$ is the independent yield of H atoms and k_6 , k_7 , and k_8 are the rate constants, respectively, for their reactions with the halouracil, uracil, and *tert*-butyl alcohol.

From the empirical expression given in ref 10 the yields for electrons which react with the solutes ($G(e_{aq}^-)$) are calculated to be 2.64 and 2.82 for the solutions containing 10^{-4} and 10^{-3} M added uracil. Using these values and taking $G(H)$ as 0.60 one calculates the solid curve given in Figure 1 for bromouracil by numerically integrating the sum of eq 6 and 7. In these calculations it is assumed that ϵ and ϵ_T are unity, that peroxide builds up linearly with $G(H_2O_2) = 0.80$, and that the increase in HUr is approximated by the loss in BrUr. This latter assumption is borne out by the fact that the sum of the BrUr and HUr (the latter as measured below) is very nearly constant. Because of the electron transfer process the buildup of peroxide has a relatively minor effect since this product is competing with an essentially constant concentration of XUr + HUr and the yield-dose curve has very little curvature. At 10^{-4} M the observed rate of decrease in BrUr is $\sim 10\%$ lower than expected from these calculations. The data can be fitted either if ϵ is taken as 0.90 (dotted curve in Figure 1) or if the H atoms which react with BrUr are assumed to consume it with an efficiency of only 50%. A combination of these two explanations is probably nearer the truth. It seems likely that at a concentration as low as 10^{-4} M the yield measured may be slightly low as the result of reaction of e_{aq}^- with trace impurities. The reaction period with the BrUr is calculated to be ~ 0.5 μsec and the electron lifetime in solutions similarly prepared was measured to be only ~ 10 μsec . From this a loss of approximately 5% can be attributed to impurities (e.g., 3×10^{-6} M O_2 would account for the observed decrease).

For the solutions with added uracil neither the peroxide buildup nor the H atom component have any significant effect and the BrUr should decrease linearly with a yield essentially equal to $\epsilon_T G(e_{aq}^-)$. The calculated curve is

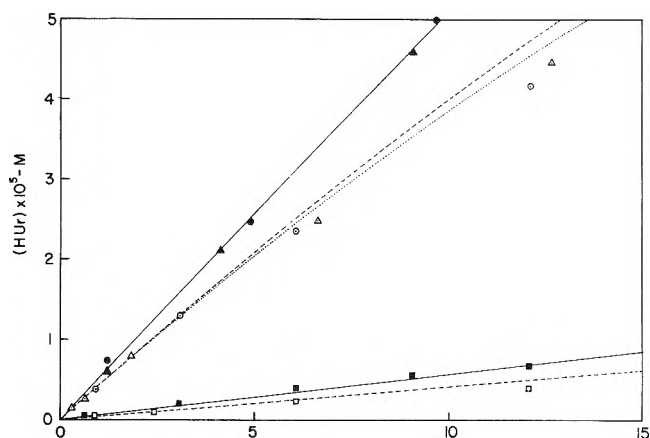


Figure 2. Production of uracil as a function of dose for solution 10^{-4} and 10^{-3} M in (○, ●) 5-bromouracil, (△, ▲) 5-chlorouracil, and (□, ■) 5-fluorouracil. Curves are calculated by integration of the sum of the right-hand side of eq 6 and 7 assuming $\epsilon_H = 0.6$. $G(e_{aq}^-)$ is assumed to be 2.64 at 10^{-4} M (solid curves) and 2.82 at 10^{-3} M (dashed curves). The efficiencies for reaction of e_{aq}^- with the halouracil were taken as 90% at 10^{-4} M and 100% at 10^{-3} M and electron transfer as 100% (dotted curve calculated for 10^{-4} M solutions with an 80% electron transfer efficiency).

given by the dashed line in Figure 1 with $\epsilon_T = 1$. The observed rate of decrease corresponds to a total yield for reaction of both solutes with e_{aq}^- of 3.0 (as compared with the value of 2.82 given above). It seems clear that both direct attack of e_{aq}^- on the bromouracil and indirect reaction via electron transfer from uracil anion radical result in consumption of the bromouracil with an efficiency very near to unity.

In the case of chloride the data at 10^{-4} M very closely parallel those from the bromouracil so that the kinetic description and the yields involved would seem to be similar. Here the experiments with added uracil show a slightly lower yield for chlorouracil consumption. By comparison with the effect on bromouracil it is estimated that electron transfer is only $\sim 80\%$ efficient. Using this value for ϵ_T the curves of Figure 1 are calculated by integrations similar to those described above. Reaction of e_{aq}^- with chlorouracil certainly results in its consumption with near unit efficiency (i.e., $>90\%$) at pH 7 and electron transfer is only slightly less efficient.

The results for fluorouracil are more difficult to treat since the dominant chemical products have not, as yet, been identified (neither fluoride ion^{3a} nor uracil (see below) are produced in high yield). The results given in Figure 1 indicate that FUr is consumed with an initial yield of ~ 2.0 and of this about 1.6 can be attributed to the direct reaction of e_{aq}^- with FUr (for an efficiency of $\sim 60\%$). The fact that fluorouracil is consumed to a significant extent qualitatively differs from the effect for uracil itself where, as pointed out above, the yield is trivially small. The yield resulting from electron transfer is 1.3 (H atom reactions should not contribute significantly here) corresponding to a slightly lower overall efficiency of $\sim 45\%$.

Production of Uracil. One can readily follow the buildup of uracil in these systems and the resulting data are displayed in Figure 2 for 10^{-4} and 10^{-3} M solutions containing 0.1 M *tert*-butyl alcohol to serve as an OH radical scavenger. From the competitive studies described below we estimate that $>98\%$ of the uracil radicals abstract hydrogen from the alcohol at a concentration of 10^{-3} M

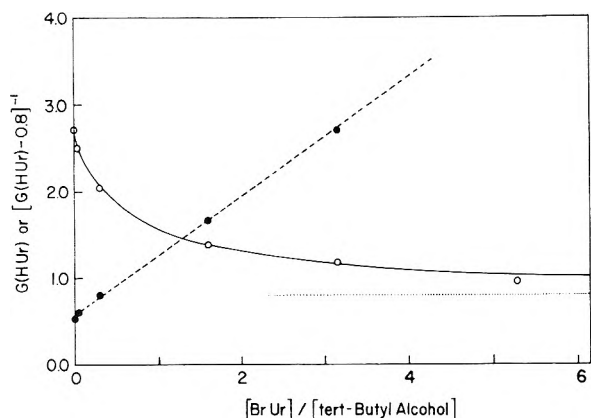
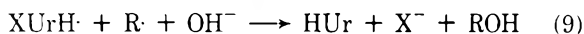


Figure 3. Competitive scavenging of the 5-uracilyl radical by *tert*-butyl alcohol. A uracil yield of 0.8 was observed in the absence of alcohol (dotted line). The yields of uracil (●) and the quantity $[G(\text{HUr}) - 0.8]^{-1}$ (○) are given as a function of the ratio $[\text{BrUr}]/[\text{tert-butyl alcohol}]$. The rate of abstraction of H from *tert*-butyl alcohol relative to the rate of addition to the bromouracil is from the latter plot 1.3.

halouracil and essentially all at 10^{-4} M. Because of the electron transfer process discussed above buildup of uracil will have no significant effect on the yield of uracilyl radicals and the effect of peroxide formation, though expected to be quite small, can readily be taken into account by integrations of expressions analogous to eq 6. Correcting the observed product concentrations for the slight losses expected from the secondary reactions we obtain initial yields of 2.7 for both BrUr and ClUr at 10^{-4} M and 3.15 at 10^{-3} M (Table I). The yields from fluorouracil are much lower being only 0.25 at 10^{-4} M and 0.4 at 10^{-3} M. Hydrogen atom addition contributes to some extent, as indicated by the low but real yields observed for 10^{-4} M solutions saturated with N_2O (where the yield from e_{aq}^- attack on XUr is expected to be <0.05), and in the case of fluorouracil would seem to be essentially the total source of uracil formation. Presumably the radical $\text{XUrH}\cdot$ formed as a result of H atom addition



is reduced in part, upon disproportionation, to give uracil



At the higher concentration of halouracils the H atoms react entirely ($>95\%$) with the halouracil (in contrast to the experiments described above with added uracil) and the contributions to uracil formation from this source are estimated to be 0.3 ± 0.1 from the experiments with N_2O -saturated solutions (see Table I). The net yields of uracil attributable to e_{aq}^- attack on BrUr and ClUr are 2.4 ± 0.1 at 10^{-4} M and 2.8 ± 0.1 at 10^{-3} M. Production curves obtained by integrating the sum of the right-hand side of eq 6 and 7 are given in Figure 2 (with $\epsilon_{\text{H}} = 0.6$). For these compounds the sum of XUr and HUr is essentially constant to doses of $\sim 5 \times 10^{17}$ eV/g so that the halouracil consumed at 10^{-4} M is almost totally accounted for by the uracil formed. At higher doses the total decreases slightly with the loss being ~ 0.3 at a dose of 1.2×10^{18} eV/g. At these doses the yield-dose plots for uracil formation have a somewhat higher curvature than can be predicted by the above scheme (see Figure 2) and indicate that unaccounted for reactions with radiation-produced

product introduce complications which reduce the yields by $\sim 20\%$.

The results at 10^{-3} M certainly indicate that e_{aq}^- reacts with both bromo- and chlorouracil very nearly quantitatively at pH 7 to form uracil. The slightly lower yields at 10^{-4} M would seem to indicate small effects of impurities as discussed above. From the additional results reported below we conclude that at this pH the overall process involves the intermediate production of the 5-uracilyl radical essentially exclusively in the case of the bromide and predominantly in the case of the chloride. The fluoro derivative obviously undergoes reaction 1b to at most a small extent and it appears that the uracil observed in this case is attributable almost entirely to the addition of H atoms.

Competitive Scavenging of Uracilyl Radical. The dependence of uracil formation on *tert*-butyl alcohol concentration for bromouracil solutions is displayed in Figure 3. In the absence of *tert*-butyl alcohol a yield ($G(\text{HUr})_0$) of ~ 0.8 is observed. Of this yield about 0.3 is attributed to the reaction of H atoms (see Table I) followed by reduction of the resultant radical and the remainder to processes involving abstraction from the bromouracil or possibly from products. In the absence of a source of readily abstractable H atoms about 80% of the uracilyl radicals react by other processes. Products from this component to the overall chemistry were not observed and presumably high molecular weight products are formed by addition to the parent compound. A competitive plot of $1/(G(\text{HUr}) - G(\text{HUr})_0)$ vs. $[\text{BrUr}]/[\text{tert-butyl alcohol}]$ is given in Figure 3. From this dependence the rate for abstraction reaction from *tert*-butyl alcohol relative to the addition reaction is determined to be 1.3 ± 0.3 . No absolute rate information is as yet available on these processes but it seems likely that the abstraction reaction will be relatively slow, very probably being somewhat less than the value of 3×10^7 $\text{M}^{-1} \text{sec}^{-1}$ observed⁸ for abstraction of hydrogen from isopropyl alcohol by *p*-hydroxyphenol radical. The present results, therefore, indicate that addition of uracilyl radical to bromouracil is similarly slow so that it is not too surprising that abstraction from the pyrimidine base itself can contribute to uracil formation. An experiment in the presence of 10^{-2} M benzene as a radical scavenger showed a uracil yield of <0.1 . In this case both H atoms and uracilyl radical are removed as a source of uracil.

pH Dependence of Uracilyl Radical Formation. The above results at pH 7 appear to be at variance with the conclusions from previous conductivity results where somewhat lower efficiencies for e_{aq}^- attack were indicated, particularly in the case of chlorouracil where the observed yield of HCl corresponded to an efficiency of only $\sim 50\%$. The conductivity experiments were necessarily carried out in more acidic solutions (pH 5–6) and it is now obvious that protonation of the chlorouracil anion radical produced in reaction 1a contributes importantly at these lower pH values. In neutral solutions Patterson and Bansal^{3b} have observed a transient with an absorption at 335 nm which decayed with a half-life of ~ 5 μsec . It now seems evident that this transient can be assigned to the chlorouracil anion radical. No similar transient was observed in the case of bromouracil^{3b,13} while in the case of fluorouracil an intermediate which has a similar absorption spectrum and did not decay on the time scale of ~ 100 μsec was present. These results indicate that the rate constants for reaction 1b are $<10^4$, $\sim 10^5$, and $>10^6$

sec^{-1} for the fluoride, chloride, and bromide. If, in the case of the chloride, we assume that the rate constant for reaction 10 is $6 \times 10^{10} \text{ M}^{-1} \text{ sec}^{-1}$ ¹⁴ then at a pH of 5.2



this reaction will compete on equal terms with reaction 1b and the uracilyl radical yield will be reduced by $\sim 50\%$. We have attempted to test this conclusion experimentally by examining the pH dependence of uracil formation.

Experiments at pH 4 on 10^{-3} M solutions of chlorouracil (plus 0.1 M *tert*-butyl alcohol) gave an initial yield of uracil of 1.9. Since the rate constants for reaction of e_{aq}^- with ClUr and H^+ are very similar about 90% of the electrons will still react with the chlorouracil at this pH and the observed yield represents about two-thirds of this reaction. From the above arguments one expects from the competition between reactions 1b and 10 that the yield of uracilyl radical will be < 0.5 . Uracil can, however, be formed by the disproportionation of the neutral radical produced in reaction 10, *i.e.*, by reduction of ClUrH \cdot *via* reaction 9. One can prevent this reduction by adding an appropriate radical oxidant to the irradiation system. Holian and Garrison¹⁵ have shown that Cu^{3+} oxidizes hydroxyhydrouracil radical quantitatively so that it would appear that Cu^{2+} should be a suitable oxidant for the ClUrH \cdot radical. The results on the pH dependence of uracil production from solutions $1.2 \times 10^{-4} \text{ M}$ in CuSO_4 and $2.0 \times 10^{-3} \text{ M}$ in ClUr (0.1 M *tert*-butyl alcohol) are reported in Figure 4. The solubility product for $\text{Cu}(\text{OH})_2$ is reported to be $5 \times 10^{19} \text{ M}^3$ ¹⁶ so that at all pH values below 6.8 the Cu^{2+} ion should be entirely in solution. Since the rate constant for reaction of e_{aq}^- with Cu^{2+} is very high ($3 \times 10^{10} \text{ M}^{-1} \text{ sec}^{-1}$)¹² a correction to the observed data must be made for electron scavenging by the Cu^{2+} . The corrected yields are indicated by the solid points in Figure 4. It is seen that the yield drops appreciably in the region below pH 6. This drop is attributed to the removal of the neutral intermediate as a precursor to uracil formation by the oxidation reaction



One possible complication in these experiments is direct oxidation of the initial radical anion by the copper



However, the high yields observed at pH values of 6.0 and 6.4 require that the rate constant for reaction 12 be less than $\sim 5 \times 10^8 \text{ M}^{-1} \text{ sec}^{-1}$ and indicate that it should not be of major importance at a copper ion concentration of 10^{-4} M . In more acidic solutions where reaction 10 dominates reaction 12 cannot contribute significantly. The results at higher pH values are difficult to interpret exactly because of the limited solubility of the copper ion (a Cu^{2+} ion concentration of $5 \times 10^{-4} \text{ M}$ is calculated for pH 7). It should be noted that oxidation by the copper is also expected to remove any uracil formed by H atom addition to the chlorouracil. Treating the sigmoidal dependence of Figure 4 as a simple competition between reactions 1b and 10 indicates that the rates of these two reactions are equal at a pH of 5.8. From this result it is estimated that at a pH 7 $\sim 95\%$ of the electrons should react with chlorouracil to give uracilyl radical *via* reaction 1b. It is noted here that the conductivity results reported below indicate a somewhat lower value for k_{10}/k_{1b} (by a factor of ~ 4) so

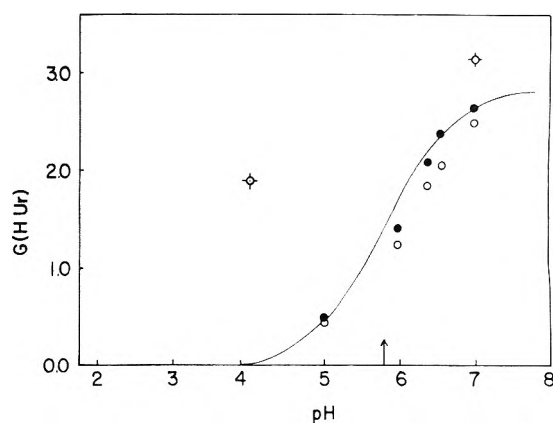


Figure 4. pH dependence of the uracil yield from $2 \times 10^{-3} \text{ M}$ solutions of chlorouracil containing 0.1 M *tert*-butyl alcohol (\oplus) neat and (O) in the presence of 10^{-4} M Cu^{2+} ion. The solid points represent the latter corrected for reaction of e_{aq}^- with the Cu^{2+} ion. The curve represents a simple competition between reaction 1b and 10 with equal rates at pH 5.8 (the arrow).

that some complications may well be present in these studies with Cu^{2+} ion.

Conductivity Experiments. The previous conductivity experiments,^{3a} which were carried out by a dc method, indicated that the fractions of electron attack that resulted in uracilyl radical formation *via* reaction 1b were 0.80, 0.50, and 0.15 respectively for BrUr, ClUr, and FUr. One cannot carry out conductivity experiments at pH 7 nor with the dc method in very acidic solutions so that these previous experiments were carried out at a pH somewhat above 5. It is now obvious that at the pH involved the yields of HCl produced initially from chlorouracil are expected to be reduced by competition from the protonation reaction so that the results obtained cannot be compared directly with those from neutral solutions. The previous results were also affected somewhat by buffering effects at the relatively high concentration of the halouracils used. Estimates assuming that the pK values of the halouracils were similar to that of uracil (pK = 9.4)¹⁷ had indicated that buffering should not be a problem. The ionization constants of the halouracils have recently been measured to be 7.9–8.1¹⁸ or ~ 1.5 units lower than that of uracil itself and it is now clear that even at a pH of 5.5 a small amount of buffering results from the ionization equilibrium of the halouracil if present at a concentration of $\sim 10^{-3} \text{ M}$. In order to avoid this, experiments must be carried out in more dilute or more acidic solutions. The development of an ac method⁹ has permitted us to examine the initial production of HX for pH values down to 2. Typical traces recorded for BrUr and ClUr solutions containing 0.5 M *tert*-butyl alcohol are given in Figure 5. At all pH values above 3 the conductivity trace observed for bromouracil solutions is flat, as is illustrated in Figure 5A. However, as is seen in Figure 5C and 5D the chlorouracil solutions show a marked growth with time. This growth is ascribed to the HCl liberated as a result of the disproportionation of the neutral radicals produced from reaction 10 at low pH.

In Figure 6 the yields of HX determined from the initial rise in conductivity for 10^{-3} M bromo- and chlorouracil solutions are illustrated and also the values at $150 \mu\text{sec}$ when the disproportionation should be $\sim 90\%$ complete. The 0.5 M *tert*-butyl alcohol will scavenge 98% of the OH

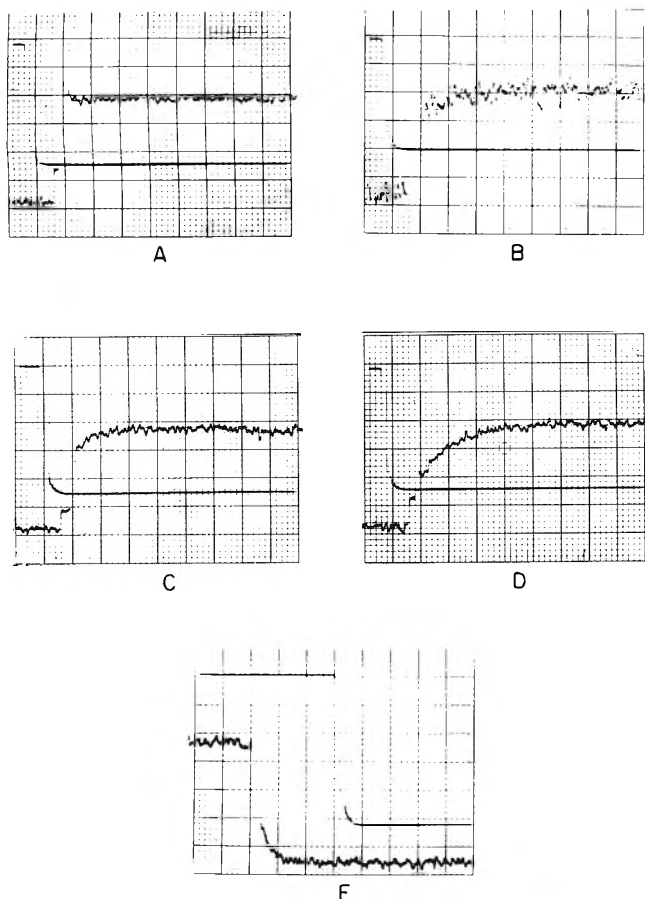


Figure 5. Dependence of conductivity on time for $10^{-3} M$ solutions of bromo- and chlorouracil containing $0.5 M$ *tert*-butyl alcohol: A, bromouracil at pH 5.4; B, bromouracil at pH 2.2; C, chlorouracil at pH 5.2; D, chlorouracil at pH 4.5; and E, chlorouracil at pH 10.5. The net yields calculated by comparing the conductivity increases to the changes observed in methyl chloride solutions correspond to $G(\text{HX})$ of A = 1.8; B = 0.60 at $10 \mu\text{sec}$ increasing to 1.8 at $100 \mu\text{sec}$; C = 1.3 at $10 \mu\text{sec}$ increasing to 1.8 at $100 \mu\text{sec}$; and D = ~ 0.7 at $10 \mu\text{sec}$ increasing to 1.8 at $100 \mu\text{sec}$. The negative increase in E corresponds to $G(\text{Cl}^- - \text{OH}^-)$ of 2.7 at $100 \mu\text{sec}$. The buffering effect of the solute is significant for all traces except D so that the yield for electron attack on the solute is somewhat greater than indicated by these net yields (see text). All traces $20 \mu\text{sec}/\text{large division}$. Conductivity of B recorded at relative gain of 2.5, all other gains are unity. Noiseless traces are output of charge monitor (E recorded on gain of 0.5) from which the relative doses are determined to be (A) 4.3, (B) 3.9, (C) 4.5, (D) 4.3, and (E) 10.6.

radicals so that only 0.05 of the observed change can be attributed to their reactions. With bromouracil the yield at a pH of 4.5 is 2.8 or identically the value expected from the reaction of e_{aq}^- via reaction 1. The drop in yield at low pH for the bromouracil solutions is clearly the result of the competing effect of the reaction of e_{aq}^- with H^+ . The solid curve represents the yields calculated from the measured pH of the solutions, the concentration of BrUr, and the known rate constants. Protonation appears to be of no major importance at a pH of 3 so that the lifetime of the BrUr anion radical can be estimated to be $< 10^{-7}$ sec. At the lowest pH values a small growth is observed to occur over a period of $50 \mu\text{sec}$ and makes accurate estimates of the initial yield difficult. This growth is attributed to the HBr liberated in the recombination of the radicals produced from H atom addition to the bromide. It is clear that in these experiments H atom addition results in very little HBr elimination.

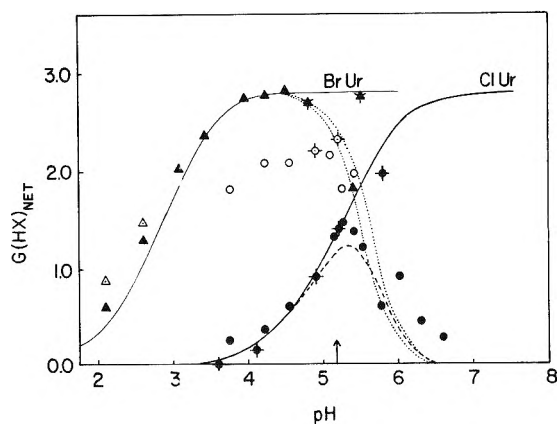


Figure 6. pH dependence for the production of HX as observed in ac conductometric pulse radiolysis experiments: (\blacktriangle , \bullet) initial yields for $10^{-3} M$ solutions of 5-bromouracil and 5-chlorouracil containing $0.5 M$ *tert*-butyl alcohol and (\blacktriangle , \bullet) initial yields for $10^{-4} M$ solutions containing $0.1 M$ *tert*-butyl alcohol. Open symbols represent yields observed at $150 \mu\text{sec}$. The solid curve labeled BrUr represents the competition between the reaction of e_{aq}^- with H^+ and $10^{-3} M$ BrUr. The data at $10^{-4} M$ have been corrected for this competition. The dotted extensions of this curve at $\text{pH} > 4$ represent the reduced yields expected to be observed as a result of buffering by $10^{-3} M$ solute if 10^{-6} and $5 \times 10^{-6} M$ HX are produced by the pulse. The solid curve labeled ClUr represents the dependence of the yield of 5-uracil radical (and HX elimination) expected from the competition between reactions 1b and 10 if the rates are equal at a pH of 5.2. The dashed curve represents the product of this dependence and the effect of the buffer.

For pH values above 5 with solutes at $10^{-3} M$ the conductivity change observed is reduced by partial removal of the H^+ liberated by reaction with the anionic form of the halouracil. At a pH of 5.4 the observed yield of HBr was only 1.8 or 64% of the expected value. Considerations of the ionization equilibrium indicate that at the doses involved a net yield of 65–70% should be observed so that the agreement is excellent. The dotted curves in Figure 6 represent the net yields expected for $10^{-3} M$ solutions if the irradiation doses are such as to produce 1 and $5 \times 10^{-6} M$ HBr.¹⁹ These calculations show that for pH values below 4.5 more than 99% of acid produced in these conductivity experiments should be observed. Experiments on a $10^{-4} M$ solution at a pH of 5.4, where at the dose used the loss from buffering $\sim 4\%$, gave an initial HBr yield of 2.73. At this solute concentration the loss of e^- from reaction with H^+ becomes severe for all pH values < 5 and buffering effects are important at values > 6 . One finds, in fact, that at all concentrations of XUr there is only a narrow pH range over which one can observe the full yield of HX.

The chlorouracil solutions show both an immediate production of HCl, as is illustrated in Figure 5C, and a long-term growth which is seen better in Figure 5D. The initial yields for both 10^{-3} and $10^{-4} M$ solutions (plotted as the solid circles in Figure 6) are very low at pH values near 4 where the bromide exhibits a yield ~ 2.8 . The solid curve given in the figure for chlorouracil is calculated on the assumption that the rates of reactions 1b and 10 are equal at a pH of 5.2. For the $10^{-3} M$ solutions the buffering effect of the chlorouracil takes over for $\text{pH} > 5$ and reduces the net yields observed so that a bell shape curve results. The dashed curve in the figure was obtained by multiplying the solid curve by the fraction of H^+ ions expected to escape the buffering action. At a given solute concentration the magnitude of the observed yield at the maximum

is strongly dependent on the ratio of the rate constants of the competition between reactions 1b and 10 and provides a critical test of this ratio. The observed value of the yield at the maximum (~ 1.4) can be accounted for only if the rates are equal at a pH very near to 5.2.

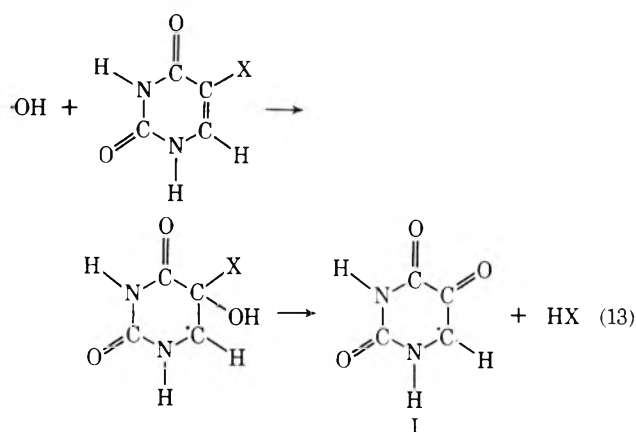
The long-term production of HCl (measured at 150 μsec) gives an upper limit of about 2 indicating that about two-thirds of the neutral radicals produced by protonation (reaction 10) are ultimately reduced in the disproportionation process. This result agrees with the yield of uracil of 1.9 measured in the chromatographic experiments at pH 4. The initial growth period ($\sim 20 \mu\text{sec}$) is about as expected from the overall radical concentration $\sim 10^{-5} M$ if a disproportionation rate constant $\sim 5 \times 10^9 M^{-1} \text{sec}^{-1}$ is assumed. The yield decreases somewhat in the more acidic solutions where e_{aq}^- is converted to H atoms. The radicals produced by H atom addition and by electron addition followed by protonation need not necessarily be the same, as has already been pointed out for the case of uracil by other workers,^{13,14} so that the yield of uracil can be expected to be dependent on pH in the region of 3. The radical produced by hydrogen atom addition (or protonation) at position 6 cannot give uracil directly upon disproportionation. Since the yields of HX and uracil are high at pH 4 protonation of the radical anion must occur to a large extent at position 5 (where uracil and Cl^- will be produced if the radical is reduced in the disproportionation process). In contrast, H atom addition to the parent molecule should be largely unselective and result in the formation of both the 5 and 6 adducts.

Experiments on bromo- and chlorouracil in the presence of 0.1 M *tert*-butyl alcohol were carried out at pH 10.0–10.5 where a decrease in conductivity results from conversion of OH^- to X^- . The conductivity trace observed at $10^{-3} M$ chlorouracil is illustrated by Figure 5E. Correcting for the relative differences in equivalent conductance ($\Delta(\text{OH}^-) - \Delta(\text{Cl}^-)/(\Delta(\text{H}^+) + \Delta(\text{Cl}^-)) = 425/117$) the increment in conductivity observed at 50 μsec corresponds to a net yield of 2.7. Interpretation of the results is complicated because one is sandwiched in between the second and third ionization equilibrium of the halouracils (loss of a proton from the halouracil anion occurs with a $pK \sim 11.4$).¹⁸ We estimate that at $10^{-3} M$ solute the conductivity change should be reduced by $\sim 20\%$ so that a total yield of ~ 3.5 is indicated of which < 0.1 can be ascribed to the reaction of OH radical. This yield is about the sum of both $G(e_{\text{aq}}^-)$ and $G(\text{H})$ so it may be that in basic solution the H atom adduct undergoes a rapid hydrolysis. At this concentration the period for the H atom addition is 3.5 μsec and could account for much of the short-term rise noted in Figure 5E. The experiments at $10^{-4} M$ involve only a minimal loss from buffering ($\sim 4\%$). The OH radical will be completely scavenged by the alcohol and the H atom component cannot contribute at short times. After making the small correction for buffering, initial yields of 2.35 and 2.75 were measured for chloro- and bromouracil. The former is $\sim 10\%$ lower than expected but agrees well with the results of the chemical experiments at this solute concentration. The latter is, if anything, slightly higher than expected. In these basic solutions the conductivity changes observed indicate that the efficiency of reaction 1 is equal to unity within experimental error.

One concludes from these conductivity experiments that attack of e_{aq}^- on bromouracil over the pH range of 3–10 results in immediate ($< 0.1 \mu\text{sec}$) quantitative loss of

Br^- . In the case of chlorouracil, however, the electron adduct is stable sufficiently long ($\sim 5 \mu\text{sec}$) that protonation can compete with Cl^- elimination at all pH values below 7. This protonation appears to be $\sim 50\%$ efficient at a pH ~ 5 , which is somewhat lower than indicated above from the results on uracil production in the presence of Cu^{2+} ion. These conductivity experiments place an upper limit of $\sim 99\%$ for Cl^- elimination from the initial anion radical at a pH of 7. The previous results on fluorouracil indicate that protonation of the anion radical produced by electron attack in that case occurs rapidly and that no large net yield of conducting species results from the initial electron attack.

OH Reactions. The esr experiments of Neta^{3c} have demonstrated quite conclusively that dehydrohalogenation follows addition of OH to the 5 position of the halouracils (reaction 13). The optical pulse radiolysis studies of Pat-



terson and Bansal^{3b} indicate that this process is complete within a few microseconds so that assuming reaction 13 to be the only source of ions on the microsecond time scale it is possible to measure its yield by determining the increase of conductivity in pulse experiments. Previous measurements^{3a} by the dc method indicated that 75, 65, and 55% of the OH radicals attacked the halouracils *via* reaction 13. Because these previous values could have been slightly low as a result of the buffering problems mentioned above we have repeated the measurements by the ac method at pH 3.9 where the starting molecule and product radical are both known to exist as neutral entities.^{3c} Solutions were saturated with N_2O so that only $\sim 1\%$ of the electrons reacted with H^+ ion. With the pulse the conductivities increased discontinuously to a level which was essentially constant out to at least 10 msec. For $10^{-3} M$ solute the yields of HX measured from the increment in conductivity were 4.7, 3.8, and 4.1 respectively for FUr, ClUr, and BrUr. At this concentration $\sim 90\%$ of e_{aq}^- reacts with N_2O and $\sim 10\%$ with the halouracil. On the short-time scale the latter will produce no conducting species in the cases of FUr and ClUr but will contribute a yield of ~ 0.3 in the case of BrUr. Correcting to 100% scavenging of e_{aq}^- by N_2O , the yields for reaction 13 are 4.8, 3.9, and 3.9. A measurement on BrUr at $10^{-4} M$, where 98% of e_{aq}^- are scavenged by N_2O gave a yield of 3.8. From these results it is concluded that 80, 65, and 65% ($\pm 5\%$) of the OH radicals attack FUr, ClUr, and BrUr at the 5 position. The present value for ClUr is identical with the previous one but those for FUr and BrUr are very slightly higher. The qualitative conclusion that the efficiency for production of HX by OH attack on the haloura-

cils is less than 100% is unaffected. From the efficiencies given here and results of the optical pulse radiolysis studies^{3b} the extinction coefficients of radical I are 8100 and 2500 $M^{-1} \text{ cm}^{-1}$ at 330 and 425 nm.

General Conclusions

Both the observations on conductivity changes and the product analysis studies indicate that at pH 7 both 5-bromouracil and 5-chlorouracil are attacked by e_{aq}^- to give 5-uracilyl radical very nearly quantitatively. At lower pH values the 5-chlorouracil radical anion initially formed *via* reaction 1a is rapidly protonated in reaction 10 to give a neutral radical which, upon disproportionation, gives a partial yield of uracil. This radical can, however, be oxidized by the addition of an appropriate electron sink to the irradiation system. The results from the conductivity experiments and from the product analysis studies appear to be in complete agreement except as to the exact value for the relative rates for the protonation and dissociation of the initial anion radical. The yields for halide ion production previously measured^{3a} in neutral solution at somewhat higher solute concentrations than used in the present studies are in reasonable agreement but still somewhat higher than would be estimated from the initial yields given here. It seems clear that trivial secondary processes can complicate the radiolysis mechanism to some extent at solute concentrations much above $10^{-3} M$.

References and Notes

(1) Supported in part by the U. S. Atomic Energy Commission.

- (2) See G. E. Adams and R. L. Willson, *Int. J. Radiat. Biol.*, **22**, 589 (1972), for a recent summary of the earlier work on this subject.
- (3) (a) K. M. Bansal, L. K. Patterson, and R. H. Schuler, *J. Phys. Chem.*, **76**, 2386 (1972); (b) L. K. Patterson and K. M. Bansal, *ibid.*, **76**, 2392 (1972); (c) P. Neta, *ibid.*, **76**, 2399 (1972).
- (4) G. E. Adams, "Current Topics in Radiation Research," Vol. III, M. Ebert and A. Howarc, Ed., Wiley, New York, N. Y., 1967, p 35.
- (5) O. Volkert, B. Bors, and D. Schulte-Frohlinde, *Z. Naturforsch. B*, **22**, 480 (1967).
- (6) J. E. Zimbrick, J. F. Ward, and L. S. Myers, Jr., *Int. J. Radiat. Biol.*, **16**, 505 (1969).
- (7) K. Bhatia, *Anal. Chem.*, **45**, 1344 (1973).
- (8) K. Bhatia and R. H. Schuler, *J. Phys. Chem.*, **77**, 1356 (1973).
- (9) J. Lilie and R. W. Fessenden, *J. Phys. Chem.*, **77**, 674 (1973).
- (10) T. I. Balkas, J. H. Fendler, and R. H. Schuler, *J. Phys. Chem.*, **74**, 4497 (1970).
- (11) M. Anbar, "Fundamental Processes in Radiation Chemistry," P. Ausloos, Ed., Interscience, New York, N. Y., 1968, p 651.
- (12) M. Anbar and P. Neta, *Int. J. Appl. Radiat. Isotopes*, **18**, 433 (1967).
- (13) M. F. Langmuir and E. Hayon, *J. Chem. Phys.*, **51**, 4893 (1969).
- (14) L. M. Theard, F. C. Peterson, and L. S. Myers, Jr., *J. Phys. Chem.*, **75**, 3815 (1971).
- (15) J. Holian and W. M. Garrison, *Nature (London)*, **212**, 394 (1966).
- (16) "Solubilities: Inorganic and Metal Organic Compounds," Vol. 1, A. Seidell and W. F. Lide, Ed., American Chemical Society, Washington, D. C., 1958, p 959.
- (17) "The Pyrimidines," D. J. Brown, Ed., Interscience, New York, N. Y., 1962, p 474.
- (18) G. A. Infante, E. J. Fendler, and J. H. Fendler, private communication.
- (19) Neglecting the water equilibrium, which is unimportant below a pH of 6, the fraction (*f*) of added hydrogen ion which appears as a change in the hydrogen ion concentration is

$$[1 + S10^{-pK}(10^{-pK} + 10^{-pH})^2]^{-1} < f < 1$$

where *S* is the concentration of buffer, 10^{-pK} the buffer equilibrium constant, and 10^{-pH} the initial H^+ ion concentration. The lower limit describes the fractional change expected for adding very small concentrations of H^+ ion. The dotted curves in Figure 6 represent the results of a complete calculation for the addition of 10^{-6} and $5 \times 10^{-6} M$ HX to $10^{-3} M$ BrUr and differ from the lower limit significantly only at pH values above 5.5.

σ - π Polarization Parameters for Oxygen-17 in Organic and Inorganic π Radicals

E. Melamud and Brian L. Silver*

Department of Chemistry, Technion—Israel Institute of Technology, Haifa, Israel (Received January 22, 1973)

Publication costs assisted by National Bureau of Standards

Using spin densities derived from oxygen-17 anisotropic dipolar tensors, it has been shown that oxygen-17 isotropic hyperfine coupling constants in inorganic and organic π radicals obey the simple relationship $a_O = Q_{OC}^O \rho_O$ where $Q_{OO}^O = -41 \pm 3 G$.

Introduction

The simplicity of McConnell's relationship $a_H = Q_{\rho}^H$ has allowed the ready estimation of spin densities on carbon atoms in π radicals from the observed proton isotropic hyperfine splittings. It would obviously be highly desirable if similar simple correlations could be made for the other atoms which commonly occur in π radicals, such as ^{13}C , ^{14}N , and ^{17}O . Symons^{1,2} has considered these nuclei and others and has come to the conclusion that the σ - π polarization constants are roughly transferrable from molecule to molecule. Values are given for these constants based on an analysis of a series of small inorganic radicals. However, the treatment of ^{17}O is based on only two molecules,

with almost identical coupling constants, for which the spin densities were rather uncertain and only the isotropic splittings were known. The analysis suggests that oxygen-17 isotropic coupling constants depend not only on the spin density on the oxygen but also on the spin density of the neighboring atoms. With improvements in instrumentation and increasing availability of oxygen-17 isotope, hyperfine splittings due to ^{17}O have been reported for a wide variety of molecules and enough data are available to form the basis for an attempted correlation between spin densities and isotropic splittings.

It is the object of this communication to show that a simple relationship of the McConnell type holds for ^{17}O iso-

tropic coupling constants, in inorganic and organic π radicals. The three approaches that are commonly used in attempting to establish values for σ-π parameters are (1) theoretical calculations, (2) semiempirical correlations of observed isotropic splitting constants and theoretically estimated spin densities, and (3) the approach used in this paper—the correlation of observed isotropic splittings with spin densities estimated from *anisotropic* dipolar tensors as measured in single crystals. The third approach is by far the most reliable, since it depends essentially only on the value taken for the parameter 2β. For ¹⁷O, this value can be pinned down to a narrow range. The results of the theoretical and semiempirical approaches will be discussed below since their failure or success may be of relevance to future work.

The Basic Data

The data upon which our analysis is based are contained in Table I,³⁻⁷ which summarizes the results of selected single-crystal studies on ¹⁷O-enriched π radicals. Some words of explanation are needed with regard to the numbers appearing in the column headed “ρ₀.” In the framework of the LCAO approximation, spin densities are most accurately described by a spin density matrix. However, when dealing with π radicals a simpler description is satisfactory, in which spin densities are allocated to individual atoms. In this spirit ρ_C for the benzene radical is put at 1/6, and ρ_O for the O₂⁻ ion at 1/2. We make no excuse for using this unsophisticated approach, since it is not only almost universal but is sufficient for almost all purposes. In the case of radicals in which the spin densities cannot be allocated by symmetry considerations alone, the best experimental determination is, as we have said, based on the anisotropic dipolar tensor. Since this tensor depends on ⟨1/r₃⟩ we can usually safely assume that the dominating contribution to the observed dipolar interaction at a given nucleus is the spin localized in orbitals based on that nucleus. Thus the dipolar tensor is taken to be due to the spin density in a single pπ atomic orbital. Densities determined in this way for the radicals in Table I add up to approximately unity when summed over all the atoms in the radical. In the case of the NO group for example,⁸ A_O^{dip} (||) = -50.6 G and A_N^{dip} (||) = 17 G. Taking the 2β values given by Morton, Rowlands, and Whiffen,⁹ (2β(¹⁷O) = -103 G, 2β(¹⁴N) = 34 G) we find spin densities of ρ_O = 0.49 and ρ_N = 0.50 adding up to 0.99.

The electronic structure of ¹⁷O₂⁻ in alkali halide lattices has been studied by Zeller and Känzig.¹⁰ In the analysis of the hyperfine tensor they took into account the orbital-nuclear interaction $\vec{L} \cdot \vec{I}$. The g values in their system were well removed from 2.0023, indicating that the degenerate π orbitals of the free ion are not strongly split by the crystal field, and thus spin-orbit coupling can introduce considerable angular momentum into the ground state. In a study³ of ¹⁷O₂⁻ in γ-irradiated K₂S₂O₈ the g values were very much closer to that of the free electron and it follows that the value of ⟨L⟩ is much less than in alkali halide crystals. The term $\vec{L} \cdot \vec{I}$ can be neglected and the estimation of the hyperfine tensor is comparatively simpler. For this reason we have preferred to take the value of a₀ for O₂⁻ from the study of irradiated K₂S₂O₈.

The value of -103 G used for 2β(¹⁷O) is that given by Morton, Rowlands, and Whiffen, and results in total spin densities close to unity when applied to the results of esr

TABLE I: ¹⁷O Isotropic Coupling Constants and Spin Densities in Selected π Radicals

Radical	-a ₀ , G	ρ ₀	Ref
O ₂ ⁻	20.5	0.500	3
O ₃ ⁻	10.5	0.264	4
	Terminal oxygen		
SO ₂ ⁻	8.96	0.214	5
ClO ₂	12.0	0.270	6
SOO ⁻	12.75	0.314	7
	Terminal oxygen		
TMPO ^a	19.4	0.500	8, 27

^a TMPO = 2,2,6,6-tetramethylpiperidone-1-oxyl.

experiments on small oxyradicals.^{3-8,11-13} We have not used the results for O⁻ in our analysis since Symons^{1,2} has shown that in atoms it is mainly the s orbitals which contribute to spin polarization, in contrast to the situation in molecules where the p orbitals of the π system play the dominant role. Consequently the value of Q_{XX}^X in atoms is very small compared to its value in molecular fragments.

In general the expression for a₀ can be written

$$a_0 = Q_{00}^0 \rho_{00} + \sum_X (Q_{CX}^0 + Q_{XO}^0) \rho_{0X} + \sum_X Q_{XX}^0 \rho_{XX} \quad (1)$$

A simpler expression, which cannot be assumed to hold a priori is

$$a_0 = Q_{00}^0 \rho_0 \quad (2)$$

We attempt to fit the data of Table I to both of these expressions. In using eq 1 we have assumed (a) that Q₀₀⁰ is a constant transferable from molecule to molecule and (b) that values of Q_{XX}^Y are determined mainly by the hybridization on the atom Y. For our analysis we have taken only terminal oxygen atoms and presume that the hybridization varies little from molecule to molecule. If this premise is accepted it implies that both Q₀₀⁰ and Q_{XX}⁰ are transferable constants. We first neglect Q_{XO}⁰ + Q_{OX}⁰ (subsequently referred to as Q_{CROSS}⁰) and carry out a least-squares fitting to eq 1. The results in gauss are Q₀₀⁰ = -39.2 and Q_{XX}⁰ = -1.0. If Q_{CROSS}⁰ is retained but assumed to be a constant the results are Q₀₀⁰ = -30.5, Q_{XX}⁰ = +4.0, and Q_{CROSS}⁰ = -13.5. It is clear that if we use the two-parameter equation for the radicals in Table I, a₀ depends overwhelmingly on ρ₀ and, in fact, the one-parameter eq 2 fits the data excellently, the least-squares fit giving Q₀₀⁰ = -41 ± 3 G.

Although the two- and three-parameter equations provide alternative frameworks for estimating ρ₀ from a₀, for practical purposes the one-parameter equation is preferable and we shall use it below in analyzing ¹⁷O splittings from a variety of radicals. The two-parameter equation shows so little dependence of a₀ on the neighboring atom that there is little point in preferring it to the one-parameter equation. Subsequently the rejection of the three-parameter equation will be justified on both practical and theoretical grounds.

Tests for Validity

If it is true that a₀ can be taken as depending only on the local spin density it follows that for a π radical containing two or more oxygens, the sum of the oxygen isotro-

TABLE II: Isotropic ^{17}O Coupling Constants in Some π Radicals^a

Radical	$-a_0$ (gauss)	$ \Sigma a_0 $ (gauss)	Ref
O_2^-	20.5, 20.5	41.0	3
O_3^-	10.5, 22.2, 10.5	43.2	4
$(\text{CH}_3)_3\text{COO}\cdot$	16.4, 21.8	38.2	14
$\text{C}_6\text{H}_5(\text{CH}_3)_2\text{COO}\cdot$	16.4, 21.8	38.2	14
$\text{ROO}\cdot$	18.0, 23.0	41.0	15
CF_3OOO	3.6, 14.0, 23.3	40.9	16

^a All coupling constants are taken to have the same (negative) sign. Where the signs of ^{17}O couplings have been determined they have invariably been found to be negative.

pic coupling coefficients is proportional to the sum of the spin densities on these atoms. There are six π radicals for which ^{17}O splittings are available and for which the π spin density is effectively entirely concentrated on the oxygen atoms. For these cases $|\Sigma a_0|$ should equal 41 G according to our results. The relevant values of a_0 and Σa_0 are listed in Table II.¹⁴⁻¹⁶ It is evident that the prediction that $|\Sigma a_0| = 41$ G holds true to $\pm 7\%$. The result for O_2^- is not surprising since it was one of the molecules used in the least-squares fit. However, it should be noted that only the terminal oxygens of O_3^- were used in the analysis. Further support can be culled from the data for FOO , for which the measured fluorine anisotropic tensor¹⁷ allows ρ_F to be estimated at 0.07. The remaining spin density on the oxygen atoms is therefore 0.93. The sum of the a_0 's (-14.50 and -22.17)¹⁵ corresponds to a calculated total ρ_0 of $36.67/41 = 0.89$, which is in good agreement with the prediction.

Another relevant example is the radical anion of ^{17}O -enriched pentamethylnitrobenzene, which was studied in solution and in frozen solution.¹⁸ The values of a_0 and $A^0(\parallel)$ are -11.3 and -39 G, respectively. Using $A^0(\parallel)$ and putting $2\beta = -103$ G leads to $\rho_0 = 0.269$, while using a_0 and $Q_{\text{OO}}^0 = -41$ G we obtain $\rho_0 = 0.275$.

A convincing case is that of transbiacetyl,¹⁹ for which the methyl splittings were used to deduce $\rho_C \approx 0.25$. In the closely related glyoxal semidione a_0 was found²⁰ to be -10.5 G, which corresponds to $\rho_0 = 10.5/41 = 0.256$ and thus to $\rho_C = 0.244$. The spin density distribution in semidiones has been discussed by Underwood and Vogel,²¹ who came to two conclusions with respect to the carbonyl group: (1) that the spin densities in all *cis*-semidiones are virtually unchanged and (2) that it is difficult to decide which is more reliable, the values $\rho_0 = 0.4$ and $\rho_C = 0.1$, given by INDO calculations, or $\rho_0 = \rho_C = 0.25$ which is normally assumed. Our results definitely favor the second choice. The splitting of -9.95 G found in a *cis*-semidione²⁰ would indicate that spin distributions are very similar in the carbonyl groups of *cis*- and *trans*-semidiones. Russell and Underwood²⁰ state that these ^{17}O splittings can be explained by putting $Q_{\text{OO}}^0 = -40$ G, $Q_{\text{CC}}^0 = 0$, and assuming that $\rho_C = 0.25$.

A rather different system is the bridged dicobalt complex μ -amido- μ -peroxobis(tetraamminecobalt)tetraniolate for which $|a_0|$ is 22.5 G.²² The g values and the small cobalt hyperfine indicate that the unpaired spin is almost entirely confined to the O-O bridge. Here $|\Sigma a_0| = 45$ G agreeing within 10% of the predicted value of 41 G.

On the basis of the above examples the use of a one-parameter equation to describe isotropic ^{17}O hyperfine

couplings in π radicals seems well justified. We now compare this result with previous work on ^{17}O σ - π parameters.

Comparison with Previous Results

In Table III²³⁻²⁸ are listed the results of previous work on ^{17}O σ - π parameters. It will be noted that previous workers have arrived at conclusions similar to that arrived at in the present work, although none has apparently attracted universal approval. In the absence of an independent method of measuring spin densities the previous results could not be satisfactorily checked against other experimental data. Pride of place chronologically must go to Dimroth, *et al.*,²³ who, on the basis of a careful study of ^1H , ^{13}C , and ^{17}O splittings in two phenoxy radicals, suggested the one-parameter relationship $a_0 = -40 \pm 4\rho_0$. Their suggestion was apparently overlooked because at the time there were almost no ^{17}O data available. The most thorough semiempirical correlation is that on a series of semiquinone radicals.²⁵ The spin densities were calculated by the Hückel or McLachlan methods and fitted to the values of a_0 using both one- and two-parameter equations. For the latter the value of Q_{OO}^0 is close to that found in this work. The value of Q_{CC}^0 depends rather more strongly on the method of calculating spin densities. However, the one-parameter relationship is not statistically much inferior to the two-parameter equation. In fact, if HMO spin densities are used the equation $a_0 = -44.9\rho_0$ holds extremely well. If the present conclusions are accepted then the agreement with the work on semiquinones implies that the HMO spin densities in these molecules are reliable. This in turn suggests that the Hückel parameters used for oxygen form a reasonable set for other calculations. Gulick and Geske's²⁴ results are based on solvent effects on ^{13}C and ^{17}O splittings but the variations in ρ_C and ρ_0 are rather small to provide a basis for reliable statistical analysis.

Of the calculated Q^0 values, those of Broze and Luz²⁵ for the carbonyl group are particularly striking in that Q_{CC}^0 is found to be negligible. The overlap spin density gives a small contribution. It is interesting to compare their results with those of Shastnev, *et al.*,²⁹ for ^{19}F isotropic couplings in π radicals, *viz.*, $Q_{\text{FF}}^{\text{F}} = 264$, $Q_{\text{CC}}^{\text{F}} = 4$, $Q_{\text{cross}}^{\text{F}} = -64$ G. As in Broze and Luz's work the neighboring atom term is completely negligible and the overlap spin density plays a secondary role compared with the dominating effect of the local spin on fluorine. Symon's¹ U values for ^{17}O which correspond to $Q_{\text{OO}}^0 = -68$ G and $Q_{\text{XX}}^0 = 11.6$ G are based on an estimated spin density of 0.4 on the oxygen of Fremy's salt, compared to the probable value of 0.5.^{8,27}

Summing up the present and previous studies, it seems that there is good reason to suppose that in π radicals the spin polarization at the oxygen nucleus is dominated by the local density to such an extent that for practical purposes the effect of the spin on neighboring atoms can be ignored.

Nevertheless, although it is clear that it is far easier to work with the one parameter equation $a_0 = Q_{\text{OO}}^0 \rho_0$, the question arises as to the physical significance of eq 1 and 2 since, although they give effectively the same result for ρ_0 , they imply a very different apportioning of contributions to a_0 . A strong point against the too ready acceptance of the values in the three-parameter equation is that

TABLE III: σ - π Polarization Parameters for Oxygen-17

Molecule or group	Method ^a	Q_{OO}^0 , G	Q_{cross}^0 , G	Q_{XX}^0 , G	Ref
Phenoxy radicals	Semiempirical HMO	-40 ± 4	23
<i>p</i> -Semibenzoquinone	Solvent effects	-40.41	...	-16.69	24
Carbonyl group	Theoretical SCF	-48.70	6.03	0.46	25
Semiquinones and semidiones	Semiempirical HMO one parameter	-44.9	25
	HMO two parameter	-43.0	...	-2.3 (Q_{cc}^0)	
	MSCF one parameter	-45.6 ± 6.0	
	MSCF two parameter	-40.7 ± 5.2	...	-9.5 ± 6.1 (Q_{cc}^0)	
Carbonyl group	Theoretical simple localized orbitals	-59 ± 5	7 ± 4.9	21 ± 3.4	26
Nitroxyl group	Theoretical simple localized orbitals	-46.6	2.5	13.9	27
Nitroxyl group	Semiempirical	-68	...	11.6	1
Carbonyl group	Theoretical SCFCI	-55.6	13.7	16.9	28
Carbonyl group	Semiempirical HMO	-22.0 ± 3	71.8 ± 9.6	75.4 ± 7.6	28
Pentamethyl nitrobenzene	Semiempirical	-49.7	...	2.92	18

^a MSCF = McLachlan Self Consistent Field. SCFCI = Self Consistent Field Configuration Interaction.

the calculated magnitudes of Q_{cross} and Q_{XX}^0 are known to be oversensitive to small changes in the values taken for ρ_O . We believe our spin densities to be reliable, but the uncertainty in their magnitudes ($\pm 5\%$) is certainly enough to allow a wide variation in these Q values.

An extreme example of this kind of sensitivity may be seen in the Q values of Yonezawa, *et al.*,²⁸ which were derived by a semiempirical correlation of calculated ρ_O 's and observed a_O 's. Broze and Luz²⁵ have also found that small changes in calculated spin densities give large changes in the Q values of the three-parameter equation.

We believe that there are good physical reasons for preferring the one-parameter equation. In relatively simple calculations on the carbonyl²⁶ and nitroxyl²⁷ group Q_{OO}^0 was found to depend heavily on the polarization of the lone pair. A calculation²⁵ based on a better wave function indicates that the overwhelming contribution to Q_{OO}^0 in the carbonyl group is from the polarization of the lone-pair electrons. It seems probable that this contribution dominates the spin polarization at the ¹⁷O nucleus in all π radicals containing oxygen, since in all cases the oxygen atoms carry at least one lone pair.

If the important role of the lone pair is accepted, it has a bearing on the solvent dependence of a_O . Solvent induced changes in hyperfine coupling constants are usually assumed to arise solely from changes in spin density distribution, the implication being that the Q matrix is insensitive to solvent. For ¹³C this is probably not a bad approximation but for ¹⁷O it is likely that the energy of the lone pair can be significantly affected by solvent molecules. In nitroxyl radicals, protonation of the oxygen causes a drastic change in a_N indicating formation of a relatively strong σ bond between the proton and the oxygen lone pair.³⁰ Whatever the nature of this bond is, it must certainly affect the energy of the lone pairs and thus directly influence the oxygen Q matrix. In general both σ - π parameters and spin densities will be affected by the environment. For this reason semiempirical estimations of Q matrices on the basis of studies of solvent effect on coupling constants are usually suspect if constant Q values are assumed. The range of variation of the Q 's may be small, but often so is that of the observed couplings.

Unsettled Problems

There are two groups of particular interest to the organic chemist for which further experimental data are needed, namely the carbonyl and peroxide groups. The peroxide group was discussed by Symons, *et al.*,² in terms of the U values derived for ¹⁷O, and it was concluded that the spin is equally distributed over both atoms, a result which was admitted to be improbable. On the other hand, Adamic, *et al.*,¹⁴ used line width variations in the ¹⁷O satellites of peroxy radicals in solution to estimate a ratio of 2:1 in the spin densities of the two oxygens. From the observed isotropic splittings we predict a ratio of about 0.56:0.44 for these spin densities. Preliminary results³¹ of a single crystal study of tetralin peroxide indicate that this prediction is fairly accurate.

There is at least one group of π radicals for which there is reason to doubt whether our results will hold, namely the orthoquinones. These compounds have previously been a source of difficulty in that they fail to fit in with the semiempirical correlations using HMO or MSCF spin densities.²⁵ It has been suggested that the Hückel parameter for orthoquinones has to be chosen differently from those for paraquinones, or that in the case of chloranilic acid there is a direct nonbonding interaction between chlorine and oxygen. An additional complication for chloranilic acid and 2,5-dioxobenzoquinone is the presence of three negative charges on the radical. It seems likely that the Q matrix for these systems is different from that for other π radicals. We are at present attempting to measure the anisotropic ¹⁷O tensors of such molecules in order to determine directly the spin densities on oxygen.

Conclusion

A simple relationship, $a_O = -41\rho_O$, has been established between isotropic ¹⁷O hyperfine coupling constants and $p\pi$ spin densities in organic and inorganic π radicals. The experimental data for a wide variety of radicals can be convincingly rationalized in terms of this equation.

References and Notes

(1) T. F. Hunter and M. C. R. Symons, *J. Chem. Soc. A*, 1770 (1967).

- (2) H. J. Bower, M. C. R. Symons, and D. J. A. Tinling in "Radical Ions," E. T. Kaiser and L. Kevan, Ed., Interscience, New York, N. Y., 1968.
- (3) A. Reuveni, Z. Luz, and B. L. Silver, to be submitted for publication.
- (4) S. Schlick, *J. Chem. Phys.*, **56**, 654 (1972).
- (5) A. Reuveni, Z. Luz, and B. L. Silver, *J. Chem. Phys.*, **53**, 4619 (1970).
- (6) S. Schlick and B. L. Silver, *Mol. Phys.*, in press.
- (7) A. Reuveni, Z. Luz, and B. L. Silver, to be submitted for publication.
- (8) H. Hayat D.Sc. Thesis, Technion—Israel Institute of Technology, 1971.
- (9) J. R. Morton, J. R. Rowlands, and D. H. Whiffen, *Natl. Phys. Lab., Gr. Brit. Circ.*, No. BPR 1.3.
- (10) H. R. Zeller and W. Kanzig, *Helv. Phys. Acta*, **40**, 845 (1967).
- (11) Z. Luz, A. Reuveni, R. W. Holmberg, and B. L. Silver, *J. Chem. Phys.*, **51**, 4017 (1969).
- (12) S. Schlick, B. L. Silver, and Z. Luz, *J. Chem. Phys.*, **54**, 867 (1970).
- (13) S. Schlick, B. L. Silver, and Z. Luz, *J. Chem. Phys.*, **52**, 1232 (1970).
- (14) K. Adamic, K. U. Ingold, and J. R. Morton, *J. Amer. Chem. Soc.*, **92**, 922 (1970).
- (15) R. W. Fessenden and R. H. Schuler, *J. Chem. Phys.*, **44**, 434 (1966).
- (16) R. W. Fessenden, *J. Chem. Phys.*, **48**, 3725 (1968).
- (17) P. H. Kasai and A. D. Kirschenbaum, *J. Amer. Chem. Soc.*, **87**, 3069 (1965).
- (18) W. M. Gulick, Jr., W. E. Geiger, Jr., and D. H. Geske, *J. Amer. Chem. Soc.*, **90**, 4218 (1968).
- (19) G. A. Russell in "Radical Ions," E. T. Kaiser and L. Kevan, Ed., Interscience, New York, N. Y., 1968.
- (20) G. A. Russell and G. R. Underwood, *J. Phys. Chem.*, **72**, 1074 (1968).
- (21) G. R. Underwood and V. L. Vogel, *J. Amer. Chem. Soc.*, **93**, 1058 (1971).
- (22) J. A. Weil and J. K. Kinnaird, *J. Phys. Chem.*, **71**, 3341 (1967).
- (23) K. Dimroth, A. Berndt, F. Bar, A. Schweig, and R. Volland, *Angew. Chem. Int. Ed. Engl.*, **6**, 34 (1967).
- (24) W. M. Gulick, Jr., and D. H. Geske, *J. Amer. Chem. Soc.*, **88**, 4119 (1966).
- (25) M. Broze and Z. Luz, *J. Chem. Phys.*, **51**, 738 (1969), M. Broze, Z. Luz, and B. L. Silver, *ibid.*, **46**, 4891 (1967).
- (26) R. Poupko, B. L. Silver, and M. Rubinstein, *J. Amer. Chem. Soc.*, **92**, 4512 (1970).
- (27) H. Hayat and B. L. Silver, *J. Phys. Chem.*, **77**, 72 (1973).
- (28) T. Yonezawa, T. Kawamura, and H. Kato, *J. Chem. Phys.*, **50**, 3482 (1969).
- (29) P. V. Shastnev, G. M. Zhidomirov, and N. D. Chuvylkin, *J. Struct. Chem.*, **10**, 885 (1969).
- (30) B. M. Hoffman and T. B. Eames, *J. Amer. Chem. Soc.*, **91**, 2669 (1969).
- (31) E. Melamud, S. Schlick, and B. L. Silver, to be submitted for publication.

Secondary and Solvent Deuterium Isotope Effects on Electronic Absorption Spectra of Anilines

J. L. Jensen* and M. P. Gardner

Department of Chemistry, California State University, Long Beach, Long Beach, California 90840

(Received November 27, 1972)

Publication costs assisted by California State University, Long Beach Foundation

The visible-ultraviolet spectra of 13 anilines have been measured in H₂O and D₂O. Spectral shifts of 130 cm⁻¹ for primary anilines and 40 cm⁻¹ for tertiary anilines are attributed to differences in solvation by specific hydrogen bonding at the amino group. Secondary isotope effects arising from exchange of amino hydrogens for deuteriums are shown to be small, 0–40 cm⁻¹. In all cases, only the effects on the primary band (¹La band) are significant. These solvent isotope effects do not seem to be measurably dependent upon electrolyte concentration.

Solvent effects on electronic absorption spectra have been widely utilized since the early systematic investigations by Burawoy.¹ These effects have provided definitive information regarding the nature of electronic transitions and structural features of ground and excited states as well as providing information regarding solute-solvent interactions.^{2,3}

For example, recently the uv spectra of a series of six nitrogen-substituted nitroanilines were determined in 31 solvents, ranging from cyclohexane to trifluoroethanol and water. It was concluded that strong hydrogen bonding by hydroxylic solvents to sp³-hybridized anilines contrasted with the absence of such solute-solvent interaction for sp²-hybridized anilines.⁴

It was our intention to extend the tool of solvent effects on electronic absorption spectra to include solvent isotope effects. To this end the electronic spectra of a variety of anilines were determined in aqueous solvent, "normal"

and deuterated. While spectral shifts are small, as expected, they are significantly measurable. As part of the process of delineating the cause and meaning of the solvent isotope effect on electronic absorption spectra of anilines, nitrogen-deuterated anilines were prepared and their absorption spectrum measured in hydrocarbon solvent. This paper discusses (for the first time) solvent isotope effects and secondary isotope effects of the first kind⁵ on electronic absorption spectra.

Experimental Section

Materials. Deuterium oxide and deuteriosulfuric acid were obtained from Stohler Isotope Chemicals and were used without further purification. Anilines obtained commercially were recrystallized from aqueous methanol or vacuum distilled until a constant melting point/boiling point and quantitative ultraviolet spectrum were obtained. Some anilines were purchased from Aldrich

TABLE I: Medium Effects on λ_{β}^{\max} ^a

Compound	λ_{β}^{\max} (band)	$\lambda_{\beta}(\text{acid}) - \lambda_{\beta}(\text{NaOH})^b$	$\lambda_{\beta}(\text{H acid}) - \lambda_{\beta}(\text{D acid})^c$	[Acid], M
Aniline	230 (¹ La)	-1	+0.5	<i>d</i>
	279 (¹ Lb)	+1	0	<i>d</i>
<i>N</i> -Methylaniline	237 (¹ La)	+0.5	+1.5	<i>d</i>
	283 (¹ Lb)	+0.5	+1.5	<i>d</i>
<i>N,N</i> -Dimethylaniline	243 (¹ La)	+0.5	+0.5	<i>d</i>
	199		0	0.0
	243 (¹ La)		+0.5	0.0
2,6-Diethylaniline	280 (¹ Lb)	0	+0.5	<i>d</i>
3-Nitroaniline	224 (¹ La)	+0.5	+0.5	<i>d</i>
4-Nitroaniline	378 (¹ La)	+1.0	+3.0	0.04
<i>N,N</i> -Dimethyl-4-nitroaniline	422 (¹ La)	0	+1.0	0.1
2-Nitroaniline	412 (¹ La)	+1.0	+3.0	0.6
<i>N,N</i> -Dimethyl-2-nitroaniline	438 (¹ La)	0	0	<i>d</i>
2-Chloro-4-nitroaniline	371 (¹ La)	+2.0	+3.0	2.1
2-Nitro-4-chloraniline	423 (¹ La)	+1.0	+3.0	1.8
2,4-Dichloro-6-nitroaniline	418 (¹ La)	+3.0	+2.0	6.0
	232		0	0.0
	282		0	0.0
	418 (¹ La)	+2.5		0.0
2,6-Dichloro-4-nitroaniline	364 (¹ La)	+3.0	+3.0	6.1
2,4-Dinitroaniline	346 (¹ La)	+2.0	+3.0	8.1
<i>N,N</i> -Dimethyl-2,4,6-trinitroaniline	408 (¹ La)	-24.0	0	10.0

^a Spectra were recorded on a Beckman DK-2A recording spectrophotometer. λ_{β}^{\max} is the wavelength of maximum absorption of a particular aniline. β . Approximate error in λ_{β}^{\max} is ± 0.5 nm if $\lambda_{\beta}^{\max} < 400$ nm and ± 1.0 if $\lambda_{\beta}^{\max} > 400$ nm. Band assignments in parentheses follow the convention used by Jaffe and Orchin.² ¹La is the primary band and ¹Lb is the secondary band. ^b $\lambda_{\beta}(\text{acid})$ is the wavelength of maximum absorbance of a particular aniline, β , in acid solution of molarity given in far right column. $\lambda_{\beta}(\text{NaOH})$ is the wavelength of maximum absorbance of a particular aniline, β , in 0.10 *N* NaOH solution. ^c $\lambda_{\beta}(\text{H acid})$ is the wavelength of maximum absorbance of a particular aniline, β , in protio acid solution of molarity given in far right column. $\lambda_{\beta}(\text{D acid})$ is the wavelength of maximum absorption of a particular aniline, β , in deutero acid solution of equivalent molarity. ^d Buffer solutions, ionic strength adjusted to 0.10 with sodium chloride.

Chemicals as Hammett indicators and were certified analytically pure. These indicators were used without further purification.

Solutions. A methanolic stock solution of each aniline was prepared. Appropriate quantities of these solutions were diluted to achieve aniline concentrations of 10^{-3} – 10^{-5} *M* in 0.1 *N* NaOH, acetic acid–sodium acetate buffers (ionic strength maintained at 0.1 using NaCl), or aqueous sulfuric acid. In all cases the final concentration of methanol in the aqueous solutions was 0.75% w/w or less. The deuterated solutions were prepared from D₂O and NaOH, acetic acid, or deuteriosulfuric acid; however, in all cases the final solutions were at least 99 atom % deuterium.

Method. The solutions were placed in a 1-cm silica cell and the visible and/or ultraviolet spectrum recorded on a Beckman DK-2A recording spectrophotometer. The cell compartment was thermostated at $23 \pm 2^\circ$. After recording the spectrum, the solutions were titrated or the pH was measured (Corning Model 12 research pH meter, expanded scale), as appropriate. Data obtained in this fashion are contained in Table I.

Spectra of *N*-deuterated anilines were obtained in the following way. A small quantity of aniline was dissolved in 3 ml of D₂O. The spectrum of the aniline-*N*-d₂ in D₂O was measured using a Cary 14 recording spectrophotometer. The aniline-*N*-d₂ was then extracted from the D₂O using cyclohexane which had been previously washed with D₂O. After allowing to stand, the layers were separated and the spectrum of the *N*-deuterated aniline in cyclohexane was obtained. For comparison, identical procedures were followed using H₂O rather than D₂O. Spectral shifts caused by changing solvent from H₂O to D₂O (Table III)

were essentially the same as those obtained as reported in the previous paragraph (Table I).

Results

Medium Effects on λ_{β}^{\max} . Absorption spectra of nitroanilines in aqueous acidic media are notoriously medium dependent. For this reason the acid molarity (or buffer conditions) are listed in Table I. At the acidity where a given aniline was studied, it was 99% unprotonated.

Another important consideration is that anilinium ions do not absorb significantly at the wavelengths being investigated. Consequently, the visible–ultraviolet spectrum measured is that exclusively of the substituted aniline.

The second data column in Table I lists changes in λ_{β}^{\max} upon changing pH, the solvents being 0.1 *N* NaOH and the aqueous acid indicated in column 4. This column essentially establishes the suitability of these kinds of anilines as Hammett indicators.⁶ In other words, a small spectral shift listed in column 2 demonstrates that a given aniline is not supersensitive to medium changes. The last compound listed is an exception in that a 24-nm shift on changing solvent from 0.1 *N* NaOH to 10 *M* H₂SO₄ is certainly significant. The cause of this shift has not been established, although it must arise from some interaction in the less acid media, since the spectrum does not change significantly over the region 9–11 *M* H₂SO₄ (except of course that *N* protonation begins to occur as acid molarity is increased much beyond 10).

Data in Table I also demonstrate that the ¹La band is normally the band which is affected most by isotopic solvents. Several bands for several compounds are reported, notably aniline, *N,N*-dimethylaniline, and 2,4-dichloro-6-

TABLE II: Solvent Isotope Effects on ${}^1\text{La}$ Band of Anilines^a

Compound	$\nu_{\beta}(\text{D}_2\text{O}) - \nu_{\beta}(\text{H}_2\text{O}), \text{cm}^{-1}$ ^a	$\text{p}K_a$
Aniline	100	4.6
3-Nitroaniline	100	2.5
4-Nitroaniline	210	1.0
2-Nitroaniline	180	-0.3
2-Chloro-4-nitroaniline	220	-0.9
2-Nitro-4-chloroaniline	170	-1.0
2,4-Dichloro-6-nitroaniline	140	-3.1
2,6-Dichloro-4-nitroaniline	230	-3.2
2,4-Dinitroaniline	250	-4.4
	180 ± 40^b	
<i>N,N</i> -Dimethylaniline	80	5.1
<i>N,N</i> -Dimethyl-2-nitroaniline	0	2.8
<i>N,N</i> -Dimethyl-4-nitroaniline	60	0.7
<i>N,N</i> -Dimethyl-2,4,6-trinitroaniline	0	-6.5
	40 ± 40^b	

^a Calculated from data in Table I, $\nu_{\beta}(\text{D}_2\text{O}) - \nu_{\beta}(\text{H}_2\text{O}) = [10^7/\lambda_{\beta}(\text{D}_2\text{O})] - [10^7/\lambda_{\beta}(\text{H}_2\text{O})] = \text{cm}^{-1}$. ^b Mean value, \pm average deviation.

nitroaniline. This effect, of course, is due to the nature of the electronic transition.^{2,3}

Since wavelength is actually inversely proportional to energy, it is more direct to consider the solvent isotope effect not as a shift in wavelength, $\Delta\lambda$, but as a change in frequency, $\Delta\nu$. Frequency shifts are tabulated in Table II. It is clear that $\Delta\nu$ for tertiary anilines is strikingly different than $\Delta\nu$ for primary anilines. Within these classes, however, $\Delta\nu$ does not appear to vary, within our experimental error. It may be that primary anilines without a nitro group conjugated with the amino group have smaller $\Delta\nu$ values than others with conjugated nitro groups. However, since individual cases are sometimes within experimental error, and since statistical analysis of the data (using standard *T* test, *Q* test, and confidence interval⁷ calculations) does not allow distinctions to be made, discussion of two values (180 cm^{-1} for primary anilines and 40 cm^{-1} for tertiary anilines) will be emphasized.

$\lambda_{\beta}^{\text{max}}$ of ArNH_2 and ArND_2 in Cyclohexane. Agreement between values of $\lambda_{\beta}(\text{H}_2\text{O}) - \lambda_{\beta}(\text{D}_2\text{O})$ and $\lambda_{\beta}(\text{H acid}) - \lambda_{\beta}(\text{D acid})$ in Table I and III demonstrates that the solvent isotope effect is not strongly medium dependent. It is also gratifying to note the absence of "instrument dependence" between comparable data in Tables I and III.

Table III clearly shows two things. (1) Secondary isotope effects on electronic absorption spectra of anilines are primarily reflected in the shift of the ${}^1\text{La}$ band. Actually, because of the small wavelength shift for the 229- and 270-nm bands of 2-nitroaniline in cyclohexane, these reported shifts may not be different from zero. However, the 0.6-nm shift reported for the 378-nm band (${}^1\text{La}$) is certainly outside experimental error. Consequently, although $\nu_{\beta}(\text{D}) - \nu_{\beta}(\text{H})$ is comparable for all three bands, it is only significantly different from zero for the ${}^1\text{La}$ band. (2) Secondary isotope effects on electronic absorption spectra of anilines are much smaller than solvent isotope effects.

Discussion

Solvent Isotope Effects on $\lambda_{\beta}^{\text{max}}$. The data presented in Table I represent the first report of solvent isotope effects on $\lambda_{\beta}^{\text{max}}$ of anilines. The quantity $\lambda_{\beta}(\text{H acid}) - \lambda_{\beta}(\text{D acid})$ will be referred to as $\Delta\lambda$ for convenience. Although

TABLE III: Secondary vs. Solvent Isotope Effects on Electronic Absorption Spectrum of Anilines

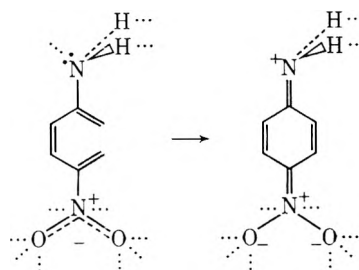
Compound	$\lambda_{\beta}^{\text{max}}$ (band)	Solvent	$\lambda_{\beta}(\text{H}) - \lambda_{\beta}(\text{D}), \text{cm}^a$	$\nu_{\beta}(\text{D}) - \nu_{\beta}(\text{H}), \text{cm}^{-1}$ ^b
Aniline	230 (${}^1\text{La}$)	H_2O or D_2O	0.7	130
	280	H_2O or D_2O	0.6	80
	234 (${}^1\text{La}$)	C_6H_{12}	0	0
	288	C_6H_{12}	0	0
2-Nitro-aniline	282	H_2O or D_2O	0.7	90
	412 (${}^1\text{La}$)	H_2O or D_2O	2.3	140
	229	C_6H_{12}	0.2	40
	270	C_6H_{12}	0.2	30
	378 (${}^1\text{La}$)	C_6H_{12}	0.6	40

^a Difference between $\lambda_{\beta}^{\text{max}}$ of aniline in H_2O and $\lambda_{\beta}^{\text{max}}$ of aniline-*N-d*₂ in D_2O or between $\lambda_{\beta}^{\text{max}}$ of aniline in cyclohexane and $\lambda_{\beta}^{\text{max}}$ of aniline-*N-d*₂ in cyclohexane. A Cary 14 spectrophotometer was used for these determinations. ^b $\nu_{\beta}(\text{D}) - \nu_{\beta}(\text{H}) = [10^7/\lambda_{\beta}(\text{D})] - [10^7/\lambda_{\beta}(\text{H})] = \text{cm}^{-1}$.

$\Delta\lambda$ is small and in several cases within experimental error of zero, the data conclusively demonstrate that there does exist a small but detectable shift to shorter wavelength of $\lambda_{\beta}^{\text{max}}$ in deuterio solvent. The solvent isotope effect, $\Delta\lambda$, is discussed as a function of two major considerations.

(1) *Differential Energy of Solvation of the Aniline.* The electronic transition related to the observed primary band for anilines may be represented as follows (using *p*-nitro-

Scheme I



aniline as an example). The principal sites of solvation are indicated by \cdots . The most important mode of solvation in aqueous acidic media is hydrogen bonding. The Franck-Condon (F-C) excited state represented in Scheme I has the same orientation (conformation) of solute and solvent cage molecules as the ground state. Since the excitation produces increased polarization, the excited state will have a greater solvation energy (i.e., be stabilized more by solvation) than the ground state.^{2,8} Note that the solvent molecules are oriented the same in the F-C excited state as in the ground state, resulting in the loss of only one site of hydrogen bonding (that due to solvent donor hydrogen bonding at the amino nitrogen electron pair). Other solvent cage molecules may be oriented properly to specifically solvate sites of increased polarity in the F-C excited state, but those solvent molecules hydrogen bonding to the ground state are oriented properly for hydrogen bonding to the F-C excited state (with the one exception mentioned above). Of course any solvent property which stabilizes charge separation (e.g., dielectric constant) will result in a more polar excited state having a greater solvation energy than a less polar ground state; however, hydrogen bonding is the stronger and more specific solute-solvent interaction.

Applying the above principles to solvent effects, the primary electronic transition of nitrobenzene should be of much lower energy in water than in the gas phase, which in fact it is by about 12 kcal/mol (a gas phase \rightarrow water bathochromic shift of 26.4 nm).² The primary electronic transition of aniline, however, is a more complex consideration. Formation of the F-C excited state results in a net loss of one hydrogen bond from solvent to the lone electron pair on nitrogen (*i.e.*, the ground state has the greater solvation energy, causing a greater energy of excitation in better hydrogen bonding solvents). In opposition to this effect is the increased polarity of the F-C excited state over the ground state and hydrogen bonding to the hydrogens on the amino nitrogen. The primary electronic transition of aniline occurs at 4 nm shorter wavelength in water than in cyclohexane (a cyclohexane \rightarrow water hypsochromic shift of 4 nm).⁹ In comparison, *N,N*-dimethylaniline has been reported to have a cyclohexane \rightarrow water hypsochromic shift of 7 nm.^{9,10} These hypsochromic shifts show that the primary electronic transitions are of lower energy in cyclohexane than water. Since *N,N*-dimethylaniline has no hydrogens on the amino nitrogen, it is apparent that less of the hydrogen bonding site predominates over the increased polarity factor mentioned above. It is also clear from the 4-nm hypsochromic shift of aniline that loss of the hydrogen bonding site predominates over increased hydrogen bonding to hydrogens on amino nitrogen; however, the latter is a significant factor.

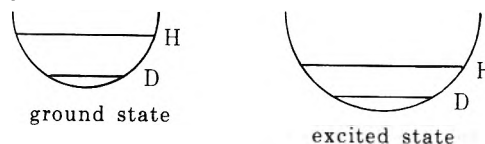
Differences in position of the primary band (¹La) upon changing the solvent from water to deuterium oxide should be much smaller than the solvent effects discussed above, but potentially much more informative. It has been tacitly assumed that water is capable of more effective hydrogen bonding than deuterium oxide.¹¹ The dielectric constants, $\epsilon(25^\circ)$, are 78.54 and 77.94, respectively.¹² Consequently, the primary electronic transition of nitroanilines should be of somewhat lower energy in water than in deuterium oxide ($\lambda_\beta(\text{H}_2\text{O}) > \lambda_\beta(\text{D}_2\text{O})$). Our data collected in Table I demonstrate that this is indeed the case.

In order to compare solvent isotope effects among anilines, it is necessary to refer to the data contained in Table II, $\nu_\beta(\text{D}_2\text{O}) - \nu_\beta(\text{H}_2\text{O})$. This quantity will be referred to as $\Delta\nu$ for the sake of simplicity. The solvent isotope effect, $\Delta\nu$, for the nine primary anilines studied is 180 cm^{-1} and for the four tertiary anilines 40 cm^{-1} (Table II). The cause of this difference is apparent by referring to Scheme I. Water molecules are oriented by weak solvation forces about N-H bonds in anilines. Consequently the F-C excited state may be stabilized by specific hydrogen bonding of the $=\text{N}-\text{H}^+$ hydrogens. Since this stabilization is greater in H_2O than in D_2O , $\nu_\beta(\text{H}_2\text{O}) < \nu_\beta(\text{D}_2\text{O})$, as is observed (Table II). However, in the case of tertiary anilines, such solvation forces are not possible, since there are no N-H bonds. It is to be emphasized that this does *not* imply that solvation at other sites is unimportant (actually the nitro group is probably a primary site of solvation); however, the data do show that the major *difference* in solvation between primary and tertiary anilines is at the NH bonds. Another possibility is that due to a secondary deuterium isotope effect. This is shown to be a minor effect in the following section.

(2) *Secondary Deuterium Isotope Effects of the First Kind.* Exchange of NH hydrogens for deuteriums appears to slightly raise the energy of the electronic transition; *i.e.*, $\nu_\beta(\text{D}) > \nu_\beta(\text{H})$ (Table III). This is a very small energy difference on the order of 0-40 cm^{-1} . This small but de-

tectable difference arises from the change in N-H (or N-D) bond upon excitation (see Scheme I). The force constant for the N-H (or N-D) bond is greater than that for the excited state $=\text{N}-\text{H}^+$ (or $=\text{N}-\text{D}^+$ bond; that is, the nitrogen-hydrogen bond in the ground state is tighter than that in the Franck-Condon excited state. This means that the deuterated ground state lies lower in the ground-state potential energy well (relative to the protio ground state) than the deuterated F-C excited state lies in the F-C excited state potential energy well (relative to the protio excited state) (Scheme II).¹³ Therefore $\Delta E_{\text{D}} > \Delta E_{\text{H}}$, which we observe as $\nu_\beta(\text{D}) > \nu_\beta(\text{H})$. The fact that this is such a small effect in cyclohexane ($\Delta\nu = 0-40 \text{ cm}^{-1}$) requires that the major effect in H_2O vs. D_2O solvents is caused by solvation differences.

Scheme II



Summary

Substitution of D_2O solvent for H_2O results in a solvent isotope effect on the primary electronic absorption band of anilines. The energy of transition in H_2O is less than in D_2O (*i.e.*, $\nu_\beta(\text{H}_2\text{O}) < \nu_\beta(\text{D}_2\text{O})$). This solvent isotope effect is a composite isotope effect, mostly composed of a solvation isotope effect^{13,14} and a smaller but significant contribution due to a secondary isotope effect of the first kind.

The solvation isotope effect arises mainly due to *differences* in solvation between the ground state and the Franck-Condon excited state amino hydrogens. Other solvation forces may contribute some to the solvation isotope effect, but the large difference in $\nu_\beta(\text{D}_2\text{O}) - \nu_\beta(\text{H}_2\text{O})$ between primary and tertiary anilines clearly points to solvation at the amino hydrogens as the main site of solvation which gives rise to differences in H_2O and D_2O solvation energies.

The secondary isotope effect for primary anilines in cyclohexane is small and presumably is small in water also, since such isotope effects are certainly not enhanced severalfold by a change in solvent. Interestingly, the energy of transition is slightly less for ArNH_2 than for ArND_2 . This is attributed to a looser nitrogen-hydrogen bond in the Franck-Condon excited state as compared with the ground state.

References and Notes

- (1) A. Burawoy, *Berichte*, **63** 3155 (1930); *J. Chem. Soc.*, 1177 (1939); 20 (1941).
- (2) H. H. Jaffee and M. Orchin, "Theory and Applications of Ultraviolet Spectroscopy," Wiley, New York, N. Y., 1962.
- (3) C. N. R. Rao, "Ultraviolet and Visible Spectroscopy," 2nd ed. Plenum Press, New York, N. Y., 1967.
- (4) M. J. Kamlet, R. R. Minesinger, E. G. Kayser, M. H. Aldridge, and J. W. Eastes, *J. Org. Chem.*, **36**, 3852 (1971).
- (5) E. Halevi, *Progr. Phys. Org. Chem.*, **1**, 109 (1963).
- (6) M. J. Jorgenson and D. R. Harks, *J. Amer. Chem. Soc.*, **85**, 878 (1963).
- (7) K. Eckschlager, "Errors, Measurement and Results in Chemical Analysis," Van Nostrand-Reinhold, London, 1969.
- (8) N. S. Bayliss and E. G. McRae, *J. Phys. Chem.*, **58**, 1002, 1006 (1954).
- (9) J. L. Jensen, unpublished results, 1972 and Table III.
- (10) H. E. Unguade, *J. Amer. Chem. Soc.*, **75**, 432 (1953).
- (11) C. A. Bunton and V. Shiner, *J. Amer. Chem. Soc.*, **83**, 42, 3207, 3214 (1961).
- (12) R. C. Weast, Ed., "Handbook of Chemistry and Physics," The Chemical Rubber Publishing Co., Cleveland, Ohio, 1969, p E67.

(13) E. K. Thornton and E. R. Thornton in "Isotope Effects in Chemical Reactions," C. J. Collins and N. S. Bowman, Ed., Van Nostrand-

Reinhold, New York, N. Y., 1970, Chapter 4.
(14) J. L. Jensen and M. P. Gadrner, *J. Phys. Chem.*, **77**, 1557 (1973).

Isotopic Exchange Reactions between Thallium(III) in Complex Compounds and $^{204}\text{Tl(I)}$

Al. Cecal* and I. A. Schneider

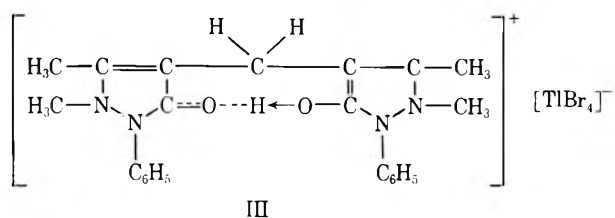
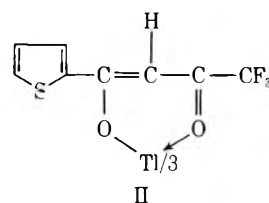
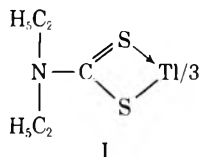
Department of Physical Chemistry, A.I.I. Cuza University, Jassy, Romania (Received July 21, 1972)

This paper presents a study of the interdependence between the kinetic and thermodynamic parameters which describe the isotopic exchange between the complexed Tl(III) and $^{204}\text{Tl(I)}$, on one hand, and the structure and the nature of the chemical bond between the central metal and ligand in the complexes $\text{Tl(III)-}N,N$ -diethyldithiocarbamate, Tl(III)- thenoyltrifluoroacetone, and $[\text{HTlBr}_4]\cdot$ diantipyrylmethane, on the other. From the experimental data, it is noted that the half time of the exchange reaction studied depends on the complexes used and decreases as follows: $\text{Tl(III)-}N,N$ -diethyldithiocarbamate $>$ Tl(III)- thenoyltrifluoroacetone $>$ $[\text{HTlBr}_4]\cdot$ diantipyrylmethane. This fact is due to the different structure and nature of the bonds which are involved between the central metallic ion and the ligand utilized. The pH influence on the exchange rates indicates the possibility of more or less hydrolysis of the given complexes and from the values of the activation entropies it can be concluded that the activated complexes which favor the electronic transfer between those two oxidation states have different probabilities of existence.

Introduction

The isotopic exchange reactions between Tl(III) and $^{204}\text{Tl(I)}$ have been studied previously by many authors using different experimental conditions. Some have researched the effect of the Tl(III) complexing by halide ions,¹⁻³ cyanide ions,⁴ and acetic acid or halide derivatives of acetic acid,^{5,6} from which they concluded that, in all cases, the isotopic exchange rate differed from the simple exchange involving Tl^{3+} and $^{204}\text{Tl}^+$. This fact was explained by the possibility of appearance at different concentrations of the added ligand of some ionic complexed species which have several concentrations and charge. These species will attract or reject the $^{204}\text{Tl}^+$ ions electrostatically, which will favor or hinder the activated complex appearance through which the electronic transfer should take place.

In this paper we have tried to establish the influence of the structure and nature of the bond between metal and ligand in the complex compounds $\text{Tl(III)-}N,N$ -diethyldithiocarbamate (I), Tl(III)- thenoyltrifluoroacetone (II), and $[\text{HTlBr}_4]\cdot$ diantipyrylmethane (III) on some kinetic and thermodynamic parameters which characterize the isotopic exchange between the complexed Tl(III) and $^{204}\text{Tl(I)}$. For this study, we have selected such complexes in which the metal-ligand bond is very different: S-Tl and S \rightarrow Tl in I, O-Tl and O \rightarrow Tl in II, and Tl-Br in III.



Experimental Section

The complex compounds of Tl(III) with N,N -diethyldithiocarbamate, thenoyltrifluoroacetone, and the addition complex between tetrabromothallic acid and diantipyrylmethane were prepared by using methods similar to those reported elsewhere.⁷⁻⁹

In preparing stock solutions, the complexes were dissolved in ethanol and then water was added to give an ethanol-water ratio of 75:25 (vol/vol). $^{204}\text{TlNO}_3$ in solid form was procured from I.F.A., Bucharest. It was dissolved in a 33% HNO_3 solution, to which a TlNO_3 solution was added. The overall concentration of monovalent thallium was determined gravimetrically.¹⁰ The different concentrations of the reactants listed in Table I were prepared from the stock solutions. The desired pH and the constant ionic strength of 0.5 was realized by adding ap-

TABLE I: Kinetic Data of the $^{204}\text{Tl}^+ - (\text{C}_8\text{H}_3\text{O}_2\text{F}_3\text{S})_3\text{TI}$ (A), $^{204}\text{Tl}^+ - (\text{C}_5\text{H}_{10}\text{NS}_2)_3\text{TI}$ (B), and $^{204}\text{Tl}^+ - [\text{HTlBr}_4] \cdot \text{C}_{23}\text{H}_{24}\text{N}_4\text{O}_2$ (C) Isotopic Exchange Systems

[Tl ⁺], mM	[Tl ³⁺], mM	<i>t</i> , °C	pH	<i>t</i> _{1/2} , hr			10 ⁷ <i>R</i> , M hr ⁻¹			<i>k</i> , M ⁻¹ hr ⁻¹		
				A	B	C	A	B	C	A	B	C
0.60	0.60	21.4	3.6	208.8	276.0	146.4	9.95	7.53	14.20	2.76	2.09	3.64
0.90	0.60	21.4	3.6	180.0	232.0	117.6	13.85	10.71	21.20	2.59	1.98	3.62
1.25	0.60	21.4	3.6	156.0	182.4	100.8	17.98	15.37	27.82	2.59	2.05	3.71
1.75	0.60	21.4	3.6	124.8	156.0	79.2	19.76	15.91	31.14	2.57	1.98	3.73
0.60	0.40	21.4	3.6	264.0	297.6	216.0	6.28	5.58	7.69	2.62	2.32	3.49
0.60	0.25	21.4	3.6	290.4	368.4	252.0	4.20	3.30	4.84	2.80	2.20	3.43
0.60	0.15	21.4	3.6	336.0	444.0	314.4	2.47	1.78	2.66	2.75	2.08	3.43
0.60	0.60	30.1	3.6	156.0	192.0	96.0	13.32	10.82	21.65	3.69	3.00	6.01
0.60	0.60	38.7	3.6	94.4	156.0	57.6	22.02	13.32	36.09	6.11	3.69	10.01
0.60	0.60	8.2	3.6	290.4	345.6	208.8	7.15	6.09	9.95	1.98	1.66	2.76
0.60	0.60	21.4	4.2	189.6	254.4	136.8	10.96	8.07	15.19	3.04	2.26	4.21
0.60	0.60	21.4	4.8	163.2	237.6	110.6	12.73	8.85	17.19	3.53	2.42	5.21
0.60	0.60	21.4	5.6	139.2	220.8	98.4	14.93	9.41	20.22	4.14	2.61	5.96

appropriate amounts of 0.2 M CH₃COOH-CH₃COONa buffer and KNO₃ solution.

In order to determine the progress of the exchange reaction, 2-ml samples were taken from each reactant mixture at the different periods of time. The separation of Tl⁺ ions from this mixture was made by using Harbottle and Dodson's method.² The Tl₂CrO₄ precipitate was filtered through a filtering G-4 crucible and water washed. The volume of the filtrate and washings that contained the Tl³⁺ ions only was adjusted to 40 ml. From this solution, 14 ml was taken for activity measurements using a Va-Z-410 immersion counter connected with a VSP-1960 electronic scaler. The exchange equilibrium was assumed when the last two-four measurements gave a constant activity.

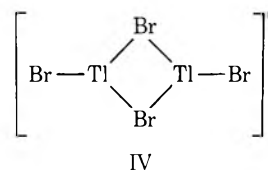
Results and Discussion

The characteristic kinetic parameters of the isotopic exchange reactions in the systems $^{204}\text{Tl}(\text{I})-\text{Tl}(\text{III})-N,N$ -diethyldithiocarbamate, $^{204}\text{Tl}(\text{I})-\text{Tl}(\text{III})$ -thenoyltrifluoroacetone, and $^{204}\text{Tl}(\text{I})-[\text{HTlBr}_4]$ -diantipyrilmethane were established using McKay's equation.¹¹ Initially the variation of $\ln(1 - F)$ vs. time was plotted from which the values of the half-times ($t_{1/2}$) were obtained. These values correspond to the case when $F = 1/2$. Knowing this parameter, the exchange rate and the rate constant were established. The experimental data obtained are presented in Table I.

From Table I, it can be seen that, under the same experimental conditions, the values of the exchange rate, for example, decrease in the following order: $[\text{HTlBr}_4]$ -diantipyrilmethane > Tl(III)-thenoyltrifluoroacetone > Tl(III)- N,N -diethyldithiocarbamate. These experimental observations can be explained through the electronic distributions.

In the case of the $[\text{HTlBr}_4]$ -diantipyrilmethane complex, the positive charge of the H⁺ ion (after its addition to a lone pair of electrons of oxygen) will be uniformly distributed over the entire organic molecule, giving it a weak positive character. For this reason, the attraction between this positively charged molecule and the negative complex ion $[\text{TlBr}_4]^-$ is very weak. This fact favors the electrostatic attraction between the negative ion and $^{204}\text{Tl}^+$, conducive to the appearance of the transition state that facilitates the electronic transfer between these two oxida-

tion states of thallium by means of some bromine bridges (IV).³

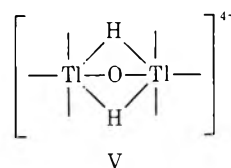


On the other hand, the observed differences between the isotopic exchange rates of the $^{204}\text{Tl}(\text{I})-\text{Tl}(\text{III})$ -thenoyltrifluoroacetone and $^{204}\text{Tl}(\text{I})-\text{Tl}(\text{III})-N,N$ -diethyldithiocarbamate systems can be explained on the basis of the inductive effect.¹²⁻¹⁴

The theophen nucleus and especially the three atoms of fluorine contained in the thenoyltrifluoroacetone molecule have a very strong inductive effect and will attract the oxygen electrons, considerably diminishing the electronic density on both atoms of oxygen. This will result in a reduction in the strength of the Tl-O and O → Tl bonds, facilitating the electronic exchange between $^{204}\text{Tl}^+$ and Tl³⁺.

In the case of the Tl(III)- N,N -diethyldithiocarbamate complex, the C=S and C-S bonds, which have a strong electronegative character, will attract the electrons of the rest of the organic molecule, consequently increasing the stability of the S-Tl and S → Tl bonds. This explains the slower electronic exchange between these two different ions of thallium.

For the last two exchange systems, the electronic transfer is assumed to occur by means of a transition state that contains water bridges between these two reactants. The activated complex (V) is similar to that proposed by Ball and King¹⁵ for the isotopic exchange in the Cr(II)-Cr(III) system.



In addition, the temperature influence on the isotopic exchange reactions in the above-mentioned systems was studied. From the Arrhenius type representations, one could estimate the values of the activation energies and

TABLE II: Values of the Energies and Entropies of Activation and the Preexponential Factors Logarithms of the Exchange Reactions Studied

System	E_a , kcal/mol	Log A	$-\Delta S_a$, cal/degree mol
$^{204}\text{Tl}^+ - (\text{C}_8\text{H}_3\text{O}_2\text{F}_3\text{S})_3\text{Tl}$	12.2	9.4	15.4
$^{204}\text{Tl}^+ - (\text{C}_5\text{H}_{10}\text{NS}_2)_3\text{Tl}$	11.4	8.7	18.4
$^{204}\text{Tl}^+ - [\text{HTlBr}_4] \cdot \text{C}_{23}\text{H}_{24}\text{N}_4\text{O}_2$	18.4	13.3	5.2

the corresponding preexponential factors. Then, the activation entropies were determined for the reactions studied. The results obtained are presented in Table II.

The values of the activation entropies indicate that the transition states (IV and V) postulated above have different probabilities of existence. The most stable state has the highest activation entropy and the most unstable state corresponds to the smallest value of this parameter. The preexponential factors permit a conclusion to be drawn about the existence of an important steric effect for the isotopic exchange between $^{204}\text{Tl}(\text{I})$ and $\text{Tl}(\text{III})$, when the latter is complexed with *N,N*-diethyldithiocarbamate or thenoyltrifluoroacetone, in comparison with the exchange reaction in which $[\text{HTlBr}_4]$ -diantiprylmethane participates. In the first two cases, the attack of Tl^+ ion is less favored than in the latter.

The study of the influence of the pH on the exchange reaction shows that different degrees of hydrolysis can occur for the three complexes used. This causes the appearance of TlOH^{2+} and $\text{Tl}(\text{OH})_2^+$ species. The exchange reactions can take place in two distinct and concurrent ways:¹ the first (k') is not dependent on the concentration of the H^+ ions and the second (k'') is dependent on this parameter. Thus, the exchange rate can be expressed as

$$R = [\text{Tl}^+][\text{Tl}^{3+}](k' + (k''/[\text{H}^+]))$$

A plot of $R/[\text{Tl}^+][\text{Tl}^{3+}]$ ($M^{-1} \text{hr}^{-1}$) vs. pH gives straight lines (Figure 1). From the intercept on the ordinate, the value of k' can be estimated and from its slope, the value of k'' can be obtained. Taking the values of k'' into account, it can be concluded that the hydrolysis of the complexes decreases in the following order: $[\text{HTlBr}_4]$ -diantiprylmethane > $\text{Tl}(\text{III})$ -thenoyltrifluoroacetone > $\text{Tl}(\text{III})$ -*N,N*-diethyldithiocarbamate.

The existence of the TlOH^{2+} ions (especially) favors the appearance of the transition state (VI) which facilitates the electronic transfer by means of the hydroxyl bridges. This activated complex will be concurrent with those presented above and will have a given lifetime.

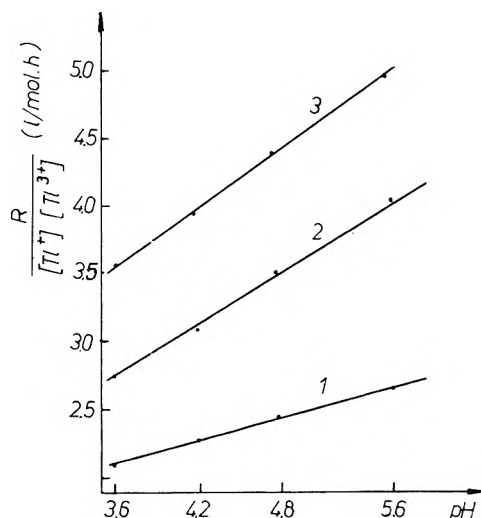
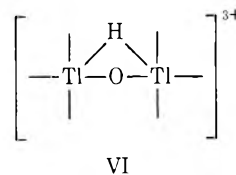


Figure 1. Plot of $R/[\text{Tl}^+][\text{Tl}^{3+}]$ vs. pH for the following exchange systems: (1) $^{204}\text{Tl}^+ - (\text{C}_5\text{H}_{10}\text{NS}_2)_3\text{Tl}$ ($k' = 2.09$ and $k'' = 0.23$); (2) $^{204}\text{Tl}^+ - (\text{C}_8\text{H}_3\text{O}_2\text{F}_3\text{S})_3\text{Tl}$ ($k' = 2.70$ and $k'' = 0.62$); (3) $^{204}\text{Tl}^+ - [\text{HTlBr}_4] \cdot \text{C}_{23}\text{H}_{24}\text{N}_4\text{O}_2$ ($k' = 3.89$ and $k'' = 0.76$). k' and k'' are expressed in $M^{-1} \text{hr}^{-1}$.



References and Notes

- (1) R. J. Prestwood and A. C. Wahl, *J. Amer. Chem. Soc.*, **71**, 3137 (1949).
- (2) G. Harbottle and R. W. Dodson, *J. Amer. Chem. Soc.*, **73**, 2442 (1951).
- (3) L. G. Carpenter, M. H. Ford Smith, R. P. Ball, and R. W. Dodson, *Discuss. Faraday Soc.*, **29**, 92 (1960).
- (4) E. Penna-Franca and R. W. Dodson, *J. Amer. Chem. Soc.*, **77**, 2651 (1955).
- (5) C. H. Brubaker, Jr., and C. Andrade, *J. Amer. Chem. Soc.*, **81**, 5282 (1959).
- (6) R. G. McGregor and D. R. Wiles, *J. Chem. Soc. A*, 323 (1970).
- (7) H. Bode, *Z. Anal. Chem.*, **144**, 165 (1955).
- (8) V. Z. Filip, Thesis, Moscow State University, USSR, 1969.
- (9) A. I. Busev and V. C. Tiptova, *Zh. Anal. Khim.*, **14**, 550 (1959).
- (10) A. I. Busev and V. C. Tiptova, *Zh. Anal. Khim.*, **14**, 28 (1959).
- (11) H. A. Mc Kay, *Nature (London)*, **142**, 997 (1938).
- (12) C. K. Ingold, "Introduction to Structure of Organic Chemistry," G. Ball and Sons Ltd., London, 1960.
- (13) C. K. Ingold, "Structure and Mechanism in Organic Chemistry," Cornell University Press, Ithaca, N. Y., 1953.
- (14) E. H. Rodd, "Chemistry of Carbon Compounds," Elsevier, Amsterdam, 1957.
- (15) D. L. Ball and L. E. King, *J. Amer. Chem. Soc.*, **80**, 1089 (1958).

Hydration and Association Equilibria in Molten Salts Containing Water.

III. The Association of Cadmium Ion with Bromide in the Solvent Calcium Nitrate–Water¹

H. Braunstein, J. Braunstein,* and P. T. Hardesty²

Reactor Chemistry Division, Oak Ridge National Laboratory, Oak Ridge, Tennessee 37830 (Received December 4, 1972)

Publication costs assisted by Oak Ridge National Laboratory

Equilibrium constants for the association of Cd(II) with bromide in $\text{Ca}(\text{NO}_3)_2\text{-H}_2\text{O}$ mixtures containing 2.8 to 10.0 mol of water/mol of $\text{Ca}(\text{NO}_3)_2$ have been determined at 50° by measurement of the emf of concentration cells. The results are interpreted in terms of a mass action model of competitive association and hydration equilibria that treats the hydration in terms of the experimental activity of water in the solvent electrolyte. Hydration equilibrium constants and bond free energies are calculated.

Introduction

An understanding of very concentrated aqueous electrolyte solutions is essential to the development of a complete interpretation of electrolyte solution behavior from the molten salt to the dilute aqueous solution.³ Some aspects of the thermodynamics of concentrated electrolyte solutions have been treated in terms of simple molten salt models.⁴ Fused salt hydrates (hydrate melts), for instance, have been discussed^{5,6} as analogs of fused salts with large weak field cations. Evidence from thermodynamic data,⁷ nmr,⁸ and Raman spectra,^{9,10} however, indicates the need for a more detailed interpretation of these melts in terms of cation–water, cation–anion competition, as had been proposed earlier.¹¹ In the concentration range below 4–6 mol of water/mol of salt, there is insufficient water to form complete hydration sheaths around the ions and the solution behavior, no longer controlled by bulk (hydrogen bonded) water properties, is controlled by molten salt properties. Figure 1 is an example of the effect of concentration on one of the properties of electrolyte–water mixtures, the enthalpy of vaporization of water, as calculated from the temperature dependence of vapor pressures reported in the literature.^{12–18} The values for pure water are indicated on the right-hand ordinate and are seen to vary very little as the water content decreases (or electrolyte concentration increases) until 6–8 mol of water/mol of salt. Here, the enthalpy begins to increase sharply, indicating the region of smooth transition from bulk water properties to the properties of individual water molecules dissolved in and interacting with the ions of the molten salt. Spectral properties of water¹⁹ and association equilibria of ionic solutes are similarly affected by varying water contents. The latter is demonstrated by the plot in Figure 1 of $RT \ln K (= -\Delta G^\circ)$ for the association of Cd^{2+} with Br^- in $\text{Ca}(\text{NO}_3)_2\text{-water}$ mixtures, as evaluated and presented later in this paper.

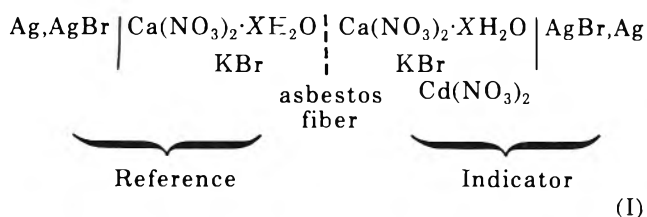
In previous publications in this series^{11,20} association equilibria have been interpreted in terms of competing hydration and association employing a simple quasi-lattice model. The success of this model for $\text{Cd}^{2+}\text{-Br}^-$ equilibria in $(\text{Li},\text{K})\text{NO}_3\text{-H}_2\text{O}$ mixtures¹¹ led to its application to other associating systems, such as Cl^- or Br^- with Ag^+ ,²¹ Cd^{2+} ,²² Pb^{2+} ²² in $\text{NH}_4\text{NO}_3\text{-H}_2\text{O}$ mixtures. The model could not, however, fit measured association equi-

libria in anhydrous calcium nitrate–alkali nitrate melts and in the hydrous melts with 4 and 6 mol of water/mol of $\text{Ca}(\text{NO}_3)_2$.^{23,24} Since the water content of the latter melts is well above the range of validity of the assumptions of the simple quasi-lattice model, the lack of fit is not surprising. As a first step toward developing a model applicable over a wide range of water contents, a mass action model of competing hydration and association was tested²⁴ and appeared promising, but over an insufficient range of water contents to provide a rigid test.

In this paper we present measurements of association equilibria of dilute Cd^{2+} with Br^- in $\text{Ca}(\text{NO}_3)_2\text{-H}_2\text{O}$ mixtures over an extended range of water mole ratios, between 2.8 and 10.0 mol of water/mol of salt. Using known water activities in these solvent melts,⁷ the calculated association constants are interpreted in terms of the mass action model of competitive hydration and association equilibria. The mass action model is applied also to published solute association equilibria in $\text{NH}_4\text{NO}_3\text{-H}_2\text{O}$ ^{21,25} and $(\text{Li},\text{K})\text{NO}_3\text{-H}_2\text{O}$ ²⁰ mixtures and compared to the quasi-lattice model of competing hydration and association equilibria.

Experimental Section

Cell. The emf of the concentration cell



where $X = 2.8, 3.0, 7.5,$ and 10.0 , was measured at several fixed KBr concentrations in the indicator half cell. The activity coefficient of the bromide component is determined from the change in emf on additions of $\text{Cd}(\text{NO}_3)_2$ to the right-hand half cell. The cell,²⁶ which is similar to that used in anhydrous molten salt studies, consisted of a 180-ml Pyrex electrolytic beaker containing melt, indicator electrode, and an asbestos fiber reference half cell; the beaker is clamped in a constant-temperature bath maintained within $\pm 0.1^\circ$. Loss of water from the solution was reduced by covering the cell with a tight-fitting cover,

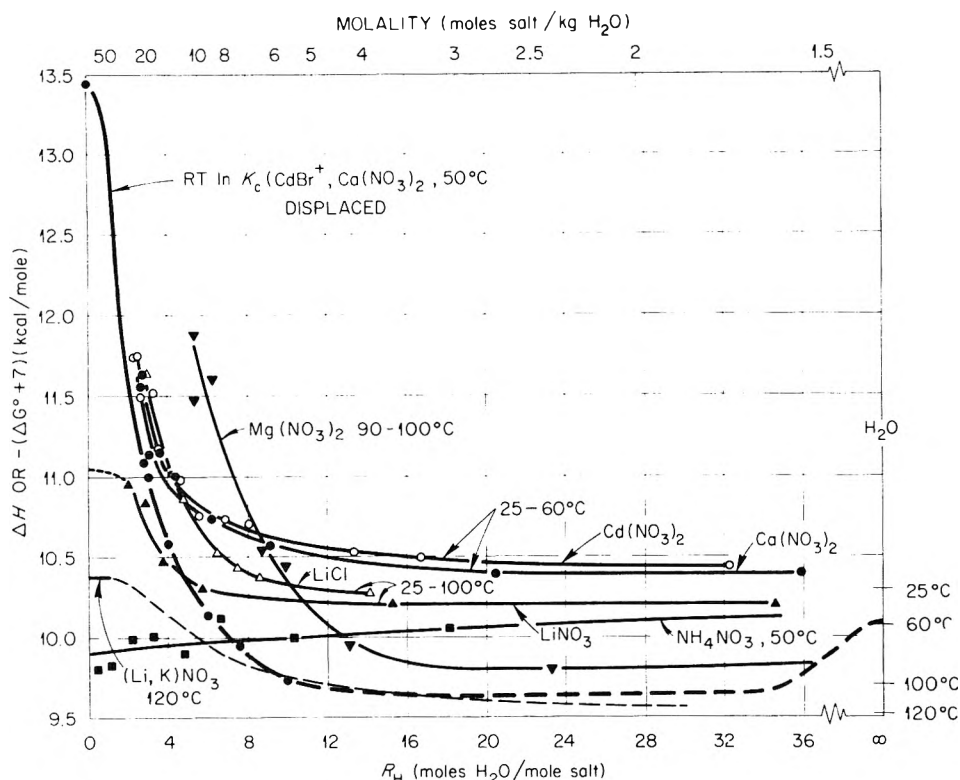


Figure 1. Enthalpy of vaporization of water from electrolyte solutions, ΔH , and free energy of association of dilute ions, $-\Delta G^\circ$, as a function of the water content.

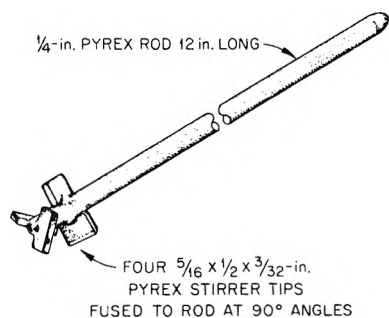


Figure 2. Stirrer for highly viscous melts

formed from Silastic (Dow Corning Corp., Midland, Mich.) with access holes for an indicator electrode, two reference electrodes, a four-blade Pyrex stirrer, and an inlet for addition of KBr and $\text{Cd}(\text{NO}_3)_2$ solutions. The height of the blade portion of the stirrer, shown in Figure 2, is approximately one-half the depth of the melt, and the outer diameter is about one-half the diameter of the beaker. The electrodes were assembled around the stirrer, which stirs the melt downward without vortex formation. The blade configuration and the dimensions relative to the melt dimensions were important for the effective stirring required for rapid equilibration in the very viscous melt containing less than 4.0 mol of water/mol of salt. Emf readings were usually completed in 2-3 hr, insufficient time for significant water loss by condensation on the slightly cooler cover, even at the higher water contents.

Chemicals. Large clear crystals of AR grade Mallinckrodt $\text{Ca}(\text{NO}_3)_2 \cdot 4\text{H}_2\text{O}$ were used without further purification. For water mole ratios less than 4, anhydrous $\text{Ca}(\text{NO}_3)_2$ (obtained by drying the tetrahydrate to the stoichiometric anhydride over P_2O_5 under vacuum at am-

bient temperature for 1 week)¹³ was added to $\text{Ca}(\text{NO}_3)_2 \cdot 4\text{H}_2\text{O}$. For water mole ratios greater than 4, distilled water was added volumetrically with a syringe or pipet. For each run, 0.5 m. of tetrahydrate was weighed directly into the cell, covered, and fused; then either water or anhydride was added before placing in the constant temperature bath.

Mallinckrodt AR grade $\text{Cd}(\text{NO}_3)_2 \cdot 4\text{H}_2\text{O}$ and KBr, the latter dried overnight at 100°, were used to prepare approximately 4 molar aqueous solutions for solute additions.

Electrode Preparation. Outer Tube. The Ag,AgBr reference electrode is made in the same way as for use in anhydrous molten salts.²⁶ A thin glass tip is drawn from the end of a 20-cm length of 6 mm o.d. Pyrex tubing; an asbestos fiber is inserted into the tip and sealed into the compartment, annealing for several minutes in a Meker burner flame. This step is important. Sealing in a gas-oxygen flame may fuse the fiber as well as the glass and has rarely yielded a low resistance, low leakage reference half cell. Choice of fiber thickness is empirical, depending upon the solution viscosity, temperature of measurement, etc., although 0.1 to 0.3-mm diameter usually produces a suitable compartment. Leakage properties of the reference junction are ascertained by submerging the tube with its sealed asbestos fiber to a depth of ca. 4 cm in a $\text{Ca}(\text{NO}_3)_2$ solution at the temperature of the emf measurement. Leakage of solution into the tube to a height of 2 cm or less in 24 hr is considered acceptable (the fiber absorbs solution and swells to prevent additional leakage) although cells with greater leakage have been used by one of the authors (J. B.) with good results.

Centering Tube. The centering tube serves a dual purpose. It prevents the silver wire electrode lead from contacting the glass wall through a film of liquid, which often

leads to spurious emf readings, and it serves as a loose fitting stopper for the reference compartment, preventing loss or gain of water in the reference half cell through contact with the atmosphere. The centering tube (~20 cm long) is prepared from Pyrex capillary tubing chosen to slip snugly into the outer compartment and to accommodate snugly in the capillary the $\sim\frac{1}{16}$ -in. o.d. Teflon tubing used for sheathing the silver wire electrode. The upper end of this tube is flared for support on the rim of the outer tube, and the lower end is heated until the capillary is slightly constricted for a tight fit around the Teflon tubing.

Silver-Silver Bromide Electrode. The end of a 50-cm length of 25 gauge silver wire is formed into a helix 2 mm in diameter and 0.5 to 1.0 cm long, heated to a red glow in a bunsen flame, then rapidly quenched in a calcium nitrate-water solution containing about 10^{-3} mole of bromide per mole of calcium and the same water content as the melt to be studied. Silver bromide is precipitated onto the electrode by addition of silver nitrate crystals to the continuously stirred solution. Best results have been obtained with reference solutions containing a small excess of bromide rather than silver.

The reference half cell is assembled by sheathing the silver wire (above the helix) with $\frac{1}{16}$ -in. o.d. Teflon tubing, threading the tubing into the centering tube so that only the helix is exposed, and placing this assembly into the outer compartment filled to a depth of 2-3 cm with the solution in which the Ag,AgBr electrode was prepared. It is important that the AgBr be completely flocculated before introduction of the solution into the outer tube to prevent precipitation of the halide in the asbestos fiber and a possible loss of conduction through the fiber. Solution is transferred using a syringe and 8 in. long Teflon needle, care being taken to transfer some solid AgBr along with solution to ensure saturation during use of the reference half cell.

When not in use and for 1-3 days before initial use, the reference cells are stored at temperature in a tube containing a $\text{Ca}(\text{NO}_3)_2$ melt of the same water composition as the reference. Electrodes prepared, aged, and stored in this manner have remained stable and conductive for months.

Indicator Electrode. The indicator Ag,AgBr electrode, which is prepared anew for each run, is made up exactly as the reference electrode except that the AgBr may be precipitated in warm aqueous solution rather than in a melt. In preparing an Ag,AgCl indicator electrode,^{23c} however, it was necessary to form colloidal silver chloride in a melt by adding an aqueous solution of AgNO_3 rather than crystals in order to obtain a lightly coated electrode. A heavy deposit of AgCl on the electrode resulted in sluggish, poorly reproducible electrodes. Emf changes for the Cd-Cl association are only about one-third as large as changes for Cd-Br association, requiring higher precision of measurement for equivalent resolution of the association constants. The indicator electrode is carefully washed with distilled water and dried gently with absorbent toweling, care being taken to transfer some of the solid silver halide into the melt with as little solution (containing excess silver or bromide) as possible.

Procedure. Additions of KBr and $\text{Cd}(\text{NO}_3)_2$ solutions were made with a syringe microburet (Micro-metric Instrument Co., Cleveland, Ohio) modified by attaching a 22 gauge flexible Teflon needle (Hamilton Co., Inc., Whittier, Calif.) between the syringe and the "St. Buret Tip"

to facilitate addition of the solutes directly into the cell. The end of the ca. 50 cm long Teflon needle was drawn out by heating gently in a draft of heated air (or a bunsen flame) and wedged tightly into the orifice of the male ground-glass joint cut from a standard glass syringe. The glass joint containing the Teflon needle was wedged tightly into the standard female ground joint of the St. buret tip and the entire ground joint assembly was coated with Silastic to prevent entrance of air during withdrawal of the syringe plunger to fill the syringe with solution. All parts of the assembly are either transparent or translucent to facilitate detection of air bubbles, which usually cease to be a problem after their initial removal. The buret tip is immersed in solution at all times except during an addition, at which time it is washed repeatedly with distilled water and dried, forcing a drop of solution out of the tip at each interval. Just prior to adding solute, a drop is forced to hang from the tip at the elevation at which the addition will be made into the solution in the cell. The hanging drop is wiped from the tip, care being taken not to draw solution from the capillary. The tip is inserted into the melt and solute is added near the rotating stirring rod to ensure that it is drawn into the melt and fully mixed. With very viscous melts, care is needed to ensure that the drop is not encapsulated by frozen melt and removed with the tip, or ejected onto the surface of the melt where the density difference hinders proper mixing. Quantities of solution added varied from 15 to 70 μl per addition, the total quantity of solution added rarely exceeding 250 μl . This quantity of added water has been shown to have negligible effect on the cell emf.^{4,23}

The emf was read to ± 0.01 mV and remained stable within ± 0.05 mV for at least 15 min.

Results

The stoichiometric activity coefficients of bromide (Although bromide is added as KBr rather than CaBr_2 , the trace of K^+ ($<10^{-3}$ ion fraction) has negligible effect and it is the activity of CaBr_2 which determines the emf.) were calculated from ΔE , the cumulative change of emf of cell I on addition of cadmium nitrate to the indicator half cell relative to the emf before adding cadmium nitrate, according to the relation^{24,26}

$$\Delta E = -\frac{RT}{2F} \ln \gamma(\text{CaBr}_2) = -\frac{RT}{F} \ln \gamma(\text{Br}) \quad (1)$$

where the symbol $\gamma(\text{Br}^-)$ represents $\gamma(\text{CaBr}_2)^{1/2}$ or $\gamma(\text{Ca}_{0.5}\text{Br})$. The use of pseudocomponents such as $\text{Ca}_{0.5}\text{Br}$ simplifies the material balance equations for charge unsymmetric solvents and especially for mixtures of salts of different charge type.²⁴ $\gamma(\text{Br})$ is equated with the ratio of free bromide concentration to the stoichiometric bromide concentration, following the conventional assumptions^{24,26,27} that deviations from Henry's law are due only to association and that the species activity coefficients are constant.

$$\gamma(\text{Br}) = \frac{R(\text{Br}^-)}{R(\text{KBr}^-)} = \frac{n(\text{Br}^-)/n(\text{NO}_3^-)}{n(\text{KBr}^-)/n(\text{NO}_3^-)} \quad (2)$$

where the n 's are numbers of moles.

The mole ratios, R , are numerically virtually equal to the Temkin ion fractions

$$R(\text{Br}^-) = \frac{n(\text{Br}^-)}{n(\text{anions})}; \quad R(\text{KBr}^-) = \frac{R(\text{KBr})}{n(\text{anions})} \quad (3)$$

commonly used in anhydrous molten salts.²⁴ The concen-

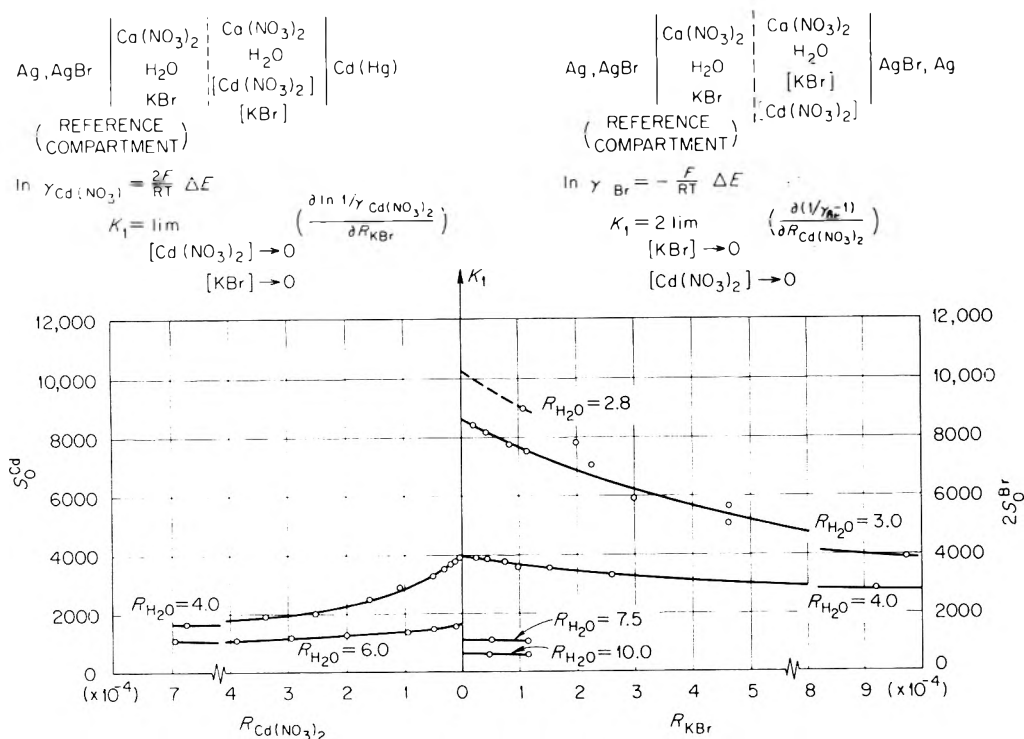


Figure 3. Graphical evaluation of K_1 and K_2 , for CdBr^+ and CdBr_2 , at water mole ratios between 2.8 and 10.0. Data at $R(\text{H}_2\text{O}) = 4$ and 6 are from ref 23.

$$S_0^{\text{Br}} = \lim_{R(\text{Cd}(\text{NO}_3)_2) \rightarrow 0} \left(\frac{\partial (1/\gamma(\text{Br}) - 1)}{\partial R(\text{Cd}(\text{NO}_3)_2)} \right)_{R(\text{KBr})} ; S_0^{\text{Cd}} = \lim_{R(\text{KBr}) \rightarrow 0} \left(\frac{\partial \ln 1/\gamma(\text{Cd}(\text{NO}_3)_2)}{\partial R(\text{KBr})} \right)_{R(\text{Cd}(\text{NO}_3)_2)}$$

trations and activity coefficients are calculated as in a molten salt, considering the water associated with the solvent salt. From the variation of the activity coefficients with the concentrations of cadmium ion and bromide ion, the consecutive association constants are calculated as previously described in detail for mixed valence solvents.²⁴

The evaluation of the association constants is shown in Figure 3, with data from cells with two different kinds of indicator electrode.²³ The plots on the right are for cells with silver-silver bromide electrodes as described above, in which bromide is titrated with cadmium. The results on the left are from previously reported data²³ for cells with cadmium amalgam electrodes, in which cadmium ion was titrated with bromide. Both cells must yield the same association constant, K_1 , obtained by extrapolating the limiting slopes, $2S_0^{\text{Br}}$ and S_0^{Cd} to infinite dilution of the solutes (the central ordinate for both sets of results). For the solvent of composition, 4 mol of water/mol of $\text{Ca}(\text{NO}_3)_2$, both curves do extrapolate to the same point, demonstrating the consistency of the two kinds of electrode. Although the intercept corresponding to K_1 should be the same for both cells, the two sets of plots are not expected to have the same slope since the slope of one is determined largely by the association constant for CdBr_2 , the other by the association constant for Cd_2Br , which are not expected to be equal.

From an analysis of the limiting slopes of the curves obtained in the right-hand cell with a bromide electrode, the association constant for the information of CdBr_2 , K_2 , was calculated according to the previously derived relations²⁴

$$K_1 K_2 = \lim_{R(\text{KBr}) \rightarrow 0} \frac{\partial S_0^{\text{Br}}}{\partial R(\text{KBr})} + \frac{1}{2} K_1^2 \quad (4)$$

where

$$S_0^{\text{Br}} = \lim_{R(\text{Cd}(\text{NO}_3)_2) \rightarrow 0} \left(\frac{\partial \left(\frac{1}{\gamma(\text{Br})} - 1 \right)}{\partial R(\text{Cd}(\text{NO}_3)_2)} \right)_{R(\text{KBr})} \quad (5)$$

and

$$K_1 = \lim_{\substack{R(\text{Cd}(\text{NO}_3)_2) \rightarrow 0 \\ R(\text{KBr}) \rightarrow 0}} 2S_0^{\text{Br}} \quad (6)$$

Values of K_2 are tabulated in Table I along with association constants from previous investigations.²³ The ratios of K_2 to K_1 for the water contents at which sufficient data were taken to obtain precise values of K_2 as well as K_1 are about 0.4, as shown in the last column. This is very close to the ratio observed for consecutive association equilibria in anhydrous molten salts^{28,29} and is the statistically expected value^{30,31} for the case of nearly equal energies of addition of successive ligands. The statistical ratio

$$\left(\frac{K_2}{K_1} \right)_{\text{stat.}} = \frac{\frac{1}{2} Z(Z-1)/Z}{Z} = \frac{Z-1}{2Z} \quad (7)$$

has the values $\frac{4}{10}$ and $\frac{5}{12}$ for assumed values 5 or 6 for Z , the coordination number.

For the water content 2.8 mol of water/mol of salt, the mixture closest to the molten salt, data were obtained as a function of cadmium concentration at only a single low bromide concentration. The value of K_1 was estimated from this one value of the slope

$$2 \lim_{R(\text{Cd}) \rightarrow 0} \frac{\partial (1/\gamma(\text{Br}))}{\partial R(\text{Cd}(\text{NO}_3)_2)} = 2S_0^{\text{Br}} \quad (8)$$

with the assumption that $K_2/K_1 \cong 0.4$, and with the relation obtained by retaining only the first power of $R(\text{Br})$ in the power series expansion of S_0^{Br} ²⁴

$$2S_0^{\text{Br}} = K_1 + K_1(2K_2 - K_1)R(\text{Br}) + \dots \text{ (higher terms)} \quad (9)$$

The resulting approximation valid at low bromide concentrations is

$$K_1 \cong \frac{2S_0^{\text{Br}}}{1 - 2\left[1 - \left(\frac{K_2}{K_1}\right)\right]S_0^{\text{Br}}R_{\text{KBr}}} \quad (10)$$

The uncertainties are estimated as usual²³ to be $\pm 5\%$ in K_1 and $\pm 10\%$ in K_2 . The values in parentheses, obtained from a smaller number of data, have an estimated uncertainty of $\pm 20\%$. The detailed tables of data will appear in the microfilm edition of this journal.³²

Discussion

The association constant of Cd^{2+} with Br^- in $\text{Ca}(\text{NO}_3)_2\text{-H}_2\text{O}$ mixtures varies with water content in much the same way as the enthalpy of vaporization of water, indicating that the dilute solute association equilibria provide a useful probe of water properties in hydrous melts. Making use of known densities³³ of $\text{Ca}(\text{NO}_3)_2\text{-H}_2\text{O}$ mixtures, the molar equilibrium constants, K_c , for the formation of CdBr^+ were calculated using the relation

$$K_c = K_1 \left(\frac{R(\text{H}_2\text{O})M(\text{H}_2\text{O}) + M(\text{Ca}(\text{NO}_3)_2)}{2\rho} \right) \quad (11)$$

where the M 's are molecular weights, ρ is the density in grams per liter, $R(\text{H}_2\text{O})$ is the concentration of water, moles of water per mole of salt, and K_1 is the equilibrium constant expressed in Temkin ion ratios as concentration units (eq 2).²⁴ The association free energy, $RT \ln K_c = -\Delta G^\circ(\text{CdBr}^+)$, is plotted as a function of water content in Figure 1. The molar scale was employed so that the free energy of association in the hydrous melts could be compared with the literature values for the association in pure water as solvent.³⁴

Association constants of Cd^{2+} with Br^- in $\text{Ca}(\text{NO}_3)_2\text{-water}$ mixtures at 4 and 6 mol of water/mol of salt have been used to test^{23,24} the fit of the quasi-lattice hydration model¹¹ without success. This is not unexpected since the water activity at the high water content of the $\text{Ca}(\text{NO}_3)_2\text{-water}$ mixtures does not satisfy the assumption of the model that water obeys Henry's law, behavior generally expected only at vanishing concentrations of water in a molten salt. For $(\text{Li,K})\text{NO}_3\text{-water}$ mixtures, however, the Henry's law region extends fortuitously to 50 mole % water,^{7,18} and this accounts for the excellent fit of the model^{11,20} up to such a high water content in this solvent.

For systems in which water is not in the Henry's law region, consistency clearly requires the incorporation of the actual composition dependence of the water activities^{7,35} into the model. A mass action model of competing hydration and association equilibria was shown earlier²⁴ to account for dependence of association equilibria of Cd^{2+} and Br^- on the water activities in $\text{Ca}(\text{NO}_3)_2\text{-H}_2\text{O}$ mixtures at 4 and 6 mol of water/mol of $\text{Ca}(\text{NO}_3)_2$. The new data presented here permit a more extensive test of the fit of the model, over the range of water contents 2.8–10.0 mol of H_2O /mol of salt.

The assumptions of the competitive hydration-association model are: (1) Ions in a very concentrated aqueous

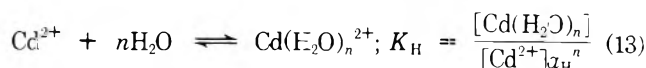
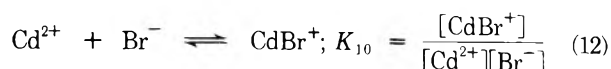
TABLE I: Association Constants in $\text{Ca}(\text{NO}_3)_2\text{-H}_2\text{O}$ at 50° for the Reactions $\text{Cd}^{2+} + \text{Br}^- \rightleftharpoons \text{CdBr}^+$; K_1 and $\text{CdBr}^+ + \text{Br}^- \rightleftharpoons \text{CdBr}_2$; K_2

$R(\text{H}_2\text{O})$, mol of water/ mol of $\text{Ca}(\text{NO}_3)_2$	K_1 mol of anion/ mol	K_2 mol of anion/ mol	K_2/K_1
0.0	7.1×10^5 ^c	—	(0.4)
2.8	10200	—	—
3.0	8600	3720	0.43
4.0	3900 ^b	1500 ^b	0.38
6.0	1550 ^b	—	—
7.5	1030	(306)	(0.3)
10.0	600	(133)	(0.2)

^a By extrapolation. ^b Reference 23.

solution are treated as a molten salt with water associated with the ions. Concentrations are Temkin ion fractions. (2) Anions and water compete to associate with solute cations in accord with their concentrations and relative energies. (3) Dilute "free" and associated species follow Henry's law in solution. (4) One hydrated solute species is dominant in the very concentrated solution range.

Water does not necessarily follow Henry's law over an extended concentration range, and the activity of water is determined by the solvent salt which is present in large excess over the solute salts ($n_{\text{solvent salt}} \cong 10^3 \times n_{\text{solute salt}}$). The last assumption of one dominant hydrated species, in this initial approach to the interpretation, is undoubtedly an over-simplification that cannot be expected to apply over an extended concentration range. The association equilibria and the equation of the model are given below.



$$K_1 = \frac{[\text{CdBr}^+]}{([\text{Cd}^{2+}] + [\text{Cd}(\text{H}_2\text{O})_n^{2+}][\text{Br}^-])} \quad (14)$$

$$\frac{1}{K_1} = \frac{1}{K_{10}} + \frac{K_H}{K_{10}} a_H^n \quad (15)$$

K_{10} and K_1 are the equilibrium constants in the anhydrous and hydrous melts, respectively, at the same temperature, a_H is the known water activity in the solvent melt, and K_H and n , the parameters in the equation, are the hydration equilibrium constant and the number of water molecules associated with the hydration equilibrium. The brackets in eq 12 and 13 refer to concentrations. The solute ions are dilute and are assumed to follow Henry's law when unassociated, an assumption justified by the Nernst behavior of the cadmium amalgam electrode in the presence of dilute cadmium ion,^{4,23} of the silver, silver-bromide electrode in the presence of dilute bromide ion^{23,36} in molten nitrates and in very concentrated aqueous nitrate melts, and by the generally small deviations from ideality in dilute simple binary molten salt mixtures.

In eq 14 the bracketed quantity $[\text{CdBr}^+]$ in the numerator corresponds to the concentration of all mononuclear cadmium species with a single bromide ligand; the sum of bracketed terms in the denominator corresponds to the concentration of all mononuclear cadmium species with

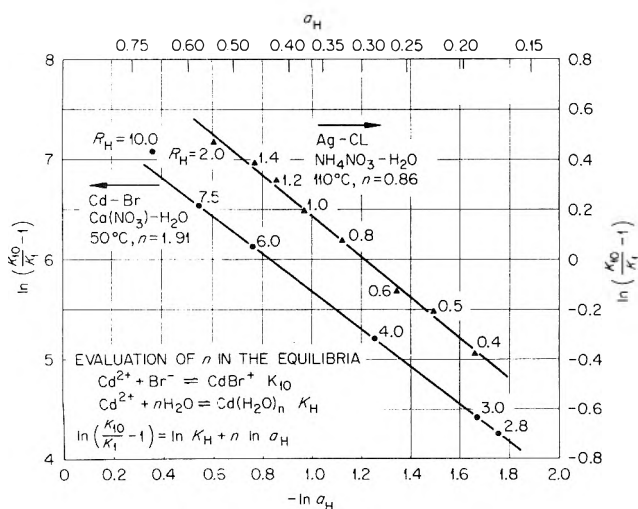


Figure 4. Evaluation of n in the hydration equilibrium of Cd^{2+} in $\text{Ca}(\text{NO}_3)_2\text{-H}_2\text{O}$ and Ag^+ in $\text{NH}_4\text{NO}_3\text{-H}_2\text{O}$. Data in $\text{Ca}(\text{NO}_3)_2$ solutions at $R_H = 4$ and 6 are from ref 23 and data in NH_4NO_3 solutions are from ref 21 and 25.

no bromide ligand; i.e., eq 12 corresponds to the displacement of nitrate ion from the coordination sphere of Cd^{2+} by Br^- ; similarly, eq 13 involves a change in the number of water molecules in the coordination shell of Cd^{2+} . These conventions are analogous to the formulation of the quasi-lattice model^{3,11} in terms of the hydration and association energies, ϵ_H and ϵ_C .

A value of n may be estimated, as seen by rearranging eq 15, from a plot of $\ln[(K_{10}/K_1) - 1]$ vs. $\ln a_H$, such as that in Figure 4. The plots are for the cadmium ion hydration equilibrium in $\text{Ca}(\text{NO}_3)_2\text{-H}_2\text{O}$ at 50° , and for silver ion in $\text{NH}_4\text{NO}_3\text{-H}_2\text{O}$ at 110° as reported by Peleg.^{21,25} The mole ratios of water to solvent salt, given next to the data points, indicate the water concentration corresponding to each water activity and association constant. The slopes of these curves yield a value of n permitting evaluation of the hydration association constant by means of eq 15, as shown in Figure 5. The reciprocal association constant is seen to be linear in the n th power of the water activity over the entire concentration range investigated in $\text{NH}_4\text{NO}_3\text{-H}_2\text{O}$ and $(\text{Li},\text{K})\text{NO}_3\text{-H}_2\text{O}$ mixtures and is linear to 7.5 mol of water/mol of salt in the $\text{Ca}(\text{NO}_3)_2\text{-H}_2\text{O}$ solvent. At a water mole ratio of 10.0 (5.5 ml), however, the model deviates from the data. This is not unexpected considering the simplifications of the model, in particular, the assumption that only one hydrated species is dominant over the entire concentration range. From the slopes of the curves in Figure 5 together with values of the association constant in the anhydrous solvent the hydration equilibrium constants have been calculated and the results summarized in Table II.

The last column in Table II lists the water-metal ion bond free energies calculated from the hydration association constants and the number of water molecules in the hydration equilibria, as given in columns 5 and 6. The $\text{Cd-H}_2\text{O}$ "bond" free energy is -2.5 kcal/mol of H_2O compared to the $\text{Ag-H}_2\text{O}$ "bond" free energy of only 0.9 kcal/mol of H_2O . The stronger $\text{Cd-H}_2\text{O}$ bond compared to $\text{Ag-H}_2\text{O}$ is reasonable in terms of the greater charge density of the cadmium ion and the consequently much stronger interaction of cadmium ion with most ligands (Br^- , Cl^- , CN^- , etc.). An interesting result whose significance remains to be investigated is the low value of n , near 2 for $\text{Cd}(\text{H}_2\text{O})_n^{2+}$ and below 1 for $\text{Ag}(\text{H}_2\text{O})_n^+$

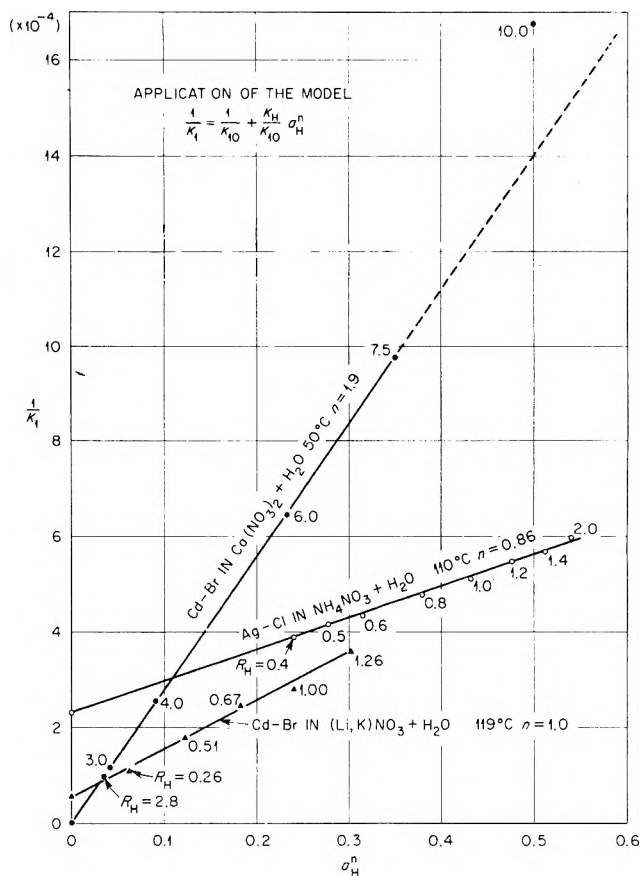


Figure 5. Application of the competitive association and hydration model to equilibria in $\text{Ca}(\text{NO}_3)_2\text{-H}_2\text{O}$, $\text{NH}_4\text{NO}_3\text{-H}_2\text{O}$ and $(\text{Li},\text{K})\text{NO}_3\text{-H}_2\text{O}$ mixtures. Data in $(\text{Li},\text{K})\text{NO}_3$ solutions are from ref 20, data in NH_4NO_3 solutions are from ref 21 and 25, data in anhydrous $\text{Ca}(\text{NO}_3)_2$ are from ref 24 and in $\text{Ca}(\text{NO}_3)_2\text{-4H}_2\text{O}$ and $\text{Ca}(\text{NO}_3)_2\text{-6H}_2\text{O}$ are from ref 23.

suggesting that Cd^{2+} may be coordinated by nitrate ions as well as water even at relatively high water contents in the melt. However, Ca^{2+} is present in large excess over Cd^{2+} , and mass action would favor its retaining water. The equilibrium may be interpreted tentatively in terms of water in two states, i.e., water in a calcium nitrate-water matrix or water adjacent to cadmium ions. The hydration reaction is envisaged as an exchange of two nitrate ions from the coordination sphere of Cd^{2+} with two water molecules from the calcium nitrate water matrix. The n value near 2 also suggests the possibility of cooperative addition of water molecules in the hydration shell. This may not be unexpected, as self-association of dissolved water in organic solvents has been reported.³⁷ The n value below 1 for silver, if it is not an artifact resulting from uncertainties in the slope determination, may suggest the possibility of dinuclear association, $\text{Ag}_2(\text{H}_2\text{O})_2^{2+}$. Although perhaps not likely, here, dinuclear association of Ag^+ with halide ligands has been reported in molten salts.³⁸

In comparing water-ion association energies (or free energies) calculated from the quasi-lattice model with those calculated from the mass action model, it should be noted that the standard states are different. In the simple quasi-lattice model of hydration-association competition, it is implicit that water follows Henry's law in the absence of Cd^{2+} and Br^- and that these solutes are the sole cause of deviations from Henry's law. This is of course not generally the case, as the water activity results show.^{7,35} Thus the quasi-lattice ion-water equilibrium constant

TABLE II: Hydration Equilibrium Constants for the Reaction $M + nH_2O \rightleftharpoons M(H_2O)_n$; K_H

Ion pair	Solvent electrolyte	Temp, °C	Range of water content,		K_H	n	$-RT \ln K_H/n$, kcal/mol of H_2O
			$R_H = \text{mol of water}$	$\text{mol of electrolyte}$			
Cd-Br	Ca(NO ₃) ₂	50	2.8	-7.5	2000	1.9	-2.5
Cd-Br	(Li,K)NO ₃ ^a	119	0.26	-1.26	19	1.0	-2.3
Ag-Cl	NH ₄ NO ₃ ^b	110	0.4	-2.0	2.86	0.86	-0.93

^a Data from ref 20. ^b Data from ref 21 and 25.

$$K_H^{\text{Q.L.}} = Z(e^{-\Delta A_H/RT} - 1) \quad (16)$$

where ΔA_H is the specific Helmholtz free energy for water-ion association and Z is the quasi-lattice coordination number, usually taken as 5 or 6, differs from the mass action equilibrium constant, even when, as for Cd²⁺-Br⁻-H₂O in the solvent (Li,K)NO₃, the value of n in the mass action model turns out to be unity ($n = 1$). The mass action equilibrium constant is defined in terms of the water activity relative to pure liquid water, *i.e.*, a Raoult's law standard state

$$a_{H_2O} = \frac{f}{f^0} \cong \frac{p}{p^0} \quad (17)$$

where f is the fugacity, p is the vapor pressure, and the superscript 0 refers to pure water at the temperature of measurement. The mass action equilibrium constant is given by

$$K_H^{\text{M.A.}} = \frac{[Cd(H_2O)_n]^{2+}}{[Cd^{2+}]a_{H_2O}^n} = e^{-\Delta G_H^0/RT} \quad (18)$$

The equation of the quasi-lattice model¹¹

$$\frac{Z}{K_1} \cong \frac{1}{\alpha} + \frac{\beta}{\alpha} R(H_2O)$$

where $\alpha = \exp(-\Delta A_{10}/RT)$ and $\beta = \exp(-\Delta A_H/RT)$, may be expressed in terms of the equilibrium constants.

$$\frac{Z}{K_1} \cong \frac{1}{\frac{K_{10}}{Z} + 1} + \frac{\frac{K_H^{\text{Q.L.}}}{Z} + 1}{\frac{K_{10}}{Z} + 1} R(H_2O) \quad (19)$$

When $K/Z \gg 1$ this may be written

$$\frac{1}{K_1} \cong \frac{1}{K_{10}} + \frac{K_H^{\text{Q.L.}}/Z}{K_{10}} R(H_2O) \quad (20)$$

Equating the second term on the right-hand side of eq 15 and 20 gives

$$\frac{e^{-\Delta A_H/RT}}{e^{-\Delta G_H^0/RT}} \cong \frac{K_H^{\text{Q.L.}}/Z}{K_H^{\text{M.A.}}} = \frac{a^n(H_2O)}{R(H_2O)} \quad (21)$$

When both $n = 1$ and the water activity is proportional to the water mole ratio, as in (Li,K)NO₃ - R(H₂O), $0 < R < 1$, the free energies differ by the excess free energy of isothermal transfer of water from pure liquid water to water at infinite dilution in the molten salt solvent. $\Delta G_H^0 = \Delta A_H + RT \ln k$ where k is the Henry's law constant

$$k = \left(\frac{a(H_2O)}{R(H_2O)} \right)_{R=0} \quad (22)$$

One point to be noted, however, is that although the model is at this stage empirical, and the physical significance of the parameters remains to be tested, the evaluation of n and K_H does rest on a number of independent

calculations, rather than entirely on a data-fitting procedure. Thus the value of the association constant K_{10} is determined from anhydrous molten salt data and cannot be varied to fit the aqueous data. Similarly, once n has been calculated, it is used to obtain K_H , but is not varied to fit the data with a "more constant" K_H .

Investigations are in progress to further test the range of validity of the mass action model and guide development of physical models such as an extension of the quasi-lattice model beyond the Henry's law region of water. The present model, it may be shown, makes no real distinction between water associated with solute cations or solute anions. While cations are undoubtedly more strongly hydrated than anions, water-negative ion interactions have been shown to be important in the gas phase³⁹ and should not be neglected in a realistic model of concentrated electrolytes. The desirability of a physical model is emphasized by the conceptual difficulty of a model based on entities such as hydrated cations and hydrated anions, since water added initially to an anhydrous molten salt will undoubtedly find itself between a cation and an anion, and interact strongly with both.

Evaluations of hydration and association equilibria for several combinations of cationic and anionic solutes in varying solvent salts are in progress, and should help to elucidate the role of anion-water interactions relative to cation-water interactions. The temperature dependence of the association equilibria also is currently being evaluated, in order to resolve the calculated free energies into entropies and enthalpies of association.

Acknowledgment. We are indebted to Professor John E. Ricci of New York University for valuable discussions and to Richard W. Poole for design and construction of the Pyrex stirrer.

References and Notes

- (1) Research sponsored by the U. S. Atomic Energy Commission under contract with the Union Carbide Corporation.
- (2) ORAU research trainee from Brescia College, Owensboro, Ky.
- (3) J. Braunstein, "Statistical Thermodynamics of Molten Salts and Concentrated Aqueous Electrolytes," in S. Petrucci, "Ionic Interactions," Vol. 1, Academic Press, New York, N. Y., 1971, pp 179-260.
- (4) J. M. C. Hess, J. Braunstein, and H. Braunstein, *J. Inorg. Nucl. Chem.*, **26**, 811 (1964).
- (5) C. A. Angell, *J. Electrochem. Soc.*, **112**, 1224 (1965).
- (6) C. T. Moynihan, *J. Phys. Chem.*, **70**, 3399 (1966).
- (7) H. Braunstein, Ph.D. Thesis, University of Maine, 1971; *Diss. Abstr.*, **32**, 6321-B (1972); University Microfilms Order #72-15,637, P. O. Box 1764, Ann Arbor, Mich. 48106.
- (8) V. S. Ellis and R. E. Hester, *J. Chem. Soc., A*, 607 (1969).
- (9) D. E. Irish and A. R. Davs, *Can. J. Chem.*, **46**, 943 (1968); D. E. Irish, A. R. Davis, and R. A. Plane, *J. Chem. Phys.*, **50**, 2262 (1969); D. E. Irish, D. L. Nelson, and M. H. Brooker, *ibid.*, **54**, 654 (1971).
- (10) M. Peleg, *J. Phys. Chem.*, **76**, 1019 (1972).
- (11) J. Braunstein, *J. Phys. Chem.*, **71**, 3402 (1967).
- (12) A. N. Campbell, J. B. Fishman, J. G. Rutherford, T. O. Schaeffer, and L. Ross, *Can. J. Chem.*, **34**, 151 (1956).
- (13) W. W. Ewing, *J. Amer. Chem. Soc.*, **49**, 1963 (1927).

- (14) W. W. Ewing and W. R. F. Guyer, *J. Amer. Chem. Soc.*, **60**, 2707 (1938).
- (15) H. F. Gibbard, Jr., Ph.D. Thesis, Massachusetts Institute of Technology, Cambridge, Mass., 1966, in Abstracts of Theses 1966-1967, MIT, p 262. The MIT Press, Cambridge, Mass., 1967.
- (16) V. P. Mashovets, N. M. Baron, and G. E. Zavodnaya, *J. Struct. Chem.*, **7**, 825 (1969).
- (17) M. Peleg, *J. Phys. Chem.*, **71**, 4553 (1967).
- (18) T. B. Tripp and J. Braunstein, *J. Phys. Chem.*, **73**, 1984 (1969).
- (19) S. Lindenbaum, private communication.
- (20) P. C. Lammers and J. Braunstein, *J. Phys. Chem.*, **71**, 2026 (1967).
- (21) M. Peleg, *J. Phys. Chem.*, **75**, 3711 (1971).
- (22) R. M. Nikolic and I. J. Gai, *J. Chem. Soc., Dalton Trans.*, 162 (1972).
- (23) (a) J. Braunstein and H. Braunstein, *Inorg. Chem.*, **8**, 1528 (1969); (b) J. Braunstein, A. R. Alvarez-Funes, and H. Braunstein, *J. Phys. Chem.*, **70**, 2734 (1966); (c) J. Braunstein and H. Braunstein, *Chem. Commun.*, 565 (1971).
- (24) J. Braunstein, H. Braunstein, R. E. Hagman, and A. Minano, *Inorg. Chem.*, **12**, 1407 (1973).
- (25) M. Peleg, *J. Phys. Chem.*, **75**, 2060 (1971).
- (26) J. Braunstein, *J. Chem. Educ.*, **44**, 223 (1967).
- (27) J. Braunstein, M. Blander, and R. M. Lindgren, *J. Amer. Chem. Soc.*, **84**, 1529 (1962).
- (28) S. H. White, D. Inman, and B. Jones, *Trans. Faraday Soc.*, **64**, 2841 (1968).
- (29) J. Braunstein and A. S. Minano, *Inorg. Chem.*, **3**, 218 (1964).
- (30) M. Blander, *J. Chem. Phys.*, **34**, 432 (1961).
- (31) N. Bjerrum, *Z. Phys. Chem.*, **106**, 222 (1923).
- (32) Detailed tables of data will appear following these pages in the microfilm edition of this volume of the Journal. Single copies may be obtained from the Journals Department, American Chemical Society, 1155 Sixteenth St., N.W., Washington, D. C. 20036. Remit check or money order for \$3.00 for photocopy or \$2.00 for microfiche, referring to code number JPC-73-1907.
- (33) W. W. Ewing and R. J. Mikovsky, *J. Amer. Chem. Soc.*, **72**, 1390 (1950).
- (34) R. G. Bates, *J. Amer. Chem. Soc.*, **61**, 308 (1939).
- (35) H. Braunstein and J. Braunstein, *J. Chem. Thermodyn.*, **3**, 419 (1971).
- (36) J. Braunstein and R. M. Lindgren, *J. Amer. Chem. Soc.*, **84**, 1534 (1962).
- (37) J. R. Johnson, S. D. Christian, and E. Afsprung, *J. Chem. Soc., A*, 77 (1966).
- (38) A. Alvarez-Funes, J. Braunstein, and M. Blander, *J. Amer. Chem. Soc.*, **84**, 1538 (1962); D. L. Manning, R. C. Bansal, J. Braunstein, and M. Blander, *ibid.*, **84**, 2028 (1962).
- (39) P. Kebarle, M. Arshadi, and J. Scarborough, *J. Chem. Phys.*, **49**, 817 (1968); **50**, 1049 (1969).

Infrared Study of the Interaction between Anhydrous Perchloric Acid and Acetonitrile

Masanori Kinugasa,* Kosaku Kishi, and Shigero Ikeda

Department of Chemistry, Faculty of Science, Osaka University, Toyonaka, Osaka 550, Japan (Received November 2, 1972)

A direct method of mixing anhydrous perchloric acid and organic compounds was established to facilitate the infrared investigation of the acid-base interaction of CH_3CN and HClO_4 . The interaction was interpreted from changes of the frequency of CH_3CN bands and of the symmetry of the ClO_4 group of HClO_4 . HClO_4 interacted with CH_3CN by hydrogen bonding in the initial stage and very slowly transferred its proton to CH_3CN . Also, CH_3COOH or CH_3COCH_3 easily accepted the proton of HClO_4 to give their ionic species in CH_3CN medium.

Introduction

Brønsted acid-base reaction have been investigated extensively by means of spectroscopic, voltametric, and thermodynamic equilibrium measurements. For systems containing perchloric acid in a nonaqueous medium, however, very few spectroscopic data have been reported. Kolthoff, *et al.*,¹ and Chantooni² reported electrochemical data for perchloric acid in acetonitrile solution (containing acetic acid) and suggested that perchloric acid is a typical strong electrolyte in acetonitrile in contrast to other Brønsted acids (H_2SO_4 , HCl , HI , etc.). For the investigation of perchloric acid-nonaqueous solvent interactions, the anhydrous acid has generally been prepared by adding acetic anhydride to 70% aqueous perchloric acid. This procedure, however, introduces acetic acid in the solution. Acetic acid thus present with perchloric acid is very difficult to remove and interferes with ir observations of the solution.

In the present study, anhydrous perchloric acid was prepared by Smith's method³ and was mixed with acetonitrile and other bases at Dry Ice temperature while guard-

ing against possible explosion of the mixture. Acetonitrile, used in this study as a solvent, is aprotic in character, with a high dielectric constant. It has been extensively adopted as a solvent in the investigation of acid-base equilibria in nonaqueous systems.⁴

Experimental Section

Extra-pure reagent acetonitrile from Nakarai Chemicals was purified by Forcier and Olver's method.⁵ Guaranteed reagent acetic acid and carbon tetrachloride were purified by the procedures given in the literature.⁶ Anhydrous perchloric acid was prepared by Smith's method³ in a closed system by means of the apparatus shown in Figure 1. Five milliliters of 70% aqueous perchloric acid and 20 ml of 20% fuming sulfuric acid were introduced successively in vessel A cooled in an ice-water bath. The inlet (1) was then sealed with a hand-torch. When the entire vacuum system was evacuated to 10^{-2} Torr and vessel B was cooled with a Dry Ice-methanol freezing mixture, anhydrous perchloric acid was distilled into it. These vessels, A and B, were cooled with liquid nitrogen and the system

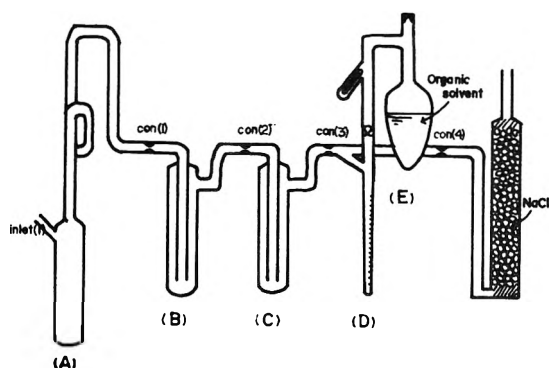


Figure 1. The apparatus for sample preparation.

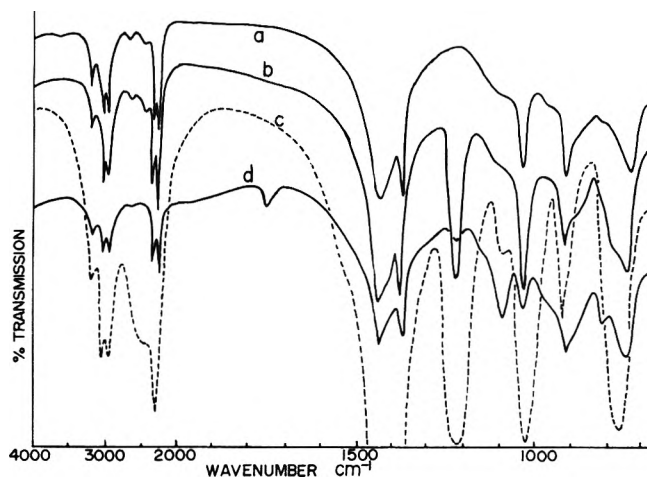


Figure 2. Ir spectra of $\text{CH}_3\text{CN}-\text{HClO}_4$ solution: (a) CH_3CN ; (b) 0.24 M HClO_4 ; (c) 1.0 M HClO_4 ; (d) change of (b) with time (5° , 50 hr).

was sealed at constrictions 1 and 4. The perchloric acid in vessel B was then distilled into vessel C cooled with an ice-salt freezing mixture for further purification. Various amounts of the acid were distilled into graduated ampoules D and sealed at constriction 3.

The compounds which were to react with anhydrous perchloric acid were poured into ampoule E, degassed, and sealed. Ampoule E was cooled with a Dry Ice-methanol freezing mixture and, after breaking the seal of the sample ampoule D, anhydrous perchloric acid was distilled onto the frozen compound in ampoule E. Perchloric acid vapor was transferred to and interacted with the organic compound at Dry Ice temperature. (Anhydrous perchloric acid is a liquid at that temperature, mp -112° .) The reaction mixture was melted and transferred into an ir cell or a conductivity cell.

Infrared spectra were recorded on a JASCO IR-G5 infrared spectrometer. The sample was put into the infrared cell with silicon disk windows in a drybox. The infrared cell was transferred to a sample compartment with KBr windows which was flushed with dry nitrogen throughout the measurement. Conductivity was measured with a Yanagimoto MY5 conductivity meter. The cell used for electrical conductivity measurement had a constant of 2.43.

Results

Figure 2 shows the infrared spectra of the pure CH_3CN (a) and of HClO_4 in CH_3CN (b, 0.24 M; c, 1.0 M). These

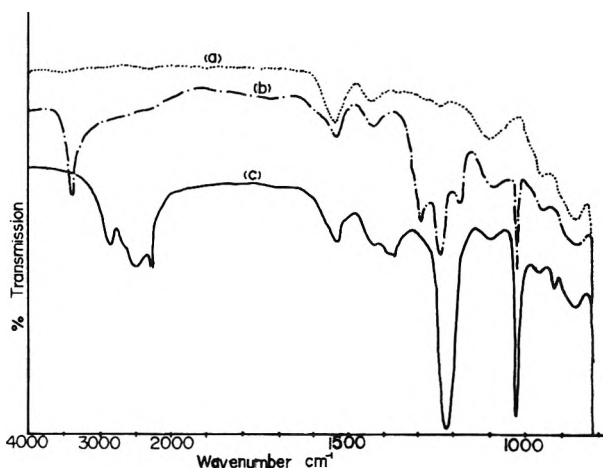


Figure 3. Ir spectra of $\text{HClO}_4-\text{CH}_3\text{CN}-\text{CCl}_4$ solution: (a) CCl_4 ; (b) $\text{HClO}_4-\text{CCl}_4$; (c) $\text{CH}_3\text{CN}-\text{HClO}_4-\text{CCl}_4$; ($\text{CH}_3\text{CN}/\text{HClO}_4 = 1$).

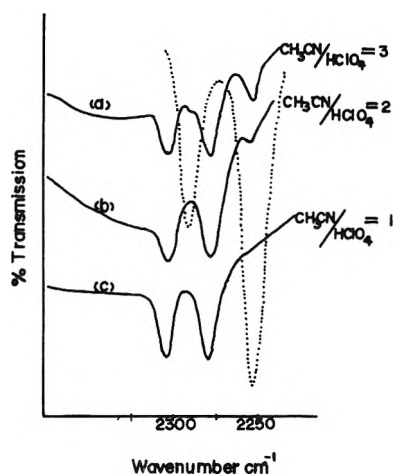


Figure 4. The relation of the $\text{C}\equiv\text{N}$ stretching bands with mole ratio of HClO_4 to CH_3CN in CCl_4 solvent; (---, CH_3CN).

spectra were obtained within 10 min after mixing. In cases b and c, new bands appeared at 2500, 2281, 1225, 1030, and 780 cm^{-1} in addition to the bands of pure CH_3CN . Spectrum b changed into (d) after 50 hr. The above new bands decreased in intensity and other bands appeared at 1750 and 1100 cm^{-1} .

In order to get more detailed information on the interaction of HClO_4 with CH_3CN , an $\text{HClO}_4-\text{CH}_3\text{CN}$ mixture (1:1 mole ratio) was dissolved in CCl_4 . The corresponding spectra are shown in Figure 3. Cases a and b show the spectra of pure CCl_4 , and HClO_4 in CCl_4 , respectively. The HClO_4 in CCl_4 gives bands at 3240, 1305, 1250, 1200, and 1040 cm^{-1} . In the case of the $\text{HClO}_4-\text{CH}_3\text{CN}$ mixture in CCl_4 (c), the bands due to HClO_4 in CCl_4 disappeared and other bands were observed at 2850, 2500, 2281, 1370-1450, 1226, 1033, and 931 cm^{-1} .

In Figure 4, the intensity changes of bands at 2304, 2290, 2281, and 2254 cm^{-1} , are shown as a function of the mole ratio of CH_3CN to HClO_4 in CCl_4 solution. The bands due to free CH_3CN at 2290 and 2254 cm^{-1} were less in intensity in (b) (2:1 mole ratio) than in (a) (3:1) and disappeared in (c) (1:1) (The dotted line is the spectrum of pure CH_3CN .)

Estimates of the relative proton affinities of CH_3CN , CH_3COOH , and CH_3COCH_3 were made from the reaction of the latter two compounds with HClO_4 in CCl_4 . This resulted in the formation of a complex species which precip-

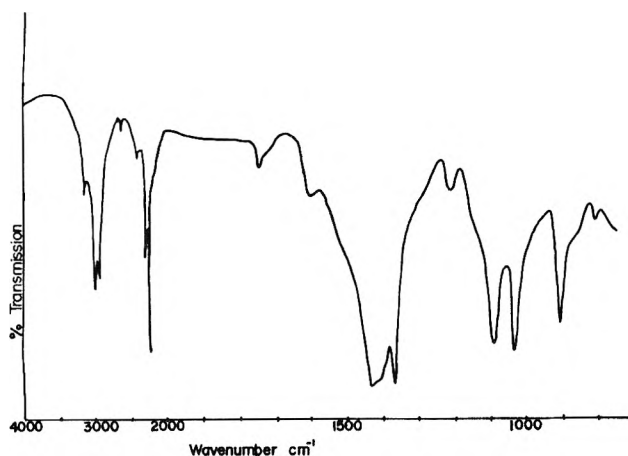


Figure 5. Ir spectra of $\text{CH}_3\text{CN-HClO}_4\text{-CH}_3\text{COOH}$ solution; ($\text{CH}_3\text{COOH}/\text{HClO}_4 = 1$).

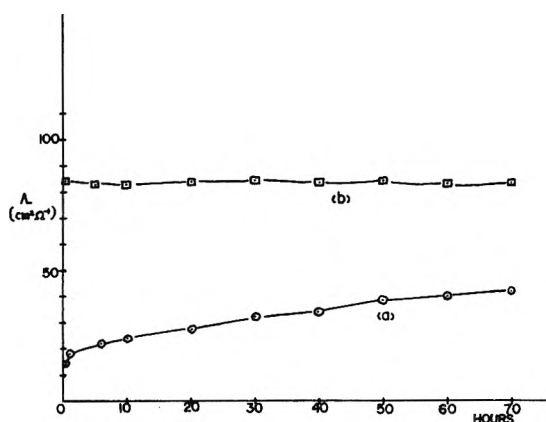


Figure 6. Change in conductivity with time: (a) $\text{CH}_3\text{CN-HClO}_4\text{-CH}_3\text{COOH}$; (b) $\text{CH}_3\text{CN-HClO}_4$ (0.12 M HClO_4).

itated in CCl_4 . In CH_3CN , neither CH_3COOH nor CH_3COCH_3 gave a precipitate with HClO_4 . After addition of CH_3COOH to a $\text{CH}_3\text{CN-HClO}_4$ solution the bands at 2281 and 1225 cm^{-1} were decreased and new bands appeared at 1720, 1600, and 1100 cm^{-1} as shown in Figure 5.

The spectra in Figures 1-5 have been displaced along the ordinate for the sake of clarity. The above spectrometric results are listed in Tables I and II together with the vibrational assignments for the CH_3CN and HClO_4 molecules.

In Figure 6, curve a shows the electrical conductivity of an $\text{HClO}_4\text{-CH}_3\text{CN}$ (0.12 M) solution as a function of time after mixing. The conductivity increased gradually but did not reach a limiting value after 70 hr. When CH_3COOH was added to the $\text{CH}_3\text{CN-HClO}_4$ system the conductivity immediately attained a practically constant value which increased only slightly with time (case b).

Discussion

The frequencies of the specific bands for the $\text{HClO}_4\text{-CH}_3\text{CN}$ system (2281, 1225, 1030, and 930 cm^{-1} , of Figure 2(b) and (c)) are almost the same as those for $\text{HClO}_4\text{-CH}_3\text{CN}$ in CCl_4 (2280, 1226, 1033, and 931 cm^{-1} of Figure 3(c)) as listed in Tables I and II. (Other bands cannot be compared due to strong absorption of solvent, CH_3CN , or CCl_4 .) This indicates that HClO_4 interacts with CH_3CN in the same manner in both solvents (CH_3CN and CCl_4).

In studies of the solvation of salts (cations) with CH_3CN and of the interaction of CH_3CN with Lewis⁸ and

TABLE I: Fundamental Infrared Frequencies and Assignments for CH_3CN in $\text{HClO}_4\text{-CH}_3\text{CN}$ Solutions (cm^{-1})

		$\text{CH}_3\text{CN-HClO}_4$ solution		Complexed CH_3CN in CCl_4
		Free CH_3CN	Complexed CH_3CN	
C-C	ν_4 (a-) ^a	918	930	931
CH_3	ν_3 (a-)	1375		1374
CH_3	ν_6 (e')	1443		
$\text{C}\equiv\text{N}$	ν_2 (a-)	2254	2281	2281
C-H	ν_1 (a-)	2945		2850
C-H	ν_5 (e')	3001		

^a P. Venkateswarlu, *J. Chem. Phys.*, **19**, 293 (1951).

Brønsted⁹ acids, the $\text{C}\equiv\text{N}$ (ν_2) and C-C (ν_4) stretching frequencies of the complexed CH_3CN have been observed at higher frequencies than those of free CH_3CN and the C-H (ν_1) and C-H (ν_5) of the complexed CH_3CN at lower frequencies.⁸ From these data, the bands at 2850, 2281, and 930 cm^{-1} for $\text{CH}_3\text{CN-HClO}_4\text{-CCl}_4$ solutions can reasonably be assigned to C-H, $\text{C}\equiv\text{N}$, and C-C stretching of the complexed CH_3CN with HClO_4 , respectively. (The band at 2290 cm^{-1} is a combination band and shifts to 2304 cm^{-1} in complexed CH_3CN . These bands, however, are not relevant to this discussion.)

The ν_2 $\text{C}\equiv\text{N}$ band of free CH_3CN in the $\text{CH}_3\text{CN-HClO}_4\text{-CCl}_4$ system decreased in intensity with increasing mole ratio of HClO_4 to CH_3CN and disappeared at a mole ratio of 1 as shown in Figure 4. At this ratio, moreover, the bands due to free HClO_4 could not be observed (Figure 3(c)). This suggests that HClO_4 gave a 1:1 complex with CH_3CN and the equilibrium lies almost entirely towards the right



The $\text{CH}_3\text{CN-C}_6\text{H}_5\text{OH}$ complex was reported to dissociate considerably in CCl_4 , showing weaker interaction in this complex.¹⁰

The magnitude of the $\text{C}\equiv\text{N}$ band shift to higher frequencies for $\text{CH}_3\text{CN-Brønsted}$ acid solutions was suggested to increase with increasing O-H distances of the hydroxyl group.⁹ The corresponding shift in CH_3CN complexed with HClO_4 , 27 cm^{-1} , is the largest for the complexes with Brønsted acids investigated so far. (In the complex with H_2SO_4 , the shift is 20 cm^{-1} .) This also indicates that HClO_4 is the strongest Brønsted acid. However, a conclusion cannot be derived from the magnitude of the band shift of the complexed CH_3CN as to whether the complex of CH_3CN with HClO_4 is a hydrogen bonded species ($\text{CH}_3\text{CN}\cdots\text{H-OCIO}_3$) or a proton transfer species (CH_3CNH^+ , ClO_4^-). This will be clarified by the discussion of the bands due to HClO_4 .

Of the fundamental vibrations of the perchlorate ion, ClO_4^- , belonging to the high symmetry point group T_d , only ν_3 and ν_4 are infrared active. When the ClO_4^- ion interacts with a metal cation as a unidentate anion, the symmetry is lowered to C_{3v} .¹¹ The degenerate ν_3 and ν_4 vibrations in T_d , split into ν_1 and ν_4 , and ν_3 and ν_5 , respectively, in C_{3v} and the Raman active ν_1 and ν_2 appear as infrared active bands (ν_2 and ν_6) as illustrated in Table II. For example, in metal complexes such as $\text{Cu}(\text{ClO}_4)_2\cdot 2\text{H}_2\text{O}$ ¹¹ and $\text{Ni}(\text{CH}_3\text{CN})_4(\text{ClO}_4)_2$,¹² strong bands are observed in the regions of 1150, 1020, and 920 cm^{-1}

TABLE II. HClO₄ Infrared Frequencies and Assignments for HClO₄-CH₃CN Systems (cm⁻¹)

ClO ₄ ⁻		Cu(ClO ₄) ₂ ·2H ₂ O ^a	Ni(CH ₃ CN) ₄ ·(ClO ₄) ₂ ^b	HClO ₄ in CH ₃ CN		HClO ₄ -CH ₃ CN in CCl ₄	HClO ₄ in CCl ₄	HClO ₄ (liq) ^c
(Td)	(C _{3v})			0.2 M	1 M			
ν ₁	932 (Raman)	ν ₂ 920	912	780	780			743
ν ₂	430 (Raman)	ν ₆ 480						440
ν ₃	1100	ν ₄ 1158	1135	1225	1225	1226	1305	1315
		ν ₁ 1030	1012	1030	1032	1033	1040	1041
ν ₄	626	ν ₃ 648			580	580	575	581
		ν ₅ 605				520		
		OH stretching ^c			2500	2500	3240	3275
		OH bending					1250	1245
		OH combination					1200	1215

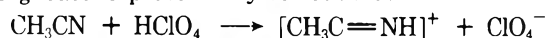
^a Reference 11. ^b Reference 12. ^c Reference 13.

which are similar to the band positions for free ClO₄⁻, but show small splittings in the ν₃ of ClO₄⁻. The spectrum of liquid HClO₄ was measured by Giguere¹³ (see Table II) and the band positions are almost the same as those of HClO₄ in CCl₄. In these systems, the ν₃ of the ClO₄⁻ group shows larger splitting (ν₁ and ν₄ of HClO₄) than those of the metal complexes. In the CH₃CN-HClO₄ complexes, strong bands were observed in the regions of 1225, 1030, and 780 cm⁻¹. The former two bands are assigned to ν₄ and ν₁, respectively, and their band positions lie between those of metal complexes and those of HClO₄-(liq). The 780-cm⁻¹ band can be assigned to ν₂ and the band shift from ν₁ of ClO₄⁻, 152 cm⁻¹, is almost of the same magnitude as that for HClO₄, 189 cm⁻¹, and larger than that of the nickel complexes, 20 cm⁻¹. This indicates that HClO₄ is linked to CH₃CN by hydrogen bonding in CCl₄ or CH₃CN and does not dissociate the OH proton in spite of being the strongest Brønsted acid. (At much higher concentrations of HClO₄, Figure 2(c), the 1100-cm⁻¹ band, indicating the presence of ClO₄⁻, was observed but with much smaller intensity than the 1225-cm⁻¹ band attributable to the hydrogen-bonded species.) This fact is also proved by the band due to the O-H group: the O-H stretching band of HClO₄, at 3240 cm⁻¹, disappeared in the presence of CH₃CN (in CCl₄) simultaneously with the other bands due to the O-H group, 1250 and 1200 cm⁻¹ (Figure 3(c)). The new bands at 2500 cm⁻¹ (very broad) can be assigned as stretching bands of the hydrogen bonded -O-H...N group, since for palmitic acid-pyridine complex in CCl₄, the broad band in the 2500-cm⁻¹ region was assigned to the -O-H...N stretching mode of the hydrogen bonded species.¹⁴

The appearance of the 1100-cm⁻¹ band in HClO₄-CH₃CN solution after 50 hr at 5° indicates the gradual dissociation of HClO₄ (Figure 1(c)) since the strong ν₃ band of the ClO₄⁻ group is observed at the same position. Also the shifted ν₁ band of ClO₄⁻ at 780 cm⁻¹ was found to go out with time² (Figure 2(b) and (d)), indicative of the disappearance of the nonionized HClO₄·CH₃CN species. Furthermore, the band at 1750 cm⁻¹ suggests the formation of a cationic species such as [CH₃C=NH]⁺ whose C=N stretching band is expected to appear in this region by comparing with the band of the imino group (C=N-H, 1640-1690 cm⁻¹).

Klages, *et al.*,¹⁵ isolated acetonitrilium hexachloroantimonate, CH₃C=NH⁺SbCl₆⁻, where the C=N stretching

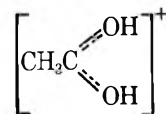
frequency shifted by 76 cm⁻¹ to higher frequency than that of the free acetonitrile, from which the presence of CH₃C=NH⁺ ions was inferred.² Such a high-frequency band of C≡N stretching was not observed during reaction: Figure 1(a)-(c). From the above discussion, the following reaction process may be deduced.



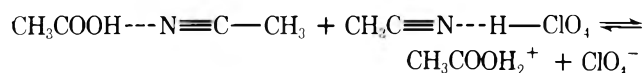
The CH₃C=NH⁺ with C=N triple bond may be unstable in CH₃CN solvent. Similar slow reactions have also been observed for the CH₃CN-HCl and CH₃CN-HBr systems.¹⁶ The resulting formation of the ionic species in the CH₃CN-HClO₄ system well satisfactorily explains the gradual increase in electrical conductivity (Figure 6(a)).

The CH₃CN-HClO₄-CH₃COOH solution, however, shows higher conductivity immediately after preparation of the solution and a much smaller time dependence than the CH₃CN-HClO₄ solution (Figure 6(b)). This experiment indicates that the addition of acetic acid brought about the rapid formation of ionic species.

More detailed information about the ionic species was obtained by ir measurement (Figure 5). The presence of the 1100-cm⁻¹ band, characteristic of ClO₄⁻, indicates the dissociation of HClO₄. The band at 1600 cm⁻¹, obtained in the presence of acetic acid, is at the same position as the C=O stretching band of the



species which was assigned to protonated acetic acid in H₂SO₄ by Nagakura, *et al.*¹⁷ The bands due to free acetic acid and hydrogen-bonded HClO₄ with CH₃CN were also observed at 1720 and 1225 cm⁻¹, respectively. Then, the following equilibrium is expected between the three components



(Chantooni investigated the CH₃COOH-HClO₄-CH₃CN system and suggested the gradual increase of the [CH₃C=NH]⁺ species by aging the system. In the present study the small time dependence of conductivity may be caused by the change from [CH₃COOH₂⁺·N≡CCH₃] to [CH₃C=NH]⁺ + CH₃COOH.)

On addition of acetone instead of acetic acid a new band is obtained at 1600 cm^{-1} which is probably due to $\text{C}=\text{O}-\text{H}^+$ stretching and a similar equilibrium will exist.

According to the charge-transfer mechanism of hydrogen bonding, delocalization energy, ΔE , is written approximately as

$$\Delta E = -\frac{2\beta^2}{I - A}$$

Here I and A are the ionization potential of the occupied orbital of the proton acceptor and the electron affinity of the vacant orbital of, for example, the O-H bond, respectively. β is the resonance integral between the two orbitals. Thus, the smaller I and the larger A and β , the larger is the stabilization energy ΔE .¹⁸ The ionization potential of the lone-pair electrons of CH_3CN (13.14 eV) is larger than those of CH_3COOH (10.70) and CH_3COCH_3 (8.71).¹⁹ Moreover, the lone-pair orbital on the nitrogen of CH_3CN may be represented by an sp hybrid and that on the oxygen of CH_3COOH or CH_3COCH_3 by an sp². A smaller β is expected for the former orbital than for the latter one. Then, CH_3COOH and CH_3COCH_3 will interact with HClO_4 more strongly than does CH_3CN .

Acetic acid has been estimated to have a smaller basicity ($\text{p}K_{\text{H}_2\text{O}} = -6.2$) than acetonitrile (-4.4)⁴ and is thought to interact negligibly with HClO_4 and not to change the equilibrium between HClO_4 and CH_3CN . Koltzoff, *et al.*, concluded that HClO_4 is a typical strong electrolyte in CH_3CN . However, as given by the present results, CH_3CN forms relatively stable hydrogen-bonded

species with perchloric acid and requires high activation energy to form the ionic species. The coexistence of acetic acid, on the contrary, facilitates the dissociation of perchloric acid extensively. Therefore, the protonated acetic acid observed in this study may contribute to the conductivity and reduction potential of $\text{CH}_3\text{CN}-\text{HClO}_4$ solutions measured by other workers.^{1,2}

References and Notes

- (1) J. F. Coetzee and I. M. Kolthoff, *J. Amer. Chem. Soc.*, **79**, 6110 (1957).
- (2) M. K. Chantooni, Ph.D. Thesis, University of Minnesota, 1960.
- (3) G. F. Smith, *J. Amer. Chem. Soc.*, **75**, 184 (1953).
- (4) G. Charlot and B. Tremillon, "Chemical Reactions in Solvents and Melts," Pergamon Press, Elmsford, N. Y., 1969.
- (5) A. Forcier and J. W. Olver, *Anal. Chem.*, **37**, 1442 (1965).
- (6) A. Weissberger, *et al.*, "Organic Solvents," Interscience Publishers, Inc., New York, N. Y., 1955, pp 390, 413.
- (7) I. S. Perelygin, *Opt. Spectrosc.*, **13**, 198 (1962); G. S. Janz, M. J. Tait, and J. Meier, *J. Phys. Chem.*, **71**, 963 (1967).
- (8) (a) K. E. Purcell and R. S. Drago, *J. Amer. Chem. Soc.*, **88**, 919 (1966); (b) H. Coerver and C. Curran, *ibid.*, **80**, 3522 (1958).
- (9) E. L. Zhukova, *Opt. Spectrosc.*, **5**, 270 (1958).
- (10) S. S. Mitra, *J. Chem. Phys.*, **36**, 3286 (1962).
- (11) B. J. Hathaway and A. E. Underhill, *J. Chem. Soc.*, 3091 (1961).
- (12) A. E. Wickenden and R. A. Kravse, *Inorg. Chem.*, **4**, 404 (1965).
- (13) P. A. Giguere and R. Savoie, *Can. J. Chem.*, **40**, 495 (1962).
- (14) R. S. Roy, *Spectrochim. Acta*, **22**, 1877 (1966).
- (15) F. Klages, *et al.*, *Ann.*, **626**, 60 (1959); G. A. Olah and T. E. Kiovsky, *J. Amer. Chem. Soc.*, **90**, 4666 (1968).
- (16) G. J. Janz and S. S. Danyluk, *J. Amer. Chem. Soc.*, **81**, 3846 (1959).
- (17) S. Hashino, H. Hosoya, and S. Nagakura, *Can. J. Chem.*, **44**, 1961 (1966).
- (18) N. Mataga and T. Kubota, "Molecular Interactions and Electronic Spectra," Marcel Decker, Inc., New York, N. Y., 1970.
- (19) D. W. Turner, "Molecular Photoelectron Spectroscopy," Wiley, New York, N. Y., 1970.

The Effect of Pressure on the Dimerization of Carboxylic Acids in Aqueous Solution

Keizo Suzuki,* Yoshihiro Taniguchi, and Takashi Watanabe

Department of Chemistry, Faculty of Science and Engineering, Ritsumeikan University Kita-ku, Kyoto, Japan (Received November 13, 1972; Revised Manuscript Received February 23, 1973)

Publication costs assisted by the Research Institute of Science and Engineering, Ritsumeikan University

The electrical conductivities of formic, acetic, propionic, and *n*-butyric acids in aqueous solution at 30° were measured at pressures up to 5910 kg/cm². From these data, the dimer dissociation constants (K_D) between dimer and monomer of these acids were calculated. The relative amount of the dimer of formic acid increases continuously with increasing pressure, while a minimum in K_D is found for acids having an alkyl group. The pressure at which this minimum appears decreases with increasing alkyl chain length. From the pressure dependence of $\log K_D$, the dimerization volume change (ΔV_D) at 1 atm was calculated to be $-14\text{ cm}^3/\text{mol}$ for formic, $-13\text{ cm}^3/\text{mol}$ for acetic, $-8.8\text{ cm}^3/\text{mol}$ for propionic, and $-6.2\text{ cm}^3/\text{mol}$ for *n*-butyric acid. The volume change at 1 atm accompanying hydrophobic bond formation was estimated from the contribution of alkyl chain length to the decrease of the absolute value of ΔV_D to be $1\text{ cm}^3/\text{mol}$ for methyl, $5\text{ cm}^3/\text{mol}$ for ethyl, and $8\text{ cm}^3/\text{mol}$ for propyl groups.

Introduction

Dimerization of carboxylic acids in aqueous solution has been studied at atmospheric pressure by various methods, including measurement of Raman spectra,¹ vapor pressure,^{2,3} freezing point,³ electrical conductivity,^{4,5} and

electromotive force.^{6,7} It has been found from these experimental results that the relative amount of dimer tends to increase with an increase in alkyl (R) chain length. Scheraga and coworkers⁸ suggested that hydrophobic bonding ($H\phi$ bonding) contributes to the stability of the carboxylic

acid dimers in aqueous solution, as well as the hydrogen bond (H bond).

In the present study, the electrical conductivities of aqueous solutions of formic, acetic, propionic, and *n*-butyric acids were measured at pressures up to 5910 kg/cm². From these conductivity data, the equilibrium constants between monomer and dimer of these acids were calculated to obtain information on pressure effects on H ϕ bonding and H bonds.

Experimental Section

Materials. Carboxylic acids (formic, acetic, propionic, and *n*-butyric acids), their sodium salts, and all other reagents were of special grade and were used without further purification. The conductivity water was prepared by repeatedly distilling the water deionized by both anionic and cationic ion-exchange resins (Amberlite IR-120 and IRA-45). The collected distilled water was aerated with air free from CO₂ to exclude CO₂. The specific conductivity of this water at 30° was 1.929×10^{-6} mho/cm under atmospheric pressure. Solutions of carboxylic acids were prepared in the concentration range of about 0.1–0.04 *M* for formic acid and 0.04–0.01 *M* for other acids. Concentrations of sodium carboxylates, sodium chloride, and hydrochloric acid were used in the range 0.01–0.001 *M*.

Apparatus and Procedures. The high-pressure apparatus and Teflon-platinum black conductivity cell for measuring electrical conductivity were described in detail elsewhere.⁹ Pressures were measured from the electrical resistance of manganin wire which was calibrated against a Heise gauge (full scale 50,000 psi, unit scale 50 psi). The resistance measurements of the solutions were made successively by a Yanagimoto MY-7 conductivity bridge (800 cps), after standing for 30 min after increasing the pressure to 5910 kg/cm² and at $30 \pm 0.05^\circ$. This process was reversible. The equivalent conductivity (Λ) under pressure was obtained from the resistance data by the following corrections. (1) The concentration change of the solution with compression was

$$\frac{V^1 - V^p}{V^1} = \frac{C}{V^1} \log \frac{B + p}{B + 1} \quad (1)$$

where V^p and V^1 are the volume of water at pressure p and 1 kg/cm², respectively, and C (0.3150) and B (3038 at 30°) are the characteristic parameters of water.¹⁰ (2) The conductivity change of water itself with compression was corrected for by subtracting the specific conductivity (κ_0) of water from that of the solution (κ) at each pressure. The conductivity of water at 5910 kg/cm² was 13.50×10^{-6} mho/cm, which is about 7 times the conductivity at atmospheric pressure. (3) The change of cell constant with pressure was calculated from the compressibility data of Teflon.¹¹ The cell constant, 0.8502 cm⁻¹ at atmospheric pressure, was estimated to be 0.8168 cm⁻¹ at 5910 kg/cm².

Results and Discussion

Ionization constants of carboxylic acids were calculated by the method of MacInnes and Shedlovsky.¹² The limiting conductivity ($\Lambda^\circ_{\text{RCOOH}}$) was determined by applying Kohlrausch's law to the known limiting conductivities of the strong electrolytes sodium carboxylates, hydrochloric acid, and sodium chloride

$$\Lambda^\circ_{\text{RCOOH}} = \Lambda^\circ_{\text{RCOONa}} + \Lambda^\circ_{\text{HCl}} - \Lambda^\circ_{\text{NaCl}} \quad (2)$$

TABLE V: Average Dimer Dissociation Constants (K_D)_{av} of Carboxylic Acids at 30° and at Various Pressures

Pressure, kg/cm ²	$(K_D)_{av}$			
	Formic acid	Acetic acid	Propionic acid	<i>n</i> -Butyric acid
1 atm	15 ± 2.1	6.6 ± 0.4	5.4 ± 0.9	4.7 ± 0.9
860	9.8 ± 1.4	4.3 ± 0.6	4.0 ± 0.6	4.0 ± 0.3
1650	7.1 ± 1.4	2.9 ± 0.1	3.2 ± 0.6	3.4 ± 0.5
2560	5.9 ± 0.4	1.5 ± 0.2	2.4 ± 0.5	4.7 ± 0.9
3410	4.1 ± 0.7	1.5 ± 0.2	2.8 ± 0.7	7.0 ± 0.7
4250	3.2 ± 0.4	1.7 ± 0.1	4.1 ± 0.2	10 ± 1.2
5020	2.2 ± 0.5	2.2 ± 0.3	5.7 ± 1.0	12 ± 1.0
5910	1.8 ± 0.8	2.9 ± 0.4	7.7 ± 0.4	17 ± 0.5

where $\Lambda^\circ_{\text{RCOONa}}$, $\Lambda^\circ_{\text{HCl}}$, and $\Lambda^\circ_{\text{NaCl}}$ were obtained as the equivalent conductivities at infinite dilution on Kohlrausch plots. A first approximation to the degree of ionization (α') of carboxylic acids was obtained by the formula

$$\alpha' = \frac{\Lambda_{\text{RCOOH}}}{\Lambda^\circ_{\text{RCOOH}}} \quad (3)$$

Then, at a concentration $\alpha'c$, the exact degree of ionization (α) was obtained by the equations

$$\alpha = \frac{\Lambda_{\text{RCOOH}}}{\Lambda^i_{\text{RCOOH}}} \quad (4)$$

$$\Lambda^i_{\text{RCOOH}} = \Lambda^\circ_{\text{RCOOH}} - \frac{(B_1\Lambda^\circ_{\text{RCOOH}} + B_2)\sqrt{\alpha'c}}{(1 + Ba\sqrt{\alpha'c})} \quad (5)$$

where

$$B_1 = \frac{0.8204 \times 10^6}{(\epsilon T)^{3/2}} \quad (6)$$

$$B_2 = \frac{82.50}{\eta(\epsilon T)^{1/2}} \quad (7)$$

$$B = \frac{50.29 \times 10^8}{(\epsilon T)^{1/2}} \quad (8)$$

$$a = \frac{e^2}{2\epsilon kT} \quad (9)$$

ϵ and η are the dielectric constant and the viscosity of water, respectively, k is the Boltzmann constant, T is the absolute temperature, e is the protonic charge, and c is the molarity.

The activity coefficient (f_{\pm}) was predicted by the Debye-Hückel limiting law at concentration c

$$\log f_{\pm} = - \frac{A\sqrt{\alpha c}}{(1 + Ba\sqrt{\alpha c})} \quad (10)$$

where A is $1.824 \times 10^6/(\epsilon T)^{3/2}$. In applying the above equation to high-pressure conditions, the dielectric constant and the viscosity were corrected using the Owen-Brinkley¹³ equation and the data of Bett and Cappi.¹⁴

The ionization constant (K_c) is given by

$$K_c = \frac{c\alpha^2 f_{\pm}^2}{(1 - \alpha)} \quad (11)$$

where the activity coefficient of the undissociated molecules is assumed to be 1. The true thermodynamic ionization constant (K), excluding the effect of the dimerization of acids, was obtained by extrapolation of the plot of $\log K_c$ against the concentration.

TABLE VI: Logarithm of Dimer Dissociation Constants (Log K_D) of Carboxylic Acids at 1 Atm Compared with Results of Other Workers

Log K_D				Temp, °C	Ref
Formic acid	Acetic acid	Propionic acid	<i>n</i> -Butyric acid		
1.19 ± 0.06	0.82 ± 0.03	0.73 ± 0.07	0.67 ± 0.07	30	This work ^a
	1.23 ± 0.015	0.98 ± 0.03	0.82 ± 0.04	30	6
	1.45		1.00	25	3
1.40	0.80	0.63	0.45	25	4
2.08 ± 0.04	1.28 ± 0.05	1.30 ± 0.03	1.04 ± 0.02	25	5
1.24 ± 0.04	0.73 ± 0.03	0.50 ± 0.04	0.26 ± 0.04	25	7

^a K_D in this work is the average value for each acid concentration.

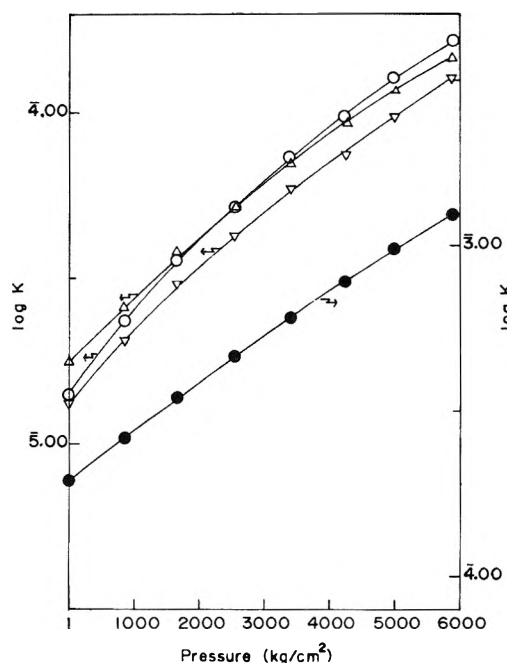


Figure 1. Effect of pressure on the thermodynamic ionization constants ($\log K$) of carboxylic acids at 30°: ●, HCOOH; Δ, CH₃COOH; ▽, CH₃CH₂COOH; ○, CH₃CH₂CH₂COOH.

Then, the dimer dissociation constant (K_D) of carboxylic acids under pressure p



was determined by the equation of Cartwright and Monk⁵

$$K_D = \frac{([\text{RCOOH}]^2)}{[(\text{RCOOH})_2]_p} \quad (13)$$

$$\alpha = \left(\frac{2x^2}{(c - c\alpha - x)} \right)_p \quad (14)$$

where x is the true concentration of carboxylic acids at pressure p , and given by the equation

$$x = \left(\frac{(\alpha c)^2 f_{\pm}}{K} \right)_p \quad (15)$$

The values of K_D of formic, acetic, propionic, and *n*-butyric acids are listed in Tables I to IV with Λ_i , Λ , K_c , and K at various pressures.¹⁵ The average values of K_D up to 5910 kg/cm² in Table V have an average error of 17% in K_D for formic, 11% for acetic, 15% for propionic, and 12% for *n*-butyric acids. These errors are a little larger than those obtained at 1 atm by other workers, in Table VI. Considering the values obtained by other methods, except

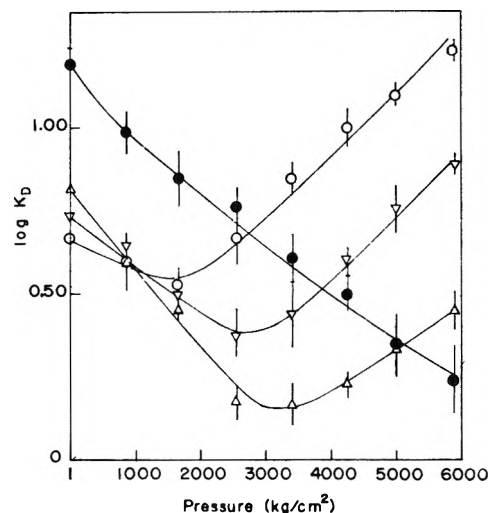


Figure 2. Effect of pressure on the dimer dissociation constants ($\log K_D$) of carboxylic acids at 30°: ●, HCOOH; Δ, CH₃COOH; ▽, CH₃CH₂COOH; ○, CH₃CH₂CH₂COOH.

Davies and Griffiths³ and Cartwright and Monk,⁵ the present values at 1 atm may be reasonable. The measurements of electrical conductivity by Cartwright and Monk were extended to the higher concentrations of 1 *M* for formic and 0.2 *M* for other acids, at which the viscosity factor becomes more important, while in the present measurements the highest concentration, 0.1 *M* for formic and 0.04 *M* for other acids, may be too low for viscosity to affect the conductivity. These results under pressure (in Table V) show that K_D of formic acid decreases with increasing pressure. That is, the amount of the dimer of formic acid continuously increases with increasing pressure, while K_D passes through a minimum for the acids having alkyl groups, and the pressure where the minimum appears decreases with increasing alkyl chain length.

The volume changes (ΔV or ΔV_D) at 1 atm accompanying ionization or the formation of acid dimers were obtained graphically from Figures 1 and 2 by the equations

$$\left(\frac{\partial \ln K}{\partial P} \right)_T = - \frac{\Delta V}{RT}; \quad \left(\frac{\partial \ln (1/K_D)}{\partial P} \right)_T = - \frac{\Delta V_D}{RT} \quad (16)$$

where R is the gas constant, K is the true ionization constant, and $1/K_D$ is the dimer formation constant. The absolute values of ΔV increase with an increase of R-chain length, as shown in Table VII. That is, the anion size influences the diminution of the volume and the amount is about 1 to 3 cm³/mol by each -CH₂- of the R chain. In Table VIII, the values of ΔV_D at 1 atm of formic, acetic, propionic, and *n*-butyric acids are -14, -13, -8.8, and

TABLE VII: Volume Changes (ΔV) for the Ionization of Carboxylic Acids at 1 Atm Compared with Results of Other Workers

$-\Delta V, \text{cm}^3/\text{mol}$				Temp., °C	Ref
Formic acid	Acetic acid	Propionic acid	<i>n</i> -Butyric acid		
8.3	11.5	13.5	15.0	30	This work
7.8	10.9	12.6	14.4	30	<i>a</i>
	10.3	12.6		30	<i>b</i>
8.0	12.5	13.7	13.7	25	<i>c</i>
8.43	11.50		14.22	25	<i>d</i>
8.8	12.2	12.9		25	<i>e</i>
9.2	11.6			25	<i>f</i>
	9.2			25	<i>g</i>
	11.46			25	<i>h</i>
	11.47			25	<i>i</i>
	12.1			25	<i>j</i>

^a W. Kauzmann, A. Bodanszky, and J. Rasper, *J. Amer. Chem. Soc.*, **84**, 1777 (1962). ^b H. H. Weber, *Biochem. Z.*, **218**, 1 (1930). ^c S. D. Hamann and S. C. Lim, *Aust. J. Chem.*, **7**, 329 (1954). ^d E. J. King, *J. Phys. Chem.*, **73**, 1290 (1969). ^e S. D. Hamann and W. Strauss, *Trans. Faraday Soc.*, **51**, 1684 (1955). ^f L. Distèche and P. Distèche, *J. Electrochem. Soc.*, **112**, 350 (1965). ^g B. B. Owen and S. R. Brinkley, *Chem. Rev.*, **29**, 461 (1941). ^h H. Wirth, *J. Amer. Chem. Soc.*, **70**, 462 (1948). ⁱ O. Redlich and J. Bigeleisen, *Chem. Rev.*, **30**, 171 (1942); O. Redlich and L. E. Nielsen, *J. Amer. Chem. Soc.*, **54**, 761 (1942). ^j A. J. Eliss and D. W. Anderson, *J. Chem. Soc.*, 1765 (1961).

$-6.2 \text{ cm}^3/\text{mol}$, respectively. The ΔV_D for formic acid, $-14 \text{ cm}^3/\text{mol}$, is attributed only to the formation of 2 mol of H bond. Therefore, the volume change per H bond mole is $-7 \text{ cm}^3/\text{mol}$, which seems to be a little large in comparison with the $-4.6 \text{ cm}^3/\text{mol}$ obtained for the association of *n*-butyl alcohol from ir spectrophotometric measurement under high pressure.¹⁶

The ΔV_D for carboxylic acids, except formic acid, is assumed to be the sum of the volume change due to H-bond formation and that due to $H\phi$ bonding. If the contribution of H-bond formation to the volume change is assumed to be the same as in formic acid, the decrease in the absolute value of ΔV_D with the increase in R chain length must be attributed to $H\phi$ bonding. The volume change ($\Delta V_{H\phi}$) accompanying $H\phi$ bonding in each carboxylic acid is calculated as follows

$$\Delta V_{H\phi} = \Delta V_D - \Delta V_D(\text{Formic Acid}) \quad (17)$$

The results are listed in Table IX, which shows that the $\Delta V_{H\phi}$ value is positive and becomes larger with an increase in R chain length. The fact that $\Delta V_{H\phi}$ is positive has been reported for model systems with $H\phi$ bonding by other workers. Masterton¹⁷ showed that the partial molal volumes of nonpolar gases in aqueous solutions are much smaller than in nonpolar solvents or than molar volumes in the liquid state. Némethy and Scheraga¹⁸ calculated the volume change for the transfer of a hydrocarbon from a nonpolar medium into aqueous solution at 25°. The values are negative, -18.1 to $-22.7 \text{ cm}^3/\text{mol}$ for experimental and -9.5 to $-14.7 \text{ cm}^3/\text{mol}$ for calculated data (when $H\phi$ bonding is broken), and the absolute value of calculated data increases with R chain length. Our experimental data are in poor agreement with the data of Masterton and Némethy and Scheraga. This disagreement may be caused by the differences in the systems concerned.

The volume change accompanying micelle formation of surface-active agents in aqueous solution is positive, 10 to $16 \text{ cm}^3/\text{mol}$ for anionic detergents¹⁹⁻²¹ and 3 to $11 \text{ cm}^3/\text{mol}$ for cationic detergents.²²⁻²⁴ This fact suggests that

TABLE VIII: Volume Changes (ΔV_D) for Dimer Formation of Carboxylic Acids at 30° and 1 Atm

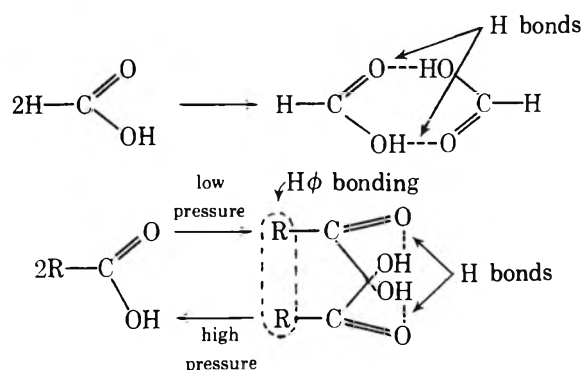
$-\Delta V_D, \text{cm}^3/\text{mol}$			
Formic acid	Acetic acid	Propionic acid	<i>n</i> -Butyric acid
14	13	8.8	6.2

TABLE IX: Volume Changes ($\Delta V_{H\phi}$) for the Formation of Hydrophobic Bonding at 30° and 1 Atm

$\Delta V_{H\phi}, \text{cm}^3/\text{mol}$		
CH ₃ -	CH ₃ CH ₂ -	CH ₃ CH ₂ CH ₂ -
1	5	8

polar groups influence the volume change accompanying $H\phi$ bond formation. Our data seem to be reasonable on the basis of this consideration, and these results show that pressure favors the rupture of $H\phi$ bonding. It is, therefore, clear that the pressure effect on the formation of H bonds is opposite to that on $H\phi$ bonding.

Summarizing the results mentioned above, the following schemes are presented



In formic acid, only H bonds are involved in dimer formation. Therefore, the relative amount of dimer increases continuously with an increase of pressure. On the other hand, in carboxylic acids other than formic acid, both H bonds and $H\phi$ bonding are involved in the dimerization process. In the lower pressure region, the contribution of H bonds predominates over that of $H\phi$ bonding, and the amount of dimer increases with pressure, and in the higher pressure region the situation is reversed. That the inversion occurs at lower pressure in the carboxylic acid having the larger R chain can be explained by considering that the contribution of $H\phi$ bonding increases with increasing R chain length.

References and Notes

- (1) P. Koteswaram, *J. Chem. Phys.*, **7**, 88 (1939); *Z. Phys.*, **110**, 118 (1938); **112**, 395 (1939).
- (2) F. H. MacDougall and D. R. Blumer, *J. Amer. Chem. Soc.*, **55**, 2236 (1933).
- (3) M. Davies and D. M. L. Griffiths, *Z. Phys. Chem. (Frankfurt am Main)*, **2**, 353 (1954); **6**, 43 (1956).
- (4) A. Katchalsky, H. Eisenberg, and S. Lifson, *J. Amer. Chem. Soc.*, **73**, 5889 (1951).
- (5) D. R. Cartwright and C. E. Monk, *J. Chem. Soc.*, 2500 (1955).
- (6) G. R. Nash and C. E. Monk, *J. Chem. Soc.*, 4274 (1957).
- (7) D. L. Martin and F. J. Rossotti, *Proc. Chem. Soc. London*, **60** (1959).
- (8) E. E. Schrier, M. Pottle, and H. A. Scheraga, *J. Amer. Chem. Soc.*, **86**, 3444 (1964).
- (9) K. Suzuki and Y. Taniguchi, *Biopolymers*, **6**, 215 (1968).
- (10) H. S. Harned and B. B. Owen, "The Physical Chemistry of Electrolyte Solutions," Reinhold, New York, N. Y., 1957, p 380.

- (11) C. E. Weir, *J. Res. Nat. Bur. Stand.*, **53**, 245 (1954).
 (12) D. A. MacInnes and T. Shedlovsky, *J. Amer. Chem. Soc.*, **54**, 1429 (1932).
 (13) B. B. Owen and S. R. Brinkley, *Phys. Rev.*, **64**, 32 (1943).
 (14) J. B. Cappi, Ph.D. Thesis, London University, 1964.
 (15) Tables I-IV will appear following these pages in the microfilm edition of this volume of the journal. Single copies may be obtained from the Business Operations Office, Books and Journals Division, American Chemical Society, 1155 Sixteenth St., N.W., Washington, D. C. 20036. Remit check or money order for \$3.00 for photocopy or \$2.00 for microfiche, referring to code number JPC-73-1918.
 (16) E. Fishman and H. D. Drickamer, *J. Chem. Phys.*, **24**, 548 (1956).
 (17) W. L. Masterton, *J. Chem. Phys.*, **22**, 1830 (1954).
 (18) G. Némethy and H. A. Scheraga, *J. Chem. Phys.*, **36**, 3401 (1962).
 (19) K. Shinoda and T. Soda, *J. Phys. Chem.*, **67**, 2072 (1963).
 (20) S. D. Hamann, *J. Phys. Chem.*, **66**, 1359 (1962).
 (21) R. G. Paquette, E. C. Lingafelter, and H. V. Tartar, *J. Amer. Chem. Soc.*, **65**, 686 (1943).
 (22) R. F. Tuddenham and A. E. Alexander, *J. Phys. Chem.*, **66**, 1839 (1962).
 (23) J. Osugi, M. Sato, and N. Ifuku, *Rev. Phys. Chem. Jap.*, **35**, 32 (1965).
 (24) J. M. Corkill, J. F. Goodman, and T. Walker, *Trans. Faraday Soc.*, **63**, 768 (1967).

COMMUNICATIONS TO THE EDITOR

Temperature-Jump Experiments on the System Acridine Orange-Poly(styrenesulfonic acid)^{1,2}

Sir: The main feature of the binding of a number of cationic dyes to biopolymers and to synthetic polyelectrolytes is the so-called "metachromasia," an effect which has been recognized as due to different binding modes of the dye molecules exhibiting different absorption spectra in the visible region. The absorption bands show that the dye molecules bind as monomer or they interact with each other on the polyelectrolyte molecule to form dimers or aggregates similar to those existing in concentrated aqueous solutions.³⁻⁷

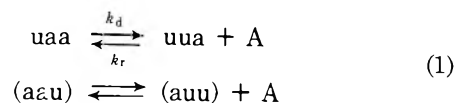
Bradley and Wolf⁸ proposed a simple model which accounts for this behavior in terms of dilution of the dye molecules along the polymer chain which is supposed to be a linear sequence of available binding sites. Several statistical approaches, based on the Ising model,⁹ can be used to treat the binding of small molecules along a polymer chain which take into account first and higher order neighbor interactions.¹⁰⁻¹³

The interaction behavior of poly(styrenesulfonic acid) (PSS) with a number of metachromatic dyes has been found particularly suitable for statistical treatment according to the linear chain model.^{14,15} The tendency of the dye molecules to aggregate along the polyelectrolyte chain (stacking tendency) is not very high and it is easily possible to detect the equilibrium monomer \rightleftharpoons dimer \rightleftharpoons aggregate of the bound dye for values of the ratio P/D (concentration of polymer available sites to bound dye concentration) just exceeding unity.¹⁶

The equilibrium properties of the system Acridine Orange-poly(styrenesulfonic acid) (AO-PSS) were recently studied in our laboratory and a good agreement was found between experimental data and the statistical treatment which includes first and second neighbor interactions.¹⁷ At 20°, the first neighbor interaction parameter (stacking coefficient), q_1 ,¹¹ was found to equal 30 in absence of

added salts, as compared with $q_1 = 1580$ for polyphosphates⁸ or $q_1 = 1700$ for poly-L-glutamic acid in neutral solution.¹⁸ So, it was thought worthwhile to obtain some information on the relaxation properties of the system AO-PSS through a set of T-jump experiments.

The kinetics of the binding of simple molecules (or ions) to linear macromolecules (or polyions) has been recently discussed by Schwarz^{13,19} and experimental data have been reported for the system AO-poly(L-glutamic acid).¹⁸ The kinetic process which was observed through T-jump measurements is the release of the dye from the polyion to the solution (reverse of growth process)

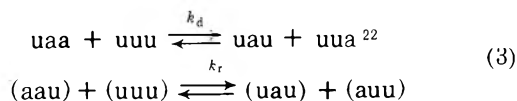


where u stands for an unoccupied binding site on the macroion chain and a for an occupied site, A being the free dye in solution. Schwarz derived an expression for the reciprocal of the mean relaxation time applicable in the case of very highly cooperative binding²⁰

$$(1/\tau^*) = 2k_r \sqrt{\sigma\{(D/P)[1 - (D/P)]\}}(P/D)D \quad (2)$$

where σ is a function of the stacking coefficient, q_1 .²¹ According to eq 2, $(1/\tau^*)$ increases by increasing the P/D ratio at constant dye concentration and increases, linearly, by increasing dye concentration at constant P/D ratio.

A different kinetic process should be expected in a T-jump experiment in the case of very strong binding with fairly weak cooperativity. In this case a negligible amount of free dye is present in solution and we expect the following main reaction to occur



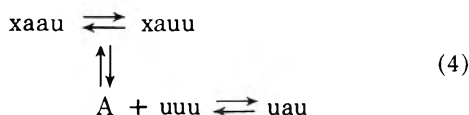
Equation 3 is the phenomenological description of the dye sequences' redistribution along the polymer chain, leading to a change in their number. Schwarz suggested that it

TABLE I: Relaxation Times for the System Acridine Orange–Poly(styrenesulfonic Acid) in 0.04 M NaCl at $T \approx 23^\circ$, Measured from the Optical Density Change at λ 500 nm^a

P/D	$(\tau^*)^{-1} \times 10^{-4}, \text{sec}^{-1}$	P/D	$(\tau^*)^{-1} \times 10^{-4}, \text{sec}^{-1}$
0.8	0.00014	50	2.65*
1	0.012	75	2.64*
2	0.12	100	2.51*
3	0.22	150	2.10*
4	0.49*	200	1.82
5	0.96	300	1.43*
7	1.13	500	1.16*
10	1.54*	700	1.00
20	2.18*	800	0.95*

^a P/D , stoichiometric ratio between PSS equivalent concentration and AO concentration. The value at $P/D = 0.8$ is only indicative. The values marked with an asterisk are average values of two or more runs.

might proceed through a transient nucleation process such as²³



Actually, the free dye, A, should be considered as a molecule within the domain of the macroion. Under these conditions, any kinetic process occurring on the polymer molecule should be independent of the stoichiometric concentration of polymer, depending only on the ratio between the available binding sites concentration and the dye concentration (P/D ratio, $1/\theta$ in the Schwarz symbolism). Every macroion with its bound dye molecules can, in fact, be thought of as an independent system.

The system AO–PSS is particularly suitable for testing a kinetic mechanism like that shown in eq 3 and 4 because of its low stacking coefficient value and because of the negligible amount of free dye, even in 0.05–0.1 M salt solution, for $P/D > 50$ –60.²⁴ Both facts are probably due to specific interactions between the benzene rings of PSS and dye aromatic rings which might favor some kind of partial intercalation.

By adding NaCl to the AO–PSS system, the stacking coefficient increases (remaining lower than 100 in 0.1 M NaCl) and the binding constant decreases; we assume, as suggested in our previous paper,¹⁷ that this effect is principally due to electrostatic interactions and that no competition for binding sites should be considered in the case of Na^+ ions that are held within the domain of the macroion mainly by the effect of electrostatic interactions according to generally accepted theories on polyelectrolyte solutions.^{25–27}

Poly(styrenesulfonic acid) was obtained, and Acridine Orange was purified as described elsewhere.¹⁷

T-jump experiments were done in 0.04 M NaCl.²⁸ The total dye concentration was 10^{-5} M (unless otherwise stated). The final temperature was $\approx 23^\circ$ (T-jump between 2 and 3°). Rise time was not greater than 5 μsec for all experiments. The relaxation process was followed by measuring the optical density increase at λ 500 nm (maximum absorption of monomer bound AO).²⁹ The accuracy of experimental results was within 10–15%. The semilogarithmic plots of the optical absorptions generally exhibit constant slopes only during the initial time which includes about one-half to two-thirds of the total absorption

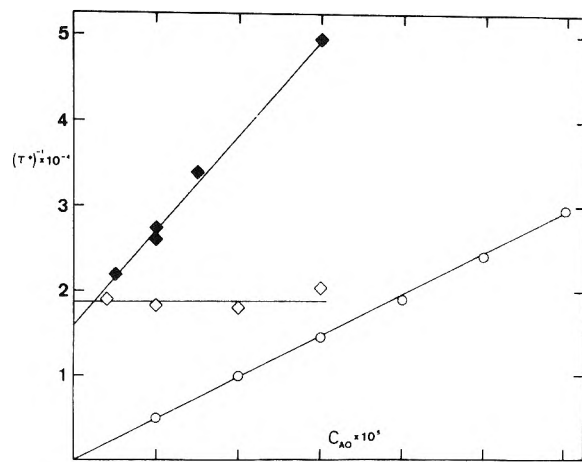


Figure 1. Mean (reciprocal) relaxation times for the system AO–PSS at constant P/D and varying dye concentration: \circ , $P/D = 4$, $\text{NaCl} = 0.04$ M; \blacklozenge , $P/D = 200$, $\text{NaCl} = 0.04$ M; \diamond , $P/D = 50$, $\text{NaCl} = 0.10$ M. The set of runs at $P/D = 50$ was taken in Palermo with the help of Professor P. Cavasino, whom the author wishes to thank. The apparent constant value of $1/\tau^*$ in the NaCl concentration range 0.04–0.10 M may be fortuitous at this P/D ratio because an ionic strength effect should be expected on the relaxation times, and it was found for the system AO–poly(L-glutamic acid).¹⁸ The higher value of the slope at $P/D = 50$ as compared with that at $P/D = 4$ follows from eq 2, as far as kinetics described by eq 1 contributes appreciably to the optical absorption increment due to the T jump; the increment of the (P/D) term is, in fact, much higher than the decrement of the term under square root.

change. Similar behavior was found by other authors¹⁸ and for this reason we did not investigate this point further, but computed only the mean relaxation times from the initial slopes.³⁰

Table I collects the $1/\tau^*$ values as a function of the ratio P/D . As predicted by Schwarz,²³ the $1/\tau^*$ values go through a maximum that must be expected when the kinetic process changes from that described by eq 1 to that described by eq 3 and 4; at $D/P = 0$, the extrapolated $1/\tau^*$ value is $\approx 6500 \text{ sec}^{-1}$. However, a quantitative agreement was not found between our experimental data and the mean relaxation times computed by introducing the stacking coefficient measured previously,¹⁷ $q_1 \approx 65$, in eq 60 of ref 23 (a value of $q_1 \approx 1000$ –1500 should be used in order to fit the experimental data).

It is not possible to explain such a disagreement on the basis of the present available τ^* data, and much more work ought to be done. Actually, in applying eq 60 of ref 23, we neglected the second neighbor interaction parameter, q_2 , but this approximation should not be critical at high P/D values where sequences higher than dimers do not contribute very much to the AO–PSS complex configurations.

A set of T-jump experiments were also made at three values of the P/D ratio, varying the total dye concentration: $P/D = 4$, 50, and 200, respectively. The results are reported in Figure 1; they show the change from the eq 1 type kinetics to that of eq 3. At $P/D = 4$, the $1/\tau^*$ values are a linear function of the dye concentration with a zero origin intercept, as predicted by eq 2. At $P/D = 50$, the $1/\tau^*$ values are still a linear function of the dye concentration, but the origin intercept has a finite value. At $P/D = 200$, the $1/\tau^*$ values are almost independent of dye concentration as expected in the absence of free dye in solution and as predicted by ref 23 eq 60.

Acknowledgments. The author wishes to thank Professor Eigen and his coworkers, especially Professor G. Maass and Dr. Mrs. M. L. Ahrens, for their kind and friendly help during his visit to the M. Planck Institut in Göttingen. He also thanks Professor G. Schwarz for his interest in and discussion of the subject of this note.

An Electron Spectroscopy for Chemical Analysis Study of Lead Adsorbed on Montmorillonite¹

Publication costs assisted by
the National Aeronautics and Space Administration

Sir: The bonding state of adsorbed species on solid surfaces is of fundamental interest. The results of using electron spectroscopy for chemical analysis (ESCA) to determine the bonding state of lead adsorbed from aqueous solutions onto montmorillonite are presented in this paper. We have measured recently the adsorption of Pb(II) from aqueous lead nitrate solutions onto sodium-saturated montmorillonite at room temperature. Changes in lead concentration due to adsorption were determined using a Perkin-Elmer 303 atomic absorption spectrophotometer. Adsorption isotherms were determined at pH 4 and 6 over the concentration range 25–1000 ppm. Significant quantities of lead are adsorbed on montmorillonite over the concentration range studied.

The clay sample was equilibrated with an initial 1000 ppm of Pb(II) solution at pH 6. The quantity of Pb(II) adsorbed per gram of montmorillonite under these conditions was determined to be 18 mg. The sample was centrifuged and the clay was oven dried at 105° for 1.5 hr. A small quantity (about 10 mg) of the dried clay was suspended in acetone and spread on the sample probe of the electron spectrometer. In a second sample preparation, a small quantity (about 10 mg) of the dried clay was pressed into indium foil.

The ESCA measurements were made using an AEI ES 100 photoelectron spectrometer employing Al K_α radiation (1486.6 eV). Data acquisition was accomplished using the AEI DS-100 data system and a Digital PDP-8/e computer. Specific spectrometer conditions are listed on the subsequent spectra. The binding energies of gold 4f levels at 87.1 and 83.4 eV² were measured during some of the runs and used to evaluate the work function of the spectrometer.

The binding energies of lead were determined in a series of known lead compounds as a basis for comparison of the binding energy of adsorbed lead. The narrow scan ESCA spectrum of Pb in lead foil pressed from lead shot is shown in Figure 1a. The shoulders at 141.1 ± 0.2 and 136.4 ± 0.3 correspond to the 4f_{5/2} and 4f_{7/2} levels of Pb metal whereas the more intense peaks at 142.4 ± 0.3 and 137.5 ± 0.4 eV correspond to the same levels of Pb in a presumed surface oxide layer. The binding energies have been corrected for the work function of the spectrometer. The sample was then argon ion etched for 10 min. The narrow scan ESCA spectrum of Pb after etching is shown in Figure 1b. The change is dramatic. The Pb metal peaks have now become the most intense whereas the lead oxide peaks have been reduced in intensity. The ESCA spectrum obtained after an additional 10-min etching is shown in Figure 1c. The peaks attributed to lead oxide are barely discernible. There was no observed shift in the binding energy of the predominant peaks.

An authentic sample (PbO) was run to support the assignments made in Figure 1. The narrow scan ESCA spectrum of Pb in lead oxide particles pressed into indium foil is shown in Figure 2. The binding energies at 143.0 ± 0.2 and 138.0 ± 0.2 eV in Figure 2 match those of the more intense peaks in Figure 1a thereby supporting the peak

References and Notes

- (1) This research has been partially supported by the Italian C.N.R.
- (2) The author is indebted to the E.M.B.O. organization for a short term fellowship for visiting the Max Planck Institut für physik. Chemie in Göttingen.
- (3) L. Michaelis, *J. Phys. Chem.*, **54**, 1 (1950).
- (4) E. Rabinowitch and L. F. Epstein, *J. Amer. Chem. Soc.*, **63**, 69 (1941).
- (5) V. Zanker, *Z. Phys. Chem.*, **199**, 225 (1952).
- (6) G. Barone, L. Costantino, and V. Vitagliano, *Ric. Sci.*, **34**, 87 (1964).
- (7) M. E. Lamm and D. M. Neville, *J. Phys. Chem.*, **69**, 3872 (1965).
- (8) D. F. Bradley and M. K. Wolf, *Proc. Nat. Acad. Sci., U. S.*, **45**, 944 (1959).
- (9) T. L. Hill, "Statistical Mechanics," McGraw-Hill, New York, N. Y., 1956, Chapter 7.
- (10) S. Lifson, *J. Chem. Phys.*, **40**, 3705 (1964).
- (11) D. F. Bradley and S. Lifson in "Molecular Association in Biology," B. Pullman, Ed., Academic Press, New York, N. Y., 1969, p 261.
- (12) G. Schwarz, *Biopolymers*, **6**, 873 (1968).
- (13) G. Schwarz, *Eur. J. Biochem.*, **12**, 442 (1970).
- (14) V. Vitagliano and L. Costantino, *Boll. Soc. Natur. in Napoli*, **78**, 169 (1969).
- (15) V. Vitagliano and L. Costantino, *J. Phys. Chem.*, **74**, 197 (1970).
- (16) In this case *P* corresponds to the sulfonic groups' equivalent concentration.
- (17) V. Vitagliano, L. Costantino, and A. Zagari, *J. Phys. Chem.*, **77**, 204 (1973).
- (18) G. Schwarz and W. Balthasar, *Eur. J. Biochem.*, **12**, 461 (1970).
- (19) G. Schwarz, *Ber. Bunsenges. Phys. Chem.*, **75**, 40 (1971).
- (20) Reference 13, eq 51–55.
- (21) According to Schwarz' treatment, σ is assumed to be a constant, $\sigma = 1/q_1$; using Lifson's model, as done in ref 15 and 17, and neglecting second and higher order neighbor interactions

$$\sigma = \left\{ \sqrt{F_1} \left[1 - \frac{1 - \sqrt{F_1}}{1 + (q_1 - 1)\sqrt{F_1}} \right] \right\} / \left\{ (q_1 + 1)\sqrt{F_1} - 1 + \left[\frac{(1 - \sqrt{F_1})^2}{1 + (q_1 - 1)\sqrt{F_1}} \right] \right\}$$

where F_1 is the fraction of monomer bound dye (C_{uau}/C_a) and the terms in square brackets account for the aua sequences

$$\frac{D}{P} = \frac{1 - \sqrt{F_1}}{1 + (q_1 - 1)F_1} \quad (\text{ref 11, eq 13})$$

$$\lim_{F_1 \rightarrow 1} \sigma = 1/q_1$$

- (22) Reactions of the type $\text{aaa} + \text{uuu} \rightleftharpoons \text{aua} + \text{uau}$ can be neglected.
- (23) G. Schwarz, *Ber. Bunsenges. Phys. Chem.*, **76**, 373 (1972).
- (24) Direct measurements of the free AO at P/D values higher than 2–3 were not made. However, from the adsorption isotherms shown in the previous paper, which were taken both in the absence and in the presence of NaCl, one can easily guess the absence of free dye at room temperature for P/D ratios higher than 50–60.
- (25) R. M. Fuoss, A. Katchalsky, and S. Lifson, *Proc. Nat. Acad. Sci. U. S.*, **37**, 579 (1951).
- (26) S. Lifson and A. Katchalsky, *J. Polym. Sci.*, **13**, 43 (1954).
- (27) F. Oosawa, *J. Polym. Sci.*, **23**, 421 (1957).
- (28) E. F. Callen, "Fast Reactions in Solution," Blackwell Science Publishers, Oxford, 1964.
- (29) Most of the T-jump experiments were carried out at the Max Planck Institut für physik. Chemie in Göttingen. Some control experiments were made in Professor Schwarz's laboratory in Basel and in Professors Accascina's laboratory in Palermo by using the same standard apparatus used in Göttingen.
- (30) G. Schwarz, *Rev. Mod. Phys.*, **40**, 206 (1968).

Istituto Chimico
Università di Napoli
80134 Napoli, Italy

Vincenzo Vitagliano

Received October 30, 1970

Revised manuscript received December 18, 1972

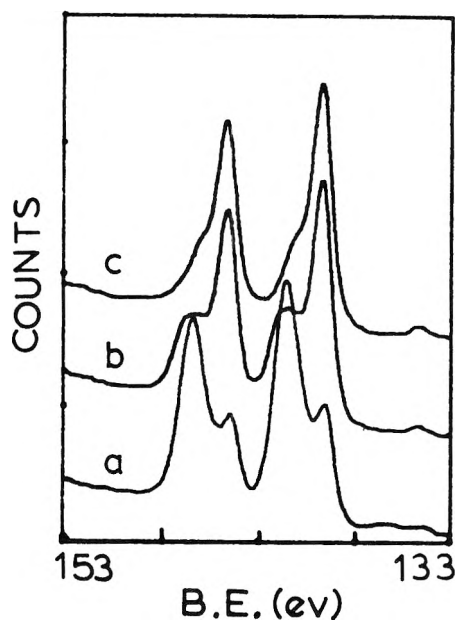


Figure 1. ESCA spectrum of lead 4f electrons obtained from lead foil: (a) as pressed, (b) after 10-min Ar^+ etch, (c) after 20 min Ar^+ etch (scanning: 200 channels, 3 sec/channel, 3 scans).

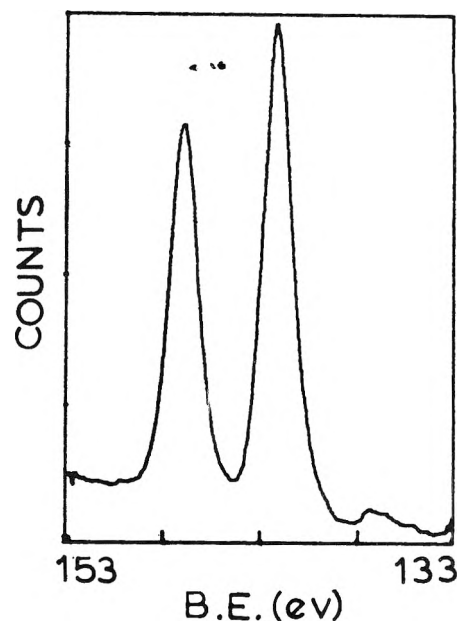


Figure 3. ESCA spectrum of lead 4f electrons obtained from lead dioxide (scanning: 200 channels, 3 sec/channel, 5 scans).

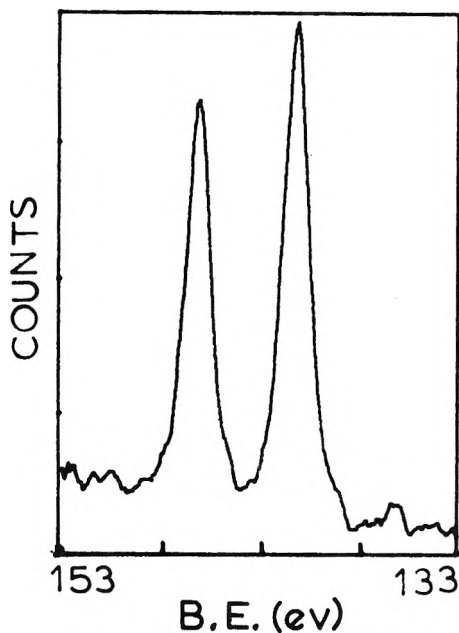


Figure 2. ESCA spectrum of lead 4f electrons obtained from lead oxide (scanning: 200 channels, 3 sec/channel, 5 scans).

assignments above. Jorgensen³ reported values of 149.0 and 144.15 eV for PbO which appear too high and may be due to sample charging discussed below.

An authentic sample of lead dioxide (PbO_2) was also run to support the subsequent assignment of lead adsorbed on montmorillonite. The lead dioxide sample was prepared by heating lead foil in an oven at 110° for 20 hr in an oxygen rich atmosphere.⁴ The narrow scan ESCA spectrum of Pb in lead dioxide is shown in Figure 3. The binding energies at 143.6 and 138.6 eV occur at significantly higher binding energies than Pb in lead oxide.

The charging of nonconducting sample is a continuing problem in ESCA studies. For example, charging effects were neglected in a recent ESCA study of Rh adsorbed on

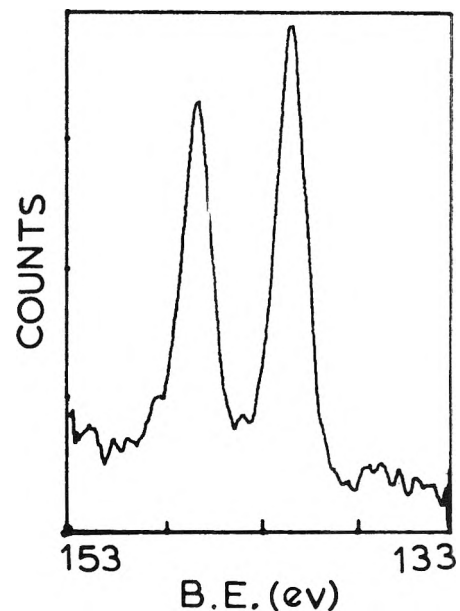


Figure 4. ESCA spectrum of lead 4f electrons obtained from lead adsorbed on montmorillonite (scanning: 200 channels, 3 sec/channel, 66 scans).

carbon.⁵ It was anticipated that the clay particles in the present work would charge and therefore the particles were either pressed into indium foil or deposited as a very thin film.

The narrow scan ESCA spectrum of clay which had not been equilibrated with lead was obtained over the binding energy range 153–133 eV. No detectable signal due to Pb was observed. The narrow scan ESCA spectrum of clay equilibrated with an aqueous lead nitrate solution is shown in Figure 4 for clay particles pressed into indium. A similar spectrum was obtained for clay particles suspended in acetone. The presence of the adsorbed lead is readily seen. Binding energies at 142.9 and 138.0 eV are very close to the values assigned for lead oxide. Thus, we have established the binding energies of lead adsorbed on mont-

morillonite and further that the adsorbed lead is in a similar bonding state as the lead in lead oxide.

Acknowledgment. We wish to acknowledge gratefully the assistance of the National Science Foundation under the Capital Equipment Grant Program in the purchase of the AEI electron spectrometer. We thank Dr. Lucian Zelazny, Department of Soils, University of Florida, for supplying the clay sample.

References and Notes

- (1) This work was supported in part by the Center for Environmental Studies and the College of Arts and Sciences at Virginia Polytechnic Institute and State University including a graduate research assistantship for one of us (M. E. C.).
- (2) K. Siegbahn, *et al.*, "ESCA—Atomic, Molecular and Solid State Structure Studies by Means of Electron Spectroscopy," Almquist and Wiksells, Uppsala, 1967.
- (3) C. K. Jorgensen, *Chimia*, **25**, 213 (1971).
- (4) J. F. Rendina, *Amer. Lab.*, **17** (Feb 1972).
- (5) J. S. Brinen and A. Melera, *J. Phys. Chem.*, **76**, 2525 (1972).

Department of Chemistry
Virginia Polytechnic Institute
and State University
Blacksburg, Virginia 24061

Mary Ellen Counts
James S. C. Jen
James P. Wightman*

Received April 11, 1973

On the Decay of Hydrated Electrons in Radiolytic Spurs at Picosecond Times¹

Publication costs assisted by the U. S. Atomic Energy Commission and Carnegie-Mellon University

Sir: A recent report on the radiolytic yield of hydrated electrons as observed at subnanosecond times by both the stroboscopic pulse radiolysis technique and by direct measurements with single pulses indicates that $G(e_{aq}^-)$ is $\sim 4.0 \pm 0.2$ on the 30–1000-psec time scale.² This yield is somewhat lower than the value of 4.8 required in the calculations of Schwarz³ to explain the net observed yield of water decomposition on the basis of the spur diffusion model. Furthermore very little decay was observed over the period 30–350 psec after irradiation in contrast to the expected $\sim 15\%$ drop. The purpose of the present communication is to point out that, to a large extent, these observations can be accommodated by the spur diffusion model provided hydration requires a period $\sim 10^{-12}$ sec.

It has previously been shown⁴ that the concentration dependence observed for scavenging hydrated electrons by both N_2O and CH_3Cl is in reasonable agreement with the calculations of Schwarz.³ This concentration dependence has been used⁴ to obtain a description of the decay of the electron population, which should be accurate for times longer than nanoseconds, as

$$G(e_{aq}^-) = 2.55 + 2.23e^{\lambda t} \operatorname{erfc}(\lambda t)^{1/2} \quad (1)$$

where λ is a constant which can be evaluated from the scavenging data as $8 \times 10^8 \text{ sec}^{-1}$. Exploration of the shorter time scale by scavenging methods requires inordi-

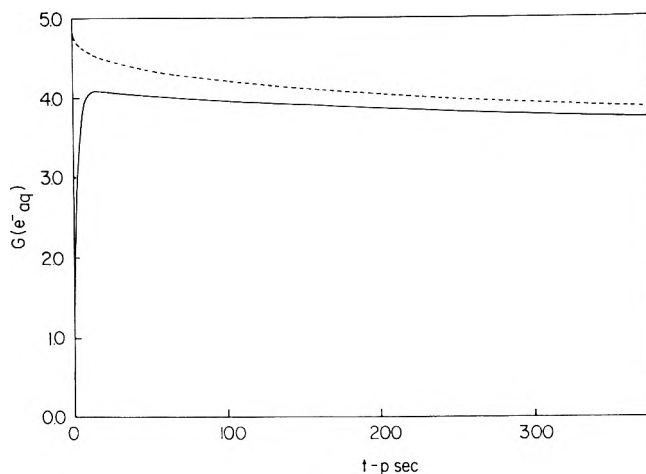


Figure 1. Time dependence of the hydrated electron population (----) as given by eq 1 with $\lambda 8 \times 10^8 \text{ sec}^{-1}$ and (—) as modified by a hydration period of 1.7 psec taking into account reaction of the electrons at a 100-fold higher rate prior to hydration.

nately high solute concentrations ($>1 M$) so that one can only infer the behavior by extrapolation of the trends observed at experimentally accessible concentrations. Yields for electron scavenging as high as ~ 3.8 have been observed and these yields are obviously still increasing with concentration in the molar region so that a limiting yield considerably in excess of 4 is indicated.⁴ Making the very reasonable assumption that the limiting yield at very high solute concentrations is in the vicinity of the value of 4.78 used in the calculations of Schwarz³ the decay on the time scale of the stroboscopic pulse radiolysis experiment as predicted by eq 1 is given by the dashed curve in Figure 1. Schwarz' predictions are very similar (see Figure 7 in ref 4). The detailed differences between the direct observations (which over the region 30–350 psec give yields very similar to the solid curve in Figure 1) and the conclusions from both the scavenging studies and also the model calculations have led a number of investigators to question the applicability of the spur diffusion model. Attention has particularly been focused on the fact that the full initial yield required in the spur diffusion calculations is not observed in the pulse experiments. Also, in the stroboscopic experiment, the yield averaged over a finite pulse of 20 psec should decay from a value of 4.6⁵ to 4.0 whereas the actual data indicate an initial yield of only 4.0 and a decay considerably less than 8%.⁶ From the experimental facts that the initial yield, which was initially thought to be only 3.3,⁷ is now observed to be 4.0⁵ or greater and also that appreciable decay occurs in a 30-nsec period, it seems obvious that the general aspects of spur diffusion theory must be incorporated into any detailed model.

It can be shown that if the relative rates for reaction of the electrons with an externally added scavenger and with the other intermediates produced within the spur are unaffected by hydration then the concentration dependence for reaction of the electrons with the scavenger will be independent of whether or not hydration occurs.⁸ Under these conditions one can, from the scavenging studies, obtain a description of the distribution of the lifetimes that the electrons would have if hydration did not occur. By use of mathematical devices similar to those employed in the discussion of hydrocarbon radiolysis,⁹ one can then explore the possible effects of the hydration period on the

time dependence of $G(e_{aq}^-)$. We have carried out such calculations assuming that prior to hydration electrons have the high mobilities characteristic of them in hydrocarbons (*i.e.*, as for the dry electron suggested by Hamill).¹⁰ For this model the initial reactions of the electron within the spur will be very rapid and will compete with hydration. The calculated time dependence of the hydrated electron population is extremely sensitive to the hydration period (in the region of 10^{-12} sec). Rentzepis and co-workers¹¹ in picosecond photolysis experiments have recently shown that the absorption spectrum of the hydrated electron is present a few picoseconds after photolysis and have suggested a rate constant for hydration of 4×10^{11} sec⁻¹. Using this value, an initial electron mobility of 0.5 cm² sec⁻¹ V⁻¹, and other parameters as determined from the scavenging experiments, we have calculated the solid curve in Figure 1 for the time dependence of the hydrated electron population on the time scale of the stroboscopic experiment. This curve is essentially identical with the experimental curve reported in ref 2. While the hydration period effectively acts as a smoothing time constant at very short times this effect is very small and the difference between the two curves in Figure 1 is largely the result of the loss of $\sim 14\%$ of the electrons initially produced in spur reactions that occur prior to hydration. With shorter hydration times or lower initial mobilities the calculated curves rapidly approach the dashed curve. For hydration periods greater than ~ 5 psec a significant rise would be observed within the time resolution of the stroboscopic experiment and more importantly the maximum yield would be less than 4.0 so that it is clear that hydration of the electrons cannot require a period of more than a few picoseconds.

While the above modification of the spur diffusion model is capable of explaining the observed data reasonably well, minor discrepancies with the detailed observations still remain. Such an explanation requires some decay to occur on the 30–350-psec time scale. However, over this period the absorbance at 575 nm decreases very little and, as recognized by Hunt and coworkers,² may possibly even increase since the apparent decay in the stroboscopic experiment must be corrected for a significant change in the background light level resulting from the decay of the electrons which occurs on the nanosecond time scale (see Figure 1 in ref 2). Also, in the experiments at nanosecond times (see Figure 2 in ref 2) the initial drop is not as sharp as expected and the yield at 5 nsec, where the hydration period is unimportant to the interpretation, appears to be ~ 0.4 units higher than given by inference from the scavenging data. Schwarz¹² has suggested that introduction of time dependent rate constants into the scavenging kinetics will result in a reinterpretation of the data in terms of a somewhat lower initial yield and a corresponding decrease in the required contribution of processes at very short times. A curve very similar to the solid curve in Figure 1 in the time region of 20–500 psec is obtained if the scavenging data are interpreted in terms of an initial yield of 4.3 and an hydration period of 10^{-13} sec or shorter. Such a refinement, however, has little effect on the interpretation of the results at times longer than 1 nsec. One cannot incorporate both a low initial yield (*i.e.*, < 4.3) and an hydration period of $\sim 10^{-12}$ sec or longer into the model since such will predict a yield at 30 psec considerably below the observed value of 4.0.

Given that the initial conditions are reasonably as as-

sumed by Schwarz³ it follows from elementary consideration of the Smoluchowski equation that there must be reaction of radiolytically produced entities within the spurs since the rate constants of the reactions involved are known to be sufficiently high that they will occur in competition with diffusion out of the spurs. It is clear from this that not all hydrated electrons have an equal probability for decay in a given time interval and, therefore, that their decay should not be a simple exponential. Rather at all times one expects to have a continuous distribution of decay probabilities (lifetimes). In a simple model not involving a delay in the production of the intermediate under observation this distribution must result in a continuously decreasing rate of decay. Any departure from this form in the actual decay requires the introduction into the model of delayed processes which act as sources of e_{aq}^- . The chemical scavenging experiments, of course, take as their time origin the time at which the intermediate appears in solution so that the effect of any such delay, which is important in the real time experiments, is lost. The presently available experimental results do not appear to allow any large contribution from delayed processes. While other authors^{2,12} have suggested that e_{aq}^- may be formed by decay of excited states it is pointed out here that any such source of e_{aq}^- must be included within the scheme used by Schwarz to account for the net yield of water decomposition and that one must be careful not to count electrons twice, *i.e.*, one cannot simply superimpose an additional yield on that given by the spur diffusion calculations. Within this limitation it can be suggested that decay of intermediate states resulting from the reaction of electrons prior to hydration might possibly lead to a delayed hydrated electron yield of ~ 0.5 in pure water. A component of this magnitude, however, cannot contribute importantly to the form of the decay on both the 30–350-psec and 1–10-nsec time scales. Obviously the present state of the subject under discussion is currently in a great state of flux and further considerations must await the development of even more detailed results from both the real time and scavenging studies.

References and Notes

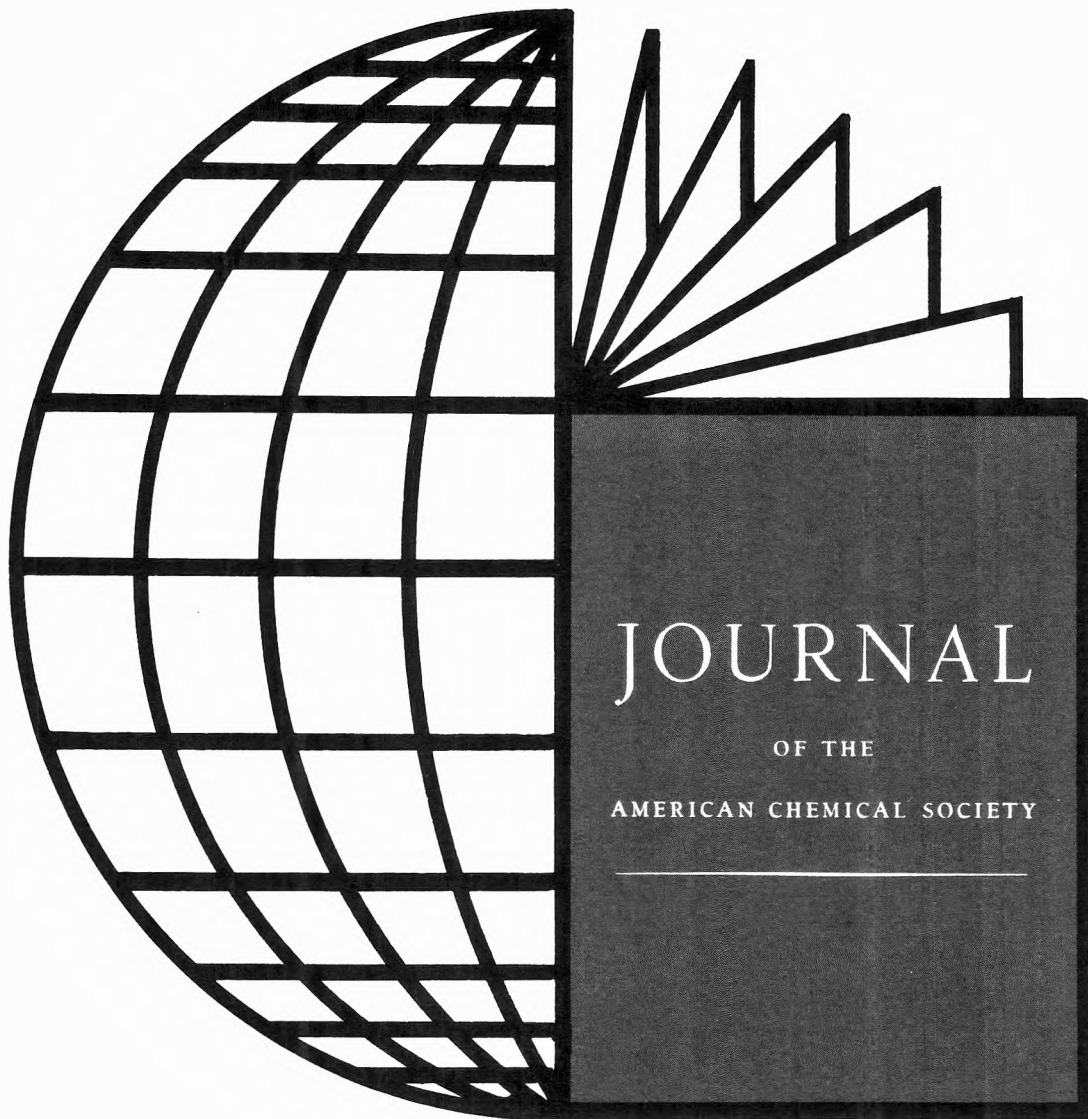
- (1) Supported in part by the U. S. Atomic Energy Commission.
- (2) J. W. Hunt, R. K. Wolff, M. J. Bronskill, C. D. Jonah, E. J. Hart, and M. S. Matheson, *J. Phys. Chem.*, **77**, 425 (1973).
- (3) H. A. Schwarz, *J. Phys. Chem.*, **73**, 1928 (1969).
- (4) T. I. Balkas, J. H. Fendler, and R. H. Schuler, *J. Phys. Chem.*, **74**, 4497 (1970).
- (5) For a decay of the form of eq 1 averaged over a finite pulse of 20 psec (with $\lambda = 8 \times 10^8$ sec⁻¹) the maximum observed value of $G(e_{aq}^-)$ will be 4.57 or ~ 0.2 units less than the initial yield. If eq 1 applies, the yield observed at 30 psec should be incremented by about 0.2 to take into account the decay which occurs during the pulse.
- (6) Because the decay in the stroboscopic experiment is the composite obtained from electrons of different ages, accurate interpretation of the decay data requires a complete description of the microstructure of the 8-nsec pulse and is certainly complex. In pure water a large background of the electrons produced do not decay at all so that the resultant time dependence of the optical absorption is a staircase. In ref 2 the average absorption was 50% indicating a very high absorption for at least a portion of the microstructure train. The resultant nonlinear averaging will further complicate the interpretation of the data. The observed decay should, however, be an upper limit.
- (7) J. E. Aldrich, M. J. Bronskill, R. K. Wolff, and J. W. Hunt, *J. Chem. Phys.*, **55**, 530 (1971).
- (8) Detailed calculations show that for a given initial lifetime distribution a change of a factor of 2 in the relative rates of the electron reactions upon hydration will have very little effect (< 0.1 in yield) on the scavenging curves. It is known that electrons react rapidly with methyl chloride in both water (ref 4) and in hydrocarbons (J. M.

- Warman, K.-D. Asmus, and R. H. Schuler, *J. Phys. Chem.*, **73**, 931 (1969)) so that the mathematical arguments employed in the present work should be reasonably accurate.
- (9) S. J. Rzad, P. P. Infelta, J. M. Warman, and R. H. Schuler, *J. Chem. Phys.*, **52**, 3971 (1970).
- (10) W. H. Hamill, *J. Phys. Chem.*, **73**, 1341 (1969).
- (11) P. M. Rentzepis, R. P. Jones, and J. Jortner, *Chem. Phys. Lett.*, **15**, 480 (1972).
- (12) H. A. Schwarz, private communication.

*Radiation Research Laboratories
Center for Special Studies
Department of Chemistry
Mellon Institute of Science
Carnegie-Mellon University
Pittsburgh, Pennsylvania 15213*

**Stefan J. Rzad
Robert H. Schuler***

Received April 6, 1973



Most cited chemical journal in the entire world

... and one of publishing's best subscription values! That's right! You pay less per page for JACS—the most widely cited journal in chemistry—than for any other major scientific journal in the world.

But don't subscribe to this internationally respected journal because it's inexpensive. Subscribe because you will receive biweekly original research articles that cover ALL chemical research areas ... together with many concise, up-to-the-minute Communications. Regardless of your major field of interest in chemistry, you'll find an abundance of authoritative and definitive data in each issue that cuts across ALL chemical research areas and is valuable and relevant to *your* work as well.

Order your own personal subscription to the number one chemical journal now. Complete and return the form.



... another ACS service

Journal of the American Chemical Society American Chemical Society

1155 Sixteenth Street, N.W.
Washington, D.C. 20036

Yes, I would like to receive the JOURNAL OF THE AMERICAN CHEMICAL SOCIETY at the one-year rate checked below:

	U.S.	Canada	Latin America	Other Nations
ACS Member Personal-Use				
One-Year Rate	<input type="checkbox"/> \$22.00	<input type="checkbox"/> \$27.00	<input type="checkbox"/> \$27.00	<input type="checkbox"/> \$28.00
Nonmember	<input type="checkbox"/> \$66.00	<input type="checkbox"/> \$71.00	<input type="checkbox"/> \$71.00	<input type="checkbox"/> \$72.00
Bill me <input type="checkbox"/>	Bill company <input type="checkbox"/>	Payment enclosed <input type="checkbox"/>		

Name _____

Street _____ Home
Business

City _____ State _____ Zip _____

J-73

For the most current information by the leaders in the field...

Kinetic Systems

Mathematical Description of Chemical Kinetics in Solution

By **Christos Capellos**, *Picatinny Arsenal*, and **Benon H. J. Bielski**, *Brookhaven National Laboratory*

Kinetic Systems contains step-by-step developments of important mathematical equations used in solving chemical kinetic systems. The authors treat each equation rigorously and in detail, eliminating the need for outside sources of information. At the same time, the level of presentation is elementary, making the book completely understandable even to those who are not fluent in these mathematical operations.

1972 138 pages \$11.95

X-Rays, Electrons, and Analytical Chemistry

Spectrochemical Analysis with X-Rays

By **H. A. Liebhafsky**, *Texas A&M University*, and **H. G. Pfeiffer, E. H. Winslow, and P. D. Zemaný**, *all of General Electric Company*

"This book is substantially a revised and updated version of *X-Ray Absorption and Emission in Analytical Chemistry* by the same authors, published in 1960, and like the previous work, it covers X-Ray spectrometry, absorbtometry and powder diffractometry. In the new work, a greater emphasis has been placed on X-Ray powder diffractometry, but less on X-Ray absorbtometry. In addition to chapters devoted to each of these three techniques, separate chapters are also devoted to such topics as X-Ray spectra, generation and properties of X-Rays, the selection of X-Ray wavelengths, counting statistics, and measurement of film thickness. . . . the book is complete enough to be used both as a basic text for beginners as well as serving as a useful reference work for more experienced users. . . ."—*X-Ray Spectrometry*

1972 566 pages \$24.95

Surface and Colloid Science

Volume 6

Edited by **Egon Matijević**, *Clarkson College of Technology*

Contents, Volume 6

Colloidal Silica—*R. K. Iler*. Radioactive Tracers in Surface and Colloid Science—*Mitsuo Muramatsu*. Biopolymers at Interfaces—*I. R. Miller and D. Bach*. Lipid Multilayers—*Kare Larsson*. Author Index. Subject Index. Cumulative Index, Volumes 1-6.

1973 320 pages \$22.50

Advances in Chemical Physics

Volumes 23 and 24

Edited by **I. Prigogine**, *University of Brussels*, and **Stuart A. Rice**, *University of Chicago*

Contents, Volume 23

Recombination of Gaseous Ions—*Bruce H. Mahan*. Vibration—Vibration Energy Transfer—*C. Bradley Moore*. ESCA—*David A. Shirley*. Ab Initio Calculations on Small Molecules—*J. C. Browne and F. A. Matsen*. Picosecond Spectroscopy and Molecular Relaxation—*P. M. Pentzepis*. Some Aspects of Exciton Theory—*Michael R. Philpott*. Author Index. Subject Index.

1973 357 pages \$22.50

Contents, Volume 24

Laser Light Scattering in Fluid Systems—*P. A. Flury and J. P. Boon*. Thermodynamics of Discrete Mechanical Systems with Memory—*B. D. Coleman*. Transition from Analytic Dynamics to Statistical Mechanics—*J. Ford*. Variational Methods in Statistical Mechanics—*M. D. Girardeau and R. M. Mazo*. Kinetic Theory of Dense Fluids and Liquids Revisited—*H. T. Davis*. Author Index. Subject Index.

1973 368 pages \$22.50

Progress in Physical Organic Chemistry

Volume 10

Edited by **Andrew Streitwieser Jr.**, *University of California, Berkeley*, and **Robert W. Taft**, *University of California, Irvine*

A relatively recent chemical discipline, physical organic chemistry seeks to explore the effects of structure and environment on reaction dynamics and mechanisms through the use of modern quantitative and mathematical techniques. Volume 10 presents six new, authoritative papers covering several of the field's current areas of importance.

Contents

Generalized Treatment of Substituent Effects in Benzene Series: A Statistical Analysis by the Dual Substituent Parameter Equation—*S. Ehrenson, R. T. C. Brownlee, and R. W. Taft*. Substituent Effects in Non-Aromatic Unsaturated Systems—*M. Chartor*. Vinyl and Allenyl Cations—*P. J. Stang*. Physical Properties and Reactivity of Radicals—*R. Zahradnik and P. Carsky*. Probing the Active Sites of Enzymes with Conformationally Restricted Substrate Analogs—*G. L. Kenyon and J. A. Fee*. The Enthalpy-Entropy Relationship—*O. Exner*. Author Index. Subject Index. Cumulative Index

1973 In press

...consult Wiley-Interscience

Prices subject to change without notice.

Available at your bookstore or from Dept. 553

WILEY-INTERSCIENCE

a division of John Wiley & Sons, Inc., 605 Third Avenue, New York, N.Y. 10016/ In Canada: 22 Worcester Road, Rexdale, Ontario



WILEY-INTERSCIENCE, Dept. 553, 605 Third Avenue, New York, N.Y. 10016

Please send me the book(s) I have checked below—

- 0 471 13450-3 _____ Capellos/Bielski: *Kinetic Systems*, \$11.95
 0 471 53428-5 _____ Liebhafsky, et al: *X-Rays, Electrons, and Analytical Chemistry* \$24.95
 0 471 57635-2 _____ Matijević: *Surface and Colloid Science, Volume 6* \$22.50
 0 471 69927-6 _____ Prigogine/Rice: *Advances in Chemical Physics, Volume 23* \$22.50
 0 471 69929-9 _____ Prigogine/Rice: *Advances in Chemical Physics, Volume 24* \$22.50
 0 471 83356-8 _____ Streitwieser/Taft: *Progress in Physical Organic Chemistry, Volume 10* . . . In press

My check (money order) for \$ _____ is enclosed.

Please bill me.*

Name _____

Address _____

City _____

State/Zip _____

Please add state and local taxes where applicable. Prices subject to change without notice.

*Restricted to the continental United States.